Influence of Humid Atmosphere on Crystallization Behavior of Slag Systems Used in Continuous Casting of Steels

To the Post-Graduation Program in Mining, Metallurgical and Materials Engineering (PPGE3M) of the Universidade Federal do Rio Grande do Sul (Brazil)
and
To the Faculty of Materials Science and Technology (Faculty 5)
of the Technische Universität Bergakademie Freiberg (Germany)
(bi-national doctorate)

THESIS

to attain the academic degree of

Doutor em Engenharia

(Dr.)

and

Doktor-Ingenieur

(Dr.-Ing.)

submitted

by Chemical Engineer Daniel dos Reis Silva
born on March 21st 1973 in Porto Alegre (Brazil)

Rewiers: Prof. Dr.-Ing. Antônio C. F. Vilela, Porto Alegre, Brazil
Prof. Dr.-Ing. Jeferson L. Klug, Porto Alegre, Brazil
Prof. Dr. Wagner V. Bielefeldt, Porto Alegre, Brazil
Dr. Magda G. François, Porto Alegre, Brazil
Prof. Dr.-Ing. Olena Volkova, Freiberg, Germany
Prof. Dr. rer. nat. habil David Rafaja, Freiberg, Germany
Prof. Dr.-Ing. habil. Horst Biermann, Freiberg, Germany
Prof. Dr.-Ing. habil. Christos G. Aneziris, Freiberg, Germany
Prof. Dr.-Ing. habil. Rüdiger Schwarze, Freiberg, Germany

Data of the award: December 16th 2020 (Brazil) and 26th February 2021 (Germany)

Influência da Atmosfera Úmida sobre o Comportamento de Cristalização de Sistemas de Escórias usados no Lingotamento Contínuo de Aços

Para o Programa de Pós-Graduação em Engenharia de Minas, Metalúrgica e de Materiais (PPGE3M) da Universidade Federal do Rio Grande do Sul (Brasil)

e

Para Faculdade de Ciência e Tecnologia dos Materiais (Faculdade 5) da Technische Universität Bergakademie Freiberg (Alemanha)

Einfluss feuchter Atmosphäre auf das Kristallisationsverhalten von Schlacken beim Stranggießen von Stähle

Der Postgraduiertenprogramm in Bergbau, Metallurgie und Materialtechnik (PPGE3M) der Universidade Federal do Rio Grande do Sul (Brasilien)

und

Der Fakultät für Werkstoffwissenschaft und Werkstofftechnologie (Fakultät 5) der Technische Universität Bergakademie Freiberg (Deutschland)

In memory of my father.

Abstract

The influence of humid atmosphere on crystallization behavior of mold powders used in continuous casting of steel is the subject of the present study. The experimental procedures were conducted at the Institut für Eisen- und Stahltechnologie of the Technische Universtität Bergakademie Freiberg, Germany, and at the Universidade Federal do Rio Grande do Sul, Brazil. In the present study, the Single Hot Thermocouple Technique (SHTT) was applied for the investigation of the influence of the humidity on crystallization behavior of mold fluxes. Five distinct mold powders compositions were prepared based on the CaO-SiO_2-Al_2O_3-MgO-TiO_2 slag system and submitted to continuous cooling and isothermal experimental measurements at inert atmosphere of argon (Ar), and at two distinct gas mixtures Ar-water vapor with 3.34 % H_2O and 12.49 % H_2O. Continuous cooling transformation (CCT) and time-temperature-transformation (TTT) diagrams were obtained and analyzed.

CCT and TTT diagrams showed a strong tendency of slags to form glass with increasing TiO_2 content (0.5 – 5.0 wt-%); conversely, additions of MgO increase considerably the crystallization rate as well as the crystallization temperature range. The effect of water vapor on the crystallization behavior of the proposed mold powders was distinct according to the slag chemical composition and the temperature.

A markedly increase of the crystallization rate and the crystallization temperature range in presence of humid atmosphere was observed in slags with higher polymerization degree. In more depolymerized slags, such an effect is less pronounced, mainly with respect to the crystallization temperature range. Other important aspect observed was the influence of temperature on the effect of water on the crystallization behavior of the mold powders. For a determined slag, water can act either a polymerizing or depolymerizing agent, according to the temperature range, exposing the amphoteric behavior of water. For a same slag system, distinct trends regarding to the effect of water on crystallization behavior as a function of temperature could be observed. It was found that the onset of crystallization was hindering at higher temperatures in measurements conducted in humid atmosphere. At intermediate temperatures, the effect of water on the crystallization was considerably small. However, the crystallization rate was improved at lower temperatures with the presence of water vapor. Such a behavior was attributed to changes of polymerization degree with the temperature. This was more evident in slags with higher nominal NBO/T. It is suggested that the influence of temperature on the effect of water on the crystallization behavior is more intense in slags with in a NBO/T range between 1.0 and 2.0, approximately.

Finally, thermodynamic calculations using the *FactSage 6.4* software were carried out aiming to estimate the water capacity of the mold powders. The thermodynamic calculation results showed an increase of water capacity of slag with increasing MgO content. The water capacity results were also expressed as a function of some calculated structural parameters, namely, NBO/T and optical basicity. The water capacity showed a large variation in a narrow optical basicity range; while a tendency toward the increase the water solubility with increasing the degree of depolymerization of the slags could be observed.

Resumo

A influência da atmosfera úmida sobre o comportamentos de cristalização de pós de molde usados no lingotamento contínuo de aços é objeto do presente estudo. Os procedimentos experimentais foram conduzidos no Institut für Eisen- und Stahltechnologie da Technische Universität Bergakademie Freiberg, Alemanha, e na Universidade Federal do Rio Grande do Sul, Brasil. No presente estudo, a técnica Single Hot Thermocouple (SHTT) foi aplicada na investigação da influência da umidade sobre o comportamento de cristalização dos pós de molde. Cinco composições distintas de pós de molde foram preparadas baseadas no sistema de escórias $CaO\text{-}SiO_2\text{-}Al_2O_3\text{-}MgO\text{-}TiO_2$ e submetidas à medições experimentais de resfriamento contínuo e isotérmicas em atmosfera inerte de argônio (Ar), e em duas misturas distintas de Ar-vapor de água com 3.34 % H_2O e 12.49 % H_2O. Diagramas de resfriamento contínuo (CCT) e de tempo-temperatura-transformação (TTT) foram obtidos e analisados.

Os diagramas CCT e TTT mostraram uma forte tendência das escórias de formarem vidro com o aumento do teor de TiO_2 (0.5 – 5.0 wt-%); em contrapartida, adições de MgO aumentam consideravelmente a taxa de cristalização, como também o intervalo de temperatura de cristalização. O efeito do vapor de água sobre o comportamento de cristalização dos pós de molde propostos foi distinto de acordo com a composição química e temperatura.

Um aumento notável da taxa de cristalização e do intervalo de temperatura de cristalização foi observado em escórias com grau de polimerização mais alto. Em escórias mais depolimerizadas, tal efeito foi menos pronunciado, com respeito, principalmente, ao intervalo de temperatura de cristalização. Outro importante aspecto observado foi a influência da temperatura sobre o efeito que a água exerce sobre o comportamento de cristalização dos pós de molde. Para uma determinada escória, a água pode agir como um agente polimerizador ou depolimerizador, de acordo com o intervalo de temperatura, expondo o comportamento anfótero da água. Para um mesmo sistema de escória, tendências distintas com respeito ao efeito da água sobre o comportamento de cristalização como função da temperatura puderam ser observadas. Verificou-se que o início da cristalização foi obstruído em temperaturas mais elevadas em medições conduzidas em atmosfera úmida. Em temperaturas intermediárias, o efeito da água sobre a cristalização foi consideravelmente pequeno. Entretando, a taxa de cristalização foi melhorada em temperaturas mais baixas com a presença de vapor de água. Tal comportamento foi atribuído à mundanças do grau de polimerização com a temperatura. Isto foi mais evidente em escórias com maior NBO/T nominal. É sugerido que a influência da temperatura sobre o efeito da água sobre o comportamento de cristalização é mais intenso em em escórias em um intervalo de NBO/T entre 1.0 e 2.0, aproximadamente.

Finalmente, cálculos termodinâmicos usando o *FactSage 6.4* foram realizados objetivando estimar a capacidade de água dos pós de molde. Os resultados dos cáculos termodinâmicos mostraram um aumento da capacidade de água com o aumento do teor de MgO. Os resultados da capacidade de água também foram expressos como função de alguns parâmetros estruturais calculados, a saber NBO/T e basicidade óptica. A capacidade de água mostrou grande variação em um intervalo estreito de basicidade óptica; enquanto uma tendência em

direção ao aumento da solubilidade da água com o aumento do grau de depolimerização das escórias pode ser observado.

Zusammenfassung

Der Einfluss der feuchten Atmosphäre auf das Kristallisationsverhalten von Formpulvern, die beim Stranggießen von Stahl verwendet werden, ist Gegenstand der vorliegenden Doktorarbeit. Die experimentellen Verfahren wurden am Institut für Eisen- und Stahltechnologie der Technischen Universität Bergakademie Freiberg und an der Universidade Federal do Rio Grande do Sul, Brasilien, durchgeführt. In der vorliegenden Studie wurde die Single Hot Thermocouple (SHTT) -Technik angewendet, um den Einfluss von Feuchtigkeit auf das Kristallisationsverhalten von Formpulvern zu untersuchen. Auf der Basis des CaO-SiO_2-Al_2O_3-MgO-TiO_2-Schlackensystems wurden fünf verschiedene Formpulverzusammensetzungen hergestellt und einer kontinuierlichen Abkühlung und isothermen experimentellen Messungen in einer inerten Atmosphäre von Argon (Ar) und in zwei verschiedenen Gasgemischen Ar-Wasserdampf mit 3,34% H_2O und 12,49% H_2O unterzogen. Diagramme zur kontinuierlichen Kühltransformation (CCT) und Zeit-Temperatur-Transformation (TTT) wurden erhalten und analysiert.

CCT- und TTT-Diagramme zeigten eine starke Tendenz von Schlacken, mit zunehmendem TiO2-Gehalt (0,5 – 5,0 Gew .-%) Glas zu bilden;jedoch die Zugaben von MgO erhöhen die Kristallisationsgeschwindigkeit sowie den Kristallisationstemperaturbereich erheblich. Die Wirkung von Wasserdampf auf das Kristallisationsverhalten der vorgeschlagenen Formpulver war je nach chemischer Schlackenzusammensetzung und Temperatur unterschiedlich. In Schlacken mit höherem Polymerisationsgrad wurde ein deutlicher Anstieg der Kristallisationsrate und des Kristallisationstemperaturbereichs in Gegenwart einer feuchten Atmosphäre beobachtet.

In stärker depolymerisierten Schlacken ist ein solcher Effekt weniger ausgeprägt, hauptsächlich in Bezug auf den Kristallisationstemperaturbereich. Ein weiterer wichtiger Aspekt war der Einfluss der Temperatur auf die Wirkung von Wasser auf das Kristallisationsverhalten der Formpulver. Für eine bestimmte Schlacke kann Wasser je nach Temperaturbereich entweder als Polymerisations- oder Depolymerisationsmittel wirken und das amphotere Verhalten von Wasser freilegen. Für dasselbe Schlackensystem konnten unterschiedliche Trends hinsichtlich des Einflusses von Wasser auf das Kristallisationsverhalten als Funktion von Wasser beobachtet werden. Es wurde festgestellt, dass der Beginn der Kristallisation bei höheren Temperaturen und bei Messungen in feuchter Atmosphäre behindert wurde. Bei Zwischentemperaturen war die Wirkung von Wasser auf die Kristallisation beträchtlich gering. Die Kristallisationsrate wurde jedoch bei niedrigeren Temperaturen in Gegenwart von Wasserdampf verbessert. Ein solches Verhalten wurde auf Änderungen des Polymerisationsgrades mit der Temperatur zurückgeführt. Dies zeigte sich am deutlichsten bei Schlacken mit einem höheren nominalen NBO/T. Es wird vermutet, dass der Einfluss der Temperatur auf die Wirkung von Wasser auf das Kristallisationsverhalten in Schlacken in einem Bereich von NBO/T zwischen ungefähr 1,0 und 2,0 stärker ist.

Schließlich wurden thermodynamische Berechnungen mit FactSage 6.4 durchgeführt, um die Wasserkapazität der Formpulver abzuschätzen. Die Ergebnisse thermodynamischer Berechnungen zeigten eine Zunahme der Wasserkapazität mit einer Zunahme des MgO-

Gehalts. Die Ergebnisse der Wasserkapazität wurden auch als Funktion einiger berechneter Strukturparameter ausgedrückt, nämlich NBO/T und optische Basizität. Die Wasserkapazität zeigte große Unterschiede in einem engen Bereich der optischen Basizität; während ein Trend zur Erhöhung der Wasserlöslichkeit mit zunehmendem Grad der Schlackendepolymerisation beobachtet werden kann.

Acknowledgements

I would like to express my heartfelt thanks to my supervisors, Prof. Dr.-Ing. Antônio C. F. Vilela for his guidance, encouragement and patience in the conduction of the present study, and Prof. Dr.-Ing. Habil Olena Volkova for his helpful support for the accomplishment of the co-tutelage.

Very deep thanks to Prof. Dr.-Ing. Nestor C. Heck for numerous hours of fruitful discussions, comments and all its scientific contribution to this study.

Special thanks to Prof. Dr.-Ing. Jeferson L. Klug for his valuable research line suggestion, experimental technique teaching, orientation, hospitality and friendship.

I'm also sincerely grateful Dr.-Ing. Hans-Peter Heller for his help and advice on measurement technology, as well as for all employees from TU Bergakademie Freiberg in special to Dr.-Ing. Armin Franke, Mr. Peter Neuhold, Mr. Günter Frank, Mr. Steffen Bajorat, Mr. Marcus Block, Mrs. Katrin Brock and Mrs Melanie Strobel.

I would like to thank to the Brazilian Science and Technology National Concil (CNPq) for the granted scholarship.

Last but not least, I would like to thank my colleagues, in special to Dr. Julio A. M. Pereira for his helpful technical contribution.

CONTENTS

List of Figures

Chapter 1

Chapter 2

Chapter 3

Chapter 4

Section 4.1

Appendix A

Appendix B

Appendix C

List of Tables

List of Symbols

CLSM:	Confocal Laser-scanning Microscope
C_{OH}:	Hydroxyl capacity (or water capacity)
DHTT:	Double Hot Thermocouple Technique
DTA:	Differential Thermal Analysis
E_a:	Activation energy of crystallization
EPMA:	Electron probe micro analysis
FTIR-RAS:	Fourier transform infrared-reflection absorption spectroscopy
HTT:	Hot thermocouple tecnhique
η	Viscosity
NBO/T:	Non-bridging oxygen atoms per number of atoms in tetragonal coordination
O^-:	Non-bridging oxygen
O^0:	Bridging oxygen
O^{2-}:	Free oxygen
SHTT:	Single Hot Thermocouple Technique
T_g:	Glass transition temperature
T_{gr}:	Reduced glass transition temperature
XDR:	X-Ray Diffraction
XPS:	X-ray photoelectronic spectroscopy
Δt:	Incubation time deviation

CHAPTER 1 – INTRODUCTION

1.1 Background

Continuous casting is a world-widely process used in the casting of steel and its alloys. It is the predominant method to solidify the steel directly into a semifinish product in a pre-determined shape – where blooms, billets (including round hollow billets), slabs and beam blanks are the more conventional forms (see **Figure 1.1**) – been responsible for more than 90% of the world steel production [1]. The process was definitely introduced in the industrial flow sheets in the 1960s and it had been continuously improved with the progress of implemented technologies as the high speed casting. In the continuous casting, the mold powders are essential to quality surface of the steel product and to the stability of casting process. In the present introduction, the continuous casting will be broached only some general topics of the process. More detailed information about the continuous casting process can be found in Mizoguchi *et al*. [2] and Garcia *et al*. [3].

1.2 Continuous Casting Process

The continuous casting is the last stage of the steel production chain that runs with steel in the liquid state. **Figure 1.1** shows an example of an overall scheme of the slab continuous casting process of steel (the process layout is substantially the same for the other shapes). This process is, in essence, a solidification process at which the liquid steel is poured from a ladle to a tundish; and from this last into one (or more) open ended water cooled copper mold. Two practices have been applied concerning the steel delivery from the tundish to the mold: without steel jet shrouds (open casting); or through a submerged entry nozzle (SEN), which distributed the liquid steel through the outlet ports directed by its angle and geometry, modifying the flow pattern inside the mold cavity (closed casting) [3-5]. Open casting technology is normally applied to billets and blooms casting; in this case, an inert shrouding gas is used instead of a SEN. For this technology, oil is employed as mold lubricant, although mold powders have been formulated to be used in open casting [6,7]. The utilization of refractory shrouds for steel transfer process from the ladle – passing by the tundish – to the mold (close casting) have been adopted for slab casting. In this case, the use of mold powders are normally deployed as a lubrication agent, and to help to control heat transfer (more details in **section 1.3**) [8].

When in contact with the mold cooled wall, the molten steel starts to solidify due to a strong heat extraction through the mold wall to the circulating water, forming a solid shell. The mold performs a vertical oscillatory movement to avoid the freezing of the steel onto the mold, and accordingly sticker breakouts [9,10]. The solid steel shell formed will constantly increase its thickness along to caster mold length, being extracted by the mold oscillation movement and drive rolls positioned below the caster machine. Mechanically, the thickness of the steel shell that leaves the mold zone is not strong enough to the containment of the non-solidified steel. The relative position of the steel shell to the mold is kept by support rolls positioned below the mold, supporting the steel and minimizing the bulging due to the ferrostatic pressure. The remaining molten steel enclosed by the solid steel shell which leaves the mold is cooled by water and air mist sprays positioned between the rolls until the molten core becomes fully

solidified. After the complete solidification of the center of the strand steel (metallurgical length), it is cut in sections by a torch, according to its application [11,12].

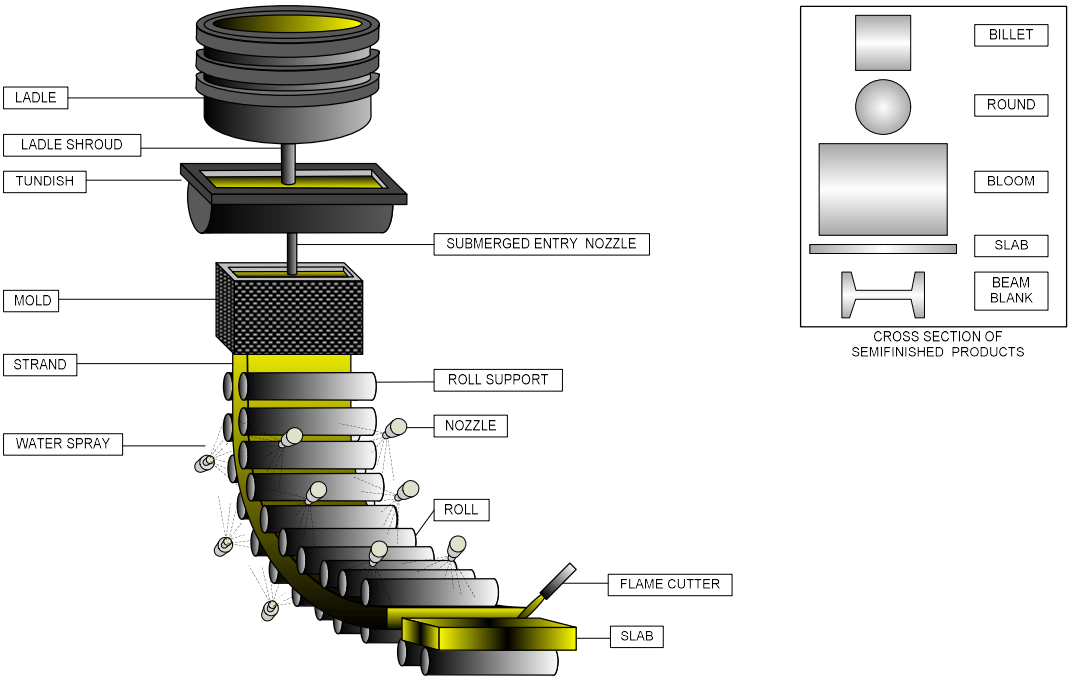

Figure 1.1 Generic representation of a slab continuous casting process; and semifinished cross section of the continuous casting steel products.

In this context, the mold powder plays a vital role along the steel solidification stage occurring at the mold level, being the subject of the present work. Thus, a concise but relevant description of the mold powders and their duties in the continuous casting process is present next. A more detailed discussion regard to the theme mold powders can be found in the work of Pinheiro *et al.* [13-24] and Mills and Däcker [1].

1.3 Mold Powders

Mold powders – also known as mold slags or mold fluxes – are synthetic slags constituted of a mixture of different oxides, silicate and fluorides. Their chemical composition varies greatly depending on the properties required by the casting process. Usually, the mold powders are composed of CaO and SiO_2 (about 70%), with varying content of other oxides as Al_2O_3, MgO, Na_2O, Li_2O *etc*. and fluorides as CaF_2, which are added to adjust important slag properties as viscosity, crystallization and melting point [14,25-27]. In the continuous casting mold, the mold powder is fed onto the free surface of the liquid steel forming first a sintered layer, a mushy and liquid layer from the top of mold to the liquid steel surface (**Figure 1.2(a)**). At this point, the powder undergoes a series of changes according to a temperature range as following: (i) evaporation of moisture at *ca*. 97 °C; (ii) decomposition of carbonates (at *ca*. 397 °C– 497 °C); (iii) sintering (at *ca*. 677 °C – 877 °C) (iv); reaction of carbon particles with oxygen forming a reducing atmosphere of $CO_{(g)}$ and $CO_{2(g)}$ (at *ca*. 497 °C – 697 °C); and (v) at temperatures higher than 877 °C occurs the melting of the powder [28,29]. Beside these events, chemical reactions between molten slag and liquid steel and inclusions pick up such as TiO_2 and Al_2O_3 would promote significant alteration in the physical

properties of the liquid slag as viscosity, break temperature, or crystalline degree of solid slag film [30,31].

The mold powders are fundamental in the control and stability of continuous casting process and in the quality of the final steel product. Their importance lies on a set of functions carried out by the mold flux along the caster process; namely (i) protect the steel meniscus against reoxidation; (ii) providing thermal insulation to prevent the steel from oxidation; (iii) absorb inclusions that rise from the steel surface into the molten slag pool; (iv) provide liquid lubrication for the strand; and (v) controlling the horizontal heat transfer across the infiltrate slag layer between the strand and mold [13,30,32]. Among the mold flux functions, lubrication of the mold and horizontal heat transfer control are the most critical to the operational stability [13] and will be discussed in more detail later. These functions are strongly affected by the crystallization tendency of the slag, which, in turn, is affected by its chemical composition, temperature and environment conditions.

At the top of the mold, the mold flux acts as a thermal and chemical insulator. It reduces the heat losses from the upper surface of the liquid steel preventing its partial solidification, mainly at the meniscus level [13,26,33]. The chemical insulating from the atmosphere protects the liquid steel surface from reoxidation [13,32]. The liquid slag layer is responsible to assimilate nonmetallic inclusions, as nitrides, Al_2O_3 and TiN, which emerge to the mold surface from steel and/or reactions between slag and steel. The kind of inclusion depends of Al-killled or [Ti] steel grade, for instance [34].

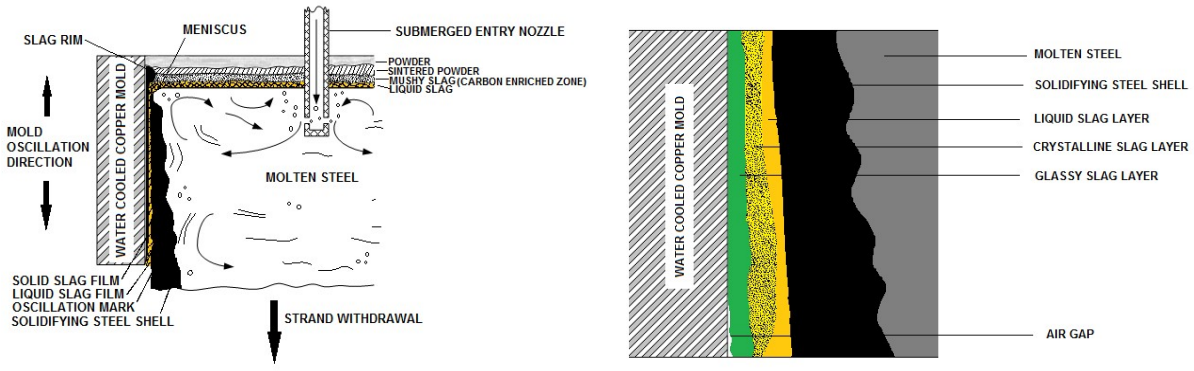

Figure 1.2 Schematic of the liquid steel and the mold flux at the mold of the continuous caster.

Figure 1.2(a) shows a schematic representation of the mold slag film evolution. The formed liquid slag pool must have an appropriated depth to provide adequate liquid slag to lubrication of strand. The infiltration of the liquid slag into the gap between the mold wall and steel shell is facilitated by the oscillation stroke of the mold and is related to the shear force created by the negative strip [4,35-38]. The infiltration of the molten flux into the gap below the meniscus is. When in contact with cooled mold wall, the molten slag forms a rim at the meniscus level. Below the frozen rim, the liquid slag in contact with mold wall forms a thin slag film (2 – 3 mm thick) which solidifies rapidly forming a glassy layer at first. Due to a large temperature gradient across the solid slag film (approximately 1000°C), the glassy phase

tends to change forming a crystalline layer with a liquid part in the hotter regions near to the strand [34]. **Figure 1.2(b)** shows the three different slag layers formed due to the large thermal gradient across the slag film. The presence of a crystalline layer can be either beneficial or deleterious to the casting process, depending of the steel grade and the casting speed. For instance, slag with high crystallization tendency increases slag scale on the steel surface and can lead to cracks or breakouts because of lower local heat transfer. In addition, crystalline slag has been shown to be harmful to high-speed casting conditions due to tendency of slag-fracture near the meniscus [39]. Therefore, the presence of crystal in the slag film has significant effect on the lubrication and heat transfer process. In this context, factors which have influence on the crystallization behavior of the slag must be investigated to provide a wide data range to aid in the mold powders development. For the present work, the interaction of factors as the environment conditions and the chemical composition of the mold powder is the main focus of research.

1.4 Aim of the Study

Understanding the behavior of molten slags under solidification, including the influence of the environment on its properties is fundamental in mold powders development. The characteristic crystallization of the mold powder has direct impact on the viscosity and heat transfer through the slag; besides being susceptible to atmosphere conditions. Thus, the aim of the present thesis is:

> *to develop an understanding about the influence of water vapor on the crystallization behavior of simple mold powder systems.*

For this purpose, the specific objectives were performed as following:

(i) to evaluate the effect of addition of MgO and TiO_2 on the crystallization behavior of the $CaO\text{-}SiO_2\text{-}Al_2O_3$ system – at constant binary basicity – by constructing continuous cooling transformation (CCT) and time-temperature-transformation (TTT) diagrams, from measurements in inert atmosphere using the Single Hot Thermocouple Technique (SHTT).

(ii) to characterize the mold powders concerning to viscosity, crystalline phase and critical cooling rate (in continuous cooling conditions); and crystal morphology (in isothermal conditions).

(iii) to investigate the influence of water vapor on the crystallization behavior of the mold slag systems above proposed by application of different atmospheric conditions (two specific water vapor partial pressures) obtaining the respective TTT-diagrams from SHTT experimental results, and comparing them with those obtained in inert atmosphere (as a parameter).

(iv) to evaluate qualitatively the influence of the chemical composition on the water solubility via thermodynamic simulations, providing data to estimate the water capacity of the mold powders; aiming to correlate the simulated data with the results obtained from SHTT and DHTT in humid atmosphere for crystallization.

1.5 Thesis Outline

Following the **Chapter** 1, a general introduction about the continuous casting process is presented accompanied by a brief description of the mold powders and their role and importance on the continuous casting process. The objectives of this thesis are also described in this chapter. In the **Chapter** 2, a mold flux review with a special focus on the relevant subjects concern to the present study such as an overview about the structure of the slags and melts, passing through a general description of the theory of crystallization, until the crystallization behavior of slags and the effect of some oxides on the crystallization tendency of slag, with special importance to MgO and TiO_2; the issues regarding to the effect of water vapor atmosphere, influence of the chemical composition of the slags and melts on the water solubility and its effect on the some properties and crystallization behavior of the slags are highlighted. In the following chapter (**Chapter 3**), materials preparation and the experimental procedures are provide; with a description of the technique employed in the crystallization experiments (SHTT), and calibration are presented. In the **Chapter 4**, the experimental data and discussion of results are showed. The effects of water on crystallization behavior as well as some thermodynamic simulations are presented separately. Finally, the findings and the general conclusions of the present study are presented in the **Chapter 5**.

References

[1] Mills, K. C., Däcker, C.: *The Casting Powders Book*; 1 ed.; Springer International Publishing, 2017.

[2] Mizoguchi, S., Ohashi. T., Saeki, T. Continuous Casting of Steel. *Annual Review of Materials Science*1981.

[3] Garcia, A., Spim, J. A., Santos, C. A. D., Cheung, N.: *Lingotamento Contínuo de Aços (portuguese)*; Associação Brasileira de Metalurgia e Materiais: São Paulo, 2006.

[4] Meng, Y., Thomas, B. G. Modeling Transient Slag-Layer Phenomena in the Shell/mold Gap in Continuous Casting of Steel. *Metallurgical and Materials Transactions B* **2003**, *34B*, 707-725.

[5] *Benefits of Increased Use of Continuous Casting by the U.S. Stell Industry - A Technical Memorandum;* States, O. o. T. A.-C. o. t. U.: Washington DC, 1979.

[6] de Wet, G. J. CFD Modelling and Mathematical Optimisation of a Continuous Caster Submerged Entry Nozzle. University of Pretoria, 2005.

[7] Carli, R., Alloni, M., Mapelli, C., Barella, S., Levrangi, L. In *Liquid Powder for Continuous Open Casting of Steel*, Graz (Austria)2014.

[8] Pehlke, R. D.: ASM Handbook. Casting; ASM International, 1998; Vol. 15.

[9] Aigner, R., Steinrück, H.: The Influence of Liquid Steel Level Fluctuations on the Formation of Oscillation Marks. In *Eurotherm 82*; A. Nowak, R. A. Bialecki: Gliwice-Cracow, Poland, 2005.

[10] Szekeres, E.: Overview of Mold Oscillation in Continuous Casting. Iron and Steel Engineer, 1996.

[11] Thomas, B. G.: *Continuous Casting, The Encyclopedia of Materials: Science and Technology*; Elsevier Science Ltd., Oxford: UK, 2001; Vol. 2. pp. 1595-1599.

[12] Mourão, B. M. *et al.*: *Introdução à Siderurgia*; Associação Brasileira de Metalurgia e Materiais: São Paulo, 2007.

[13] Pinheiro, C. A., Samarasekera, I. V., Brimacombe, J. K. Mold Flux for Continuous Casting of Steel, Part I. *Iron and Steelmaker* **1994**, 55-56.

[14] Pinheiro, C. A., Samarasekera, I. V., Brimacombe, J. K. Mold Flux for Continuous Casting of Steel, Part II. *Iron and Steelmaker* **1994**, 62.

[15] Pinheiro, C. A., Samarasekera, I. V., Brimacombe, J. K. Mold Flux for Continuous Casting of Steel, Part III. *Iron and Steelmaker* **1994**, 12-14.

[16] Pinheiro, C. A., Samarasekera, I. V., Brimacombe, J. K. Mold Flux for Continuous Casting of Steel, Part XIV. *Iron and Steelmaker* **1995**, 54-56.
[17] Pinheiro, C. A., Samarasekera, I. V., Brimacombe, J. K. Mold Flux for Continuous Casting of Steel, Part XV. *Iron and Steelmaker* **1995**, 43-44.
[18] Pinheiro, C. A., Samarasekera, I. V., Brimacombe, J. K. Mold Flux for Continuous Casting of Steel, Part VII. *Iron and Steelmaker* **1995**, 45-47.
[19] Pinheiro, C. A., Samarasekera, I. V., Brimacombe, J. K. Mold Flux for Continuous Casting of Steel, Part IV. *Iron and Steelmaker* **1995**, 43-44.
[20] Pinheiro, C. A., Samarasekera, I. V., Brimacombe, J. K. Mold Flux for Continuous Casting of Steel, Part VI. *Iron and Steelmaker* **1995**, 76-77.
[21] Pinheiro, C. A., Samarasekera, I. V., Brimacombe, J. K. Mold Flux for Continuous Casting of Steel, Part XI. *Iron and Steelmaker* **1995**, 41-43.
[22] Pinheiro, C. A., Samarasekera, I. V., Brimacombe, J. K. Mold Flux for Continuous Casting of Steel, Part IX. *Iron and Steelmaker* **1995**, 43-44.
[23] Pinheiro, C. A., Samarasekera, I. V., Brimacombe, J. K. Mold Flux for Continuous Casting of Steel - Part V. *Iron and Steelmaker* **1995**, 37-39.
[24] Pinheiro, C. A., Samarasekera, I. V., Brimacombe, J. K. Mold Flux for Continuous Casting of Steel, Part XVIII. *Iron and Steelmaker* **1996**, 85.
[25] Orrling, C. Crystallization Phenomena in Slags. Carnegie Mellon University, 2000.
[26] Mills, K.C.; Fox, A. B.; Li, Z.; Thackray, R. P. Performance and properties of mould fluxes. *Ironmaking and Steelmaking* **2005**, *32*, 26-34.
[27] Turkdogan, E.T.: *Physicochemical properties of molten slags and glasses*; The Metal Society: London, 1983. pp. 201-208.
[28] Mills, K. C. Structure and Properties of Slags Used in the Continuous Casting of Steel: Part 1 Conventional Mould Powders. *ISIJ Internacional* **2016**, *56*, 1-13.
[29] Mills, K. C., Fox, A. B. The Role of Mould Fluxes in Continuous Casting – So Simple Yet So Complex. *ISIJ International* **2003**, *43*, 1479-1486.
[30] Liu, H., Wen, G., Tang, P. Crystallization Behaviors of Mold Fluxes Containing Li_2O Using Single Hot Thermocouple Tecnhique. *ISIJ Internacional* **2009**, *49*, 843-850.
[31] Fox, A. B., Valdez, M. E., Gisby, J., Atwood, R. C., Lee, P. D., Sridhar, S. Dissolution of ZrO_2, Al_2O_3, MgO and $MgAl_2O_4$ Particles in a B_2O_3 Containing Commercial Fluoride-free Mould Slag. *ISIJ Internacional* **2004**, *44*, 836-845.
[32] Mills, K. C.: *Mould Powder for Continuous Casting*; Escola de Engenharia Industrial Metalúrgica de Volta Redonda - Centro Tecnológico, 1995.
[33] Mills, K. C.: *The Making, Shaping and Treating of Steel - Mould Powders for Continuous Casting (Chapter 8)*; The AISE Steel Foundation: Pittsburgh, 2003.
[34] Kromhout, J. A. Mould powders for high speed continuous casting of steel. Doctoral, Technische Universiteit Delft, 2011.
[35] Sengupta, J., Thomas, B. G., Shin, H-J., Lee, G-G., Kim, S-H. A New Mechanism of Hook Formation during Continuous Casting of Ulta-Low-Carbon Steel Slabs. *Metallurgical and Materials Transactions A* **2006**, *37A*, 1597-1611.
[36] Bezuidenhout, G. A. The effect of alumina pick-up on mould flux behavior in continuous casting. University of Pretoria, 1999.
[37] Araki, T., Ikeda, M. Optimization of Mold Oscillation for High Speed Casting - New Criteria for Mold Oscillation. *Canadian Metallurgical Quarterly* **1999**, *38*, 295-300.
[38] Shin, H, Choi, W., Kang, S., Park, J., Kim, S., Thomas, B. G.: Effect of Mold Oscillation on Powder Consumption and Hook Formation in Ultra Low Carbon Steel Slabs. In *AISTech*; Assoc. Iron Steel Technology, Warrendale, PA.: Nashville, TN, 2004.
[39] Meng, Y. Modeling Interfacial Slag Layer Phenomena in the Steel Shell/Mold Gap in Continuous Casting of Steel. University of Illinois at Urbana-Champaign, 2004.

CHAPTER 2 – LITERATURE REVIEW

2.1 Essentials on Structure of Silicate Melts, Glasses and Slags

Slags are present in most high temperature metallurgical processes upon which the metal is in a liquid state. These slags are submitted to a series of processes and atmospheric conditions which alters their characteristics and, as a consequence, their performance. Attempts to quantify the physical properties of silicate melts that affect such processes – diffusion, nucleation, crystal growth, convection or formation of immiscible liquids – requires at least an elementary understanding of the structure of these melts [1]. Silicates and/or other complex-forming components are the base of the most of slags applied in all metallurgical processes [2]; and their thermo-physical properties are strongly dependent upon their structure [3]. Since the structure of silicate melts provides a basis for understanding the relations between the structure and the physical, chemical, and thermal properties of the melts, the knowledge of the structure of silicates gains a relevant role in the understanding of behavior of the slags [4]. As will be seen later, the water solubility in silicate melts and glasses has been shown as a function of water partial pressure, chemical composition and basicity, which are directly related to the structure of melt.

Silicate slags are predominantly structured on Si cations surrounded by 4 oxygen anions forming a SiO_4^{4-} tetrahedron that constitutes a basic unit. Such tetrahedral units are joined together forming chains or rings by bridging oxygens (BO). Other oxides (*e.g.*, B_2O_3 and GeO_2) can easily build up a characteristic network structure similar to that formed by silica, *i.e.*, structures consisting of triangles or tetrahedral units. These oxides are classified as network formers. When a metal oxide (*e.g.* Na_2O and CaO) is added to silica melts, the oxygen bonds tend to be broken by cations such as Na^+, Ca^{2+}, Mg^{2+}, and Fe^{2+}, promoting the formation of non-bridging oxygen (NBO) atoms – as O^- and free oxygens O^{2-} – in the structure, in a process called depolymerization of silicate melt. These oxides are named network modifiers (or breakers). The NBO are bonded to both network modifier metal cations and tetrahedrally coordinated cations in the silicate network. Thus, metal cations act as linkage between various anionic structural units with tetrahedrally coordinated cations occurring in the melt [2,4-6]. **Figure 2.1** shows an illustrative scheme of the regular structure of crystalline silica, the irregular structure of glassy silica and the structure of sodium silicate glass. Some oxides behave as either network former or network modifier, depending upon the melt environment. Oxides such as TiO_2, Al_2O3 and Fe_2O_3 belong to this group and are named as amphoteric oxides. Cations of these oxides (*e.g.* Ti^{4+}, Al^{3+}, P^{5+} and Fe^{3+}) also form tetrahedral structures and can be incorporated into the silica network as TiO_4^{4-}, PO_4^{3-}, AlO_4^{5-} and FeO_4^{5-} [2,6]. However, these cations need to maintain its electrical charge balance, and this demands other cations for charge-balancing, *e.g.* if an Al^{3+} is incorporated into a Si^{4+} chain, it must have a Na^+ (or one half of a Ca^{2+}) sitting near the Al^{3+} to maintain local charge balance [3].

Silicate melts are constituted by a distribution of different polymeric silicate anions of different molecular weights, which are three-dimensionally interconnected units such as SiO_2, $Si_2O_5^{2-}$, $Si_2O_6^{4-}$, $Si_2O_7^{2-}$, and SiO_4^{4-} coexisting in the melt. The proportion of these structural

units is influenced by the nature of the cation in the silicate melt. The SiO_2 and SiO_4^{4-} units are stabilized by small cations with high valence, *e.g.* $Mg^{2+} > Ca^{2+} > Na^{+}$ [7]. There is a gradual breakdown of the silicate network with the addition of basic metal oxides to vitreous or molten silica, which can be represented by the **reaction 2.1** [8]

$$\cdots \equiv Si - O - Si \equiv \cdots + M_2O = \cdots \equiv Si - O^-(M^+) + (M^+)O^- - Si \equiv \cdots \quad (\mathbf{2.1})$$

where M and M^+ represent the metal of the oxide and the metal ion, respectively.

For the case of the disilicate composition represented in the **reaction 2.1**, the structure of the silicate melt would consist of infinite two-dimensional sheets represented by the $Si_{2n}O_{5n}^{2n-}$ structural formula. With the increment of the metal oxide content, the sheets breakdown to chains such that at the metasilicate composition the system would be formed of infinite chains of SiO_4 tetrahedra and /or a metasilicate ring structure; with further addition of the metal oxide, this dissociative process will take place until the system consist of discrete SiO_4^{4-} anions at the orthosilicate composition [8]. The silicate polymers are dissociate according to the following pattern: $Si_6O_{18}^{12-} \rightarrow Si_4O_{12}^{8-} \rightarrow Si_3O_9^{6-} \rightarrow Si_2O_7^{6-} \rightarrow SiO_4^{4-}$. This explains why in industrial slag there are no isolated SiO_2 molecules [7,9].

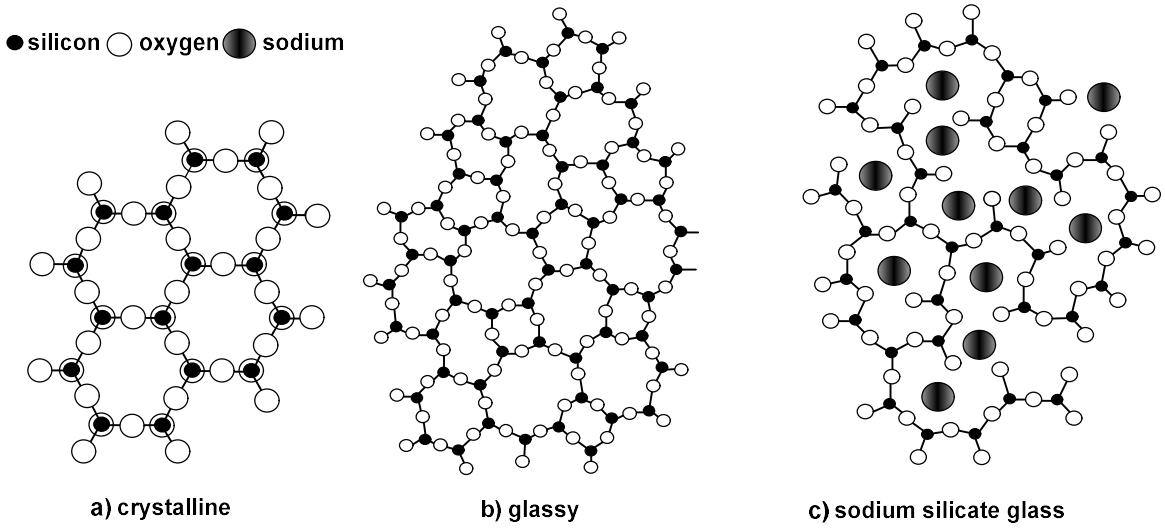

Figure 2.1 Schematic representation of 2-dimensional structures of (a) crystalline silica state; (b) glassy silica state and; (c) sodium silicate glassy state. Illustration adapted from [2,5,8].

Some studies point to changes of the structure of glasses and melts with temperature. Data obtained by Majérus *et al.* [10] from *in situ* neutron diffraction measurements showed structural changes in potassium dissilicate glasses and melts as a function of temperature. The polymerized parts of the network are stretched and relaxed with increasing temperature. Other structural change observed was the narrowing of the Si-O-Si bond angle distribution and the increase of the proportion of small rings in the melt compared to the glass. In alkali silicate melts such as $Na_2Si_2O_5$, the glass network can be described by reactions of the type $2Q^3 = Q^2 + Q^4$ (see **Section 2.1.1.1**, **equation 2.5**). Studies performed using NMR (nuclear magnetic resonance) spectroscopy on glasses prepared at different cooling rates point to that the early referred reaction tends to move to right side at high temperatures [11].

2.1.1 Degree of Polymerization of Silicate Melts and Slags

The structure of the silicate slags is defined by factors as its degree of polymerization, the nature of the constituent cations (network or network-breaking) and the physical state of the slag – liquid, glass or crystalline phase. The influence of the degree of polymerization has different extent on the properties of the slag; so that a hierarchy of dependence of the polymerization on the slag properties can be established, as follow: viscosity > electrical resistivity ≈ diffusivity > thermal conductivity (k) > thermal expansion coefficient > density (ρ) > heat capacity (C_p) [3]. Experimental techniques have been used to determine the structural aspects of the melts and glasses as X-ray, Raman Spectroscopy and Fourier Transformed Infrared Spectroscopy (FTIR) [2,8]. Usually, the degree of polymerization of a melt has been represented by using some parameters as NBO/T ratio and optical basicity (Λ).

2.1.1.1 NBO/T Ratio

The NBO/T is a structural parameter which indicates the degree of depolymerisation of silicate melts, where NBO is the number of non-bridging oxygen atoms, while T (usually Si for silicate melts) represents the number of tetrahedrally-coordinated atoms. The tetrahedral cation besides Si^{4+} can be Ti^{4+}, P^{5+}, Al^{3+}, and Fe^{3+} [12]. The formation of these non-bridging oxygen atoms occur with the addition of metal oxide to silica melts. Once these oxygens are boned to both network-modifying metal cations and tetrahedrally coordinated cations in the silica network, the metal cations works as linkage between the various anionic structural units and the tetrahedrally coordinated cations [4]. A variety of properties of the silicate melts such as viscosity, thermal conductivity and so on are dependent of its structure [2,13,14]. Furthermore, rate and equilibrium reactions are directly related to degree of depolymerization of the melt. For instance, a study carried out by Brooker *et al*. [15] correlates NBO/T ratio to the solubility of CO_2 in slags, showing strong influence of the structure on the solubility capacity of the slag. The NBO/T can be estimated by following the **equations** (**2.2**)**,** (**2.3**) and (**2.4**)**. Figure 2.2** shows an illustrative representation of the concept of the bridging and non-bridging oxygen in the structure of the silicate

$$Y_{NB} = \sum 2\,[X_{CaO} + X_{MgO} + X_{FeO} + X_{MgO} + X_{CaO} + X_{MnO} + X_{Na_2O} + X_{K_2O} + 3fX_{Fe_2O_3} - 2(1-f)X_{Fe_2O_3}] \quad (\mathbf{2.2})$$

$$X_T = \sum X_{SiO_2} + 2X_{Al_2O_3} + 2fX_{Fe_2O_3} + X_{TiO_2} \quad (\mathbf{2.3})$$

$$(NBO/T) = Y_{NB}/X_T \quad (\mathbf{2.4})$$

where X represents the molar fraction of the slag constituents CaO, Al_2O_3, SiO_2 etc., f is the fraction of Fe^{3+} in (IV) coordination (which is zero for the most of the steel slags), Y_{NB} is the total charge on the network breaking cations and X_T is the sum of the molar fraction of the network formers.

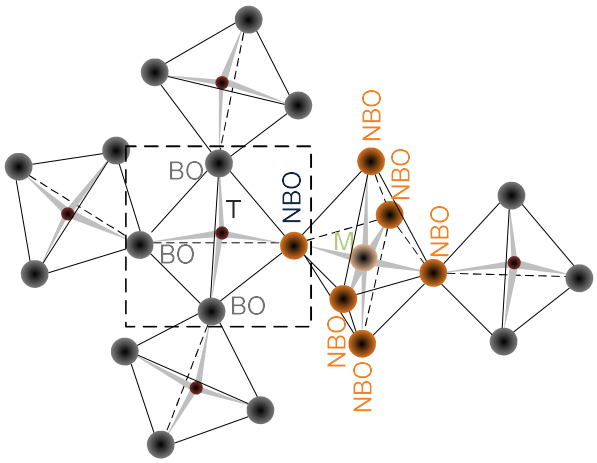

Figure 2.2 Structural representation of the concept of bridging (BO) and non-bridging (NBO) oxygen. Figure adapted from [16].

Another way to represent the structure of slags is the *Q*-notation (defined by **equation (2.5)**) or stucton term. Such structure representation, Q^n (where n can be 0, 1, 2, 3 or 4) is defined as single atom (ion or molecule) surrounded by others in a specific manner. The anionic structure of metal oxide-silica melts may be described in terms of individual anionic structural units such as monomers (NBO/Si = 4), dimmers (NBO/Si = 3), chains (NBO/Si = 2), sheets (NBO/Si = 1) and three-dimensional network units (NBO/Si = 0) (see **Figure 2.3**) [4].

$$Q = 4 - NBO/T \tag{2.5}$$

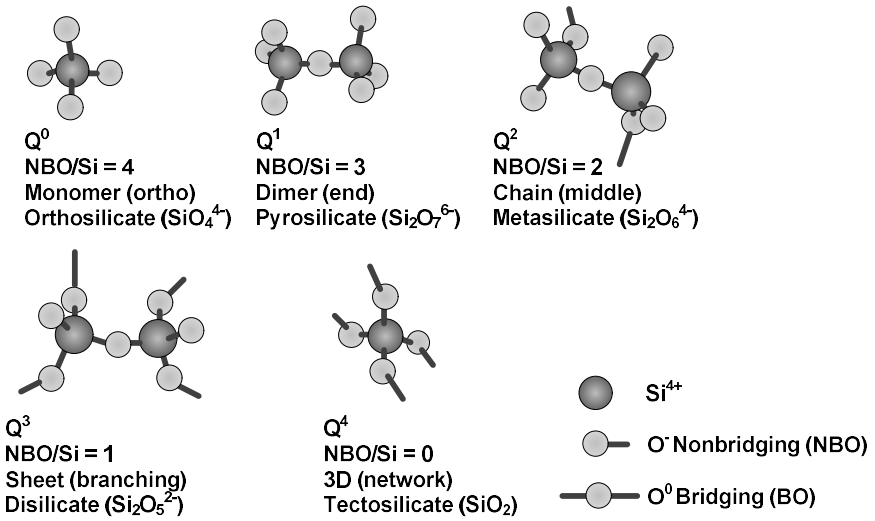

Figure 2.3 Models of silicate melts structural units whit their respective Q-notation and NBO/Si ratios. Illustration adapted from [7].

The structure of melts containing low silica contents are dominated by SiO_4 monomers. With increasing SiO_2 content, these silicate species polymerize forming larger branch and ring structures [1]. Mysen *et al*. [17] proposed equilibrium reactions relating the coexisting anionic units in silicate melts according to its degree of polymerization (reactions (**2.6**), (**2.7**) and (**2.8**)):

$$For\ 4 > \frac{NBO}{Si} > 2:\quad 2Si_2O_7^{6-}(dimer) \rightleftarrows\ 2SiO_4^{4-}\ (monomer) +\ Si_2O_6^{4-}\ (chain) \qquad (\mathbf{2.6})$$

$$For\ 2 > \frac{NBO}{Si} > 1:\quad 3Si_2O_6^{4-}\ (chain) \rightleftarrows 2Si_2O_5^{2-}\ (sheet) +\ 2SiO_4^{4-}\ (monomer) \qquad (\mathbf{2.7})$$

$$For\ 1 > \frac{NBO}{Si} > 0.1:\ 2Si_2O_5^{2-}\ (sheet) \rightleftarrows Si_2O_6^{4-}\ (chain) +\ 2SiO_2\ (3D) \qquad (\mathbf{2.8})$$

Mysen *et al.* [17] reported that the same expressions hold true regardless of the type of network-modifying cation.

The NBO/T can also provide an indicative of the crystallization tendency of slags. Correlation between NBO/T and crystallization tendency of mold fluxes have been suggested as a way to predict the % crystallinity in slag films [18]. The authors recommended the follow equation to calculate the % crystallinity of mold fluxes:

$$\%\ crystallinity = 141.1\left(\frac{NBO}{T}\right) -\ 284.0 \qquad (\mathbf{2.9})$$

where % crystallinity is given in % mole. Such equation is restricted to NBO/T > 2. Below this values, the slag is considered completely glassy (very low % crystallinity); characterizing the NBO/T = 2 as a critical point.

2.1.1.2 Basicity Indices

As the NBO/T and *Q*-notation, the basicity is also a parameter used to represent the structure of the slag [18,19]. Slag-metal reactions are dependent upon the activity of the slag and metal components. However, there is scarcity of activity data of multicomponent slags. In polymeric melts, the component activity is directly related to changes in the silicate network. Changes in the polymerization degree of the melt are attributed to the kind and co-existent cations and temperature, being the degree of polymerization of a slag directly influenced by the alkali oxide activity [8,20,21]. Qualitatively, the basicity is defined as the concentration ratio between network modifiers oxides and network former oxides, giving us a sense of slag structure, which works as a simple indicator of the trend in changes of oxide activities with composition [8]. The basicity of slags and melts can be defined in different ways. The simplest index of the basicity is the concentrate ratio of network modifier CaO to network modifier SiO_2 – known as the *V* ratio (= %CaO/%SiO_2) – which has been widely used by steelmakers. One problem related to *V* ratio is the fact that it does not take account the effect of other oxides as MgO, Al_2O_3, FeO etc. which are constantly present in metallurgical slags. Another important problem lies on the arbitrary decision if a slag component, mainly for amphoteric oxides, is either network modifier or network former. Furthermore, it is impossible of assign a basicity value to slags, in basicity ratio, that contain no recognized acid component [2,8,22,23]. Due to these issues, many others basicity indices have been proposed considering the effect of a more extensive oxide range. A variety of basicity index examples are summarized in the Slag Atlas (pg. 10, **Table 2.1**) [2] and in [24,25]. On the other hand, the optical basicity can provides a reasonable measurement of the polymerization of the melt.

Optical basicity is an entirely physic based concept which allows to characterize fluxes according to their compositions relating slag basicity to the state or relative freeness of the

oxygen ions in the slag. The values of optical basicity for various oxides (Λ_i) can be calculated from Pauling electronagativities (**Table 2.1**). For slags, the values of optical basicity can be derived using the **equation 2.10**, where *n* represents the number of oxygen atoms in the molecule [2,26].

$$\Lambda = \frac{\sum_i (x_i n_i \Lambda_i)}{\sum_i (x_i n_i)} \qquad (\mathbf{2.10})$$

where x_i, n_i and Λ_i represent molar fraction, the number of oxygen atoms in the molecule and the optical basicity of the oxides, respectively.

Table 2.1 Optical basicity calculated values of some oxides [2].

Oxide	Calculated values of Λ_i	
	Pauling eletronegativity	Electron density
Li_2O	1.0	1.06
Na_2O	1.15	1.11
MgO	0.78	0.92
TiO_2	0.61	0.65
Al_2O_3	0.60	0.66
SiO_2	0.48	0.47
CaO	1.0	1.0
B_2O_3	0.42	0.42
P_2O_5	0.40	0.48
Fe_2O_3	0.48	0.72

Mills [14] point to that the use of the optical basicity provide a reasonable measure of the depolymerization of the alumino-silicate slags when corrected for the cations required to charge-balance of any AlO_4^{5-} tetrahedra present. The author suggest that, although the NBO/T is superior polymerization parameter than the Λ, the last has advantages that it is applicable to non-silicate melts.

References

[1] Hess, P. C. Polymer model of silicate melts. *Geochimica et Cosmochimica Acta* **1971**, *35*, 289-306.

[2] Mills, K. C.: *Slag Atlas*; 2nd Edition ed.; Verlag Stahleisen GmbH Düsseldorf, 1995.

[3] Mills, K. C. Structure and Properties of Slags Used in the Continuous Casting of Steel: Part 1 Conventional Mould Powders. *ISIJ Internacional* **2016**, *56*, 1-13.

[4] Mysen, B. O. The structure of silicate melts. *Ann. Rev. Earth Planet Sci.* **1983**, 75-97.

[5] Callister, JR., W. D.: *Material Science and Engineering: An Introduction 7th ed.*, 2007.

[6] Waseda, Y., Toguri, J. M.: *The Structure and Properties of Oxide Melts*; World Scientific Publishing Co. Pte. Ltd., 1998.

[7] Mohassab, Y., Sohn, H. Y. Analysis of Slag Chemistry by FTIR-RAS and Raman Spectroscopy: Effect of Water Vapor Content in H_2-H_2O-CO-CO_2 Mixtures Relevant to a Novel Geen Ironmaking Technology. *Steel Research International* **2014**, *85*.

[8] Turkdogan, E.T.: *Physicochemical properties of molten slags and glasses*; The Metal Society: London, 1983. pp. 201-208.

[9] ŽIvković, Ž., Mitevska, N., Mihajlović, I., Nikolić, D. The influence of the silicate slag composition on copper losses during smelting of the sulfide concentrates. *Journal of Mining and Metallurgy* **2009**, *45*, 23-34.

[10] Majérus, O., Cornier, L., Calas, G., Beuneu, B. A neutron diffraction study of temperature-induced structural changes in postassium disilicate glass and melt. *Chemical Geology* **2004**, *213*, 89-102.
[11] Stebbins, J. F., McMillan, P. F., Dingwell, D. B.: *Structure, Dynamics, and Properties of Silicate Melts*; Mineralogical Society of America, 1995; Vol. Vol. 32.
[12] Mysen, B. O., Virgo, D., Harrison, W. J., Scarfe, M. Solubility mechanisms of H_2O in silicate melts at high pressures and temperatures: a Raman spectroscopic study. *American Mineralogist* **1980**, *65*, 900-914.
[13] Hasegawa, H., Kowatari, T., Shiroki, Y., Shibata, H., Otha, H., Waseda, Y. Thermal Conductivity of Molten Silicate of Al_2O_3-CaO-Na_2O-SiO_2 Measured by Means of a Front Heating-Front Detection Laser Flash Method. *Metallurgical and Materials Transactions B* **2012**, *43B*, 1413-1419.
[14] Mills, K. C. The Influence of Structure on the Physico-chemical Properties of Slags. *ISIJ Internacional* **1993**, *33*, 148-155.
[15] Brooker, R. A., Kohn, S. C., Holloway, J. R., McMillian, P. F. Structural controls on the solubility of CO_2 in silicate melts Part I: bulk solubility data. *Chemical Geology* **2001**, *174*, 225-239.
[16] Mysen, B. O. Water-melt interaction in hydrous magmatic systems at high temperature an pressure. *Progress in Earth and Planetary Science* **2014**, *1:4*.
[17] Mysen, B. O., Virgo, D., Scarfe, C. M. Relations between the anionic structure and viscosity of silicate melts - a Raman spectroscopic study. *American Mineralogist* **1980**, *65*, 690-710.
[18] Li, Z., Thackray, R., Mills, K. C.: A test to determine crystallinity of mould fluxes. In *VII International Conference on Molten Slags, Fluxes and Salts* The South African Institute of Mining and Metallurgy: South Africa, 2004; pp 813-819.
[19] Mills, K. C., Yuan, L., Jones, R. T. Estimating the physical properties of slags. *The Journal of the Southern African Institute of Mining and Metallurgy* **2011**, *111*, 649-658.
[20] Ban-Ya, S., Hino, M., Nagasaka, T. Estimation of Water Solubility in Molten Silicates by Quadratic Formalism Based on the Regular Solution Model. *ISIJ Internacional* **1993**, *33*, 12-19.
[21] Mueller, M., Willenborg, W., Hilpert, K., Singheiser, L.: Structural dependence of alkali activity in coal ash slags. In *Conference on Molten Slags, Fluxes and Salts - MOLTEN*; The South African Institute of Mining and Metallurgy: South African, 2004; pp 615-618.
[22] Daya, Z. A. The Thermodynamics of Water Vapour Dissolution in Tundish Fluxes. University of Toronto, 1997.
[23] Elahipanah, Z. Therno-Physical Properties of Mould Fluxes Slags for Continuous Casting of Steel. Royal Institute of Technology, 2012.
[24] Mohassab, Y., Sohn, H. Y. The Effect of Water Vapor on O_2- Content in Ironmaking Slag. *Journal of Iron and Steel Research International* **2015**, *22*, 909-915.
[25] Sommerville, I. D.: The Capacities and Refining Capabilities of Metallurgical Salgs. In *Foudry Process: Their chemistry and physics*; Landefeld, S. K. C. F., Ed.; Plenum Press: New York, 1988; pp 101-119.
[26] Schulz, T., Janke, D., Heller, H. P., Lychatz, B. Entwicklung umweltfreundlicher Stranggießschlacken (german). *Stahl und Eisen* **2008**, *128*, 65-78.

2.2 GENERAL THEORY OF CRYSTALLIZATION

2.2.1 The Glass Transition

Glasses and slags exhibit similar characteristics due to the proximity of their chemical composition, which are classified as polymeric melts. Glasses are defined as non-crystalline solids that undergo a glass transition in the course of their preparation [1]. According to Shelby [2], any material inorganic, organic or metallic, which exhibits glass transformation behavior can be considered a glass. For homogeneous, amorphous or glass materials, the most striking feature of the glass transition is the abrupt change in physicochemical properties of a liquid, such as the thermal expansion coefficient (α) and heat capacity (c_p), as it is cooled through the range of temperature where its viscosity (η) approaches to a range between 10^{13}- 10^{12} Pa.s ≈ $\eta(T_g)$, where T_g is the glass transition temperature [1,3]. For most inorganic liquids, the viscosity at T_g corresponds to a structural relaxation time in the region of 100 s [4].

Figure 2.4 shows the variation of the first-order thermodynamic properties (energy, enthalpy or specific volume) as a function of temperature. When a liquid is cooled at slow cooling rates (**Fig 2.4**, path a), it may crystallize at the melting point, T_m. When to liquid is cooled at high cooling rates, fast enough to avoid crystal nucleation and growth, a supercooled liquid would be produced (**Fig 2.4**, path b) [3].

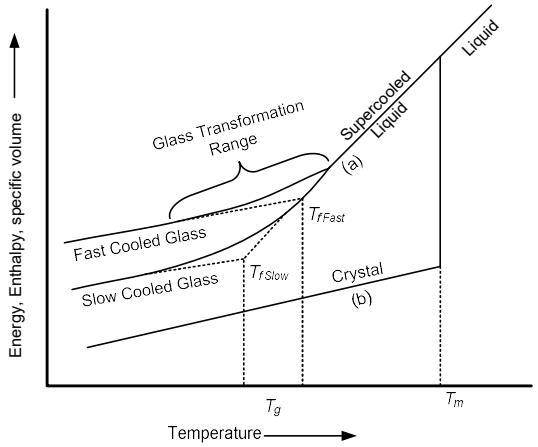

Figure 2.4 Effect of temperature on the thermodynamic properties energy, enthalpy or specific volume where of a glass forming (a) glass transition and (b) crystallization of a liquid; where T_m, T_f and T_g denote the melting point, fictive temperature and glass transition temperature, respectively. Figure adapted from [2-4].

In a general way, as a molten material is cooled, the atomic structure of the melt will gradually change and will be characteristic of the exact temperature at which the melt is held; in other words, the atomic structure of the glass is representative of its parent liquid, frozen in time and characteristic of the temperature at which the liquid was thermally equilibrated for the last time. The referred temperature is named as fictive temperature (T_f) and depends on the cooling rate of the liquid. Faster cooling rates will give higher fictive temperatures and vice-versa. Cooling the melt to any temperature below the melting point (T_m) of the crystal, would normally result in the conversion of the material to the crystalline state. However, under determined conditions, the spontaneous nucleation and crystallization can be delayed forming a metastable supercooled liquid. This metastable condition lies in a temperature range between melting temperature and fictive

temperature. The reordering of the liquid structure advances as the temperature decreases. Nevertheless, as the liquid is cooled further, the viscosity became so high that large-scale atomic rearrangements of the system are no longer possible and the structure became fixed, *i.e.*, the structural rearrangements required to the liquid keeps itself in the appropriate metastable equilibrium state cannot follow any more the change of temperature. The temperature lying between the limits where the thermodynamic property (enthalpy, volume etc.) is that of the equilibrium liquid and that the frozen solid is called the glass transformation region, and the liquid is now a glass [1,3-5].

The formed glasses are very stable at room temperatures because their high viscosity inhibits structural rearrangements required for nucleation and crystal growth occur. However, when a glass is held for a sufficiently long period of time at high temperatures within or above the glass transition region – where its crystallization potential is significant – the glass tends to reaches the stable crystalline condition. This process, known as devitrification of glass, readily starts via heterogeneous or homogeneous nucleation [1,6]. The variation of the thermodynamic properties across the glass transition depends on the cooling (or heating) rate of the liquid. Therefore, the occurrence of nucleation and crystal growth, as the transition from liquid to glass or glass to liquid, is essentially a kinetic phenomenon [4].

2.2.2 Kinetics of Phase Transformation

2.2.2.1 Nucleation Theory

The crystallization phenomenon could be considered as a process which occurs into two steps, in which the phase separation or appearing of new crystals – known as nucleation process – and their growth to larger sizes – known as crystal growth. Nucleation is the start of crystallization process and involves the birth of a new crystal, characterized by appearing of small regions with atoms (in the case of metals) or molecules (for other materials) ordered in a periodic array. Crystal growth occurs when the nuclei have been formed in a supersaturated or supercooled system became stable, beginning to growth into crystals of visible size [5,7-9]. When a liquid is cooled below its melting point, the crystal nucleation may be either homogeneous (in the volume), *i.e.*, forming spontaneously within the melt, or heterogeneous, *i.e.*, forming at a pre-existing surface, such as that due to an impurity, crucible wall etc. If no nuclei are present, crystal growth cannot occur and the material will form a glass [3,5]. The thermodynamic considerations for homogeneous nucleation were developed by Gibbs (1928), Volmer (1939), Tunrbull and Fischer (1949), Nielsen (1964) and others. It is based on the thermodynamics description of heterogeneous systems developed by Gibbs, in which a real inhomogeneous system is replaced by a model system consisting of two homogeneous phases. Classical nucleation theory (CNT) has been applied extensively to predict the nucleation rates of different materials [8,10]. It assumes that clusters are formed in solution by an addition mechanism that continues until a critical size is reached. According to the CNT, nucleation is controlled by the competition between the free energy gain due to the liquid-crystal transformation and the free energy loss associated with the formation of the liquid-crystal interface. The description of homogeneous and heterogeneous nucleation can be basically performed by the same methods. This theory considers a initial state, which is a homogeneous disordered liquid and a final order crystal phases as the only key players of nucleation [1,11].

There are two barriers to the formation of a nucleus: a thermodynamic barrier – which involves the free energy change in a system when a nucleus is formed; and a kinetic barrier – which is the result of the requirement that mass be moved or rearranged in space to allow the growth of an ordered particle (crystal) from a disordered liquid [5]. Assuming homogeneous nucleation, the total free-energy cost to form a spherical particle with radius r is given be **Equation** (**2.11**).

$$\Delta G = \frac{4}{3}\pi r^3 \Delta G_v + 4\pi r^2 \gamma \quad (\mathbf{2.11})$$

where the first term is the free energy difference between the solid and liquid phases, or the volume free energy, ΔG_v. Its value will be negative if the temperature is below the equilibrium solidification temperature [5,12,13]. The value of the surface free energy, γ, is always positive whereas ΔG depends upon the temperature below the melting point, ΔT. ΔG is a negative value if ΔT is positive. This behavior leads to occurrence of a maximum in the value of ΔG when the melt is undercooled. This maximum can be regarded as being the activation energy which has to be overcome in order to form a crystal nucleus, which will continue to grow [14]. Taking the derivate of ΔG with respect to r and setting it equal to zero, it is possible to determine the critical radius, r^*, *i.e.*, the nucleus radius above which the clusters growth will continue with a concomitant decrease in free energy. If the nuclei are small, the surface energy term will dominate at very low values of r, ΔG will increase with increasing r, and nucleus will be unstable, shrink and redissolve into the melt [5,12]. Thus, the critical radius is obtained from the maximum of the total energy (**Equation 2.12**).

$$r^* = -2\gamma/\Delta G_V \quad (\mathbf{2.12})$$

Substituting the expression for r^* into **Eq**. **2.11**, gives

$$W^* = 16\pi\gamma^3/3\Delta G_v^2 \quad (\mathbf{2.13})$$

The rate of nucleus formation by the addition mechanism for the overall process is described by an Arrhenius type expression

$$I = A\, exp[-(W^* + \Delta G_D)/kT] \quad (\mathbf{2.14})$$

where A is a constant, W^* and ΔG_D are the thermodynamic and kinetic free energy barriers to nucleation, respectively, k is the Boltzmann's constant, and T is the absolute temperature (K). The thermodynamic barrier to nucleation, W^*, is actually the work required to form a nucleus of critical size, *i.e.*, one which will grow instead of redissolve into de melt. The free energy change for the formation of the nucleus surface (a positive quantity) and the free energy change for phase transformation is a negative quantity for undercooled melt. The formation of a nucleus promotes a change in the thermodynamic barriers of the system. The volume free energy is lowered by the formation of a crystalline arrangement due to the lower free energy of the crystalline state compared to that of the melt. This decrease in free energy is countered by an increase in surface energy due to the formation of a new interface between regions of different structures.

Determination of the ΔG_D is subject to some controversy. Assuming that the molecular re-arrangement for the nucleation process can be described by an effective diffusion coefficient, D, expressed by

$$D = \nu\lambda^2 exp(-\Delta G_D/kT) \quad \textbf{(2.15)}$$

where λ is the jump distance of the order of atomic dimensions. The effective diffusion coefficient can be related to the viscosity (η) by means of the Stokes-Einstein equation:

$$D = kT/3\pi\lambda\eta \quad \textbf{(2.16)}$$

Combining the **Equations 2.15**, **2.16** and **2.11** gives

$$I = \left(\frac{Ah}{3\pi\lambda^3\eta}\right) exp\left[-\left(\frac{W^*}{kT}\right)\right] \quad \textbf{(2.17)}$$

The pre-exponential factor A is a constant over the temperature range of nucleation measurement. It depends only weakly on temperature, where A is typically $10^{41} – 10^{42}$ $m^{-3}s^{-1}$ for different condensate systems [1,3,5]. A good approximation this factor can be obtained by the following expression

$$A = n_v(kT/h) \quad \textbf{(2.18)}$$

where n_v is the number of molecules or formula units of nucleation phase per unit volume of parent phase (typically $10^{28}10^{29}$ m^{-3}) and h is the Planck's constant. Replacing the exponential factor A by **Eq. 2.18**, the homogeneous nucleation rate I in condensed systems can be writing as

$$I = (n_v kT/3\pi\lambda^3\eta)\exp(-W^*/kT) \quad \textbf{(2.19)}$$

A foreign solid substance and phase boundaries present in a supersaturated solution are generally known reduce the energy required for nucleation. For the heterogeneous nucleation, the formation of a nuclei on preexisting surfaces or interfaces reduces the interfacial energy term (γ) and, consequently, the activation energy barrier for nucleation (W^*) is lower than in the case of homogeneous nucleation. Volmer (1939) found that the decrease in free energy depended on the contact (or wetting) angle of the solid phase. Considering a cluster as a spherical cap forming from a liquid phase on a solid flat surface with a contact angle θ. Assuming that both the liquid and the solid phases wet this flat surface, the contact angle is obtained taking a surface tension force balance, assuming that the interfacial tensions solid-surface (γ_{IL}), solid-liquid (γ_{SI}), and liquid-surface (γ_{SL}) are in static equilibrium between the three phases [1,7,12,13]. An illustrative scheme of the tension forces acting in a heterogeneous nucleation is shown in the **Figure 2.5**. The surface tension balance is represented by the follow expression

$$\gamma_{IL} = \gamma_{SI} + \gamma_{SL}cos\theta \quad \textbf{(2.20)}$$

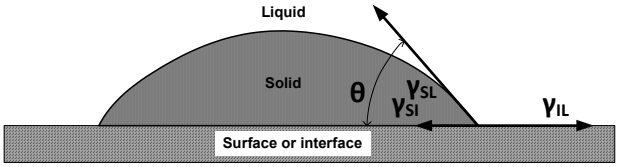

Figure 2.5 Heterogeneous nucleation of a solid from a liquid on a flat solid surface. The vectors represent the interfacial energies and the wetting angle is represented by θ. Figure adapted from [12].

The same mathematical procedures developed for homogeneous nucleation can be applied to heterogeneous nucleation. In this case, an equation similar to **Eq. 2.14** for heterogeneous nucleation can be writing as

$$I = A_{het} exp\left[-\left(\frac{\Delta G_D + W^*_{het}}{kT}\right)\right] \quad (\mathbf{2.21})$$

where the subscript *het* is referent to heterogeneous nucleation values. The decrease in free energy is related to wetting angle of the solid phase, or better saying, W^*_{het} is a function of θ, as following

$$W^*_{het} = W^*.\emptyset \quad (\mathbf{2.22})$$

$$\emptyset = \frac{1}{4}(2 + cos\theta)(1 - cos\theta) \quad (\mathbf{2.23})$$

The parameter $\emptyset$ varies from zero to unity, depending on the value of the θ between the crystal nucleus and the substrate. Its value depends on the mechanism of nucleation catalysis [1,5,7,12]. Following the expression for homogeneous nucleation exponential factor A_{het} can be expressed as

$$A_{het} = n_S(kT/h) \quad (\mathbf{2.24})$$

where n_S is the number of formula units of the melt in contact with the substrate per unit area. Thus, the expression for steady-state rate for heterogeneous nucleation can be written as

$$I_{het} = n_S(kT/h)exp[-(W^*_{het} + \Delta G_D/kT)] \quad (\mathbf{2.25})$$

According to energy considerations, occurrence of spontaneous nucleation is possible for a system where there is no contact angle; however, no such systems exist in practice. Partial attraction would occur if the foreign substance and the crystal have almost identical atomic arrangement. These foreign substance, or catalyzing surfaces, may be represented, for instance, by dispersed solid particles that act as nucleation sites. In this case, their curvature and number may strongly affect the nucleation kinetics [1,7]. If the viscosity of the melt is low, there will be a little kinetic obstruction to nucleus formation, and the nucleation rate will increase rapidly with decreasing temperature as ΔG_V increases. It is important take account that viscosity is highly temperature-dependent, so that the kinetic barrier to nucleation will also increase rapidly with decreasing temperature [5].

2.2.2.2 Crystal Growth

The degree of undercooling of the melt has influence on the rate of the crystal growth. Studies performed by Tammann (1898) exhibited an increase of rate of crystal growth with increasing undercooling, being zero at the liquidus, increasing to a maximum, then decrease with further increase in undercooling. For instance, considering a time-temperature-transformation diagram construction, as the temperature at which a determined degree of transformation take place decreases, the time required for such transformation became shorter, until reaches a minimum (**Figure 2.6**). This point is called as nose and indicates the isothermal temperature were the higher crystal growth rate is obtained. Upon further lowering of the supercooling temperature, the time for the transformation increases again depends upon other factors, primarily, upon the rigidity of the phases involved with respect to the movements of the constituent particles [15]. Clearly, the rigidity is referred to the viscosity of the solution or melt which, in turn, has influence on the diffusivity of the crystal forming component. The growth rate will increase with increasing undercooling, but will decrease with increase of viscosity [16].

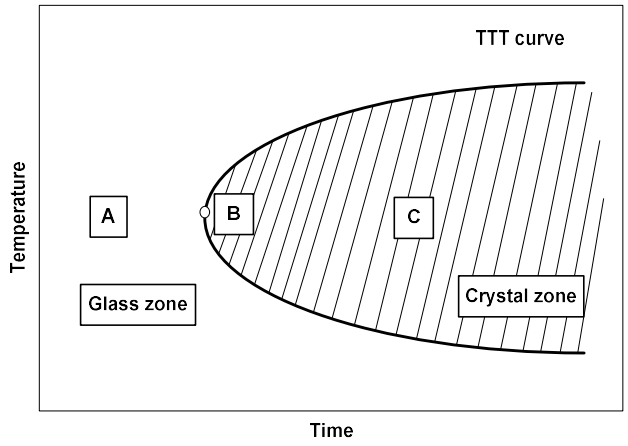

Figure 2.6 Typical TTT curve: (A) represents the zone of glass formation, (B) represents the start of crystallization at the nose and (C) represents the zone of occurrence of crystallization.

The crystal growth is controlled, primarily, by three rate processes, namely: thermal diffusion (flow of latent heat away from the growing crystal), mass diffusion (either long- or short-range) or crystal/melt interface reaction. The relative importance of each rate processes depends upon the substance and upon the solidification conditions. The viscosity of the silicate melt is higher than that of metal. On this wise, the mass diffusion process in polymeric melts is much slower than thermal diffusion. In this case, the thermal diffusion is less effective on controlling of crystal growth, especially in multicomponent systems in which are susceptible to marked composition changes at the crystal/melt interface. [14,16].

The existence of composition gradients and associated diffusion near the crystal-melt interface (short-range diffusion) can affect growth by causing the crystal to break up into a cellular morphology. The growth rate is controlled by a steady-state rate of mass transfer through a diffusion boundary layer near the crystal/melt interface. In this case, the linear growth rate is independent of time. If flow of latent heat away from the crystal-melt interface is the rate-controlling process, the interface generally has a cellular morphology. As with a

diffusion-induced instability the rate is generally independent of time [17]. If the reaction at the crystal-melt interface is the slowest step in the growth process, *i.e.*, when the crystallization is controlled by an interfacial reaction between the crystal and melt in a homogeneous melt, the growth rate is independent of position and, therefore, independent of time [16,17]. The general theory for the rate of interface-controlled growth, developed by Volmer and Mader (1931) and Turnbull and Cohen (1960), is based on the absolute reaction rate and invoking by the Stokes-Einstein relation (**Eq. 2.16)**. According to reaction-rate theory, when an atom or molecular group moves from melt to crystal, it must leave its energy state in the melt, pass through an activated state, and then into the crystalline state [16,17]. The mechanism of growth may be defined as the manner in which atoms or molecules groups attach to the growing crystal surface. Jackson *et al*. [18] suggested that there are two broad categories of mechanism: lateral growth and continuous growth.

Usually, a large distribution of crystal sizes occurs as result of continuous nucleation and crystal growth, *i.e.* the first nucleated crystal has the largest size and so forth [1]. Avrami [15] suggest that there is an impingement of grain upon another as a result of grain growth from center begins at different times; this implies in the interruption of growth of that grains which nucleated later (as represented in **Figure 2.7**).

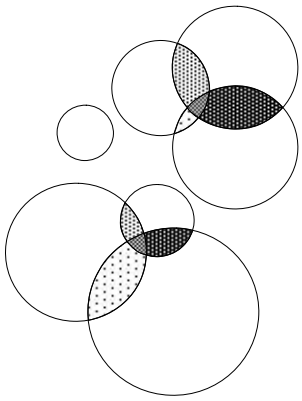

Figure 2.7 Schematic representation of the impingement of grains of a crystal aggregate [15].

According to Avrami [15] the nucleation of a new phase occurs from tiny germ nuclei, or ultra-nuclei, which already exist in the parent phase. The effective number of germ nuclei can be altered by temperature and duration of superheating. Considering the overall crystallization of a liquid, *i.e.*, the combination of nucleation and growth, the kinetic of this process is usually described by Avrami equation (as described later). It is assumed that (i) nucleation occurs randomly, *i.e.* the probability of forming a nucleus in unit time is the same for all infinitesimal volume elements of the assembly, and homogeneously; (ii) nucleation occurs from a certain number of embryos, which are gradually exhausted. The quantity of embryos decreases in two ways: by growing to critical size (becoming critical nuclei) and by absorption by the growing phase; (iii) the growth rate is constant until the growing regions impinge on each other and growth ceases [1,3,15].

The equation proposed by Avrami is derived based on the conditions aforementioned [15,19,20]. The volume fraction of the new phase for a three-dimensional nucleation and growth is given by following general relation

$$\alpha' = 1 - exp(-Kt^n) \quad (\mathbf{2.26})$$

where α' is the volume fraction of new phase; t is time; n depends on both nucleation and growth mechanisms; and the coefficient K includes the nucleation and growth rates. The **Eq. (2.16)** is, in general, applied in the form

$$\ln(-\ln(1-\alpha')) = \ln K + n \ln t \quad (\mathbf{2.27})$$

The values of coefficients K and n can be estimated by fitting the experimental data of α' to **Eq. (2.27)**. The knowledge of the Avrami coefficient n is helpful to understand the mechanism of phase transformation at isothermal condition [1]. A more detailed development of mathematical of the kinetic of the phase transformation can be found in the references used in the present section.

References

[1] Fokin, V. M., Zanotto, E. D., Yuritsyn, N. S., Schmelzer, J. W. P. Homogeneous crystal nucleation in silicate glasses: A 40 years perspective. *Journal of Non-Crystalline Solids* **2006**, *352*, 2681-2714.

[2] Shelby, J. E.: *Handbook of Gas Diffusion in Solids and Melts*; ASM International: Ohio, USA, 1996.

[3] Zanotto, E. D. Crystallization of Liquids and Glasses. *Brazilian Journal of Physics* **1992**, *22*, 77-84.

[4] Greaves, G. N., Sen, S. Inorganic glasses, glass-forming liquids and amorphizing solids. *Advances in Physics* **2007**, *56*, 1-166.

[5] Shelby, J. E.: *Introduction to Glass Science and Technology*; Second ed.; The Royal Society of Chemistry: Cambridge, 2005.

[6] Bowen, N. L. Devitrification of Glass. *Journal of American Ceramic Society* **1919**, *2*, 261-281.

[7] Myerson, A. S.: *Handbook of Industrial Crystallization*; 2nd Edition ed.; Butterworth-Heinemann, 2002.

[8] Manrich, S., Zanotto, E. D., Hage Jr., E. Aplicabilidade da Teoria Clássica de Nucleação Modificada (CD-CNT) à Cristalização de Polímeros (portuguese). *Polímeros: Ciência e Tecnologia* **1992**, 15-20.

[9] Mullin, J. W.: *Crystallization*; Fourth Edition ed.; Butterworth-Heinemann, 2001.

[10] Fokin, V. M., Abyzov, A. S., Zanotto, E. D., Cassar, D. R., Rodrigues, A. M., Schmelzer, J. W. P. Crystal nucleation in glass-forming liquids: Variation of the size of the "structural unit" with temperature. *Journal of Non-Crystalline Solids* **2016**, *447*, 35-44.

[11] Kawasaki, T., Tanaka, H. Formation of a crystal nucleus from liquid. *Proceedings of the National Academy of Science (PNAS)* **2010**, *107*, 14036-14041.

[12] Callister, JR., W. D.: *Material Science and Engineering: An Introduction 7th ed.*, 2007.

[13] Orrling, C. Crystallization Phenomena in Slags. Carnegie Mellon University, 2000.

[14] Kurz, W., Fisher, D. J.: *Fundamental of Solidification*; Trans Tech Publication, 1986.

[15] Avrami, M. Kinetics of Phase Change. I*. *Journal of Chemical Physics* **1939**, *7*, 1103-1112.

[16] Turkdogan, E.T.: *Physicochemical properties of molten slags and glasses*; The Metal Society: London, 1983. pp. 201-208.

[17] Kirkpatrick, R. J. Crystal Growth from the Melt: A Review. *American Mineralogist* **1975**, *60*, 798-814.
[18] Jacson, K. A., Uhlmann, D. R., Hunt, J. D. On the Nature of Crystak Growth from the Melt. *Journal of Crystal Growth* **1967**, *1*, 1-36.
[19] Avrami, M. Kinetics of Phase Change. II. *Journal of Chemical Physics* **1940**, *8*, 212-224.
[20] Avrami, M. Granulation, Phase Change and Microstructure. *Journal of Chemical Physics* **1941**, *9*, 177-184.

2.3 Solidification Behavior of Mold Powders and Slags

The understanding of the crystallization phenomenon of slags is crucial to determine the optimum conditions of the continuous casting process as well as the surface quality of the cast product. The main functions of the mold powders, namely lubrication and horizontal heat transfer capacity, are severely altered by the presence of crystals [1]. The solidification mechanism of the slags differs substantially of those that occur in the liquid metals. The process of solidification as from liquid metals is controlled predominantly by heat transfer. In the case of slags, the solidification is controlled initially by diffusion in the liquid and all solidification occurs predominantly in an undercooled melt [2]. During cooling processes, the slags can form glassy, partially or fully crystalline structures, depending on their chemical composition and thermal history [2,3]. Due to the wide composition range upon which the mold fluxes are disposed, the study field of the crystallization behavior of the slags is complex and wide. For instance, the effect of the basicity on the crystallization of the mold slags has been reported by several researches [4-9]. Wen *et al*. [5] point to that the crystallization tendency of the mold fluxes increases strongly with increasing the binary basicity. The same crystallization tendency was reported by Yang *et al.* [6], Lu *et al.* [8], and Zhang *et al*. [10], in which an improvement of the crystallization temperature was also observed. Several techniques as differential thermal analysis (DTA), differential scanning calorimetric (DSC), confocal laser-scanning microscopy (CLSM), single- (SHTT) and double-hot thermocouple technique (DHTT) have been extensively have been developend to investigate the crystallization behavior of slags and mold powders. Complementary analysis techniques as scanning electron microscope (SEM), energy dispersive X-ray (EDX), infrared emitter technique (IET) and X-ray diffraction (XRD) have been used to assist in the characterization of the crystalline phases. From the results provided by DTA, DSC and hot thermocouple technique, the construction of diagrams TTT and CCT became useful in the understanding of the solidification behavior of the mold slags. These diagrams allow to determine important characteristics as the time required to start the crystallization (incubation time) and the critical cooling rate of the slag.

In the present review, more attention will be give to the effect of MgO and TiO_2 on the crystallization behavior of the mold powders. The effect of other oxides is eventually mentioned along to the crystallization review and in the **item 2.3.3**. Finally, the effect of the sample fluid flow observed in hot thermocouple technique measurements on the crystallization of mold slag is discussed.

2.3.1 MgO-bearing Mold Powders

Magnesium oxide is a component present in the most of the steelmaking slags. It is added next to saturation to equilibrate the MgO-C refractory lining ladles, reducing the refractory wear rate [2,11-13]. In fluorine-free (F-free) mold fluxes, MgO is usually added with other oxides in a compositional range of 0 – 10 wt% aiming to modify the negative effect of the absence of fluorides and optimize the properties of the slag [14].

Although extensively used as a component in the mold powders composition, few studies regarding the exclusive effect of MgO on the crystallization behavior have been reported.

Kashiwaya *et al*. [15] investigated the crystallization behavior of a based $CaO-SiO_2-Al_2O_3-MgO$ blast furnace slag (BF). TTT and CCT diagrams were constructed from the SHTT results and complementary analyses were carried out with XRD and EDS, SEM observation was used in the crystallization behavior analysis. The TTT diagram obtained exhibited a double nose. According to the authors, the existence of the double nose indicates the existence of more than two kinds of crystals (**Fig. 2.8**). The higher nose position of the BF slag was about 9 seconds at 1250 °C, and the lower was 4 seconds at 1050 °C. The XRD analysis results pointed to the presence of merwinite ($3CaO.MgO.2SiO_2$), which precipitated faster, and gehlenite ($2CaO.Al_2O_3.SiO_2$). A pseudo-ternary phase diagrams of the $CaO-SiO_2-Al_2O_3$ system with 5 % and 10 % MgO are show in **Figure 2.9**.

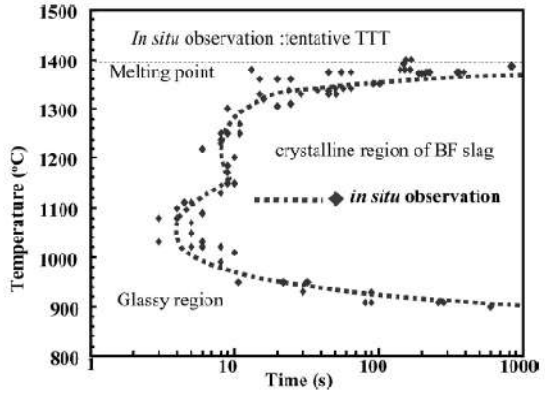

Figure 2.8 TTT diagram for a blast furnace slag (BF) constructed from SHTT results [15].

According to Kashiwaya *et al*. [15] the phase diagram (**Fig. 2.9**) shows a decrease in the merwinite region with decreasing of MgO content from 10 % to 5 %; an increase of the melilite (gehlenite) region is observed as the precipitation of merwinite occurs with decreasing MgO content. Feng *et al.* [16] reported the melilite as the basic phase in $CaO-Al_2O_3-SiO_2-V_2O_5$ with different MgO and TiO_2 contents; for this systems, a decrease of melilite diffraction peak intensity and a concomitant increase of the magnesia-alumina spinel amount with increasing MgO content from 10 % to 14 %, was also observed. Such increase in the MgO content implies in an increase of the *liquidus* temperature of the system, increasing the crystallization capacity of the slag at high temperatures.

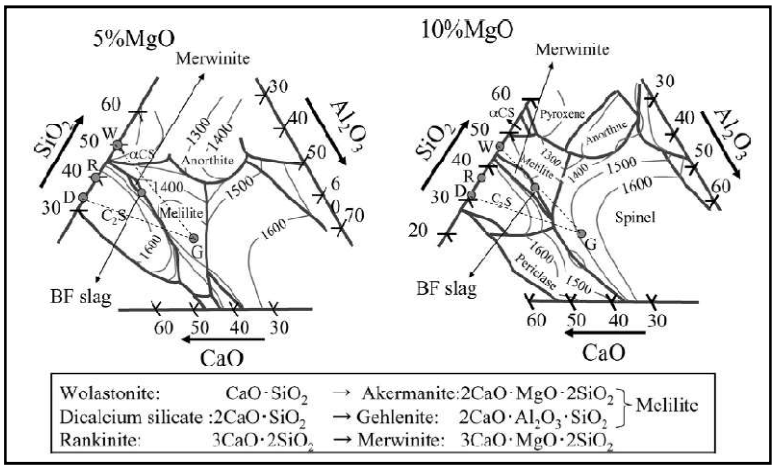

Figure 2.9 Pseudo-ternary phase diagrams for a $CaO-SiO_2-Al_2O_3$ system containing 5 % and 10 % MgO [15].

The combination of confocal laser-scanning microscope (CLSM), SEM-EDS and XRD analysis was used by Jung and Sohn [17] to construct the TTT and CCT diagrams to investigate the crystallization behavior of the $CaO-Al_2O_3-MgO$ system. The results showed a decrease of the incubation time with increasing MgO content from 2.5 to 5 wt-%; further MgO addition (to 7.5 wt-%) strongly increases the incubation time. An increase in the crystallization temperatures with increasing MgO content was also observed, *i.e.* addition of MgO promotes the formation of crystals at higher temperatures. Rocabois *et al*. [18] observed that increasing the MgO content from 0 to 7 wt-% in a $CaO-Al_2O_3-SiO_2$ system, the rate of crystallization becomes higher at 1100°C only for MgO contents larger than 6 %.

Praprakorn and Cramb [11] investigate the effect of MgO on the initial solidification of $CaO-Al_2O_3$ based slags using the DHTT. The authors reported that the addition of 7 mass% and 9 mass% MgO to calcium aluminate system increases significantly the temperature of crystallization and enhances the growth velocity of the system $CaO-Al_2O_3$. Results of X-ray diffraction showed that a mixture of $3CaO.Al_2O_3$ and $3CaO.2Al_2O_3.MgO$ crystalline phases precipitated above 1200°C, and a mixture of $5CaO.3Al_2O_3$ and $MgO.Al_2O_3$ precipitated below this temperature. Such results denotes the existence of two different crystallization events, characterized by the two noses in the TTT diagrams, as showed in **Figure 2.8**. More recently, the effect of MgO on fluorine-free mold fluxes were investigated by Yang *et al*. [19] by means of SHTT/DHTT and IET. TTT and CCT diagrams showed a shortening of incubation time and an increase of the critical cooling rate, pointing to an increase in the crystallization tendency of the mold fluxes with increasing MgO content.

2.3.2 TiO_2-bearing Mold Powders

The influence of titanium dioxide on the physicochemical properties of glasses, slags and mold powders has been subject of investigation by several researches. In glasses, the effect of TiO_2 on the optical, mechanical and thermal properties, viscosity, as well as on their structural and gas diffusion characteristics has been the focus of many researches [20-24]. In its turn, the influence of TiO_2 on properties as viscosity and crystallization tendency is the mainstream in a massive series of slags, electroslags and mold powders studies, which encompass a wide range of titanium dioxide content [16,25-44].

According to Turkdogan [45], there is a miscibility gap between 19 and 93 wt-% TiO_2 in the TiO_2-SiO_2 binary system. Studies have been pointing to the existence of Ti^{4+} in the form of $[TiO_4]$ in glasses and slag [16,34,40]; the presence of titanium with five- (Ti^{5+}) or six- (Ti^{6+}) coordination numbers has been also reported, depending of the TiO_2 content. However, there are some divergences concerning the existence of these coordination species. For instance, Greegor *et al.* [46] inferred the occurrence of Ti^{6+} in compositions along the TiO_2-SiO_2 join with very low TiO_2 contents. In contrast, no evidence of presence of this coordination was found by Henderson *et al.* [47], which suggest the existence of Ti^{5+} as the predominant coordination below 3.6 wt-% TiO_2. According to Mysen and Neuville [48], the structural role of Ti^{4+} in alkali silicate melts and glasses is a complex function of Ti concentration, with Ti existing both in four-fold and six-fold coordination. At low TiO_2 content, the Ti is in six-fold coordination and acts as a network modifier; whereas, at high TiO_2 content, Ti^{4+} (four-fold

coordination) behaves as a network modifier. Once Ti^{4+} cation have larger ionic radius than Si^{4+} cation, it appears to be unfit to replace the position of the Si^{4+} in the tetrahedral structure; bonds as Ti-O-Al and Ti-O-Ti are expected to be weaker than those present in Si-O-Al and Si-O-Si. Therefore, the viscosity of high polymerized aluminosilicate melts decreases with addition of TiO_2, although the overall NBO/T ratio decreases with increasing TiO_2 content [42,45]. In contrast, results from X-ray photoelectronic spectrocopy (XPS) analysis of calcium silicate melts containing 17 wt-% Al_2O_3 and 10 wt-% MgO showed a reduction of the bridging oxygen (O^0) and the non-bridging oxygen (O^-) fractions, and a concomitant increase of the free oxygen (O^{2-}), with addition of TiO_2; which, according to the authors, higher TiO_2 content provides higher potential to depolymerize the slag network structure [39].

Wang *et al*. [49] investigated the effect of TiO_2 on the viscosity and crystallization behavior of P-bearing steelmaking slags. Continuous cooling transformation diagrams constructed from DTA results showed that the addition of TiO_2 lowered the crystallization temperature and the crystallization tendency of the slags. Typically, the presence of TiO_2 on the mold powders composition is due to impurities and, in many cases, it has been used as a potential candidate to replace CaF_2 in F-free mold powders due to its tendency to precipitate perovskite ($CaO.TiO_2$) as a substitute of cuspidine ($3CaO.2SiO_2.CaF_2$) [4,25,27,36,50,51]. McRae *et al*. [52] reported that, for CaO-rich slags of the $CaO\text{-}SiO_2\text{-}Al_2O_3\text{-}MgO\text{-}TiO_2$ system, the primary phase to crystallize is perovskite, followed by $4(MgO.2TiO_2).(Al_2O_3.TiO_2)$. For slags rich in MgO, the crystallization order is inverted, $4(MgO.2TiO_2).(Al_2O_3.TiO_2)$ followed by $CaO.TiO_2$. Nakada *et al*. [50] investigated the use of TiO_2 as a possible substitute of fluorine in the mold fluxes composition. The authors had constructed CCT diagrams from results obtained from DTA and subsequently converted they into TTT diagrams by using the Scheil additivity rule. They found that, in $CaO\text{-}SiO_2\text{-}TiO_2$ slags, the crystals – which crystallize in a basicity range of 0.8 – 1.4 – were $CaO.SiO_2.TiO_2$, $CaO.SiO_2$ and $CaO.TiO_2$. The crystallization of $CaO.TiO_2$ promotes an increase of the viscosity; since CaO is consumed to form the crystal, the slag acidity is increased due to the excess of silicon. Such effect on the viscosity is not desired and, therefore, the precipitation of $CaO.TiO_2$ is not suitable. On the other hand, the precipitation of $CaO.SiO_2.TiO_2$ and $CaO.SiO_2$ do not alter the viscosity meaningfully, since these crystals consume both CaO and SiO_2. The incubation time of $CaO.SiO_2$ is much longer than that of cuspidine; while $CaO.SiO_2.TiO_2$ exhibited incubation times as short as those of cuspidine, present in the most of the industrial mold powders. In the referred study [50], the crystallization of $CaO.SiO_2.TiO_2$ and $CaO.SiO_2$ occurred at high temperatures for the slag with 12.05 mol % TiO_2, while for slags with 17.25 mol % TiO_2, these crystals precipitated in a lower crystallization temperature range, far below the melting point. Based on these results, the authors suggest that $CaO.SiO_2.TiO_2$ crystal in the $CaO\text{-}SiO_2\text{-}TiO_2$ system can replace the cuspidine in commercial mold fluxes.

A series of mold powders containing different contents of CaO, SiO_2, B_2O_3, MgO, Li_2O, Na_2O, MnO and TiO_2 were investigated to determine a range of composition with similar properties (melting temperature, viscosity and heat flux) of F-bearing mold powders [53]. Based on the results obtained, it was suggested that $CaO.TiO_3$ may replace $3CaO.SiO_2.CaF_2$ in conventional mold powders. Following the same research line, the crystallization behavior

and the change of activity for crystallization of slags composed by the CaO-SiO_2-Al_2O_3-MgO-B_2O_3-Na_2O-Li_2O-MnO-TiO_2 system were investigated by Qi *et al*. [54]. They concluded that increasing TiO_2 content in the mold powder, the crystallization ratio and the crystallization rate of the slag film also increase. Mold powders with TiO_2 contents higher than 6.5 wt-% exhibited lower activation energy for crystallization from glassy and liquid slag mold fluxes than that of industrial slags containing CaF_2. For contents between 1 – 6 wt-% TiO_2, the precipitated crystal was arkemanite ($2CaO.MgO.2SiO_2$); increasing titanium dioxide content above 8 %, the main crystal which precipitates was perovskite. For further TiO_2 content increment, the phases changed from arkemanite to perovskite.

In order to determine the substitution viability of CaO-SiO_2-CaF_2 (CSF) based mold powders, the crystallization properties of several types of CaO-SiO_2-TiO_2 (CTS) based slag system were investigated [27]. Properties as viscosity, break temperature, crystallization ration and solidification mineragraphy were measured and compared to those of CSF mold powders. The CST based system was composed by CaO-SiO_2-Al_2O_3-MgO-Na_2O-TiO_2-B_2O_3-Li_2O systems; while the CSF was composed by CaO-SiO_2-Al_2O_3-MgO-Na_2O-CaF_2. The authors reported the existence of $CaO.TiO_2$ or $CaO.TiO_2$ and $CaO.SiO_2$ in the CST based slags. Due to $CaO.TiO_2$ precipitation from the liquid slag, a change in the crystallization ratio occurs, which, in turn, alters the composition of the remained melt. As a consequence, the slag becomes more acid and its viscosity is increased. An interesting point discussed in the study conducted by He *et al*. is the interaction between TiO_2 and C. In high TiO_2 content slags, the titanium dioxide can reacts with N and C to form high melting point species namely TiN, TiC or T(C,N). The presence of these high temperature species increases the viscosity, which can be responsible by occurrence of sticking or breaking in the use of TiO_2 bearing slags. Therefore, the CST system could not be expected to be used as a fluorine replacement in slag with high fluorine content.

Zhang *et al*. [4] investigated the crystallization behavior of fluorine-free mold fluxes composed by CaO, SiO_2, Al_2O_3, Na_2O, B_2O_3 and TiO_2 or ZrO_2 by means of CSLM and electron diffraction scattering (EDS). In TiO_2-free mold powders, the results pointed to the presence of two mineral phases – Ca_2SiO_4 and $Ca_3Si_2O_7$ – which may growth together. Addition of TiO_2 to the slag promotes the formation of $CaTiO_3$; crystals of $CaSiO_3$ and Ca_3SiO_7 were also observed, suggesting that the presence of TiO_2 in the slag composition alters the thermodynamics of the crystal growth.

Similar result concerning the influence of TiO_2 content on the crystallization behavior of CaO-Al_2O_3 based mold powders were founded by Li *et al*. [32]. DTA results showed the presence of two peaks for TiO_2-free mold fluxes, indicating two successive crystallization events, and three peaks for TiO_2- bearing mold fluxes, denoting three crystallization events. CCT curves were constructed taking the DTA results as the onset of crystallization (**Figure 2.10**). The onset of crystallization for different TiO_2 contents (0, 5, 7 and 10 % TiO_2) indicated an increasing of the crystallization temperature with increase of TiO_2 content. One interesting fact observed was the lower variation of the crystallization temperature – at which the second and the third crystals are formed – with the cooling rate. Li *et al.* [32] suggested that, at lower temperatures, the thermodynamic drive force is the main factor acting on the

nucleation and growth of the second and third crystals; the effect of kinetic factors as viscosity on the crystallization is insignificant at lower temperatures. The enhancement of the crystallization promoted addition of TiO_2 was attributed to a decreasing in viscosity, and accordingly, the degree of polymerization of the aluminate network. Water-quenched mold powder samples were submitted to XRD and SEM to determination of the crystalline phases. For the TiO_2-free mold powders, MgO first precipitated from the liquid at higher temperature, whereas $Ca_{12}Al_14O_{33}$ crystal co-precipitated at lower temperature; for the TiO_2-bearing mold powders, crystals of $CaTiO_3$ precipitated at high temperature, while MgO and $CaTiO_3$ crystals, and MgO, $CaTiO_3$ and $Ca_{12}Al_{14}O_{33}$ at intermediate temperature and low temperatures.

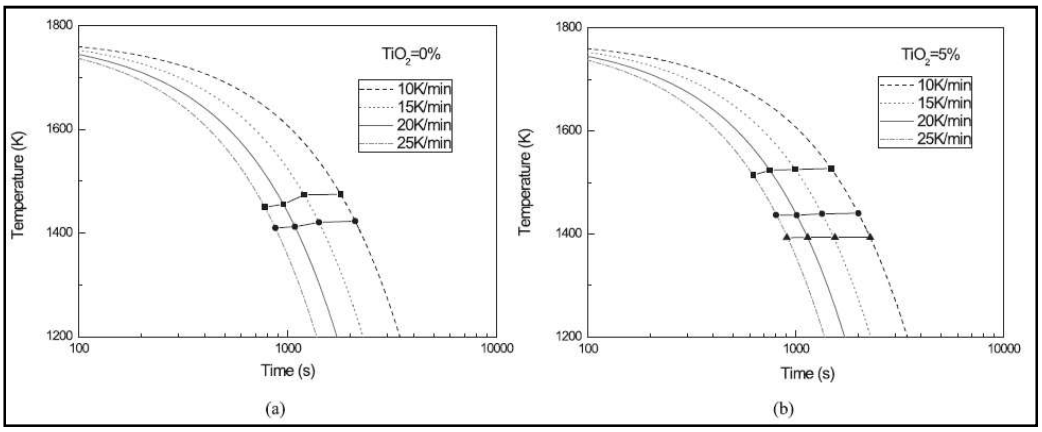

Figure 2.10 CCT curves of $CaO\text{-}Al_2O_3$ with (a) 0 mass % TiO_2 and (b) 5 mass % TiO_2 [32].

The use of portland cement clinker as a raw material for continuous casting mold powders was investigated by Arefpour *et al.* [25]. Results from viscosity measurements and crystalline composition of portland cement clinker with additions of CaF_2, TiO_2 and Na_2O were presented. The authors suggested that TiO_2 and Na_2O are not suitable to replace fluorine in the mold powder composition because it does not provide the same lubrication potential than the CaF_2. Such conclusion is in accordance with that reported by He *et al*. [27].

Studies carried out by Nakada *et al*. [50] revealed the coexistence of $CaO.SiO_2.TiO_2$ and $CaOSiO_2$ crystalline phases for the $CaO\text{-}SiO_2\text{-}TiO_2$ system, in a narrow isothermal temperature range, and with relatively high crystallization temperatures. In addition, the crystallization temperature rate which both crystal phases precipitated is large. Despite the incubation time of $CaO.SiO_2.TiO_2$ is shorter than that of cuspindine, it does not promoted increase in viscosity. The authors concluded that the $CaO.SiO_2.TiO_2$ is suitable to replace the cuspidine. Such conclusion is in disagreement with those reported by He *et al*. [27] and Arefpour *et al*. [25].

Rocabois *et al*. [18] reported that addition of TiO_2 as nucleation agent – in $Al_2O_3\text{-}CaO\text{-}SiO_2\text{-}Na_2O\text{-}CaF_2$ liquid compositions containing less that 30 wt-% SiO_2 – does not decrease the time of appearance of first crystals, and the overall crystallization rate remains practically unchanged. Li *et al*. [31] found that additions of 3 wt-% TiO_2 do not increased the % crystallinity of the slag; while for additions of 6 wt-%, only a small increase in crystallinity was observed. In slags containing TiO_2, Ti^{4+} can act as both network former and modifier,

however for a range 1 – 7 wt-% TiO_2, which includes most steelmaking slags, it plays as a network former [55].

The effect of MgO and TiO_2 on the crystallization behavior of the slags and mold powders aforementioned was focused mainly on the kind of crystalline phase are formed according to the chemical composition of the melt slag. Nevertheless, the addition (or subtraction) of a determined oxide can alters the crystallization kinetic of the mold flux. For instance, Rocabois *et al*. [18] observed that the dominant nucleation mechanism change from heterogeneous to homogeneous when MgO or TiO_2 is present in the liquid slag. The free energy barrier for heterogeneous nucleation is smaller than that for homogeneous crystallization; this suggests that MgO or TiO_2 additions may to decrease the free energy to formation of the new phase; in addition, the supercooling required to heterogeneous nucleation is lower than that for homogeneous nucleation. Thus, it is can be also suggested that additions of MgO or TiO_2 reduce of supercooling necessary to promote homogeneous nucleation [56,57]; for more details about nucleation mechanisms see **Chapter 2**, **section 2.2**.

2.3.3 Effect of Other Components on the Solidification Behavior

The effect of usual component in mold fluxes as Al_2O_3 and CaF_2 have been reported by some researches. Park [58] investigated the solidification behavior of the $CaO\text{-}SiO_2\text{-}Al_2O_3\text{-}CaF_2$-10 wt-% MgO system using XRD, SEM-EDS, and an image analyzer. The author reported an increase of the *liquidus* temperature of the oxides containing 5 wt-% CaF_2 with increasing Al_2O_3 content from 10 wt-% to 30 wt-%. For the oxide system containing 30 wt-% Al_2O_3, the *solidus* temperature significantly decreases with increasing CaF_2 content. In addition, the size of spinel ($MgAl_2O_4$) crystals in the final structure increases with increasing Al_2O_3 due to the fact that the oxides spend more time at higher temperatures below the *liquidus* temperature – where the crystal growth is generally faster than nucleation; the opposite effect on the crystal size was observed by increasing CaF_2 content, as a consequence of the oxides spending more time at relatively lower temperatures – where nucleation is faster than growth. The amphoteric character of the Al_2O_3 has also reported by Park *et al*. [59], in which a network former behavior of alumina is observed about 10 wt-%, while for higher contents, in parts, it acts as a network modifier. The effect to Al_2O_3 and CaF_2 on the solidification of mold slags was also investigated by Lachmann and Scheller [60] by means of the SHTT and DHTT. The start temperature of crystal formation decreases with increasing alumina content, while addition of fluorine shows an opposite effect. The addition of CaF_2 favors the precipitation of cuspidine ($3CaO.SiO_2.CaF_2$) at higher temperatures. For Al_2O_3 addition, pseudo-wollastonite forms at higher temperatures followed by gehlenite; with increasing of alumina content, pseudo-wollastonite can be retarded and gehlenite appears first, but at lower temperatures.

The effect of addition of CaF_2 on a $CaO\text{-}SiO_2\text{-}Al_2O_3$ system was recently reported by Susa *et al*. [61]. For the F-free system, the results point to a preference to precipitation of gehlenite to wollastonite. With the addition of CaF2, cuspidine precipitates in preference to gehlenite.

The effect of high Li_2O content on the crystallization behavior of $CaO\text{-}SiO_2\text{-}Al_2O_3\text{-}CaF_2\text{-}Na_2O$ slag system was investigated by Liu *et al.* [62]. Addition of Li_2O to the slag system promotes an increase in the critical cooling rate and the crystallization rate of the samples – in compositions with or without the presence of Na_2O. For Li_2O contents higher than 6 wt-%,

reductions in the incubation time were also observed. Results from SHTT measurements reported by Wang *et al.* [7] indicate a decreasing trend in the crystallization temperature of the CaO-SiO_2-Al_2O_3-B_2O_3-Li_2O slag system with increasing Li_2O content. TTT curves suggested that Li_2O would tend to inhibit the crystallization in high-temperature region of F-free mold fluxes and greatly accelerate the crystallization in low-temperature region. Based on SEM/EDS and XRD results the authors suggested that the main crystal phase ($Ca_{11}Si_2B_2O_{22}$) founded in F-free mold fluxes can replace cuspidine formed in fluorine-bearing mold fluxes.

Studies have focused on the potential use of ZrO_2 as a candidate to replace CaF_2 in fluorine-free mold powders. According to Rocabois *et al*. [18], the use of ZrO_2 as a nucleating agent in complexes mold powders (SiO_2-Al_2O_3-CaO-MgO-CaF_2-Na_2O-TiO_2) – containing less than 30 wt-% SiO_2 – do not decreases the time of appearance of first crystal, and the overall crystallization rate remains practically unaltered; however, ZrO_2 crystals work as heterogeneous sites for cuspidine nucleation. Similar results are reported by Li *et al.* [31]. Additions of ZrO_2 in slags containing CaF_2 did not cause significant increase in slag crystallinity, *i.e.* it presence causes little effect on the amount of the crystalline phase formed; nevertheless, additions of CaO promoted a dramatic increase in the amount of the precipitated crystalline phase (cuspidine). In the other hand, additions of ZrO_2 to CaO-SiO_2-Al_2O_3-Na_2O-B_2O_3 and CaO-SiO_2-Al_2O_3-B_2O_3-Li_2O slag systems improves the crystallization tendency of fluorine-free mold powders, acting as a heterogeneous nucleation agent due to its limited solubility. Small amounts of ZrO_2 promotes heterogeneous crystallization, since the ZrO_2 particles acts as nucleation sites, reducing the energy barrier for the precipitation of crystals [10,14].

Other usual oxides which effect on the solidification of slag is constantly investigated are Na_2O and B_2O_3. In mold powders, the presence of Na_2O has been reported as an effective crystallizing agent. According to He *et al.* [63] the CaO-Si_2O-Na_2O (1 wt-% F) based mold powders is suitable to replace CaF_2 in CaO-Al_2O_3-CaF_2 based slag with high fluorine content due to its similarity on crystallization performance. It is suggested that precipitation of $Na_2O.CaO.3SiO_2$ and $Na_2O.2CaO.2SiO_2$ in the F-free mold powders can substitute for cuspidine in commercial mold powders. Studies carried out using hot thermocouple technique point to a reduction in incubation time of fluorine-free mold powders with Na_2O addition [64,65]. An expressive effect of the wt-% Na_2O on the critical cooling rate in CaO-Si_2O-TiO_2 fluorine-free slag systems was reported. It was concluded that is possible to control the crystallization kinetics in referred slag systems by changing Na_2O content [64]. For more complexes fluorine-free mold powders, the effect of Na_2O content on critical cooling rate was similar but less intense [65]. The effect of Na_2O replacement for SiO_2 on non-isothermal crystallization behavior of CaO-BaO-Al_2O_3 based mold powders was investigated by Zhang *et al*. [66]. An increase of the initial crystallization temperature and a decrease of the crystallization activation energies with increasing Na_2O content were observed. In addition, the presence of Na_2O inhibited the precipitation of CaF_2 crystals and enhances the precipitation of $CaAl_2O_4$ crystals.

The applicability of B_2O_3 as substitute of CaF_2 in F-free mold powders have been extensively investigated by several researches. Study conducted by Choi *et al*. [67] suggests the utilization of Na_2O and B_2O_3 to replace CaF_2 in commercial mold powders composition due to the precipitation of CaB_2SiO_7 and $CaAl_4B_2(SiO_4)_8$ as substitute of cuspidine. SHTT results obtained by Zhou *et* al. [68] showed that the initial crystallization temperature of low fluorine mold powders reduces with the increase of Na_2O content due to its network breaker characteristic. Conversely, addition of B_2O_3 increases the crystallization temperature, since it acts as a network former inhibiting the slag crystallization. Li *et al.* [69] investigated the use of B_2O_3 in replacement to components as Na_2O, CaF_2 and NaF in commercial mold powders. The B_2O_3-containing mold powder exhibited low crystallization tendency, since it was predominantly glassy. According to Li *et* al., the use of B_2O_3 accelerate the formation of network structures, in a similar way to SiO_2, inhibiting the separation of crystal phases. The authors suggest that fluorine-free B_2O_3-containing mold fluxes had great potential for application in continuous casting of rare-earth steel, stainless steel, and ultra-low-carbon steel as well as high speed casting. Shu *et al*. [70] observed a decrease of *liquidus* temperature and a significant increase of incubation time for crystallization in a Al_2O_3-CaO-MgO-Na_2O-SiO_2-TiO_2 system with increasing B_2O_3 content. Similar results were found by Lu *et al*. [8] using the DHTT. It was found that the mold flux crystallization would be restrained by B_2O_3 additions reported. More recently, Zhang *et al*. [71] reported an initial inhibition of the crystallization behavior of CaO-SiO_2-B_2O_3 based F-free mold powder systems with addition of B_2O_3 (up to 6 wt-%); further B_2O_3 content increment leads to an increase in the crystallization of the system.

The influence of La_2O_3 content on the crystallization behavior of fluorine-free mold fluxes were investigated by Zhang *et al.* [72] using SEM-EDS and thermal analysis. An improvement of crystallization ratios of mold powders from 2 % to 90 % with increasing La_2O_3 content (from 0 wt-% to 20 wt-%) could be observed. The addition of La_2O_3 also promotes an increase in the crystallization temperature due to the formation of a low melting point substance. The effect of FeO on the formation of spinel phases in synthetic slag samples of the CaO-SiO_2-MgO-Al_2O_3-Cr_2O_3 system have been reported by Li *et al.* [73]. The authors found an increase of size and amount of spinel mineral with increasing FeO content in the samples. In addition, the Cr content in the spinel phase showed an increase when FeO content was increased to 6 wt-%. Lei *et al*. [74] investigated the effect of quartz on the crystallization behavior of mold powders. A decreasing in the crystallization temperature, as well as reduction in the critical cooling rate and incubation time with increasing quartz content were reported. The precipitation of cuspidine is restrained by quartz; the crystallization rate and the cuspidine content decrease when quartz content exceeds 20 wt-%.

2.3.4 Crystal Morphology

The solidification structure of the slag is extremely sensitive to the exact solidification thermal conditions [2]. During the investigation of the effect of TiO_2 and B_2O_3 on the crystallization behavior of the Al_2O3-CaO-MgO-Na_2O-SiO_2 system using the SHTT, Shu *et al.* [70] observed a gradual change of morphology from high to low temperatures. A large

number of small crystals were observed at lower temperature (900°C). With increasing temperature, needle-like, facet crystals and columnar crystals were appearing concomitant or separately, according to the temperature range. At 1100°C, large equiaxied dendrites were formed on the thermocouple wall or in the center of sample. Orrling [75,76] developed a TTT diagram to different crystal morphologies as function of temperature for two different slag samples (**Figure 2.11**).

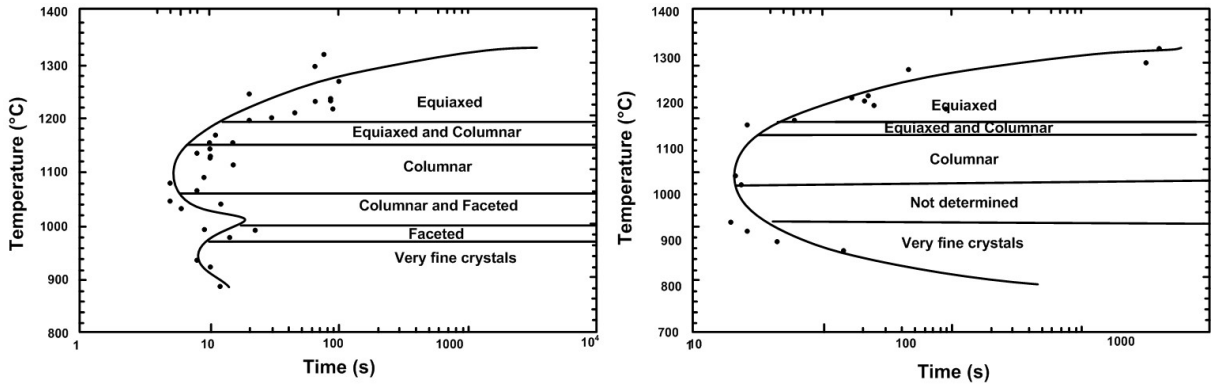

Figure 2.11 TTT diagrams showing the morphology dependence temperature of two different slag samples. Figure adapted from [76].

The variation of the crystal morphology with temperature was also reported by Klug *et al*. [64]. Crystals with dendritic structure could be observed in slag samples at high temperatures; the crystals became small and dense as the temperature decreases. At 900°C, the crystals were very fine and with a cloud-like appearance with the increasing of density. The effect of chemical composition and temperature on the crystal morphology of CaO-Al_2O_3-based slag was investigated by Jung and Sohn [17]. For a slag sample slowly cooled (with CaO/Al_2O_3 ratio equal to 1 and with 5 wt-% MgO), the morphology of the first crystal was equiaxed faceted; for higher MgO contents the crystals showed a dendritic structure. At high cooling rates, the crystal morphology was finely dispersed and with several shapes, namely spherical nodules, faceted polygonals, needles and dendrites (for higher CaO/Al_2O_3 ratios). Variation in the crystal morphology as a function the cooling rate of blast furnace slag containing high TiO_2 content was reported by Liu *el al*. [77]. At cooling rate of 10 and 30 $K.min^{-1}$, the perovskite crystal morphology was dendritic; it changes to orthogonal at a cooling rate of 20 $K.min^{-1}$ and to hexagonal at cooling rate of 40 and 50 $K.min^{-1}$. Zheng *et al*. [78] report a change in the crystal morphology of electroslag remelting with TiO_2 addition from $11CaO.7Al_2O_3.CaF_2$ faceted and bonelike to $CaTiO_3$ elliptically faceted and blocky crystals. Results from SEM analysis of CaO-Al_2O_3 based mold powders containing TiO_2 indicate a relationship between crystal morphology and crystallization control mechanism [33]. Crystals of MgO and $CaTiO_3$ exhibited a non-faceted morphology, suggesting a crystallization rate controlled by diffusion. On the other hand, crystals of $Ca_{12}Al_{14}O_{33}$ showed larger faceted morphology, suggesting a crystallization controlled by interfacial reaction. Shear stress is also reported as a factor which can exert influence on the microscopic morphology of the crystals, leading to smaller grain size, but without affect on the crystalline phase formed [79].

2.3.5 Effect of the Marangoni Convection on Mold Powders Crystallization

The Marangoni convection or thermocapillary is a liquid flow caused by an unstable surface tension modulation due local variations of the chemical composition (solute concentration gradient) or by temperature gradients through the sample. This temperature gradient or solute concentration gradient leads to unstable gradient of interfacial tension. Such instability in the interfacial tension promotes convection currents which cause unequal solute distribution in the sample interface which, in turn, promotes a spontaneous interfacial turbulence, affecting the transport mechanism – heat and mass diffusivity – in melts [45,80,81]. In SHTT/DHTT experiments, the existence of convection within the melt implies on the occurrence of temperature oscillations in the sample [65,82-84]. Kashiwaya *et al.* [82] verified that the fluid flow is dominated by Marangoni convection caused by thermal gradient in samples during SHTT experiments. At steady state, the sample region in contact with the thermocouple has the highest temperature and a small thermal gradient from the tip of thermocouple to the free contact sample region is established. When the sample undergoes a heating cycle, the temperature of the sample region in contact with thermocouple wire is hotter than that contact free region. When the sample is quenching, the heat conduction occurs from the sample to the thermocouple. The direction of convection follows the same "movement" of the heat transfer in the sample. **Figure 2.12** shows a representation of the liquid flux movement inside the liquid sample for both cases above cited.

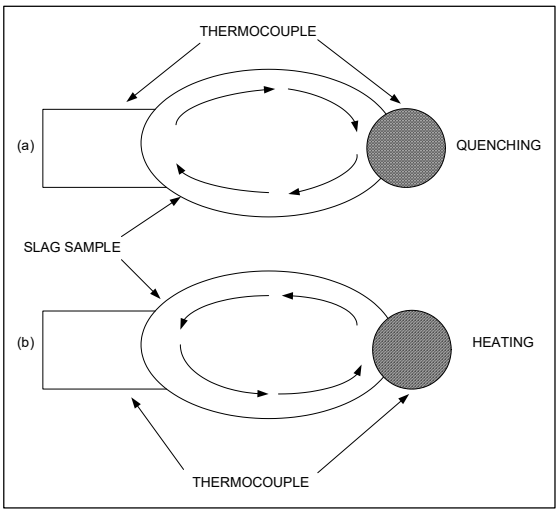

Figure 2.12 Convective mass motions in the slag sample at unsteady state under (a) cooling and (b) heating cycles. Figure adapted from Kashiwaya *et al*. [82].

Orrling *et al*. [83] observed the effect of fluid flow on the crystal stability of a calcium aluminate, where growing equiaxed dendrite crystals fragment under the action of a shear flow. The authors suggested that the shear flow was generated by Marangoni or natural convection in the sample. They has noted that this mechanism leads to an increase in the number of crystals, since the crystal fragment also starts to grow, leading to a one nucleation event forming several growing crystals. Similar behavior was reported by Yang *et al*. [65], where some equiaxed crystals formed in the liquid layer and the crystals fragments from weak crystalline layer were dragged to the high temperature region by Marangoni convection flow and remelted within the liquid sample. Zhou *et al*. [84] point out that, in DHTT experiments, only the temperature of the mold slag in contact with the thermocouple wall can be measured, causing significant effects on crystallization, such as spatial variations in

temperature and fluid flow inside the mold slag sample. It was also observed a movement of crystalline aggregations in the molten slag due to fluid flow recirculation along the surface of the slag sample driven by Marangoni flow.

References

[1] Hao, Z., Chen, W., Lippold, C., Mao, H. Crystallization Extent and Phase Constitution of Slag Films Takan from Continuous Casting Moulds for Stainless Steels. *Steel Research International* **2009**, *80*, 761-766.

[2] Cramb, A. W. The Solidification Behavior of Slags: Phenomena Related to Mold Slags. *ISIJ International* **2014**, *54*, 2665-2671.

[3] Pinheiro, C. A., Samarasekera, I. V., Brimacombe, J. K. Mold Flux for Continuous Casting of Steel - Part V. *Iron and Steelmaker* **1995**, 37-39.

[4] Zhang, Z. T., Li, J., Liu, P. Crystallization Behavior in Fluorine-Free Mold Fluxes Containing TiO_2 / ZrO_2. *Journal of Iron and Steel Research International* **2011**, *18*, 31-37.

[5] Wen, G., Liu, H., Tang, P. CCT and TTT Diagrams to Characterize Crystallization Behavior of Mold Fluxes. *Journal of Iron and Steel Research, International* **2008**, *15*, 32-37.

[6] Yang, J., Zhang, J., Sasaki, Y., Ostrvski, O., Zhang, C., Cai, D., Kashiwaya, Y. *In-situ* Study of Crystallization Behavior of CaO-SiO_2-Na_2O-B_2O_3-TiO_2-Al_2O_3-MgO-Li_2O Fluorine-free Mould Fluxes with Different CaO/SiO_2 ratios. *ISIJ Internacional* **2016**, *56*, 574-583.

[7] Wang, W., Yan, X., Zhou, L., Xie, S., Huang, D. Influences of Basicity and Li_2O on the Properties of Fluorine-Free Mold Flux for the Casting of Medium Carbon Steels. *Metallurgical and Materials Transactions B* **2016**, *47B*, 963-976.

[8] Lu, B., Wang, W., Li, J., Zhao, J., Huang, D. Effect of Basicity and B_2O_3 on the Crystallization and Heat Transfer Behaviors of Low Fluorine Mold Fluxes for Casting Medium Carbon Steels. *Metallurgical and Materials Transactions B* **2013**, *44B*, 365-377.

[9] Huang, X., Ba, X., Gao, J., Zhang, X. Exploring the crystallinity of mold fluxes by Pulse Electric Current. *Steel Research International* **2019**, *91*.

[10] Zhang, Z., Wen, G., Zhang, Y. Crystalization behavior of F-free mold fluxes. *International Journal of Minerals, Metallurgy and Materials* **2011**, *18*, 150-158.

[11] Prapakorn, K., Cramb, A. W. Initial Solidification Behavior in Continuous Casting: The Effect of MgO on the Solidification Behavior of CaO-Al_2O_3 Based Slags. *MS&T* **2004**, 3-10.

[12] Gran, J., Wang, Y., Sichen, D. Experimental determination of the liquidus in the basicity region in the Al_2O_3 (30 mass%)-CaO-MgO-SiO_2 system. *CALPHAD* **2011**, *35*.

[13] De Aza, A. H., Pena, P., De Aza, S. Ternary System Al_2O_3-MgO-CaO: I, Promery Phase Field of Crystallization of Spinel in the Subsystem $MgAl_2O_4$-$CaAl_4O_7$-CaO-MgO. *Journal of American Ceramic Society* **1999**, *82*, 2193-2203.

[14] Zhou, L., Li, H., Wang, W., Sohn, I. Effect of ZrO_2 on the melting, viscosity, and crystallization behaviors of fluorine-free mold flux for casting medium carbon steels. *Steel Research International* **2017**, *87*.

[15] Kashiwaya, Y., Nakauchi, T., Pham, K. S., Akiyama, S., Ishii, K. Crystallization Behavior Concerned with TTT and CCT Diagrams of Blast Furnace Slag Using Hot Thermocouple Technique. *ISIJ Internacional* **2007**, *47*, 44-52.

[16] Feng, C., Chu, M-S., Tang, J., Qin, J., Li, F., Liu, Z-G. Effects of MgO and TiO_2 on the viscous behaviors and phase compositions of titanium-bearing slag. *International Journal of Minerals and Materials* **2016**, *23*, 868-880.

[17] Jung, S. S., Sohn, I. Crystallization Behavior of the CaO-Al_2O_3-MgO System Studied with a Confocal Laser Scanning Microscope. *Metallurgical and Materials Transactions B* **2012**, *43B*, 1530-1539.

[18] Rocabois, P., Pontoire, J. N., Lehmann, J., Gaye, H. Crystallization of Al_2O_3-CaO-SiO_2 based oxide inclusions. *Journal of Non-Crystalline Solids* **2001**, *282*, 98-109.

[19] Yang, J., Zhang, J., Sasaki, Y., Ostrovski, Zhang, C., Cai, D., Kashiwaya, Y. Effect of MgO on crystallization and heat transfer of fluorie-free mold fluxes. *Metallurgical and Materials Transactions B* **2018**.
[20] Henderson, G. S. The structure of silicate melt: A glass perspective. *The Canadian Minaralogist* **2005**, *43*, 1921-1958.
[21] Karlsson, S., Bäck, L. G., Kidkhunthod, P., Lundstedt, K., Wondraczek, L. Effect of TiO_2 on optical properties of glasses in the soda-lime-silicate system. *Optical Materials Express* **2016**, *6*, 1198-1216.
[22] Limbach, R., Karlsson, S., Scanell, G., Mathew, R., Edén, M. The effect of TiO2 on the structure of Na2O-CaO-SiO2 glasses and its implications for thermal and mechanical properties. *Journal of Non-Crystalline Solids* **2017**, *471*, 6-18.
[23] Behrens, H. Noble gas diffusion in silicate glasses and melts. *Mineralogy & Geochemistry* **2010**, *77*, 227-267.
[24] Flueguel, A. Glass viscosity calculation based on a global statistical modelling approach. *Glass Technology: European Journal of Glass Science and Technology Part A* **2007**, *48*, 13-30.
[25] Arefpour, A. R., Monshi, A., Saidi, A. Effects of Replacing Fluorine with Sodium and Titanium Oxides on Mold Powders Lubrication in Continuous Casting of Steel. *Journal of Advanced Materials and Processing* **2015**, *3*, 59-66.
[26] Gosh, D., Krishnamurthy, V. A., Sankaranarayanan, S. R. Application of optical basicity to viscosity of high alumina blast furnace slags. *Journal of Mining and Metallurgy Section B* **2010**, *46*, 41-49.
[27] He, S., Huang, Q., Zhang, G., Lu, Y., Wang, Q. Solidification Properties of $CaO-SiO_2-TiO_2$ Based Mold Fluxes. *Journal of Iron and Steel Research International* **2011**, *18*, 15-19.
[28] Jiao, K., Zhang, J., Wang, Z., Liu, Y., Xu, R. Melting features and viscosity of TiO_2-containing primary slag in a blast furnace. *High Temperature Materials and Processes* **2018**, *37*, 149-156.
[29] Kim, J. B., Sohn, I. Influence of TiO_2/SiO_2 and MnO on the viscosity and structure in the TiO_2-MnO-SiO_2 welding flux system. *Journal of Non-Crystalline Solids* **2013**, *379*, 235-243.
[30] Lei, Y., Xie, B., Ma, W.-H. Analysis of crystallization behavior of mold fluxes containig TiO2 using the single hot thermocouple techique. *Journal of Iron and Steel Research International* **2016**, *23*, 322-328.
[31] Li, Z., Thackray, R., Mills, K. C.: A test to determine crystallinity of mould fluxes. In *VII International Conference on Molten Slags, Fluxes and Salts* The South African Institute of Mining and Metallurgy: South Africa, 2004; pp 813-819.
[32] Li, J., Shu, Q., Hou, X., Chou, K. Effect of TiO_2 Addition on Crystallization Characteristics of $CaO-Al_2O_3$-based Mould Fluxes for High Al Steel Casting. *ISIJ Internacional* **2015**, *55*, 830-836.
[33] Li, J. L., Shu, Q., Hou, X., Chou, K. C. Effect of TiO_2 addition on viscosity and structure of $CaO-Al_2O_3$ based mould fluxes for high Al steel casting. *Canadian Metallurgical Quarterly* **2015**, *54*, 85-91.
[34] Li, J., Shu, Q., Chou, K. Structural study of glassy $CaO-SiO_2-CaF_2-TiO_2$ slag by Raman spectrocopy and MAS-NMR. *ISIJ Internacional* **2014**, *54*, 721-727.
[35] Marschall, I., Kölbl, N., Harmuth, H., Xia, G. Investigation of continuous casting slag films sampled on site and comparison with laboratory results. *Journal for Manufacturing Science & Production* **2013**, *13*, 103-114.
[36] Mills, K. C. Structure and Properties of Slags Used in the Continuous Casting of Steel: Part 1 Conventional Mould Powders. *ISIJ Internacional* **2016**, *56*, 1-13.
[37] Mills, K. C. Structure and properties used in the continuous casting of steel: Part 2 specialist mould powders. *ISIJ Internacional* **2016**, *56*, 14-23.
[38] Sajid, M., Bai, C., Aamir, M., You, Z., Yan, Z., Lv, X. Understanding the structure and structural effects on the properties of blast furnace slag (BFS). *ISIJ Internacional* **2019**, *59*, 1153-1166.

[39] Sohn, I., Wang, W., Matsuura, H., Tsukiashi, F., Min, D. J. Influence of TiO_2 on the Viscous Behavior of Calcium Silicate Melts Containing 17 mass% Al_2O_3 and 10 mass% MgO. *ISIJ Internacional* **2012**, *52*, 158-160.
[40] Wang, Z., Shu, Q., Chou, K. Structure of CaO-B_2O_3-SiO_2-TiO_2 Glasses: a Raman Spectral Study. *ISIJ Internacional* **2011**, *51*, 1021-1027.
[41] Wang, Z., Sun, Y., Sridrar, S., Zhang, M., Zhang, Z. Investigation on viscosity and nonisothermal crystallization behavior of P-bearing steelmaking slags with varying TiO_2 content. *Metallurgical and Materials Transactions B* **2016**.
[42] Zhang, G. H., Chou, K. C., Zhang, J. l. Influence of TiO_2 on viscosity of aluminosilicate melts. *Ironmaking and Steelmaking* **2014**, *41*, 47-50.
[43] Zhang, S., Zhang, X., Liu, W., Lv, X., Bai, C., Wang, L. Relationship between structure and viscosity of CaO-SiO_2-Al_2O_3-MgO-TiO_2 slag. *Journal of Non-Crystalline Solids* **2014**, *402*, 214-222.
[44] Ma, H., Jiao, K., Zhang, J. The influence of basicity and TiO_2 on the crystallization behavior of high Ti-bearing slags. *CrystEngComm* **2020**, *22*, 361-370.
[45] Turkdogan, E.T.: *Physicochemical properties of molten slags and glasses*; The Metal Society: London, 1983. pp. 201-208.
[46] Greegor, R. B., Lytle, F. W. Investigation of TiO_2-SiO_2 glasses by X-ray absorption spectroscopy. *Journal of Non-Crystalline Solids* **1983**, *55*, 27-43.
[47] Henderson, G. S., Liu, X., Fleet, M. E. A Ti *L*-edge X-ray absorption study of Ti-silicate glasses. *Physical Chemistry Minerals* **2002**, *29*, 32-42.
[48] Mysen, B. O., Nouville, D. Effect of temperture and TiO_2 content on the structure of $Na_2Si_2O_5$-$Na_2Ti_2O_5$ metls and glasses. *Geochimica et Cosmochimica Acta* **1995**, *59*, 325-342.
[49] Wang, Z., Sun, Y., Sridrar, S., Zhang, M., Zhang, Z. Investigation on Viscosity and Nonisothermal Crystallization Behavior of P-Bearing Steelmaking Slags with Varying TiO_2 content. *Metallurgical and Materials Transactions B* **2017**, *48*, 527-537.
[50] Nakada, H., Nagata, K. Crystallization of CaO-SiO_2-TiO_2 as a Candidate for Fluorine Free Mold Flux. *ISIJ International* **2006**, *46*, 441-449.
[51] Wang, Z., Shu, Q., Chou, K. Viscosity of Fluoride-Free Mold Fluxes Containing B_2O_3 and TiO_2. *Steel Research International* **2013**, *84*, 766-776.
[52] McRae, L. B., Pothas, E., Jochens, P. R., Howat, D. D. Physico-Chemical Properties of Titaniferous Slags. *Journal of the South African Institute of Mining and Metallurgy* **1969**, 577-594.
[53] Wen, G., Sridhar, S., Tang, P., Qi, X., Liu, Y. Development of Flouride-free Mold Powders for Peritectic Steel Slab Casting. *ISIJ International* **2007**, *47*, 117-1125.
[54] Qi, X., Wen, G., Tang, P. Investigation on heat transfer performance of fluoride-free and titanium-bearing mold fluxes. *Journal of Non-Crystalline Solids* **2008**, *354*, 5444-5425.
[55] Mills, K. C.: *Slag Atlas*; 2nd Edition ed.; Verlag Stahleisen GmbH Düsseldorf, 1995.
[56] Challerjee, A. M. Heterogeneous nucleation in the crystallization of high polymers from melt. University of Massachusset Anherst, 1974.
[57] Fokin, V. M., Zanotto, E. D., Yuritsyn, N. S., Schmelzer, J. W. P. Homogeneous crystal nucleation in silicate glasses: A 40 years perspective. *Journal of Non-Crystalline Solids* **2006**, *352*, 2681-2714.
[58] Park, J. H. Solidification structure of CaO-SiO_2-MgO-Al_2O_3 (-CaF_2) systems and computational phase equilibria: Crystallization of $MgAl_2O_4$ spinel. *Computer Coupling of Phase Diagrams and Thermochemistry* **2007**, *31*, 248-437.
[59] Park, J. H., Min, D. J., Song, H. S. Amphoteric Behavior of Alumina in Viscous Flow and Structure of CaO-SiO_2 (-MgO)-Al_2O_3 Slags. *Metallurgical and Materials Transactions B* **2004**, *35B*, 269-275.
[60] Lachmann, S., Scheller, P.: Effect of Al_2O_3 and CaF_2 on the solidification of mould slags and the heat transfer through slag films. In *VIII International Conference on Molten Slags, Fluxes and Salts*: Santiago, Chile, 2009; pp 1101-1110.
[61] Susa, M., Sasaki, K., Yamauchi, T., Watanabe, T., Endo, R., Hayashi, M., Hanao, M. Crystallization of silicate glasses and melts with chemical compositions in primary phase region of gehlenite. *ISIJ Internacional* **2020**, *60*, 58-64.

[62] Liu, H., Wen, G., Tang, P. Crystallization Behaviors of Mold Fluxes Containing Li_2O Using Single Hot Thermocouple Tecnhique. *ISIJ Internacional* **2009**, *49*, 843-850.
[63] He, S., Wang, Q., Xie, D., Xu, D., Li, Z. S., Mills, K. C. Solidification and crystallization properties of CaO-SiO_2-Na_2O based mold fluxes. *International Journal of Minerals, Metallurgy and Materials* **2009**, *16*, 261-264.
[64] Klug, J. L., Hagemann, R., Heck, N. C., Vilela, A. C. F., Heller, H.P., Scheller, P. R. Fluorie-Free Mould Powders for Slab Casting: Crystallitation Control in the CaO-SiO_2-TiO_2-Na_2O-Al_2O_3 System *Steel Research International* **2012**, *83*, 791-799.
[65] Yang, J., Zhang, J., Sasaki, Y., Ostrvski, O., Zhang, C., Cai, D., Kashiwaya, Y. Crystallization behavior and heat transfer of fluorine-free mold fluxes with different Na_2O concentration. *Metallurgical and Materials Transactions B* **2016**, *47*, 2447-2458.
[66] Zhang, S., Li, M., Zhu, L., Wang, Q., He, S., Wang, Q. Effect of substitution Na_2O for SiO_2 on the non-isothermal crystallization behavior of CaO-BaO-Al_2O_3 based mold fluxes for casting high Al steels. *Ceramics International* **2019**, *45*, 11296-11303.
[67] Choi, S., Lee, D., Shin, D., Choi, S. Properties of F-free glass system as a mold flux: viscosity, thermal conductivity and crystallization behavior. *Journal of Non-Crystalline Solids* **2004**, *345&346*, 157-160.
[68] Zhou, L., Wang, W., Wei, J., Lu, B. Effect of Na_2O and B_2O_3 on Heat Transfer Behavior of Low Fluorine Mold Flux for Casting Medium Carbon Steels. *ISIJ Internacional* **2013**, *53*, 665-672.
[69] Li, G., Wang, H., Dai, Q., Zhao, Y., Li, J. Physical Properties and Regulation Machanism of Fluoride-Free and Harmless B_2O_3-containing Mold Flux. *Journal of Iron and Steel Research, International* **2007**, *14*, 25-28.
[70] Shu, Q., Wang, Z., Klug, J. L., Chou, K., Scheller, P. R. Effects of B_2O_3 and TiO_2 on Crystallization Behavior of Slags in Al_2O_3-CaO-MgO-Na_2O-SiO_2 System. *Steel Research International* **2013**, *84*, 1138-1145.
[71] Zhang, L., Wang, W., Sohn, I. Crystallization behavior and structure analysis for molten CaO-SiO_2-B_2O_3 based fluorine-free mold fluxes. *Journal of Non-Crystalline Solids* **2019**, *511*, 41-49.
[72] Zhang, F., Chen, Y., Wang, Y., Dong, F., Wu, M. Influence of La_2O_3 on crystallization behavior of free-fluorine mould flux and heat transfer of slag films. *Journal of Rare Earths* **2011**, *29*, 173-177.
[73] Li, J., Xu, A., He, D., Yang, Q., Tian, N. Effect of FeO on the formation of spinel phase and chromium distribution in the CaO-SiO_2-MgO-Al_2O_3-Cr_2O_3 system. *International Journal of Minerals, Metallurgy and Materials* **2013**, *20*, 253-258.
[74] Lei, L., Xiuli, H., Mingduo, L., Di, Z. Effects of quartz on crystallization behavior of mold fluxes and microstructural characteristics of flux film. *Journal of Biomaterials & Functional Materials* **2018**, *16*, 3-9.
[75] Orrling, C., Sridhar, S., Cramb, A. W. *In situ* Observations and Thermal Analysis of Crystallization Phenomena in Mold Slags. *High Temperature Materials and Processes* **2001**, *20*, 195-199.
[76] Orrling, C. Crystallization Phenomena in Slags. Carnegie Mellon University, 2000.
[77] Liu, L., Hu, M., Bai, C., Lü, X., Xu, Y., Deng, Q. Effect of cooling rate on the crystallization behavior of perovskite in high titanium-bearing blast funance slag. *International Journal of Minerals, Metallurgy and Materials* **2014**, *21*, 1052-1061.
[78] Zheng, D., Li, J., Shi, C., Ju, J. Crystallization characteristics and in-mold performance of electroslag remelting-type TiO_2-bearing slag. *Metallurgical and Materials Transactions B* **2019**, *50*, 1148-1160.
[79] Gu, S., Wen, G., Ding, Z., Tang, P., Liu, Q. Effect of shear stress in the isothermal crystallization behavior of CaO-Al_2O_3-SiO_2-Na_2O-CaF_2 slags. *Materials* **2018**, *11*, 1085.
[80] Svensson, J., Bulgakova, N. M., Nerushev, O. A., Campbell, E. E. B. Marangoni effect in SiO_2 during field-directed chemical vapor deposition growth of carbon nanotubes. *Physical Review B* **2006**, *73*, 205413-205411 - 205413-205415.

[81] Kumar, V., Basu, B., Enger, S., Brenner, G., Durst, F. Role of Marangoni convection in Si-Czochralski melts, part I: 3D predictions without crystal. *Journal of Crystal Growth* **2003**, *235*, 142-154.
[82] Kashiwaya, Y., Cicutti, C. E., Cramb, A. W. An Investigation of the Crystallization of a Continuous Casting Mold Slag Using the Single Hot Thermocouple Technique. *ISIJ Internacional* **1998**, *38*, 357-365.
[83] Orrling, C., Cramb, A. W., Tilliander, A., Kashiwaya, Y. Obeservations of the Melting and Solidification Behavior of Mold Slags. *Iron & Steel Society* **2000**, *27*, 53-63.
[84] Zhou, L., Wang, W., Liu, R., Thomas, B. G. Computational Modeling of Temperature, Flow, and Crystallization of Mold Slag During Double Hot Thermocouple Technique Experiments. *Metallurgical and Materials Transactions B* **2013**, *44B*, 1264-1279.

2.4 Effect of Water Vapor on the Slags Behavior

2.4.1 Reaction of Gases with Slags, Glasses and Oxide Melts

In high temperature manufacturing processes that involve polymeric-oxide melts such as glass-forming melts and pyrometallurgical slags, gases are evolved from volatile components present in the bulk composition of these substances. These gases can react with gases present in the atmosphere and with the molten material itself, redissolving into the melt or released into the atmosphere. The atmospheric gases can also react directly with the polymeric melt by means of solubility of these gases in the molten slag or glass. From the steelmaker`s viewpoint, water vapor present in the atmosphere is the greater concern, since it is related to hydrogen pick-up by the steel and the occurrence of so-called hydrogen induced sticker breakout. Water vapor present in the atmosphere is dissolved into the slag and reacts with it and with volatiles released from the slag. In the case of mold powders, the presence of water strongly affects significant properties such as viscosity and crystallization tendency which are directly related to the lubrication and horizontal heat transfer at continuous casting mold level.

2.4.1.1 Water Solubility in Glasses, Slags and Silicate Melts

Water solubility in silicate melts and slags have been extensively investigated by diverse researchers [1-10]. From the steelmaker's viewpoint, the growing interest regarding water solubility has begun after the perception of detrimental effects on the mechanical properties of the steel due to hydrogen pick-up by the molten bath from the slag during steelmaking processes such as electric arc furnace (EAF). Walsh *et al*. [2] reported that hydrogen in steel originates from reactions between slag and water vapor present in the atmosphere. Later, this interest was extended to slags of several new pyrometallurgical processes known collectively as secondary steelmaking [11-13].

Studies carried out by Tomlinson [1], Russel [3] and Walsh *et al*. [2] regarding to the solubility of water in molten silicates and glasses found that water dissolves in these medias as H_2O instead H_2. The water solubility mechanisms are related to the degree of polymerization of the melt according to the reactions **2.28** – **2.31** [12]:

In polymerized melts (acidic),

$$\equiv Si - O - Si \equiv + H_2O = 2(\equiv Si - OH) : \boldsymbol{DEPOLYMERIZATION} \quad (\mathbf{2.28})$$

In depolymerized melts (basic)

$$\equiv Si - O - M - O - Si \equiv + H_2O = 2\,(\equiv Si - O - Si \equiv) + 2\,OH^- + M^{2+} : \boldsymbol{POLYMERIZATION} \quad (\mathbf{2.29})$$

or

$$\equiv Si - O - M - O - Si \equiv + H_2O =$$
$$2\,(\equiv Si - O - Si \equiv) + 2\,(\equiv Si - OH) + O^{2-} + M^{2+}: \boldsymbol{DEPOLYMERIZATION} \quad (\mathbf{2.30})$$

In highly depolymerized melts

$$H_2O + O^{2-} = 2\,OH^- \quad (\mathbf{2.31})$$

Based on the solubility mechanisms represented by **reactions (2.28)** – **(2.31)**, this empirical observation can be explained by means of a overall reaction (**Equation 2.32**):

$$(O^*) + H_2O = 2(OH^*) \quad \textbf{(2.32)}$$

where O^* represents double or single bonded oxygen, or O^{2-}, and OH^* is single boded to silicon or as free ion [14].

The solubility of water in silicate melts and slags is proportional to square root of the water vapor partial pressure. The proportional increase of water content in the melt with the square root of the partial pressure of H_2O has been confirmed by further studies [6,7,15,16], expressed by the following relationship:

$$(H_2O) = K.{p_{H_2O}}^{1/2} \quad \textbf{(2.33)}$$

where K is the equilibrium constant involving the activity coefficient of the OH^- ion and the activity of the oxygen ion, indicating the formation of two OH groups per molecule of H_2O. The equilibrium relation for reaction of water with silicate melts, slags or glasses can be represented by hydroxyl capacitiy (C_{OH}) [14] or water capacity (C_{H_2O}) [17] as follow

$$C_{OH} = C_{H_2O} = (ppm\ H_2O)/\left(\mathrm{p}_{H_2O}\right)^{1/2} \quad \textbf{(2.34)}$$

where p_{H_2O} is the water vapor partial pressure in *bar*. The C_{OH} represents the ability of a slag to absorb water and it is a function of the chemical composition, temperature and pressure (the last mainly in geological processes). Sommerville [18] reports hydroxyl capacity as a function of wt-% OH^* group, with its charge being dependent of the basicity of the environment, while ppm H_2O is used to determine the water capacity. For a better understanding of the literature data presented in this work, the author will adopt the notation C_{OH} as a measure of water solubility.

Water behaves as a very amphoteric oxide in polymeric melts, *i.e*. it will behave as a network former or network modifier, depending on the basicity of the slag. The water dissolution mechanism in the slag depends – due to its dual characteristic – on the degree of polymerization of the melt, working as an acidic or a basic oxide, according to the reactions (**2.28**) – (**2.31**) [14,19].

Water can occurs as hydroxyl ions bonded to the basic building blocks of the structure, or as molecular water (mostly at elevated pressures) dispersed in the interstices of the network [12,20]. The hydroxyl formed by reaction between atmospheric water vapor and the melt is very stable. Infrared spectroscopy measurements have been shown that much of dissolved water in volcanic and synthetic silicate glasses are in molecular form [21]. Stolper [22] proposed a model to predict the variations in the concentrations of molecular water and hydroxyl groups in melts as functions of the total dissolved water content, similar to those observed in glasses. The model relates the proportion of molecular water and hydroxyl groups in melts by the following reaction, which describes the homogeneous equilibrium between melt species:

$$H_2O_{molecular}(melt) + oxygen\ (melt) = 2OH\ (melt) \quad (2.35)$$

Being the solubility of molecular water in melts is described by the following reaction:

$$H_2O\ (vapor) = H_2O_{molecular}(melt) \quad (2.36)$$

As above mentioned, the presence of dissolved molecular water occurs predominantly at high pressure ranges. Since slags are processed at ambient conditions (pressure), molecular water dissolution is out of the scope of the present study.

2.4.1.2 Influence of Composition on Water Solubility

Water vapor is soluble in all aluminossilicates, phosphates, borates and other similar polymeric-oxide melts [14]. The solubility of water has been directly related to the basicity of melts, which is essentially a quantification of the non-bridging oxygen (NBO) present in the structure. Experimental data of water solubility in melt silicate, glasses and slags have been reported by several researches, with some referring to existence of a minimum in solubility, where the water content in the melt as a function of the basicity follows a parabolic shape. The position of the minimum of solubility– for some oxide system – lies at about unity basicity or near to the metasilicate composition (*e.g.* in **Figure 2.13**) [1-4,6-9,16,23-26]. For instance, the existence of a minimum of solubility for potassium borate and sodium borate system melts was reported; as for lithium borate melts, such minimum of solubility was not observed, considering the investigated composition range [16].

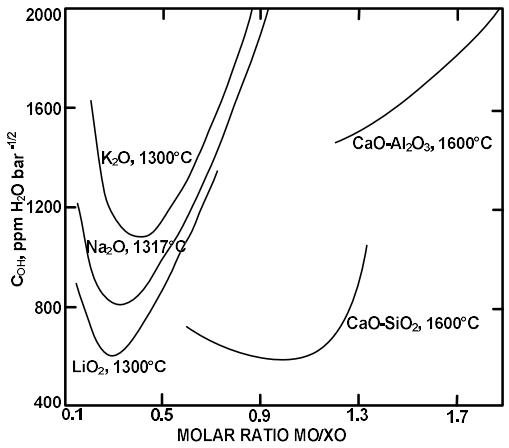

Figure 2.13 Hydroxyl capacity of molten silicate and aluminates as a function of basicity: M_2O-SiO_2 [27], CaO-Al_2O_3 [28] and CaO-SiO_2 [6]. Figure reproduced from [14].

Taking the minimum as a starting point, the solubility will increase with increasing basic or acidic character of the melt, a fact that characterizes the position of the minimum of solubility as a "neutral point" of an acidity-basicity scale. The position of the neutral point reported by Franz [16] varies for different alkali borate systems, which is in agreement with the increasing basicities of the alkali oxides in the aqueous solution ($Li_2O < Na_2O < K_2O$). However, the concept of basicity is somewhat questionable due to the high structural disruption of the melt, which constantly alters the concentration of the non-bridging oxygens [20] (see **Chapter 2**, **section 2.1.1.2**). In addition, due to difficulties related to the amphoteric character of some oxides, among other issues in the basicity determination, some authors have presented the

solubility of water in slags as a function of optical basicity [11,29]. Data from a large range of oxide systems [11,18] show the lowest water solubility values lie in a optical basicity range between 0.60 and 0.65, independently of temperature for a range of 1375 – 1600°C. The solubility of water in silicates melts increases with increasing alkali oxide content. However, addition of alkali earth oxides will either increase or decrease water solubility, according to its role in the structure of the glass. If the alkali earth oxide replaces silica, it will increase the solubility, but will decrease water solubility if the alkaline earth oxide replaces an alkali oxide. For instance, in the case of borate and germanate melts, addition of alkali oxides decrease the water solubility [20]. Study performed by Iguchi *et al*. [4] regarding to the effect of different oxide additions on the water solubility of $CaO\text{-}SiO_2$ system shows a markedly decrease in water solubility with TiO_2 addition, as can be seen in **Figure 2.14**.

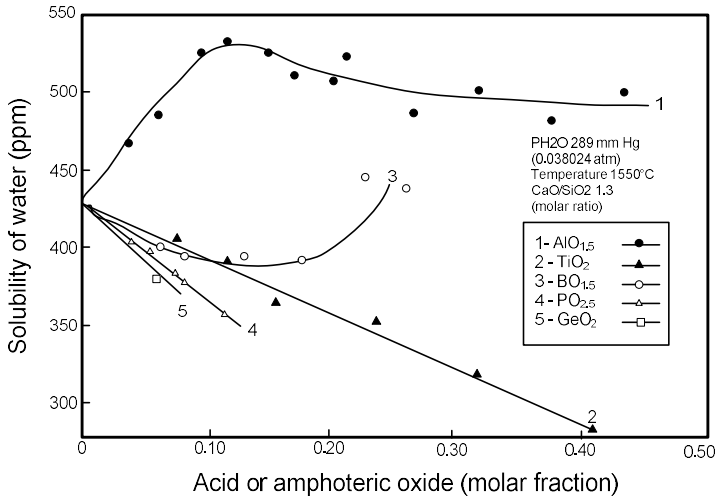

Figure 2.14 Effect of different oxide additions on the water solubility of the $CaO\text{-}SiO_2$ system. Figure reproduced from Iguchi *et al*. [4].

Imai *et al*. [30] investigated the hydrogen equilibrium in the systems atmosphere-molten slag-molten steel using infrared spectra measurements carried out on the ternary and quaternary $CaO\text{-}SiO_2$-(mono, di, trivalent metal oxide) systems. They found that water vapor dissolves into molten slag as a free, hydrogen bonded and a strongly hydrogen bonded hydroxyl, as represented in the **Figure 2.15**.

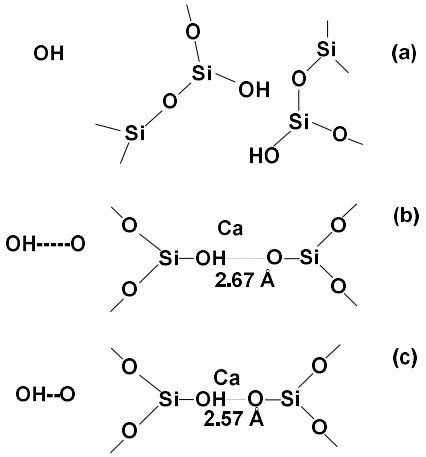

Figure 2.15 Three forms of hydroxyl: (a) free; (b) hydrogen bonded; and (c) strongly hydrogen bonded hydroxyl. Figure reproduced from Imai *et al*. [30].

Imai *et al.* [30] reported that the existence ratio of each form of hydroxyl to total amount of hydroxyl varies characteristically with the basicity of the slag (**Figure 2.16**). The results obtained by Imai *et al*. showed that the ratio of free hydroxyl form increases with increasing of ion-oxygen attraction force of M^{n+}, at the expense of the two other forms, which became smaller, for the $CaO\text{-}SiO_2\text{-}M_xO_y$ systems (where M_xO_y= Na_2O, BaO or Al_2O_3, 10 mol% each in the ternary systems or M_xO_y= 13 mol% MgO and 20 mol% Al_2O_3 in the quarternary system).

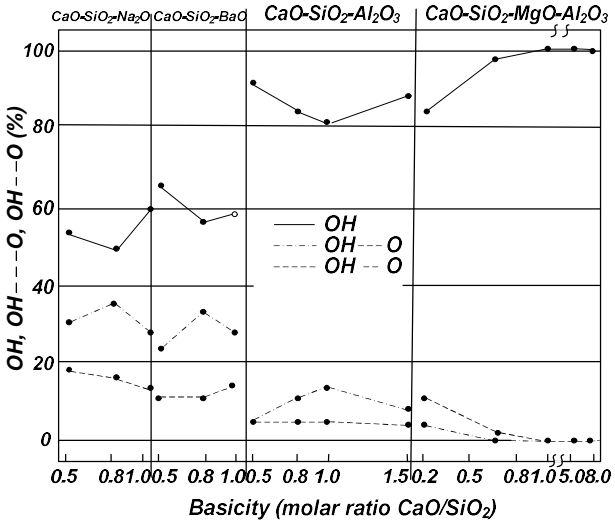

Figure 2.16 Variation of different water dissolved species as a function of basicity for the $CaO\text{-}SiO_2\text{-}Na_2O$, $CaO\text{-}SiO_2$-BaO, $CaO\text{-}SiO_2\text{-}Al_2O_3$ and $CaO\text{-}SiO_2\text{-}MgO\text{-}Al_2O_3$ systems [30].

Figure 2.17 shows an illustrative diagram of the influence of different metal cations on the ratio of the hydroxyl forms. As an example, the replacement of Na^+ with Mg^{2+} promotes a transition from bonded to free hydroxyl form. As previously mentioned, silicate melts are composed by different anionic structural units. The nature of the network-modifying cation has influence on the coexisting anionic species and on the portion of these units in the silicate melts [12,17,31]. However, such cations do not alter the overall degree of polymerization of the slag. The formation of the more extreme units as SiO_2 and SiO_4^{4-} are favored by small cations of high valence *e.g.* $Mg^{2+} > Ca^{2+} > Li^+ > Na^+ > K^+$ [17].

Schwerdtfeger *et al*. [6] investigated the water solubility in $CaO\text{-}Al_2O_3$ melts by applying the thermogravimetric method. An atmosphere consisting of Ar-H_2O mixture was used in the experiments by bubbling 140 ml/min of argon through a water column held at constant temperature in a thermostat. Water vapor pressures of 150, 338 and 600 mm Hg (0.2, 0.44 and 0.79 atm, respectively) were used. According to **Eq**. **2.33**, the equilibrium constant *K* is dependent on slag composition and increase with increasing CaO/Al_2O_3 ratio. The authors found that $CaO\text{-}Al_2O_3$ pick-up much more water than $CaO\text{-}SiO_2$ melts by a factor from two to three at 1600°C and at giving water vapor pressure (**Figure 2.18**).

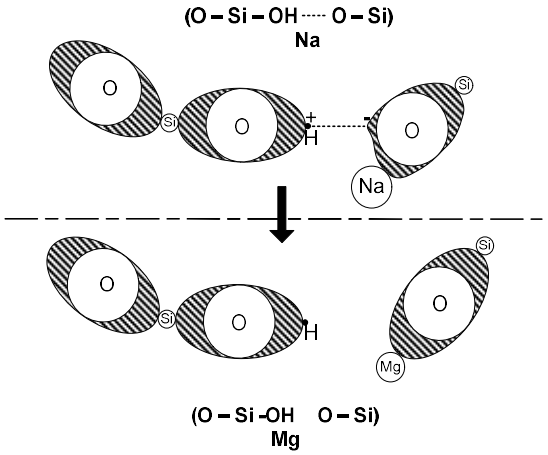

Figure 2.17 Transition of hydroxyl from hydrogen bonded form to free form. Figure reproduced from Imai *et al.* [30].

In a previous study, Sachdev *et al*. [7] observed a decrease in the water solubility of the CaO-SiO_2 system with addition of Al_2O_3, reaching a minimum of solubility for additions about 20 wt-% Al_2O_3 (at a constant basicity); while for higher Al content, the water solubility of lime-silica melts increases. An interesting result showed by Sachdev *et al.* is the relation between the water solubility and the oxygen density of the melt. The latter represents the absolute number of oxygen atoms – irrespective of their coordination number – and can be considered as a structural parameter. It was found an inverse proportionality between oxygen density and solubility of lime-silica-alumina melts.

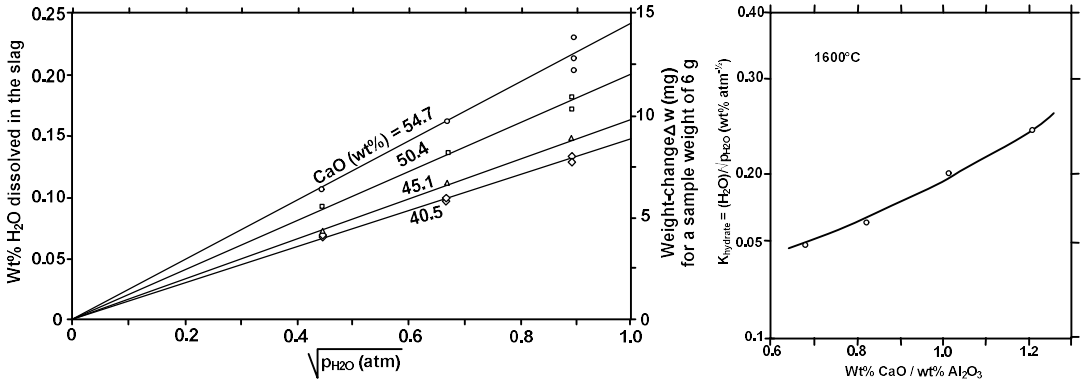

Figure 2.18 (a) Solubility of water in weight % as a function of water vapor partial pressure at 1600°C; (b) hydrate capacity as a function of CaO/Al_2O_3 ratio at 1600°C. Figure reproduced from [6].

Iguchi and co-workers [4,23] measured the hydroxyl capacities (C_{OH}) of CaO-SiO_2-MgO, CaO-SiO_2-TiO_2 and CaO-SiO_2-Al_2O_3 silicate melts at 0.375 bar H_2O and 1550°C. The results showed that the C_{OH} increases with increasing MgO in "detriment" of CaO content. The additive effect of Al_2O_3 on the solubility of water changes depending on the basicity of slag (CaO/SiO_2). In alumino-silicate melts, the hydroxyl capacity decreases in acidic composition, reaches a minimum, and then increases with increasing the CaO/Al_2O_3 ratio; however, aluminates dissolve more water than silicate melts (as can be seen in the **Fig. 2.13**). Additions of TiO_2, in turn, decrease the C_{OH} of the CaO-SiO_2 system. Beyond a determined amount, TiO_2 exhibits amphoteric nature in relation to the CaO-SiO_2 system and the minimum of

solubility is no longer observed with increase TiO_2 content [32]. In order to determine the water vapor dissolution in CaO-MgO-SiO_2 ternary and Al_2O_3-CaO-SiO_2-MgO quarternary systems, different techniques as thermogravimetric and inert gas fusion have been applied [8,25,33,34]. In all these works, the relation between water solubility and square root of partial pressure of water vapor has been confirmed.

Zuliani *et al.* [5,33] reported that the replacement of CaO by MgO had a negligible effect on the water vapor solubility in the slag. This result is adverse to that reported by Iguchi and Fuwa [23]. Study performed by Jo and Kim [34] using inter gas fusion pointed out the improvement of hydroxyl capacity in different Al_2O_3-CaO-SiO_2-MgO slag systems with MgO additions. It was concluded that hydroxyl capacity is independent on the relative amount of CaO and MgO in the slag and, therefore, the contribution of these oxides on the hydroxyl capacity are equivalent on molar basis. In addition, Al_2O_3 shows better effect on the hydroxyl capacity than SiO_2. Such effect of alumina on the C_{OH} is in accordance to those founded by Schwerdtfeger and Schubert [6] comparing the water solubility of CaO-Al_2O_3 and CaO-SiO_2 melts. Similar results were obtained by Brandberg *et al*. [25,35] for the Al_2O_3-CaO-SiO_2-MgO system using thermogravimetric technique. It was observed that C_{OH} does not vary substantially with composition. On the other hand, a considerable increase of hydroxyl capacity was noticed when the slag composition approaches CaO saturation.

Mathematical models and thermodynamic simulations have been performed to predict the water solubility in slag systems. Ban-ya *et al*. [19] estimated the hydroxyl capacity of Na_2O-SiO_2, Li_2O-SiO_2, CaO-SiO_2 binaries and CaO-SiO_2-Al_2O_3, CaO-SiO_2-MgO, CaO-SiO_2-MnO, and CaO-SiO_2-P_2O_5 ternaries slag systems by quadratic formalism based on the regular solution model. The dissolution of water in the CaO-MgO-Al_2O_3-SiO_2-FeO slag system was investigated by Jung [36] using a thermodynamic model and FACT oxide database. An important result pertinent to the present study shows that addition of MgO increases the water capacity in the CaO-SiO_2-Al_2O_3 system. Zorzato [37] studied the hydrogen pick-up of steel from water dissolved in CaO-SiO_2-Al_2O_3-MgO slag system using the thermodynamic software FactSage. The results showed an increase in water solubility with increasing CaO and MgO content for the slag systems investigated. Although these mathematical models and thermodynamic simulations showed good agreement with the literature, these methods to predict water capacity may show some limitations inherent to the reliability of thermodynamic database, in the case of *FactSage*, for instance.

2.4.1.3 Influence of the Structure on the Water Solubility

The relation between water solubility and structure of silicate melts and slags have been reported by some researchers [10,12,38,39]. The solubility mechanism of H_2O silicate melts was investigated by Mysen *et al.* [10]. Based on Raman spectra results of quenched silicate samples, it was suggested by the authors the existence of two different solubility mechanisms which are dependent of the presence or absence of non-bridging oxygen in the silicate melts.
The Raman spectra of different Na_2O-Al_2O_3-SiO_2 hydrous samples showed the existence of four structural units, namely: units involving only Si and OH, chain units without OH but with both Si and Al (were Al^{3+} must be locally charge-balanced with Na^+), a portion of the three-dimensional network units that is not affected by the presence of H_2O in the melt, and

the additional water dissolved as OH^-, locally charge-balanced by Na^+. This implicates that, in melt with three-dimensional network structure, water reacts with bridging oxygen to form two OH groups per broken oxygen bond. Some of this three-dimensional network is broken down to chain units, accompanied by the expulsion of Al^{3+} from tetrahedral coordination. In melts that have non-bridging oxygen (less polymerized), water reacts with both non-bridging and network modifiers to form Si-OH bonds and M(OH) and $M(OH)_2$ complexes – where M is a modifying cation. Solution of water in highly polymerized melts results in an increase of NBO/T. Mysen *et al.* [10] suggest that the crystal-liquid partition coefficient (wt-% of oxide in crystal/wt-% of oxide in liquid) will decrease with increasing H_2O content. The reason for this decrease occurs due to the formation of the less polymerized chain units in the melt. On the other hand, solution of water probably will decrease the NBO/T in melt with large NBO/T.

The relation between water content in silicate melts and its polymerization degree was also found by Deubener *et al*. [38]. They observed that the concentrations of OH in more depolymerized sodium trisilicate (NBO/T≈0.66) are significantly higher than in fully polymerized rhyolitic glass (NBO/T≈0). A quantitative study concerning the interaction of water with the structure of silicate glasses and melts was carried out by means examination of the structure of alkali (Li^+, Na^+, K^+) tetrasilicate glasses using Raman and ^{29}Si SP MAS NRM spectroscopy [39]. The authors concluded that the chemical composition of silicate melts affects the solution mechanisms of water, resulting in different effects on the melt structures at T_g; the alkali affects the speciation of dissolved water between H_2O_{mol} species and OH groups, as well as the bonding of the OH groups with the quenched melt structure. Variations in the solubility of water with ionic radius of the alkali in tetrasilicate melts were also reported, indicating that the solubility of water is affected by the interaction between the melt composition, water solution mechanism, and the melt structure. The effect of water vapor on the chemistry of ironmaking slags was investigated by Mohassab and Sohn [12] using reflection absorption spectroscopy (FTIR-RAS) and Raman analysis. Based on the spectroscopy and XRD analysis, it was concluded that water stabilizes the more polymerized silicate anions rather than the depolymerized monomers. The higher water content in the gas atmosphere the more polymerized the silicate in the slag.

Some parameters have been proposed as index to measure the water solubility in slags and silicate melts. Based on water vapor solubility measurements using a thermogravimetric technique, Sosinsky *et al.* [8] suggest the activity of SiO_2 as a parameter to evaluates the solubility of water in CaO-MgO-SiO_2 slag systems. Therefore, a relationship between water concentration in the slag phase and the activity of silica was developed in the form of the **Equation 2.37**.

$$H_2O_{,ppm} = \left(1095 - 2180a_{SiO_2} + 3146a_{SiO_2}^2 - 1365a_{SiO_2}^3\right)P_{H_2O}^{1/2} \quad (\mathbf{2.37})$$

where a_{SiO_2} is the silica activity. Other structural parameter which has been correlated to water solubility in slags is the optical basicity (Λ). The basicity indices have been empirically

derived, which involve an arbitrary decision as a component is an acidic or a basic oxide. This peculiarity of the basicity indices has been considered a problem, mainly for intermediate oxides such as TiO_2 [40]. In this context, the use of optical basicity as a water solubility index has been proposed to overcome such issue (for more detail about optical basicity see **Chapter 2, section 2.1.1.2**). Sosinsky [29] estimated the water capacity of CaO-MgO-SiO_2 slag system in terms of optical basicity, Λ, as derived from Pauling electronegativity by the **Equation 2.38**.

$$\log C_{H_2O} = 12.04 - 32.63\Lambda + 32.71\Lambda^2 - 6.62\Lambda^3 \quad (\mathbf{2.38})$$

The results showed good agreement with those reported by Zuliani [41] and with those from a previous Soinsky´s work [8]. Daya [11] proposes two different equations to estimate the water vapor capacity as a function of the optical basicity, according to the optical basicity range, namely: derived from Pauling eletronegativity for a range of 0.55 – 0.80, (**Equation 2.39**), and derived from Electron density for a range of 0.55 – 0.83 (**Equation 2.40**).

$$\log C_{H_2O} = 41.92 - 164.92\Lambda + 226.42\Lambda^2 - 100.31\Lambda^3 \quad (\mathbf{2.39})$$

$$\log C_{H_2O} = 30.47 - 116.26\Lambda + 159.18\Lambda^2 - 70.36\Lambda^3 \quad (\mathbf{2.40})$$

In terms of temperature, its effect on the water solubility shows some controversial results [42,43]; although a negligible effect of temperature on the water solubility for a range of 1400°C – 1600°C have been reported by some researchers [8,11,25,44].

2.4.1.4 Effect of Water on the Physicochemical Properties of the Slags, Melts and Glasses

The physicochemical properties of glasses are susceptible to changes in presence of water. Significant properties such as electrical conductivity, thermal expansion, refractive index, density and viscosity are strongly affected by melted glass-water reaction [9,45,46]. Shelby and McVay [47] found a decrease of the transformation range viscosity, the activation energy for viscous flow and the dilatometric critical temperature of sodium trisilicate glasses. Min'ko and Varavin [48] reported a strong effect of water on the technological and physicochemical properties of glass, even when only traces amounts of water are present (approximately 10^{-2} %). Changes in glass transition temperature T_g and viscosity have been reported by Shelby [20], Deubener *et al.* [38] and Hurley *et al.* [49]. For glass former oxides, the effect of water on T_g and viscosity is more pronounced. The T_g of glasses decreases with increasing water content and its intensity varies with the glass composition; for instance, the decreasing of T_g is much more effective in sodium silicates than in lithium borate glasses [20]. Deubener *et al.* [38] found that T_g decrease with increasing water content, and this effect is much more pronounced in silicates with the lowest water content where water entirely dissolves to hydroxyl. For water-rich melts, T_g decreases is more subtle.

A relationship between the effect of water on the T_g and the degree of polymerization of four different water-free glasses was reported by Bouhifd *et al.* [50]. It was found that the decrease in T_g due to the presence of water was more effective in the more polymerized melt (NBO/T = 0) than in those with lower polymerization degree (NBO/T = 0.19 and 0.21).

Reduction of viscosity of glasses and mold slags in presence of water has been discussed by Shelby [9,20] and Orrling *et al*. [51], respectively. Shelby attributed the strong effect of hydroxyl on the viscosity to the formation of additional non-bridging species in the network by conversion of bridging oxygens in non-bridging hydroxyls. Orriling *et al*. suggest – as will be seen further – that the increase of crystallization rate in presence of water probably occurs by reduction of the viscosity of the slag. According to the Stoke-Einstein relation (**Equation 2.41**), viscosity is inverse to diffusivity in slag melts

$$D_L = \frac{kT}{6\pi r} \tag{2.41}$$

where η represents the liquid viscosity. A decrease in viscosity implicates in an increase of the mass-transfer rate. However, the author points to an unavailability of viscosity data of system under humid atmosphere. According to Shelby [9], the diffusivity of water increases as viscosity decreases as a consequence of changes of the melt structure with increasing temperature. A study concerning the effect of atmosphere on the viscosity of coal slags was conducted by Hurley *et al.* [49]. Coal slag viscosity measurements were carried out in air and in an air + 10 % water vapor atmosphere. The presence of water do not changes significantly the viscosity and critical temperature (T_c) of the coal slag. However, it is possible observe that, for temperatures immediately below T_c, the viscosity of slag at humid atmosphere increase considerably compared to that measured in air atmosphere. This higher increase of viscosity may be related to an increase of crystallization rate attributed to the presence of water in the melt. Hurely *et al.* also reported that the effect of water on the T_c and viscosity is more substantial when measured in air + 10% water vapor in case of alumina addition, but less substantial in the case of magnesia additions (**Figure 2.19**).

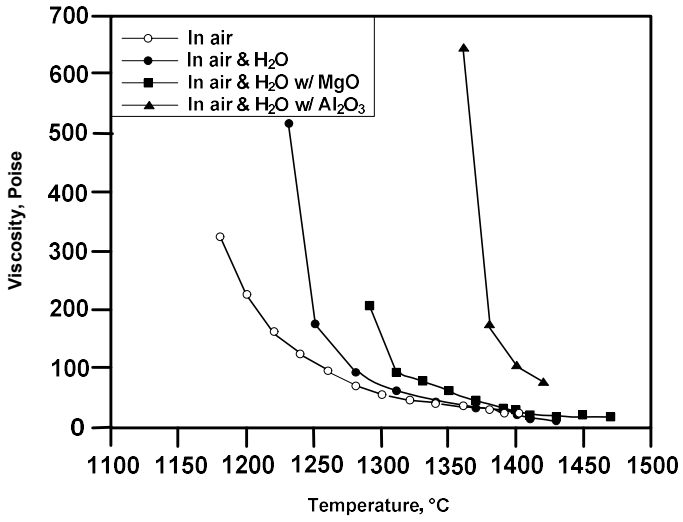

Figure 2.19 Effect of water and addition of Al_2O_3 and MgO on the viscosity of the coal slag in air. Figure adapted from [49].

More recently, the influence of water vapor on the viscosity behavior of coal slags was investigated by Cao *et al*. [52,53]. Small decrease in the viscosity and T_c in presence of water could be observed; however, its effect tends to increase with increasing water content. On the other hand, a slight increase in the viscosity at the same temperature and T_c was found for

high silicon-aluminum slags with increasing water vapor proportion. Mysen *et al*. [10] suggest that because H_2O in effect increases NBO/T in less polymerized melts, the viscosity of some geologic melt (*e.g.* picrite, komatiite and basanite composition) may increase as a result of the dissolution of water. This increase of viscosity in presence of water was also observed by Mohassab *et al.* [12] as a result of the increase of the degree of polymerization of silicate anions.

2.4.2 Effect of Water on the Crystallization Rate of Silicate Melts and Slags

Although there is a large number of studies concerning the water solubility in glasses, molten silicates and slags, few investigations regarding on the effect of water on the crystallization behavior of mold powders have been reported. The presence of hydroxyl group in oxide glasses and melts promotes the crystallization for melts which are already prone to crystallize [9,54]. According to Shelby [55], the increase of crystallization rate is a consequence of the decreasing in network connectivity, which is responsible to decrease of viscosity and glass temperature. The reaction between atmospheric water and oxide glasses results in the replacement of an oxygen atom occupying a vertex of silicon-oxygen tetrahedron by hydroxyl groups, decreasing the network connectivity [20,48]. According to Wagstaff and Richards [56,57], water tends to enhance the crystallization rate of silicate glasses in two different ways: (1) by acting as a source of oxygen, and (2) by weakening the glass structure through the reaction of [Si–O–Si] bonds with water to form [SiO–OH HO–Si] groups. In one of these studies, Wagstaff and Richards [56] examined the crystallization kinetics of stoichiometric vitreous silica in N_2, H_2O and vacuum atmospheres. The results point out to an enhancement of crystallization in presence of water vapor compared to nitrogen and vacuum atmospheres; the intrinsic crystallization rate measured in vacuum was much lower of the than the rates measured in either nitrogen or water vapor atmospheres (**Figure 2.20**(**a**)). The effect of water content on the crystal growth length of cristobalite with the time is shown in the **Figure 2.20**(**b**) [58].

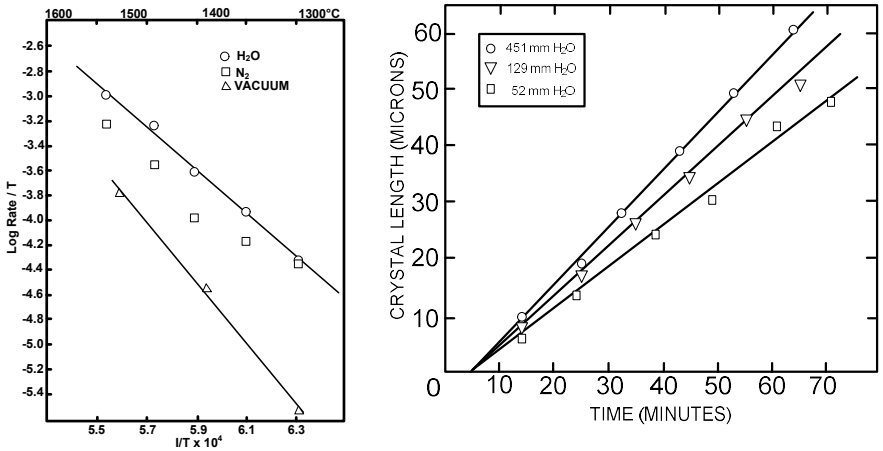

(a) **(b)**

Figure 2.20 (a) Comparison of crystallization rates of stoichiometric SiO_2 glass in different atmospheres, and (b) cristobalite crystal length as a function of time for different partial water vapor pressures. Figures adapted from [56] and [58], respectively.

There is a linear time dependence of all growth rates for stoichiometric vitreous silica in presence of H_2O-vapor; while an increase of the cristobalite thickness with increasing water vapor partial pressure could be also observed.

In order to determine the influence of water vapor on the crystallization behavior of CaO-Al_2O_3 join, TTT diagram was constructed from isothermal experiments results using the DHTT [59]. When in presence of humid atmosphere, the formation of crystals occurred at 1350°C and 1450°C, however, no crystallization was observed at these temperatures in dry atmosphere; in argon, the higher crystallization temperature lied between 1270°C and 1280°C. Such a behavior denotes that water do not only enhances crystallization as well as extend the crystallization temperature of the slag. Results from X-ray diffraction analysis of samples from continuous cooling experiments in argon and humid atmospheres showed change of the precipitated crystal phase in presence of water [59]. The phases $Ca_5Al_6O_{14}$ (major phase) and $Ca_3Al_2O_6$ (second phase) were found in samples cooled at $1°C.s^{-1}$ in argon atmosphere; while $Ca_{12}Al_{14}O_{33}$ (mayenite) was detected for the same cooling rate of samples exposed to water vapor atmosphere. According to the CaO-Al_2O_3 phase diagram (see ***Slag Altlas*** [17], page 39) the expected phases for the referred composition are $Ca_{12}Al_{14}O_{33}$, $CaAl_2O_4$ and $Ca_3Al_2O_6$. The same crystal phase change was also observed in samples submitted to isothermal experiments. For the sample held at 1200°C in argon, the crystalline phases were the same as those founded in the continuous cooling carried out in argon; on the other hand, for a sample held at 1400°C in a water vapor saturated atmosphere, the precipitated phases were determined as been $Ca_3Al_2O_6$ and $CaAlO_4$. According to the author, the presence of only 0.04 % H_2O in the slag melt is enough to change which phase is the most favorable to precipitate. However, it is unlikely that such water concentration could promote significant structural changes in order to alter the viscosity of the molten slag.

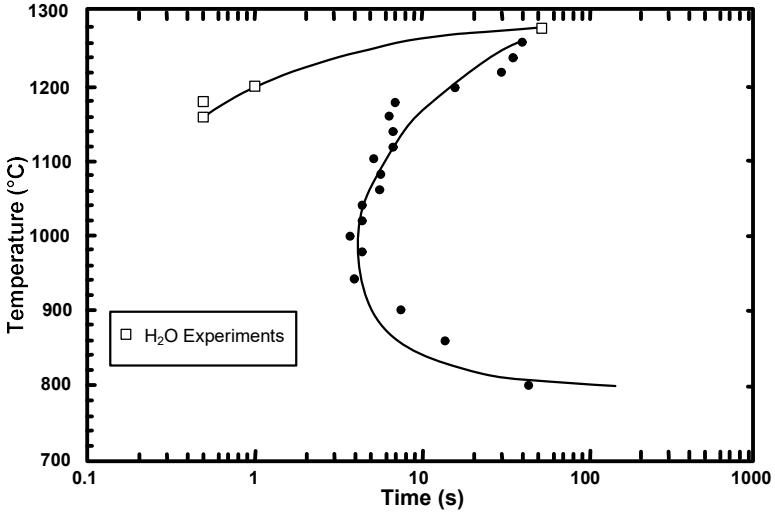

Figure 2.21 Isothermal experiment results in dry atmosphere and humid atmosphere [51].

According to Nurse *et al.* [60], the phase mayenite is stabilized by hydroxyl groups, being considered as a hydrate $Ca_{12}Al_{14}O_{32}(OH)_2$ that can't be found in the CaO-Al_2O_3 system; the phases $Ca_3Al_2O_6$ and $CaAlO_4$ were determined at 1400°C.

The effect of water on the crystallization behavior of more complex slag systems were also investigated by Orrling and Cramb [51] using the DHTT. Results from isothermal experiments for a CaO- SiO_2-Al_2O_3-Na_2O-CaF_2 slag exhibited strong effect of water on the nucleation rate and crystal growth rate. In the measurements carried out in water vapor atmosphere, the technique allowed to identify the start time of crystallization only at the temperatures of 1160°C, 1180°C and 1200°C. At lower temperatures, the crystallization started during the quench, about 1 s after the beginning of the experiment (**Figure 2.21**). A set of experiments was performed at 1280°C (20°C above the *liquidus* temperature measured in argon). An intermittent water vapor flux was applied as follow: water vapor was introduced 30 seconds before the beginning of the experiment and was turned off and on along the experiments [51]. Initially, the slag sample became fully crystalline right after crystallization started; and the crystal density was intense due to the faster crystal growth rate. In absense of water vapor, the crystals formed in humid atmosphere started to dissolves and the sample became liquid again. According to authors, the crystalline phase is stabilized by the presence of water, which promotes not only an increase in the nucleation and crystal growth rate, but also extends the thermal stability of the crystalline phase. After a determined time of the experiment, the water vapor was turned on again; however, the crystallization no longer occurred. Orrling and Cramb [51] suggest that the interaction of slag with water changes its chemical composition. This change in chemical composition is caused by the loss of fluorine and sodium due to vaporization of NaF promoted by the presence of H_2O in the atmosphere. Assuming the increase of the crystal density as an indicative of an increase in the nucleation rate, the authors suggested, based on the classical nucleation theory, that the presence of water must reduce the energy barrier for nucleation as a consequence either the reduction of interfacial energy between solid crystal and the liquid, or the reduction of the volume free energy change for precipitation (see **Chapter 2**, **section 2.2**,) [51,59].

In a previous study, Wagstaff and Richards [56] reported a decrease of the activation energy for crystallization of SiO_2 glass in presence of H_2O vapor. The heat of activation for growth of cristobalite from hydrous vitreous silica decreases markedly with increasing H_2O vapor concentration in atmosphere, from 134 kcal/mol to 77 kcal/mol. Li *et al*. [61] reported activation energy values of 408 kJ/mol and 529 kJ/mol for surface crystallization of cristobalite from fused silica powders heat-treated in air and nitrogen atmospheres, respectively. The authors attributed the lower activation energy to a decrease of oxygen vacancies due to reaction of the vacancies with O_2 and H_2O presents in the air. This decrease in the oxygen vacancies was considered beneficial to the nucleation of cristobalite on the surface of the SiO_2 powder.

The effect of water vapor on the crystallization behavior of CaO-Al_2O_3 and CaO-Al_2O_3-MgO slag systems was investigated by Prapakorn and Cramb [62,63] by means of DHTT. Results obtained from continuous cooling and isothermal experiments showed distinct effect of water vapor on the crystallization behavior for each system investigated. For the eutectic CaO-Al_2O_3 system, the position of TTT curves changes significantly toward higher temperatures and shorter incubation times, denoting the enhancement effect of water on the solidification behavior of the calcium aluminate system. For the CaO-Al_2O_3-MgO slag system, the

influence of humid atmosphere was subtle. According to the authors, the addition of MgO attenuates the effect of water vapor on the crystallization. For the MgO-bearing system, the crystallization at high temperatures was hindered in presence of water vapor. A similar behavior was found for continuous cooling experiments, where water tend to hinders the crystallization of $CaO-Al_2O_3$-MgO system for cooling rates equal or lower than 7 $°C.s^{-1}$. For higher cooling rates, the water vapor has no effect on the crystallization behavior as well as on the critical cooling rate.

In order to observe the influence of water vapor on the crystallization behavior of F-bearing and F-free mold powders, continuous cooling measurements were carried out by Beak *et al*. [64] using the SHTT. For the F-bearing mold powder, the change of the primary crystalline phase from cuspidine to Ca_2SiO_4 by increasing water vapor pressure was reported. The Ca_2SiO_4 has higher crystallization temperatures than that founded for cuspidine. The crystallization of F-bearing mold powder has been considerably accelerated by evaporation of fluorine as SiF_4. Such fluorine evaporation should be enhanced in presence of water vapor by the formation of hydrogen fluoride (HF). The authors conclude that the presence of water vapor enhances the melt crystallization of mold fluxes containing fluoride by acceleration of fluorine evaporation. The influence of water vapor on the crystallization behavior of F-free mold powders was reported as no significant.

More recent study has been pointed to an inhibitor effect of water vapor on the crystal growth for coal slags [52]. A decrease of the average particle size of solid phases with increasing water vapor proportion of the atmosphere was observed, suggesting that water impedes the growth of crystals. For high silicon-aluminum coal slags, the degree of polymerization is enhanced with increasing water vapor proportion, since the formation of Si-O-Si bridges and the transformation of $[AlO_6]^{9-}$ to $[AlO_4]^{5-}$ is favored by increasing water content [53]. In addition, the presence of water also promotes the crystallization and growth of crystals, differently from what was observed in the previous study.

References

[1] Tomlinson, J. W. A note of the solubility of water in a molten sodium silicate. *Journal of Society Glass Technology* **1956**, *40*, 25T-31T.
[2] Walsh, J. H., Chipman, J., King, T. B., Grant, N. J. Hydrogen in Steelmaking Slags. *Journal of Metals - Transactions AIME* **1956**, 1568-1576.
[3] Russell, L. E. Solubility of Water in Molten Glass. *Journal of Society Glass Technology* **1955**, *41*, 304T-317T.
[4] Iguchi, Y., Ban-Ya, S., Fuwa, T. The Solubility of Water in Liquid $CaO-SiO_2$, with Al_2O_3, TiO_2 and FeO at 1550°C. *Transactions ISIJ* **1969**, *9*.
[5] Zuliani, D. J., Iwase, M., McLean, A. The Thermodynamics of Water Vapour Dissolution in $CaO-MgO-SiO_2$ Slags. *Trans. ISIJ* **1982**, *1*, 61-67.
[6] Schwerdtfeger, K., Schubert, H. G. Solubility of Water in $CaO-Al_2O_3$ Melts at 1600°C. *Metallurgical Transactions B* **1978**, *9B*, 143-144.
[7] Sachdev, P. L., Majdic, A., Schenck, H. Solubility of Water in Lime-Alumina-Silica Melts. *Metallurgical Transactions* **1972**, *3*, 1537-1543.

[8] Sosinsky, D. J., Maeda, M., McLean, A. Determination and Prediction of Water Vapor Solubilities in CaO-MgO-SiO_2 Slags. *Metallurgical Transactions B* **1985**, *16B*, 61-66.
[9] Shelby, J. E. Diffusion and solubility of water in alkali borates melts. *Physics and Chemistry of Glasses* **2003**, *44*, 106-112.
[10] Mysen, B. O., Virgo, D., Harrison, W. J., Scarfe, M. Solubility mechanisms of H_2O in silicate melts at high pressures and temperatures: a Raman spectroscopic study. *American Mineralogist* **1980**, *65*, 900-914.
[11] Daya, Z. A. The Thermodynamics of Water Vapour Dissolution in Tundish Fluxes. University of Toronto, 1997.
[12] Mohassab, Y., Sohn, H. Y. Analysis of Slag Chemistry by FTIR-RAS and Raman Spectroscopy: Effect of Water Vapor Content in H_2-H_2O-CO-CO_2 Mixtures Relevant to a Novel Geen Ironmaking Technology. *Steel Research International* **2014**, *85*.
[13] Mohassab, Y., Sohn, H. Y. The Effect of Water Vapor on O_2- Content in Ironmaking Slag. *Journal of Iron and Steel Research International* **2015**, *22*, 909-915.
[14] Turkdogan, E.T.: *Physicochemical properties of molten slags and glasses*; The Metal Society: London, 1983. pp. 201-208.
[15] Yokokawa, T. Gas solubilities in molten salts and silicates. *Pure & Applied Chemistry* **1986**, *58*, 1547-1552.
[16] Franz, H. Solubility of Water Vapor in Alkali Borates Melts. *Journal of American Ceramic Society* **1966**, *49*, 473-477.
[17] Mills, K. C.: *Slag Atlas*; 2nd Edition ed.; Verlag Stahleisen GmbH Düsseldorf, 1995.
[18] Sommerville, I. D.: The Capacities and Refining Capabilities of Metallurgical Salgs. In *Foudry Process: Their chemistry and physics*; Landefeld, S. K. C. F., Ed.; Plenum Press: New York, 1988; pp 101-119.
[19] Ban-Ya, S., Hino, M., Nagasaka, T. Estimation of Water Solubility in Molten Silicates by Quadratic Formalism Based on the Regular Solution Model. *ISIJ Internacional* **1993**, *33*, 12-19.
[20] Shelby, J. E.: *Introduction to Glass Science and Technology*; Second ed.; The Royal Society of Chemistry: Cambridge, 2005.
[21] Stolper, E. Water in silicate glasses: an infrared spectroscopy study. *Contributions to Mineralogy and Petrology* **1982**, *81*, 1-17.
[22] Stolper, E. The speciation of water in silicate melts. *Geochimica et Cosmochimica Acta* **1982**, *46*, 2609-2620.
[23] Iguchi, Y., Fuwa, T. The Solubility of Water in Liquid CaO-SiO_2-MgO, with and whitout "FeO" at 1550°C. *Transactions ISIJ* **1970**, *10*, 29-35.
[24] Iguchi, Y., Fuwa, T.: *Hydrogen in Liquid Silicates*; Editions Science et Industrie ed., 1972; Vol. 2. pp. 1-3.
[25] Brandberg, J., Sichen, D. Water Vapor Solubility in Ladle-Refining Slags. *Metallurgical and Materials Transactions B* **2006**, *37B*, 389-393.
[26] Fuwa, T., Ban-Ya, S., Fukushima, T., Iguchi, Y. The Solubility of Water in Liquid Silicate. *Tetsu-to-Hagané* **1967**, *53*, 91-100.
[27] Kurkjian, C. R., Russell, L. E. Solubility of water un molten alkali silicates. *Journal of Society Glass Technology* **1958**, *42*, 130-144T.
[28] Fukushima, T., Iguchi, Y., Ban-Ya, S., Fuwa, T. The Solubility of Water in the Liquid Silicate. *Trans ISIJ* **1966**, *6*, 19-26.
[29] Sosinsky, D. J, Sommerville, I. D., McLean, A.: Sulphide, Phosphate, Carbonate and Water Capacities of Metallurgical Slags. In *Process Technology Conference ISS-AIME*, 1986; Vol. 6; pp 697-703.

[30] Imai, M., Ooi, H., Emi, T. On Hydrogen Equilibria in the System Water Vapour-Molten Slag-Molten Iron. *Tetsu-to-Hagané* **1964**, *50*, 878-887.
[31] Mysen, B. O., Virgo, D., Scarfe, C. M. Relations between the anionic structure and viscosity of silicate melts - a Raman spectroscopic study. *American Mineralogist* **1980**, *65*, 690-710.
[32] Iwamoto, N. Gas Solubility of Slag. *Transactions JWRI* **1976**, *5*, 135-142.
[33] Zuliani, D. J., Iwase, M., McLean, A., Meadowcroft, T. R. An Experimental Study of the Kinetics and Thermodynamics of Water Vapour Dissolution in a $CaO-SiO_2-MgO$ Slag. *Canadian Metallurgical Quarterly* **1981**, *20*, 181-187.
[34] Jo, S-K., Kim, S-H. The Solubility of Water Vapour in $CaO-SiO_2-Al_2O_3-MgO$ Slag System. *Steel Research International* **2000**, *71*, 15-21.
[35] Brandberg, J. Solubility of hydrogen in slags and its impact on ladle refining. Royal Institute of Technology, 2006.
[36] Jung, I-H. Thermodynamic Modeling of Gas Solubility in Molten Slags (II) - Water. *ISIJ Internacional* **2006**, *46*, 1587-1593.
[37] Zorzato, M. G. Análise Termodinâmica da Incorporação da Hidrigênio pelo Aço Líquido através da Escória da Refino Secundário (portuguese). Universidade Federal do Rio Grande do Sul - UFRGS, 2013.
[38] Deubener, J., Müller, R., Behrens, H., Heide, G. Water and the glass transition temperature of silicate melts. *Journal of Non-Crystalline Solids* **2003**, *330*, 268-273.
[39] Le Losq, C., Mysen, B. O., Cody, G. D. Water and magmas: insights about the water solution mechanisms in alkali silicate melts from infrared, Raman and ^{29}Si solid-satate NMR strectroscopies. *Progress in Earth and Planetary Science* **2015**, *2*.
[40] Sommerville, I. D.: Foundry Processes. In *Their Chemistry and Physics*; 1 ed.; Springer US; pp 101-133.
[41] Zanotto, E. D., Sosinsky, D. J., McLean, A.: Thermodynamic and Kinetic Aspects of Water Vapour Dissolution in Molten $CaO-MgO-SiO_2$ Slags. In *2nd. International Symposium of Metallurgical Slags and Fluxes Met. Society AIME*, 1984; pp 625-642.
[42] Mysen, B. O. The Solubiity of H_2O and CO_2 Under Predicted Magma Genesis Conditiond and Some Prological and Geophysical Implications. *Reviews of Geophysics and Space Physics* **1977**, *15*, 351-361.
[43] Kennedy, G. C., Wasserburg, G. J., Heard, H. C. The upper three-phase region in the system SiO_2-H_2O. *American Journal of Science* **1962**, *260*, 501-521.
[44] Zuliani, D. J., Hasegawa, M., Heard, R. A., Sosinsky, D. J., McLean, A.: Hydrogen Dissolution Reactions and their Influence on the Production of Low Sulfur Steel. In *International Symposium of Physical Chemistry of Iron and Steelmaking*, 1982; pp l-40 - l-46.
[45] Abe, Y., Clark, D. E. Determination of combined water in glasses by infrared spectroscopy. *Journal of Materials Science Letters* **1990**, *9*, 244-245.
[46] Naraev, V. N. The Influence of Water on the Glass Properties. *Glass Physics and Chemistry* **2004**, *30*, 367-389.
[47] Shelby, J. E., McVay, G. L. Influence of water on the viscosity and thermal expansion of sodium trisilicate glasses. *Journal of Non-Crystalline Solids* **1976**, *20*, 439-449.
[48] Min'ko, N. I., Varavin, V. V. Effect of water in the structure and properties of glass (review). *Glass and Ceramics* **2007**, *64*, 71-74.
[49] Hurley, J. P., Watne, T. M., Nowok, J. W. The Effect of Atmosphere and Additives on Coal Slag Viscosity. 691-694.
[50] Bouhifd, M. A., Whittington, A., Roux, J., Richet, P. Effect of water on the heat capacity of polymerized aluminosilicate glasses and melts. *Geochimica et Cosmochimica Acta* **2006**, *70*, 711-722.

[51] Orrling, C., Cramb, A. W. The Effect of Water Vapor on Mold Slag Cristallization. *Metallurgical and Materials Transactions B* **2000**, *31B*, 403-406.
[52] Cao, X., Kong, L., Bai, J., Ge, Z., He, C., Li, H., Bai, Z., Li, W. Effect of water vapor on coal slag ash viscosity under gasification condition. *Fuel* **2019**, *237*, 18-27.
[53] Cao, X., Kong, L., Bai, J., Zhao, H., Ge, Z., Li, H., Bai, Z., Li, W. Effect of water vapor on viscosity behavior of coal slags with high silicon-aluminum level under gasification condition. *Fuel* **2020**, *260*.
[54] Shelby, J. E. A Limited Review of Water Diffusivity and Solubility in Glasses and Melts. *Journal of the American Ceramic Society* **2008**, *91*, 703-708.
[55] Shelby, J. E.: *Handbook of Gas Diffusion in Solids and Melts*; ASM International: Ohio, USA, 1996.
[56] Wagstaff, F. E., Richards, K. J. Kinetics of Crystallization of Stoichiometric SiO_2 Glass in H_2O Atmospheres. *Journal of American Ceramic Society* **1966**, *49*, 118-121.
[57] Wagstaff, F. E., Richards, K. J. Preparation and Crystallization Behavior of Oxygen-Deficient Vitreous Silica. *Journal of the American Ceramic Society* **1965**, *48*, 382-383.
[58] WagstafF, F. E., Brown, S. D., Cutler, I. B. The influence of H_2O and O_2 atmospheres in the crystallization of vitreous silica. *Physics and Chemistry of Glasses* **1964**, *5*, 76-81.
[59] Orrling, C. Crystallization Phenomena in Slags. Carnegie Mellon University, 2000.
[60] Nurse, R. W., Welch, J. H., Majumdar, A. J. The CaO-Al_2O_3 System in a Moisture-Free Atmosphere. *Trans. British Ceramic Society* **1965**, *64*, 409-418.
[61] Li, X., Yin, X., Zhang, L., He, S. The devitrification kinetics of silica powder heat-treated in different conditions. *Journal of Non-Crystalline Solids* **2008**, *354*, 3254-3259.
[62] Prapakorn, K., Cramb, A. W. Initial Solidification Behavior in Continuous Casting: The Effect of MgO on the Solidification Behavior of CaO-Al_2O_3 Based Slags. *MS&T* **2004**, 3-10.
[63] Prapakorn, K., Orrling, C., Cramb, A. W.: The Solidification Behavior of Calcium Aluminate in Dry and Wet Atmospheres. In *European Casting Conference*, 2002; Vol. 2; pp 733-742.
[64] Baek, J-Y., Cho, J-W., Kim, S-H. Effect of Water Vapor on Evaporation and Melt Crystallization of Mold Fluxes. *Metallurgical and Materials Transactions B* **2016**, *47B*, 32-36.

Chapter 3 – Experimental

3.1 Materials and Samples Preparation

In order to investigate the effect of water vapor on the crystallization behavior of mold powders, a set of binary, ternaries and quartenaries oxide systems were prepared based on commercial mold powders used in continuous casting practice. The mold powders were prepared by mixing of the pure raw materials SiO_2, Al_2O_3, TiO_2, MgO, and $CaCO_3$ as source of CaO. The components were chosen based on main constituents of usual industrial mold powders, where SiO_2, CaO, Al_2O_3 are the most abundant components. MgO is usually added either intentionally or as impurity from raw materials [1]. TiO_2 oxide has been added as a candidate to replace fluorine in the mold powder composition due to its effect on the viscosity and crystallization [2-4]. The nominal compositions of the slags are shown in **Table 3.1**.

Table 3.1 Nominal chemical compositions of the slag systems.

SLAG SYSTEM	WEIGHT (wt- %)					
	CaO	SiO_2	Al_2O_3	TiO_2	MgO	Basicity (CaO/SiO_2)
CA	50	-	50	-	-	1*
CSA_T	35	35	25	5	-	1
CSA_M	33	33	19	-	15	1
CSA_TM1	40	40	14	1	5	1
CSA_TM2	38	38	16.25	0.75	7	1
CSA_TM3	35	35	19.5	0.5	10	1

*The ratio CaO/Al_2O_3 was used as a parameter.

After mixing, the raw materials were pre-melted in an induction furnace and subsequently decarburized in a muffle furnace at 600°C during 6 hours. The final chemical composition of the slags was determined by means of X-ray fluorescence (XRF) analyses. Residual carbon content was analyzed by combustion infrared detection technique (LECO CS 244). The chemical compositions of the slag systems investigated in the crystallization measurements are shown in **Table 3.2**.

Table 3.2 Weight contents of oxides components of the slag systems after pre-melting and decarburization.

SLAG SYSTEM	WEIGHT (wt- %)								
	CaO	SiO_2	Al_2O_3	TiO_2	MgO	K_2O	P_2O_5	C**	Basicity (CaO/SiO_2)
CA	48.99	0.01	49.83	-	0.19	-	-	0.09	0.98*
CSA_T	35.56	35.21	25.33	4.95	0.10	0.01	0.01	0.02	1.01
CSA_M	33.75	33.89	19.69	0.02	13.4	-	-	0.02	1.00
CSA_TM1	39.07	40.24	14.23	0.99	4.60	-	-	0.03	0.97
CSA_TM2	39.00	38.44	16.44	0.77	6.35	0.02	-	0.04	1.01
CSA_TM3	36.01	35.29	19.94	0.53	9.13	0.02	-	0.03	1.02

* The ratio CaO/Al_2O_3 was used as a parameter.
** Average value.

3.2 Hot Thermocouple Technique (HTT) – Single (SHTT) and Double (DHTT)

3.2.1 Description of the Technique

The essence of Hot Thermocouple Technique (HTT) was first developed by Ordway [5] for the study of single crystal growth, followed by Welch [6] in 1950's. Since then, many adaptations and improvements in the electronic arrangement have been implemented to the technique by other researchers for different applications. At present, the HTT have been applied in the investigation of the crystallization behavior of slags, since it provides

advantages that fulfill the restrictions inherent to others techniques as the differential thermal analysis (DTA). The hot thermocouple technique allows to observe *in situ* the crystallization behavior of slag samples under determined temperature conditions [7]. This technique can be applied using a single thermocouple (SHTT) or two thermocouples (Double Hot Thermocouple Technique). In SHTT, the sample is placed on thermocouple tip and can be either submitted to heating/cooling rates with variable rates or be held at constant temperature. With the DHTT, temperature gradients can be applied keeping the thermocouples at different temperatures, simulating the conditions between steel shell and copper mold wall in continuous casting process. In this kind of configuration, the sample is placed between the two thermocouples. The **Figure 3.1** shows a schematic of both single and double techniques.

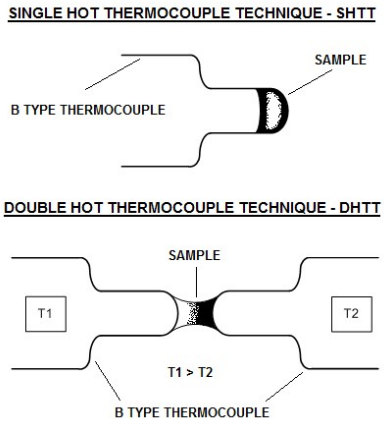

Figure 3.1 Illustration of the single and double hot thermocouple techniques.

Both single and double arrangements had low thermal inertia due the low mass of the system sample and thermocouple, easily allowing the application of high heating and cooling rates [8]. The HTT was basically developed from the principle of the hot stage microscope. **Figure 3.2** illustrates the scheme of the fast sequence of heating and measuring temperature of the HTT setup. Due to its high frequency, all this process gives the impression of simultaneous temperature measurement and control. The heating process is carried out conductively by means of an alternating electrical current with a wave being supplied by a diode. In this way, heating take place in the released half-wave and temperature measurement in the period of the suppressed half-wave. The "simultaneous" setting and measurement of temperature occurs at the welding point of the thermocouple (see **Figure 3.9**).

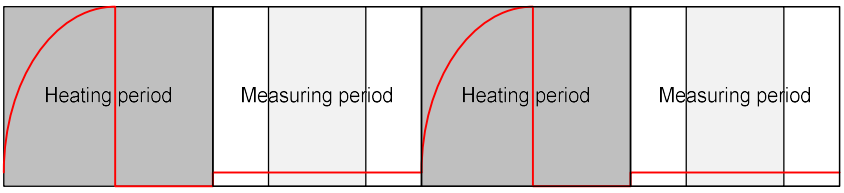

Figure 3.2 Schematic draw of principle of measurement of the HTT setup. Figure adapted from [9].

The cycle initially consists of a heating period followed by a measuring period. The high frequency of these processes gives the impression of simultaneous temperature measurement and control. More details concerning the development of HTT can be found in [10].

3.2.2 The HTT Setup

Figures 3.3 and **3.4** show a schematic view and a picture of the HTT setup at the *Institut für Eisen- und Stahltechnologie* (IEST) of the *Technische Universität Bergakademie Freiberg* (TUBAF), respectively. It includes a vacuum chamber with two water cooled inserts located diametrically opposed to each other (**Figure 3.5)**. The thermocouples are fixed at the end of inserts in a manner that your tips are situated inside an additional heating element. This element (*Kanthal* coil) aims to reduce the thermal losses from the sample to surrounding, reaching temperatures up to 1000°C. The heating and cooling process of each thermocouple is controlled independently. The HTT setup has an integrated observation system that includes a CCD camera connected to a computer, which allows to watch and register digital video images directly from the thermocouples in real time.

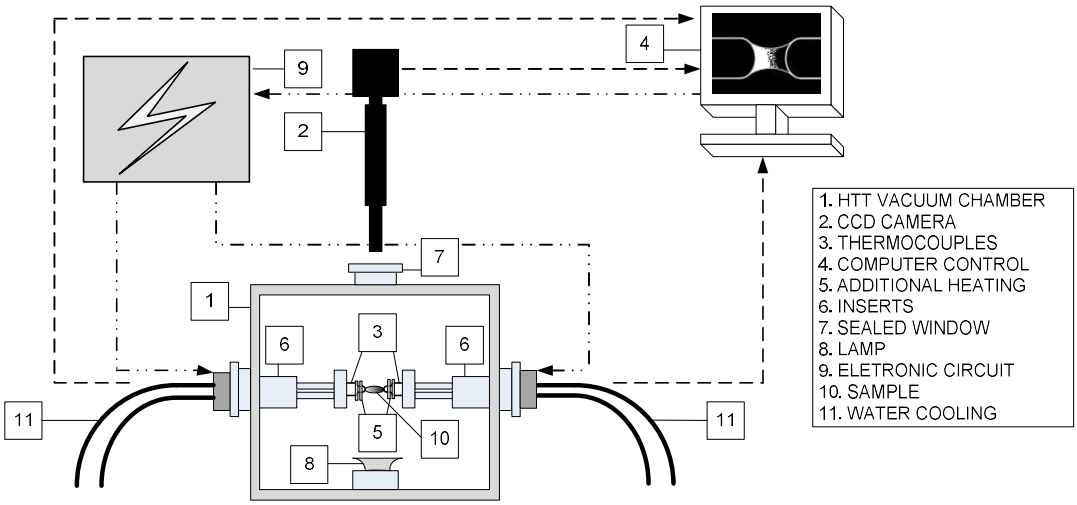

Figure 3.3 Schematic representation of the HTT set up at the Institute of Iron and Steel Technology of the *Technische Universität Bergakademie Freiberg* – Germany

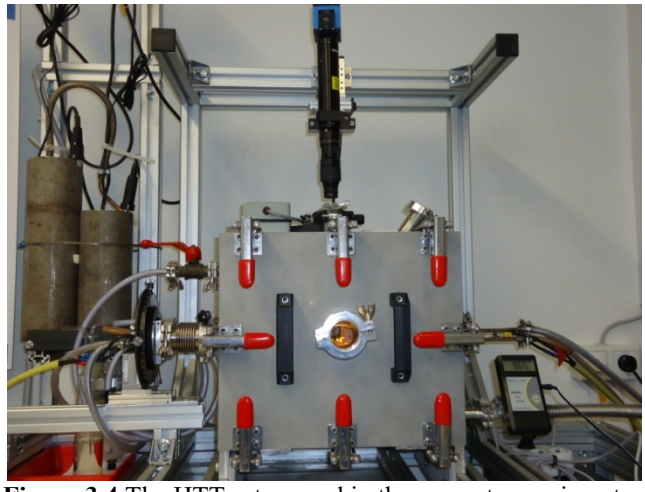

Figure 3.4 The HTT setup used in the present experiments.

The sample is melted directly at the thermocouple tip (or between the tips in DHTT measurements) and it can be subjected to defined cooling and heating conditions, enabling to apply heating and cooling rates up to 3000 °C.min^{-1}.

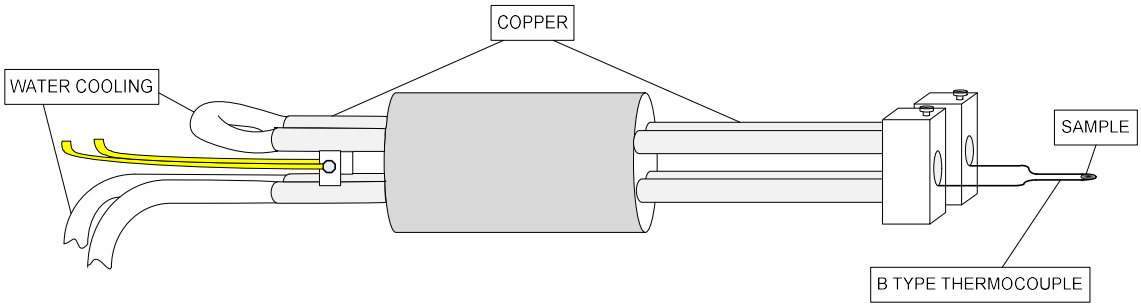

Figure 3.5 Schematic representation of HTT water cooled insert.

3.2.3 Experimental Procedures

The experiments were divided in two stages: (i) experiments with argon atmosphere (inert atmosphere), and (ii) experiments with humid atmosphere (reactive atmosphere). The first was conducted initially submitting the sample to vacuum (10 mbar) during 10 minutes; subsequently argon was admitted inside the chamber. The argon flux rate imposed in all measurements with inert atmosphere was 300 $l.h^{-1}$ (5000 $ml.min^{-1}$), and kept until the end of experiment. Experiments carried out with humid atmosphere followed the same vacuum time period (10 min), followed by insertion of a water vapor + argon gas mixture during 20 minutes before turn on the thermocouple. The flow rate used during experiments with water vapor atmosphere was lower than that used in the experiments carried out in argon atmosphere – approximately 19.8 $l.h^{-1}$ (330 $ml.min^{-1}$).

The crystallization behavior of the slags proposed were investigated based on visual observations of the beginning of crystallization, constructions and interpretation of their respective time-transformation-temperature (TTT) diagrams and continuous-cooling-transformation (CCT) diagrams, both obtained from measurement result with SHTT. **Figure 3.6** shows the thermo cycle applied in both experiments, inert and humid atmosphere.

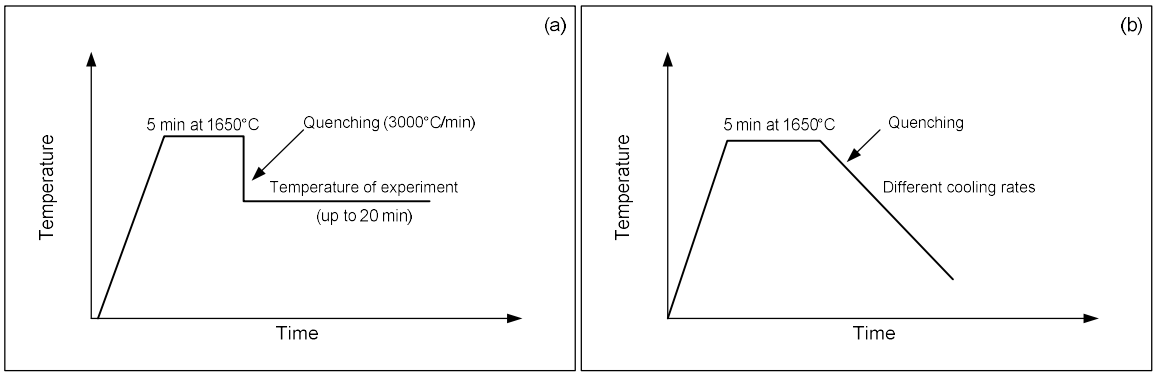

Figure 3.6 Thermal cycle applied to the mold powders samples in all SHTT experiments for (a) isothermal measurements and (b) continuous cooling measurements.

The continuous cooling experiments were conducted only in inert atmosphere, whereas the investigation of the effect of water vapor on the crystallization behavior was carried out only for isothermal measurements. In the both cases, samples between 5 and 10 mg are placed on the tip of the thermocouple (see **Figure 3.1**). The slag sample is subjected to a moderate heating rate (1.67°C.s^{-1}) until reaching 1650°C and retained at this temperature during 5 minutes to homogenization.

In the isothermal measurements, the sample was cooled at a high cooling rate about 50°C.s^{-1} up to a predetermined temperature and hold it at this temperature until the experimental time (time for crystallization observation) ends, which was stipulated as being 20 minutes. For the continuous cooling measurements, after the 5 minutes at 1650°C, different cooling rates were applied until 900°C (below this temperature, the visualization of any crystallization event becomes impaired).

The TTT diagrams were constructed taking the time at which the first trace of crystallization was able to be observed (incubation time) at each isothermal temperature. The same procedure was adopted for the CCT diagrams for each applied cooling rate. The measurements were reproduced circa 10 runs for each isothermal temperature or cooling rate. The total number of measurements per mold powder composition varies with the crystallization temperature range (for isothermal experiments) or with the cooling rate range.
All data obtained from *in situ* observation were statistically analyzed assuming the mean values and standard deviation as normal distribution. **Figure 3.7** shows a TTT curve of the CSA_TM2 mold powders with its respective mean and standard deviation.

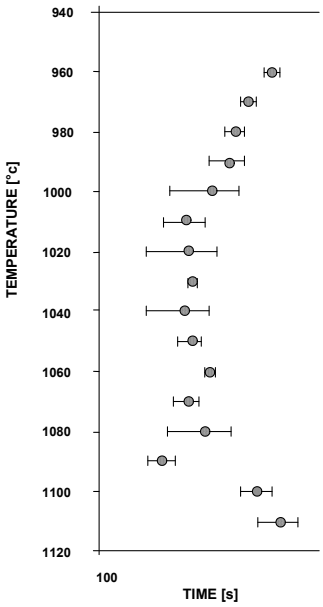

Figure 3.7 TTT curve of the CSA_TM2 mold powder from SHTT measurement in argon atmosphere. The statistical parameters of normal distribution (mean and standard deviation) are also exhibited.

3.2.4 Thermocouples Manufacturing

The experimental measurements were conducted using thermocouples type B (Pt30Rh and Pt6Rh for positive and negative components, respectively). The type B thermocouples are indicated for use in clean air, inert and oxidation atmospheres at a temperature range of 0 - 1820°C. These thermocouples are very stable, very reproducible, and are more reliable than the most other thermocouples, when properly used in uncontaminated oxidizing atmospheres. They are very highly resistant to oxidation and its maximum optimum temperature for prolonged operations is approximately 1700°C [11]. For the present study, thermocouples were constructed by means of cutting 0.5 mm diameter wires and 32 and 35 mm length for the positive and negative legs, respectively. After cutting, the wires tips, which will form the

contact junction, were polished to asseverate a good wire connection during welding process. **Figure 3.8** shows images of the thermocouple wires alignment and welding process.

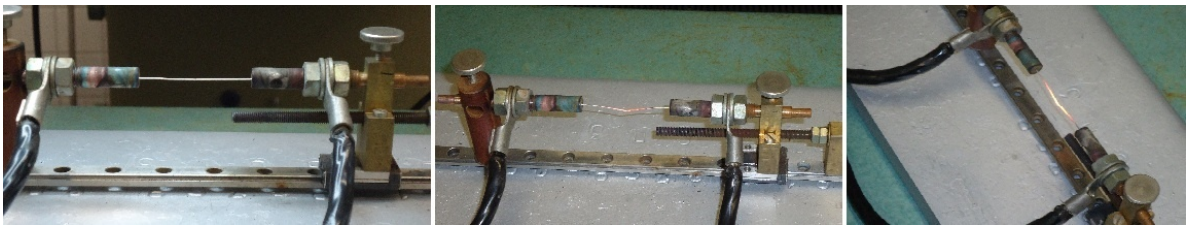

Figure 3.8 Thermocouple welding device. The images sequence: thermocouple wires alignment; star of welding process and; end of welding process.

The wires are fixed to copper supports tubes using a propane-butane torch at temperatures about 1925°C. The copper supports are connected to electrodes which enable to apply a voltage along the wires. The electrical current finds some resistance at the junction point due to the reduction of the contact area, leading to an increase of the temperature up to the wire melts, creating a junction welding point. **Figure 3.9** and **Figure 3.10** show a magnified image of the thermocouple tips during the alignment and welding process, and the final shape of the thermocouple, respectively.

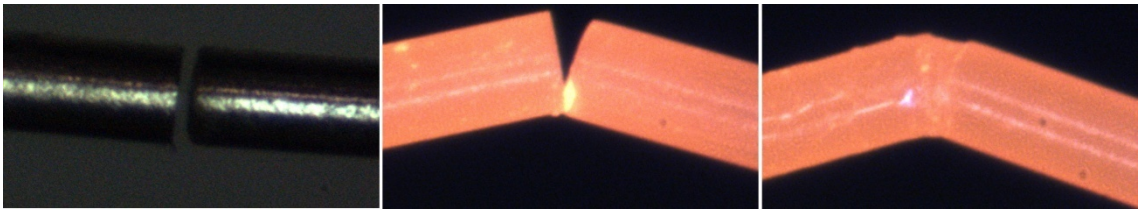

(a) **(b)** **(c)**

Figure 3.9 Thermocouples welding process: (a) wires alignment; (b) welding starting and; (c) welding ending.

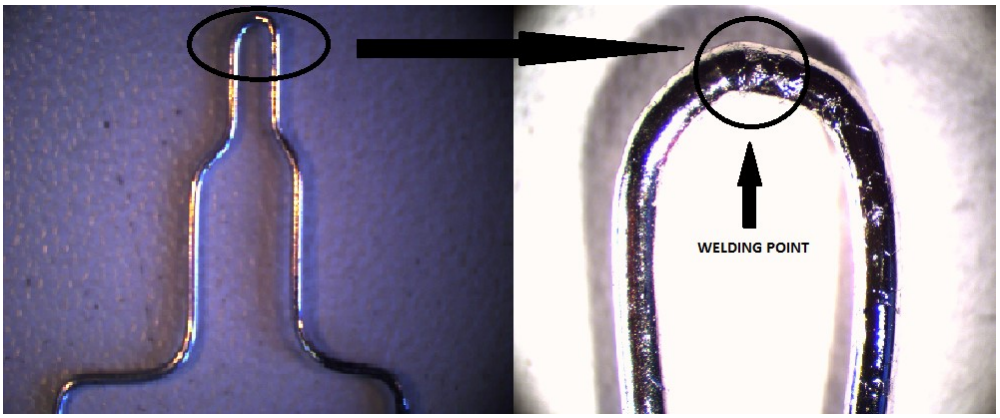

Figure 3.10 Final shape of the thermocouple and its welding point position.

3.3 Water Vapor Generation

The water vapor used during the SHTT analysis with humid atmosphere was generated by an apparatus according to **Figure 3.11**. The water vapor set consist in two cylinders: a presaturator and a condenser, both filled with water. Argon is injected in the presaturator through a copper coil tube immersed in the water column at a predetermined temperature (high temperature water). The argon gas is released at the water column bottom in a “trap” cylinder. It consists in an open bottom copper cylinder inserted in the center of the copper coil

as a core, with the opened part positioned exactly above the coil argon exit point. The copper coil tube works as a heat exchanger, allowing heating the argon flux at or next to the water temperature. As the argon flow ascends through the hot water, it is enriched with humidity. When the moisture-enriched argon emerges on the water surface inside the trap, it found an enclosed water vapor saturated atmosphere. Subsequently, humid argon follows to the condenser, where the excess of humidity present in the argon stream is retained. The water partial pressure is regulated by adjusting the temperature of water of the presaturator and condenser by means of two thermostats. Due to inertia of the system, the presaturator temperature was kept about 10°C above the desired saturation temperature. The water vapor partial pressure was controlled based on the thermodynamic data by adjusting the temperature of the condenser cylinder. To reach the desired water vapor partial pressure, the temperature difference between presaturator and condenser water was kept at maximum 25°C. In order to obtain the adequate water vapor partial pressure in equilibrium with the temperature of the condensation spiral tube, a low argon flow rate of 330 $ml.min^{-1}$ was admitted in the presaturator. The water vapor partial pressure control adopted in the present study was similar to that used by Orrling *et al.* [12] and Prapakorn *et al*. [13]. The partial water pressures applied on the crystallization measurements using the SHTT are listed in **Table 3.3**.

Table 3.3 Water vapor partial pressures of the argon + water vapor gas mixture applied in the experiments carried out in humid atmosphere.

	Water vapor partial pressure		Saturation temperature
Water vapor 1	3.384 kPa	0.0334 atm	26°C
Water vapor 2	12.349 kPa	0.1219 atm	50°C

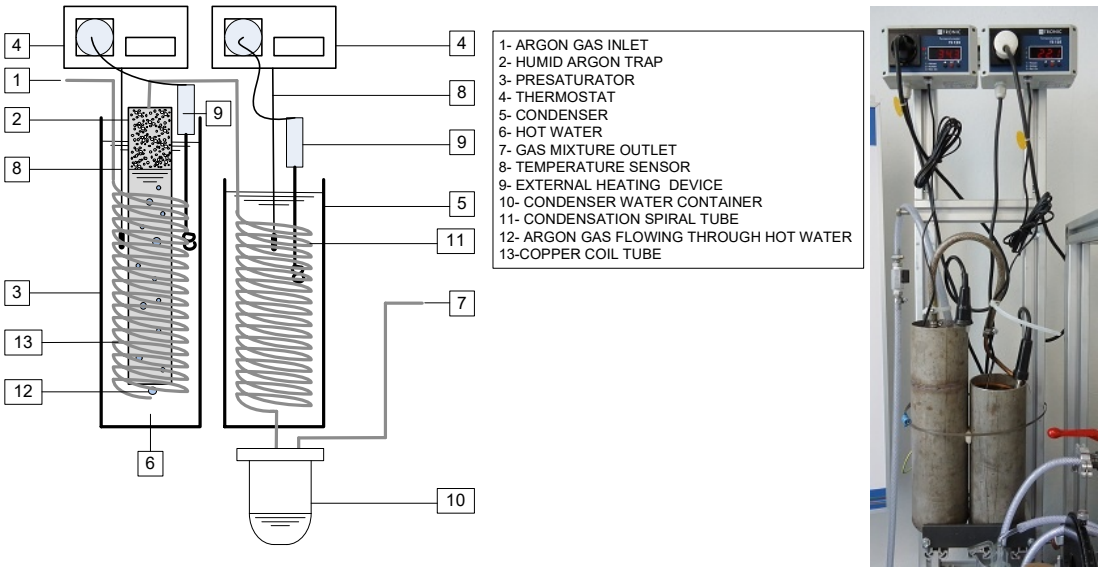

Figure 3.11 Water vapor generation system used during the SHTT experiments with humid atmosphere.

The high temperature around the thermocouples promotes an intense convective mass motion inside the HTT chamber. **Figure 3.12** shows a schematic illustration of the convective mass motion inside the HTT chamber. When the thermocouples are in operation, the water partial pressure in the region around the sample gradually falls due to the high temperature provided by the additional heating, the lamp (see **Fig. 3.13**) and mainly by the thermocouples.

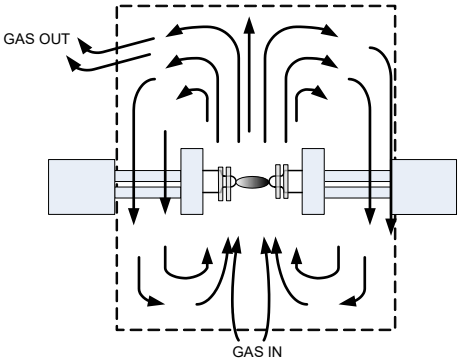

Figure 3.12 Gas-mass convection motion inside HTT chamber due high-temperature promoted by thermocouples.

Although the occurrence of natural convection is not favorable to reach an equilibrium temperature due to the generated instability, the ascendant mass convection was used as a "transport medium" to carry the humid argon closer to the sample. Aiming at controlling the air convection, a ceramic tube was positioned above the thermocouples to create a continuous humid stream flux passing through the sample, as showing in **Figure 3.13**. The ceramic tube works as a conductor of the ascendant gaseous mass. In order to ensure the desired water vapor partial pressure in the thermocouples region, a circular copper tube was positioned 5 cm below the thermocouple to inject the water vapor directly on the slag sample. At this position, the water vapor is carried by the ascendant convective mass, providing a water vapor flow with a controlled partial pressure around the slag samples.

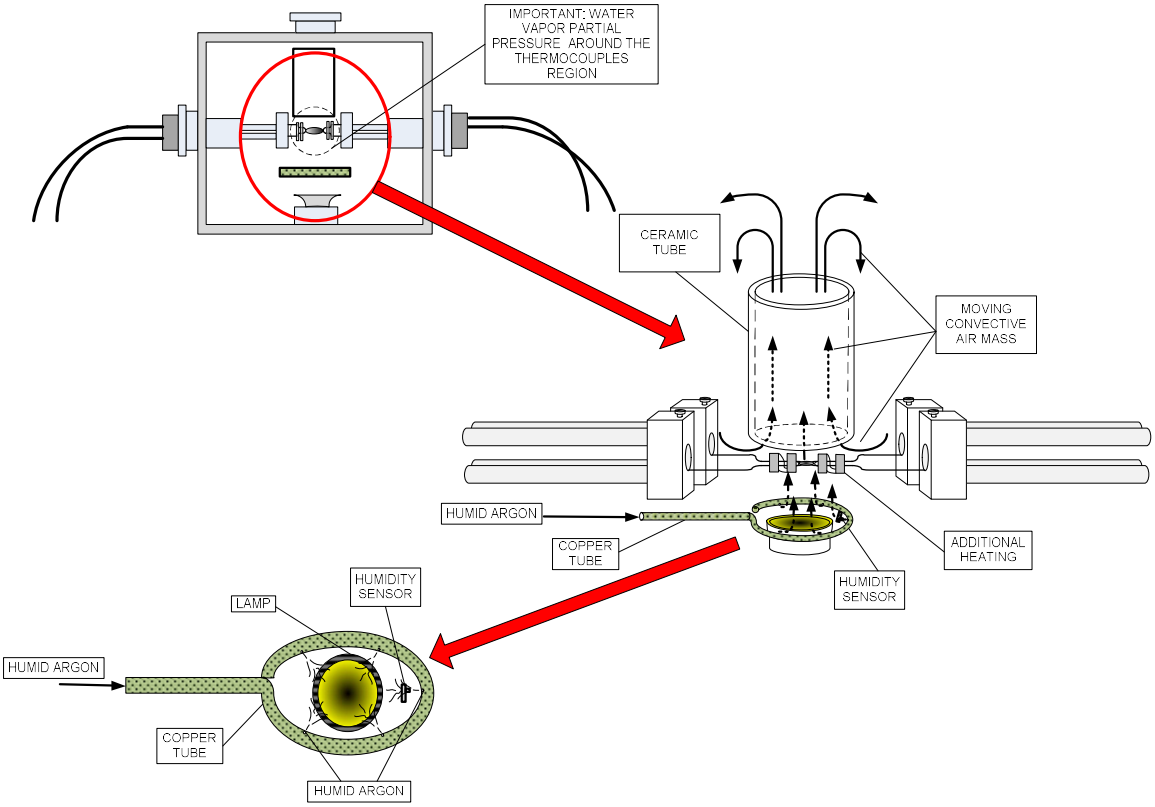

Figure 3.13 Schematic of the internal water vapor distribution setup in the HTT vacuum chamber.

3.3.1 Water Vapor Monitoring

The humidity content in the argon stream injected into the HTT chamber was continuously monitored using a hygro-thermometer positioned exactly before one of the five holes of the copper tube, distant 5 cm below and 5 cm right of the slag sample (see **Fig. 3.13**). The sensor was connected to software that allows recording several parameters such as relative and absolute humidity, saturation partial pressure, water partial pressure among others (**Figure 3.14**). The software provides information of the evolution of humidity every 2 seconds, allowing measuring the real water vapor partial pressure during the observation of the start of crystallization.

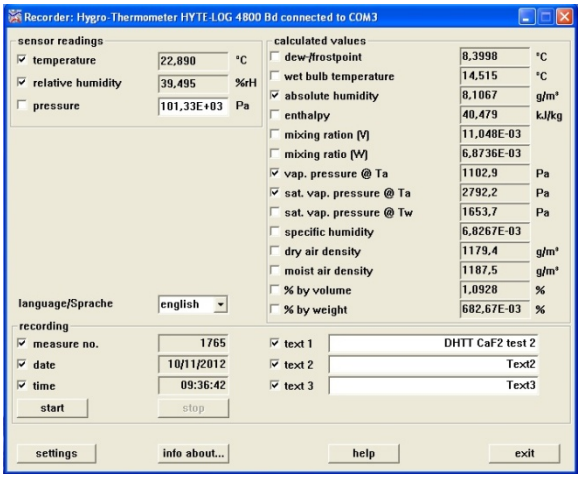

Figure 3.14 Display of the humidity sensor software interface with the respective parameters measured.

3.3.2 Water Vapor Partial Pressure – Preliminary Tests

In order to adjust the water vapor partial pressure, some preliminary crystallization measurements with water vapor atmosphere were carried out with CaF_2 using both thermocouples (DHTT). In these tests, a cooling rate of 5 °C.s^{-1} was applied for different water vapor partial pressures. The water vapor partial pressures were arbitrary chosen. Initially, the crystallization measurement was carried out with the water of the presaturator and condenser at room temperature. The water vapor partial pressure obtained was 0.00086 atm (0.086 % H_2O), which correspond to 100 % humidity at a saturation temperature of 4.08 °C. The temperature of presaturator was gradually increased and the argon flux was constantly adjusted up to attain a specified water partial pressure. In this way, was possible to verify the optimum temperature range between the presaturator and condenser. The others water vapor partial pressures applied in the preliminary tests were 0.01021atm (1.021 % H_2O) and 0.01464 atm (1.464 % H_2O) corresponding to 100 % humidity at, 7.34 °C and 12.82 °C, respectively. The same procedure was adopted in the crystallization measurements carried out in humid atmosphere in the present study. **Figure 3.15** shows the temperature and the time of crystallization as a function of the water vapor partial pressure. There is an evident increase of the temperature of crystallization and a decrease of the crystallization time with increasing water pressure. As shown in **Figure 3.16**, the sample becomes opaque in a short time range (in a few seconds); the sample opacity decrease with increasing water vapor partial pressure. This opacity can be caused by formation of calcium oxide according **Equation 3.1** [14].

$$(CaF_2) + H_2O_{(g)} = (CaO) + 2HF_{(g)} \quad \textbf{(3.1)}$$

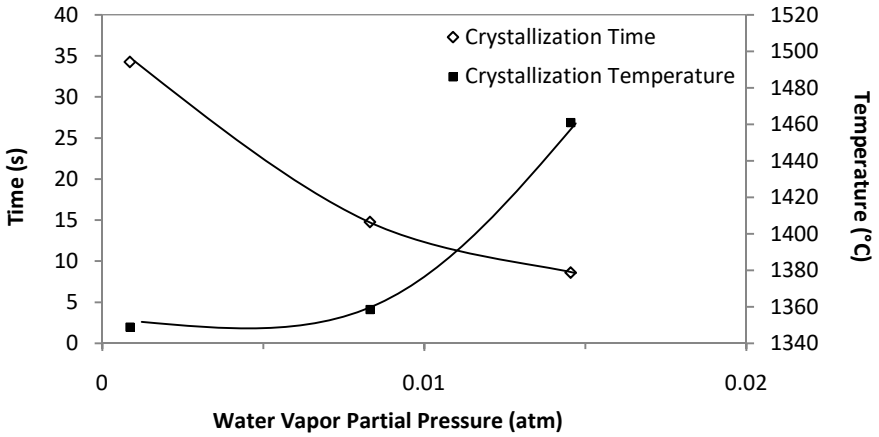

Figure 3.15 Crystallization temperature and crystallization time of CaF_2 sample as a function of the water vapor partial pressure.

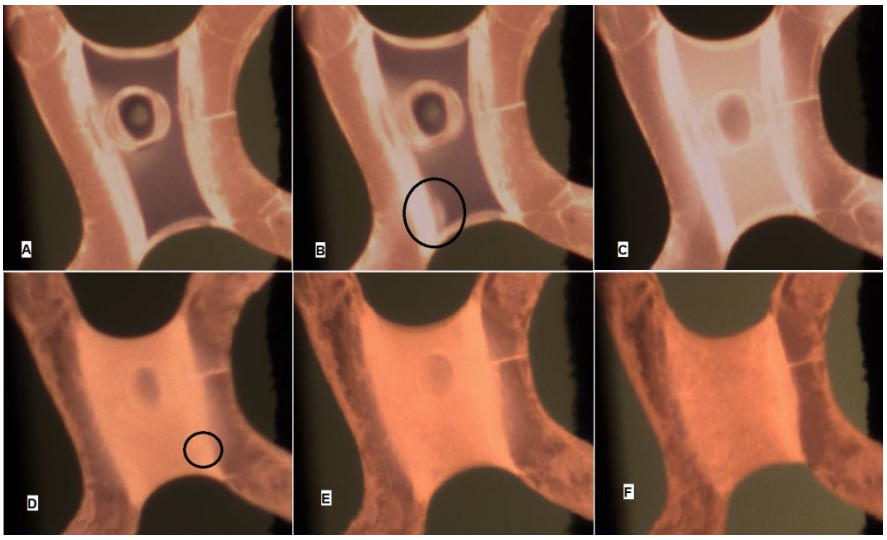

Figure 3.16 Images from preliminary crystallization tests of CaF_2 sample using the DHTT in humid vapor atmosphere. The images show the CaF_2 sample: (a) completely melted; (b) beginning of opacity; (c) sample full opaque; (d) start of crystallization; (e) sample partially crystallized and (f) sample fully crystallized.

Some results about the effect of atmospheric conditions on the crystallization behavior of CaF_2 samples were reported by Gusarova [9] and Klug [15] using the SHTT. The experiments were carry out exposing the sample to atmospheric air, however, no information about the water vapor partial pressure during the experiments were mentioned. There was the formation of several lumps on the thermocouple surface in presence of air. In addition, the mass of lumps increase with the time; after formed, it no was possible to melt them, even at high temperatures for a long time. Such lump is also attributed to the formation of CaO as described in **Equation 3.1.** Calcium oxide has an higher melting point (2572°C [16]) than calcium fluoride (between 1418°C and 1423°C [16,17]), which in turn is insoluble in water. According to the CaF_2-CaO phase diagram (**Figure 3.17**) the melting temperature increase sharply for CaO contents above 17 % mass.

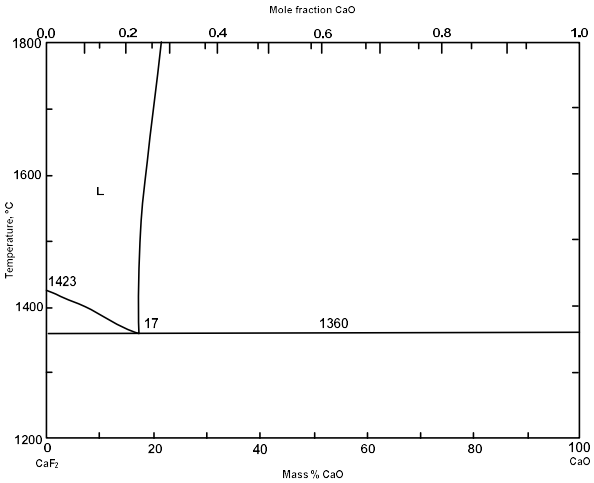

Figure 3.17 CaF_2-CaO phase diagram. Figure reproduced from [17].

Additional crystallization experiments with CaF_2 in humid atmosphere were carried out applying a thermal gradient and different water vapor partial pressures and in atmospheric air. In these pre-tests, a thermal gradient of 200°C was applied (left thermocouple: hot side; right thermocouple: cold side). The sample was placed at the tip of the both thermocouples – distant 0.5 mm to each other – and melted at 1520°C (approximately 100°C above the melting point); after the sample is completely melted, the temperature of the right thermocouple is cooled until 1320°C at a cooling rate of 1.67°C.s^{-1}. **Figure 3.18** shows images of the CaF_2 samples taken *in situ* at a temperature gradient and different water vapor partial pressures.

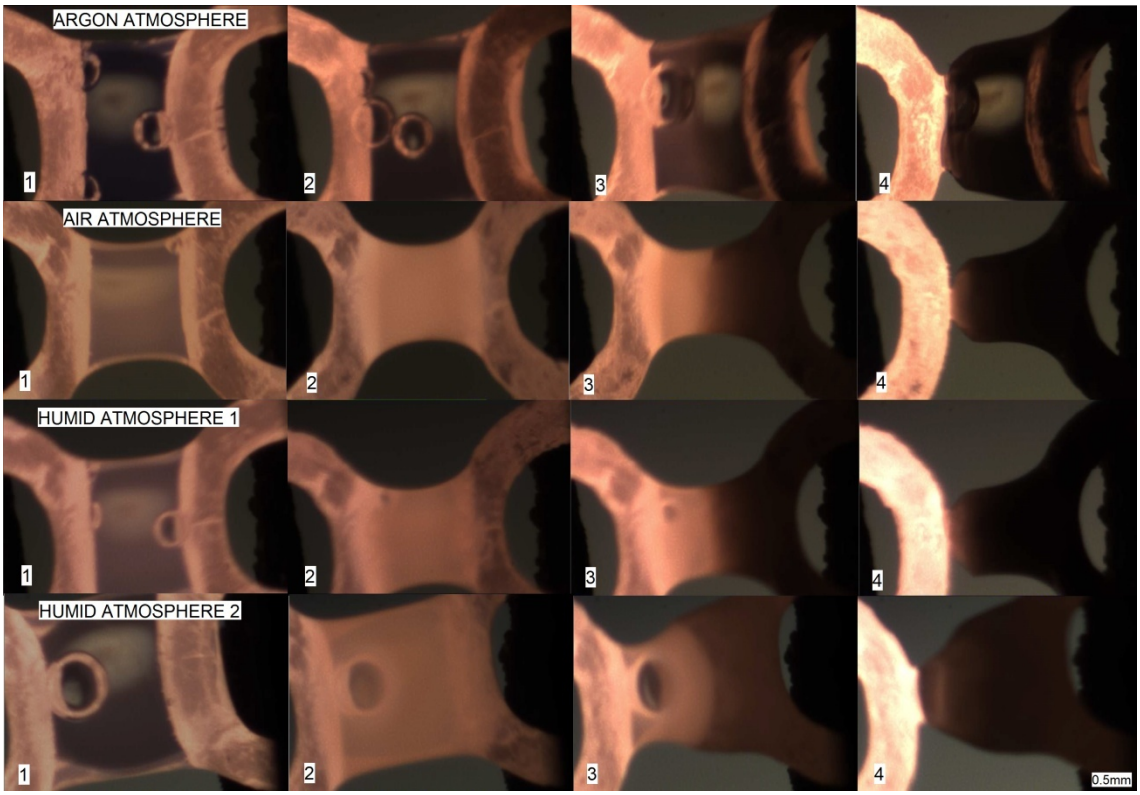

Figure 3.18 Crystallization progress comparison of the CaF_2 under a thermal gradient of 200°C and in different humidity atmosphere contents: (1) both thermocouples at 1520°C; (2) and (3) decrease of temperature of right thermocouple at 1.67°C.s^{-1}; (4) gradient temperature of 200°C already established.

Each number (1, 2, 3 and 4) in the image represents images taken at the same time for samples in atmospheres with different water vapor contents. The water vapor partial pressure used in the pre-tests with CaF_2 were the same used in the SHTT in humid atmosphere: argon atmosphere (0.0 % H_2O), air atmosphere (0.87 % H_2O - corresponding to a relative humidity of 34 % at 22°C); and humid atmosphere 1 and 2 corresponding to the 3.34 % H_2O and 12.19 % H_2O, respectively (see **Table 3.3**). The crystallization was improved in presence of humidity, increasing slightly with increasing water vapor partial pressure. The opacity of the sample was more intense for the sample exposed to air and decrease with increasing the water pressure. In contrast to the other atmospheric conditions, no bubbles were formed in the samples bulk.

3.4 Calibration

The calibration experiments were performed using CaF_2 (with 0.2% free Ca and 0.1% SiO_2) and Na_2SO_4 ($NaHSO_4$ as reagent grade) as standard samples. The melting temperature of the samples was taken by observation of the formation of the first liquid of the sample during the heating process at a rate of 0.5°C.s^{-1}. The melting point measurements were performed in argon atmosphere, preceded by vacuum during 30 minutes. An argon flow rate of 300 l.h^{-1} was applied along the measurements. According to the Slag Atlas [17] (phase diagram of Ca-CaF_2) the melting point of CaF_2 is 1423°C. Other literature sources report melting points of 1418 °C, 1403°C or even 1382°C to calcium fluoride [16,18,19]. In this case, a temperature range of 1418°C - 1423°C was assumed as a melting point region of CaF_2 for calibration purposes. The calibration measurements were carried out in both thermocouples (left and right); for the left side thermocouple (used in all SHTT experiments) 21 and 10 measurements were performed with CaF_2 and Na_2SO_4, respectively. For right side thermocouple, were carried out 8 measurements with CaF_2 and 10 measurements with Na_2SO_4. The melting point results with CaF_2 and Na_2SO_4 are shown in **Figure 3.19** and **Figure 3.20**, respectively.

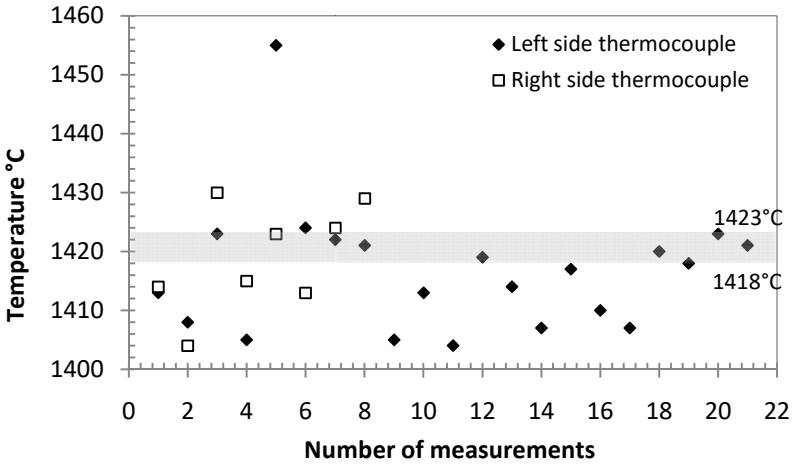

Figure 3.19 Melting point results of calibration measurements carried out with CaF_2.

The average values and its respective standard deviation are shown in the **Table 3.4**.

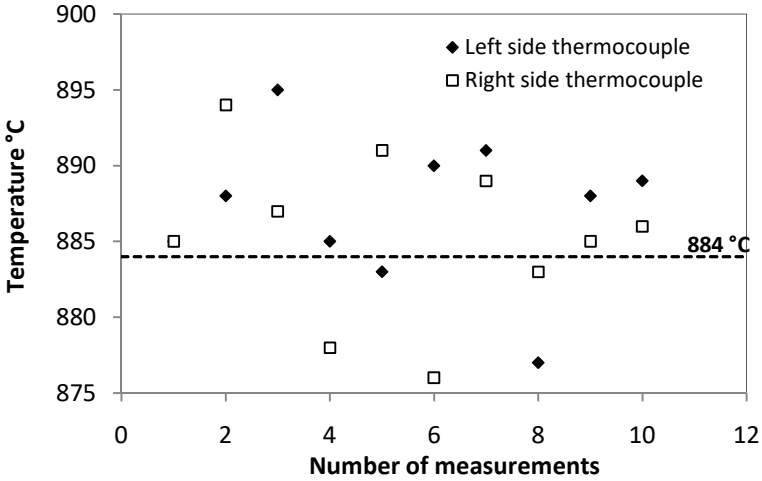

Figure 3.20 Melting point results of calibration measurements carried out with Na_2SO_4.

Table 3.4 Average melting point of CaF_2 and Na_2SO_4 calibration measurements.

Samples species	Left thermocouple measured m.p. (°C)	Left thermocouple standard deviation	Right thermocouple measured m.p. (°C)	Right thermocouple standard deviation	Literature melting point (°C)
CaF_2	1416.62	11.09	1419	8.97	1418-1423 [16,17]
Na_2SO_4	887.1	4.93	885.4	5.48	884 [16]

Figure 3.21 shows a deviation of the heat curve the calibration measurements with CaF_2 at a heating rate of 0.5°C/s for the left thermocouple. The curve was plotted taking the average time-temperature data; deviations at 1410°C and 1418°C can be clearly observed. Kashiwaya *et al.* [7] reported a deviation in the heating curve as occurred at 1423 °C for a average heating rate of 7.4 °C.s^{-1}. Taking the melting temperature range of CaF_2 founded in the literature as a standard, corroborated by the results reported by Kashiwaya *et al.*, the calibration results were considered in good agreement with the melting point range, 1480°C – 1423°C.

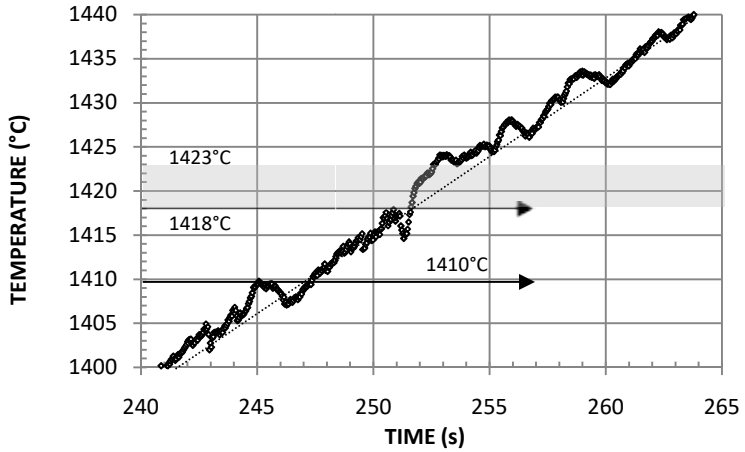

Figure 3.21 CaF_2 melting profile for a heating rate of 0.5 °C.s^{-1}.

A continuous cooling measurement using the CaO-Al_2O_3 binary system as standard was carried out and adopted as a complementary calibration measurement. The results were

compared with some data found in literature and shown in the **Appendix A** of the present study.

3.5 Viscosity Measurements

The viscosity of slag systems were measured using an Anton Paar MC 301 rheometer at the Technische Universität Bergakademie Freiberg, Germany. The samples were prepared by remelting the samples processed to SHTT experiments in a molybdenum crucible. This procedure was carry out with intent to remove some dissolved gases that could form bubbles during viscosity measurements, which can alters the final results. **Figure 3.2** shows a picture, an illustration of the viscometer as well as the geometrical parameters of the rotating bob and the crucible. Before start the heating processes and melting of the sample, the position of crucible and the centricity of the rotating bob are controlled and adjusted using a video recording and image processing [20].

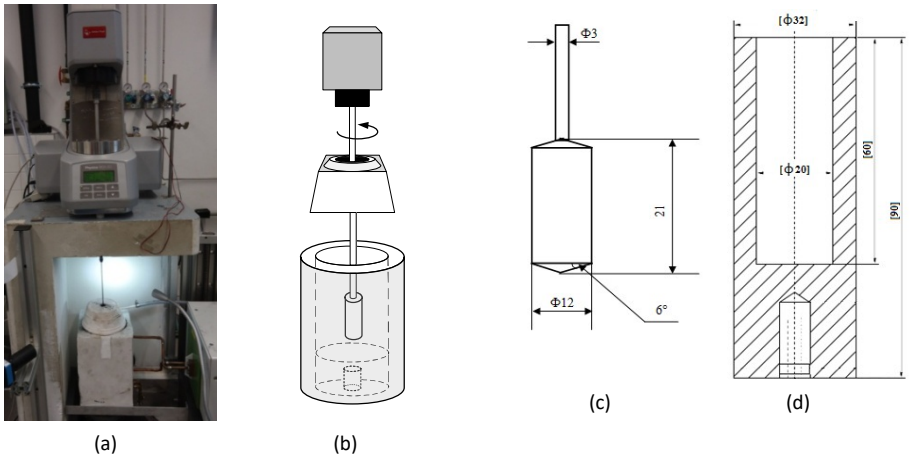

Figure 3.22 Experimental facility for viscosity measurements: (a) and (b) image and schematic draw of the viscometer, respectively; geometrical parameters of (c) the rotating bob and (d) the crucible. Letters (c) and (d) reproduced from [21].

The mold powders were melted in an induction furnace at 1600°C in Ar atmosphere. Subsequently, the molybdenum bob is slowly immersed in the crucible while the torque is measured. A cooling rate of 0.17°C.s^{-1} was applied with a molybdenum bob with a rotating speed of 15 rpm. The torque generated by the rotation of the bob is measured and converted to viscosity values by a computer system. The viscosity measurements were performed during the cooling cycle and interrupted when a torque of 200 µNm was exceeded.

References

[1] Yang, J., Zhang, J., Sasaki, Y., Ostrovski, Zhang, C., Cai, D., Kashiwaya, Y. Effect of MgO on crystallization and heat transfer of fluorie-free mold fluxes. *Metallurgical and Materials Transactions B* **2018**.

[2] Zhang, Z. T., Li, J., Liu, P. Crystallization Behavior in Fluorine-Free Mold Fluxes Containing TiO_2 / ZrO_2. *Journal of Iron and Steel Research International* **2011**, *18*, 31-37.

[3] Qi, X., Wen, G., Tang, P. Investigation on heat transfer performance of fluoride-free and titanium-bearing mold fluxes. *Journal of Non-Crystalline Solids* **2008**, *354*, 5444-5425.

[4] Yang, J., Zhang, J., Sasaki, Y., Ostrvski, O., Zhang, C., Cai, D., Kashiwaya, Y. *In-situ* Study of Crystallization Behavior of CaO-SiO_2-Na_2O-B_2O_3-TiO_2-Al_2O_3-MgO-Li_2O Fluorine-free Mould Fluxes with Different CaO/SiO_2 ratios. *ISIJ Internacional* **2016**, *56*, 574-583.
[5] Ordway, F. Techniques for growing and mounting small singles crystals of recfractory compounds. *Journal of Research of the National Bureau of Standards* **1952**, *48*, 152-158.
[6] Welch, J. H. A simple microscope attachment for observing high-temperature phenomena. *Journal of Scientific Instruments* **1954**, *31*, 458-462.
[7] Kashiwaya, Y., Cicutti, C. E., Cramb, A. W., Ishii, K. Development of Double and Single Hot Thermocouple Technique for *in Situ* Observation and Measurement of Mold Slag Crystallization. *ISIJ International* **1998**, *38*, 348-356.
[8] ORRLING, C., CRAMB, A. W., TILLIANDER, A., KASHIWAYA, Y. Observations of the Melting and Solidification of Mold Slags. *I&SM* **2000**, 53-63.
[9] Gusarova, T. Neue Meßmethod zur Qualitätsprüfung von metallurgischen Schlacken (german). Technische Universität Bergakademie Freiberg, 2005.
[10] Esfahani, S. Crystallization of synthetic blast furnace slag pertaining to heat recovery. University of Toronto, 2016.
[11] Pollock, D. D.: *Thermocouples: Theory and Properties*; CRC Press: Boca Raton, Florida, 1991.
[12] Orrling, C., Cramb, A. W. The Effect of Water Vapor on Mold Slag Cristallization. *Metallurgical and Materials Transactions B* **2000**, *31B*, 403-406.
[13] Prapakorn, K., Cramb, A. W. Initial Solidification Behavior in Continuous Casting: The Effect of MgO on the Solidification Behavior of CaO-Al_2O_3 Based Slags. *MS&T* **2004**, 3-10.
[14] Yuan-Sun, H., Yuan-Hsi, C., Fu-Lien, L. A study of the equilibrium between HF-H_2O gas and slags of the CaO-CaF_2 and CaO-SiO_2-CaF_2 system. *Acta Metallurgica Sinica* **1964**, *7*, 24-31.
[15] Klug, J. L. Crystallization control for fluorine-free slags using the Single Hot Thermocouple Technique. UFRGS-Brazil / TU Bergakademie Freiberg-Germany, 2012.
[16] Patnaik, P.: *Handbook of Inorganic Chemicals*; McGraw-Hill: New York, 2003.
[17] Mills, K. C.: *Slag Atlas*; 2nd Edition ed.; Verlag Stahleisen GmbH Düsseldorf, 1995.
[18] Falbe, J., Regitz, M.: *RÖMPP Chemie-Lexikon*; Thieme Georg Stuttgart - New York, 1996; Vol. 9.
[19] SCHACKELFORD, J. F., ALEXANDER, W.: *Materials Science and Engineering Handbook*; CRC Press, 2001.
[20] Heller, H. P., Schürmann, M., Scholl, K., Haustein, N., Lychatz,B., Falkus, J. Calibration problems with the viscosity measurements of liquid metallurgical slags. *Journal of Phyicas: Conference Series* **2017**, *790*, 1-5.
[21] Wu, L. Viscosity measurements of slags with rotation viscometer. Diplomarbeit, Technische Universität Bergakademie Freiberg, 2011.

4 – Results and Discussion

In the present chapter, the crystallization behavior results obtained from experiments carried out with the Single Hot Thermocouple Technique (SHTT) of the five mold powders proposed are presented. The continuous-cooling-transformation (CCT) diagrams in inert atmosphere (argon) and the temperature-time-transformation (TTT) diagrams in inert and humid atmospheres (argon-water vapor gas mixture) are shown and discussed in the **Sections 4.1**. The water vapor partial pressures applied in each experiment are related in the **Chapter 3** (see **Table 3.3**). Aiming to avoid the influence of the basicity on crystallization behavior of the slags, the binary basicity or V ratio (%CaO/%SiO_2) was tailored to be 1 (unity) for all mold powder compositions. Although a basicity equal to unity have been considered as moderately basic [1]; the slags may be more basic or acid, since the binary basicity does not contemplate the presence of the other oxides as Al_2O_3, TiO_2 and MgO, as previously mentioned in **Chapter 2**, **sub-section 2.1.1.2**. This fact may be relevant on the crystallization results, mainly regarding to the solubility of water in slag. Calculations of water solubility in the slags were carried out using the thermodynamics software *FactSage 6.4* and the results are presented in the **Section 4.2**.

4.1 Crystallization Behavior Results

4.1.1 CCT Diagrams, Critical Cooling Rate, Viscosity and Crystalline Phases

The CCT diagrams of the CA system, and the CSA_M, CSA_TM2 and CSA_TM3 mold powders are presented below. These diagrams were constructed aimed to determine the critical cooling rate (CCR) and the crystallization temperature of the slag systems proposed during cooling process. The CCR is the maximum cooling rate where occurrence of crystallization still is possible; above it no longer crystals precipitate. The SHTT experiments were performed undergoing the slag sample to distinct cooling rates under argon atmosphere. When observed, the start of crystallization for each cooling rate – time and temperature – was recorded. The melting temperatures of the mold fluxes were taken during the heating stage. They were considered when the first liquid fraction could be observed, since a multi-component mixture has no fixed melting point [2]. This temperature was compared to the *liquidus* temperature provided by *FactSage* software.

4.1.1.1 CSA_M Mold Powder

The CCT curves of CSA_M mold powder (33.75 wt-% CaO – 33.89 wt-% SiO_2 – 19.69 wt-% Al_2O_3 – 13.4 wt-% MgO) are shown in the **Figure 4.1.1**. The critical cooling rate for glass formation was 1.67°C.s^{-1}, *i.e.* for higher cooling rates the sample will solidify only with glassy structure.

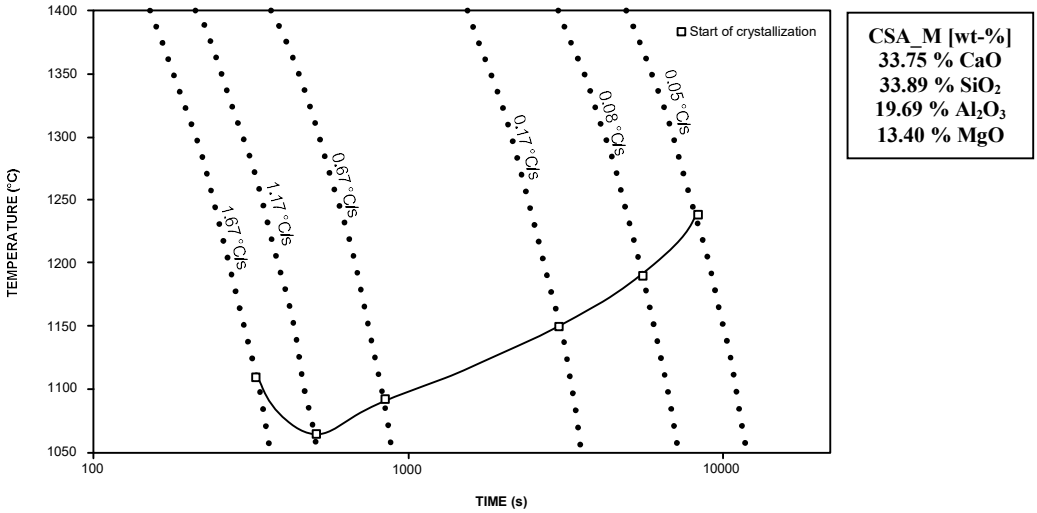

Figure 4.1.1 CCT diagram of the CSA_M mold powder in inert atmosphere.

An increase in the crystallization temperature at 1.67°C.s-1 (critical cooling rate for this slag) was clearly observed. As previously mentioned, Orrling [3] reported an increasing in the crystallization temperature for $CaO\text{-}Al_2O_3$ system; however, it was observed from lower cooling rates region until to a specific cooling rate ($8.0°C.s^{-1}$), which was characterized as a maximum crystallization temperature. For cooling rates above $8.0°C.s^{-1}$, the crystallization temperature became lower with increasing cooling rate. As will be seen further, the CSA_M slag samples exhibit two distinct crystallization event (characterized by the presence of two noses in the TTT diagrams). The increase of the crystallization temperature at a cooling rate of $1.67°C.s^{-1}$ may be related to a change of the precipitated crystalline phase. Other possible factor is related to kinetic aspects inherent to the crystallization under non-steady conditions. However, the reason of this increasing in the crystallization temperature at high cooling rate remains unclear.

At determined cooling rates, a convective mass motion inside the sample could be observed, through the crystal particles translation in the bulk of the sample. This convective motion can be attributed to Marangoni convection or natural convection caused by the temperature gradient between thermocouple and sample. In the **Figure 4.1.2** it is possible to observe a opposite movement of the little particles into the bulk melted sample during cooling. Kashiwaya *et al*. [4] pointed to the existence of a Marangoni convection in the melt oxide.

Orrling *et al*. [5,6] reported the occurrence of a crystal growth instability in presence of a high rate of internal recirculation; the presence of Marangoni or natural convection can generate a shear flow, causing a fragmentation of the growing crystals, increasing the number of crystals in the bulk molten slag. In SHTT experiments, such phenomena transports the crystalline particles from the heating source (thermocouple side) to colder region of the sample (thermocouple contact free) during heating process; or from the colder to the hotter region of the sample, during cooling process [4,6]. For the present study, the fluid flow inside the sample was verified during quenching (see **Figure 2.12 (a)**).

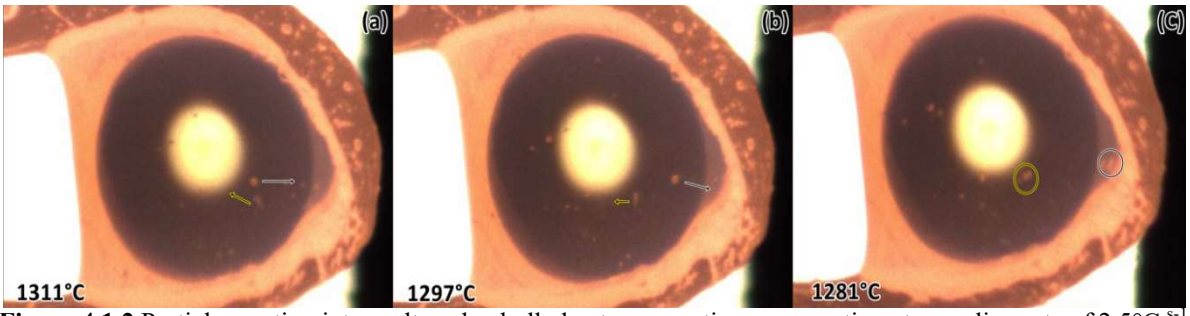

Figure 4.1.2 Particles motion into molten slag bulk due to convective mass motion at a cooling rate of 2.5°C.$^{s-1}$.

Figure 4.1.2 shows an image takes *in situ* from a CSA_M sample at cooling rate of 2.5°C.s^{-1}. At such a cooling rate, the formation of crystals was not observed; however, little particles similar to fine crystals emerged during the sample cooling, moving in opposite directions, following a convective motion inside the sample. These particles were not stable enough to promote the crystal growth, redissolving during the cooling process. The convective mass motion tends to be more intense at higher cooling rates due to the large thermal gradient formed between the thermocouple surface and the center of the slag sample. The occurrence of Marangoni convection in HTT experiments, although knew, was unexpected. Since it is not an issue in the present study, the discussion presented here about the phenomenon and its influence on the crystallization is only superficial. As reported by Orrling *et al*. [5] there is a striking effect of the fluid flow on the crystal stability; however, the influence of Marangoni convection on inhibition of crystallization was not clear, and to attribute the particles dissolution occurred at high cooling rates to the striking or any other effect caused by convective motion would be only speculative. Therefore, more specific studies about the influence of the Marangoni convection on the nucleation and crystal growth stability are necessary.

Figure 4.1.3 shows the viscosity profile of the CSA_M mold powder from measurements carried out with the high temperature viscometer. The viscosity at 1300°C (standard temperature for mold fluxes) is 16.5 P.

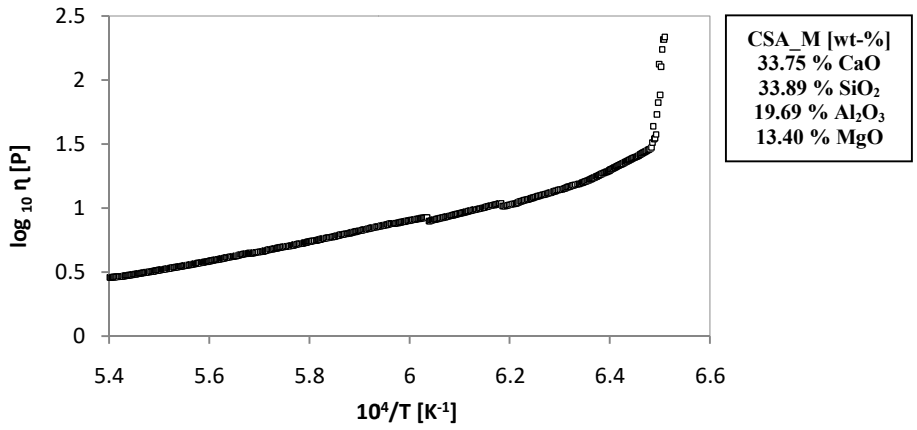

Figure 4.1.3 Viscosity profile of CSA_M mold flux obtained from high temperature viscometer measurements.

Table 4.1.1 compares viscosity values of the CaO-SiO_2-Al_2O_3 slag system (containing 5 wt-% and 10 wt-% MgO) at different temperatures [7] with the viscosity values of CSA_M (15

wt-% MgO) at the correspondent temperatures. The numbers from 101 to 104 denote the slags containing 5 wt-% MgO, while the number from 201 to 204 correspond to that containing 10 wt-% MgO. The referred slags have a basic character (V ratio > 1) and 30 – 55 wt-% less silica content.

Table 4.1.1 Viscosity values of slags containing -5 and -10 wt-% MgO [7], and CSA_M at different temperatures.

TEMPERATURE [K]	SAMPLE 5 wt-% MgO	VISCOSITY [P] 5 wt-% MgO	VISCOSITY [P] CSA_M	TEMPERATURE [K]	SAMPLE 10 wt-% MgO	VISCOSITY [P] 10 wt-% MgO	VISCOSITY [P] CSA_M
1765	101	4.535	4.340	1727	201	5.641	5.328
1800	102	2.950	3.570	1751	202	3.742	3.632
1795	103	2.907	3.660	1776	203	2.755	4.058
1748	104	3.116	4.723	1720	204	4.648	5.561

Comparing the results, an interesting aspect is the distinct effect of MgO on the viscosity with temperature. The variation of viscosity with the temperature becomes more sensitive to MgO additions – the higher MgO content, the higher the viscosity change with temperature. In general way, there is an increase in the viscosity with increasing MgO content. Taking account the differences of basicity, and MgO and SiO_2 contents, the viscosity values presented are consistent regarding to the effect of MgO content on the viscosity.

4.1.1.2 CSA_T Mold Powder

The CSA_T mold powder do not exhibited any visual trace of crystallization at any cooling rate applied. The low crystallization tendency of the CSA_T system was characteristic of the mold powders with high TiO_2 content in the present study. Similar results were obtained by Klug [8] for CaO-SiO_2-TiO_2 slag systems, where no crystals were observed for all cooling rates tested. **Figure 4.1.4** shows the viscosity profile of the CSA_T mold powder. For this slag, the viscosity at 1300°C was 43.72 P and no break temperature was observed, which is in accordance with its strong tendency of CSA_T to form glass.

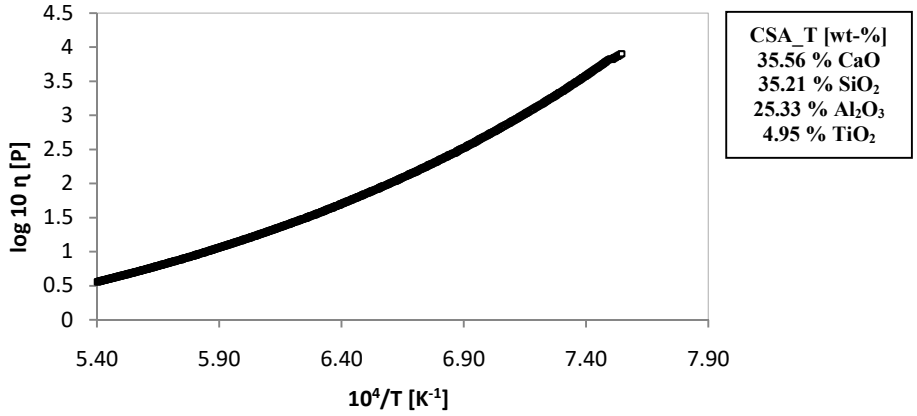

Figure 4.1.4 Viscosity profile of CSA_T mold powder obtained from rotation viscometer measurements.

4.1.1.3 CSA_TM1 Mold Powder

Similar to the CSA_T system, no crystal precipitation was observed in the continuous cooling measurements carried out with the CSA_TM1 mold powder. The viscosity profile of the CSA_TM1 mold powder is shown in the **Figure 4.1.5**.

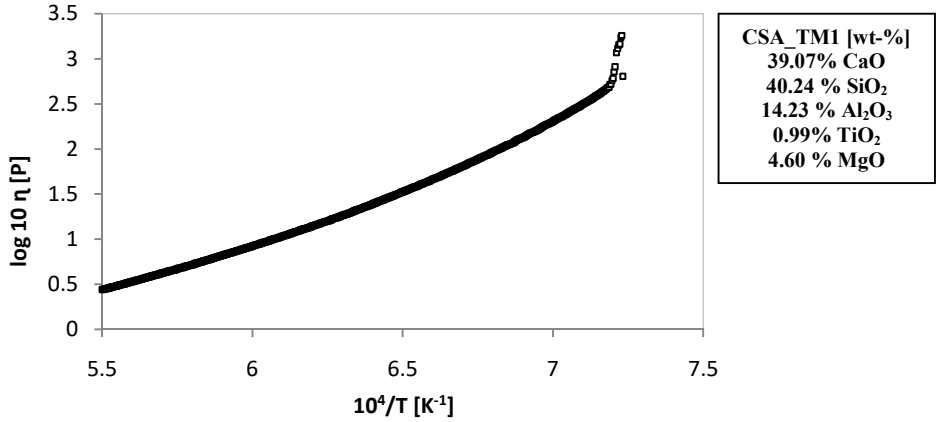

Figure 4.1.5 Viscosity profile of CSA_TM1 mold powder obtained from rotation viscometer measurements.

The viscosity of the CSA_TM1 mold powder at 1300°C was 21.73 P. Note that, for this slag, a break temperature was observed at approximately 1121.42°C. Assuming the break temperature as an indicator of crystal precipitation [9], the presence of a break temperature is inconsistent with the glassy character exhibited by the referred slag. The existence of a break temperature involving the occurrence of crystal precipitation can be attributed to shear strain caused by rotating bob, which may promotes the crystal precipitation [10]. Comparing the viscosity profiles of both mold powders containing TiO_2, it is possible to verify a decreasing in the viscosity from CSA_T to CSA_TM1, which may be related to the additional effect of MgO addition.

4.1.1.4 CSA_TM2 Mold Powder

Figure 4.1.6 shows the CCT curves of the CSA_TM2 mold powder. The SHTT results reveal the occurrence of crystallization in a narrow cooling rate range, accompanied by a relatively low critical cooling rate (0.17°C.s^{-1}).

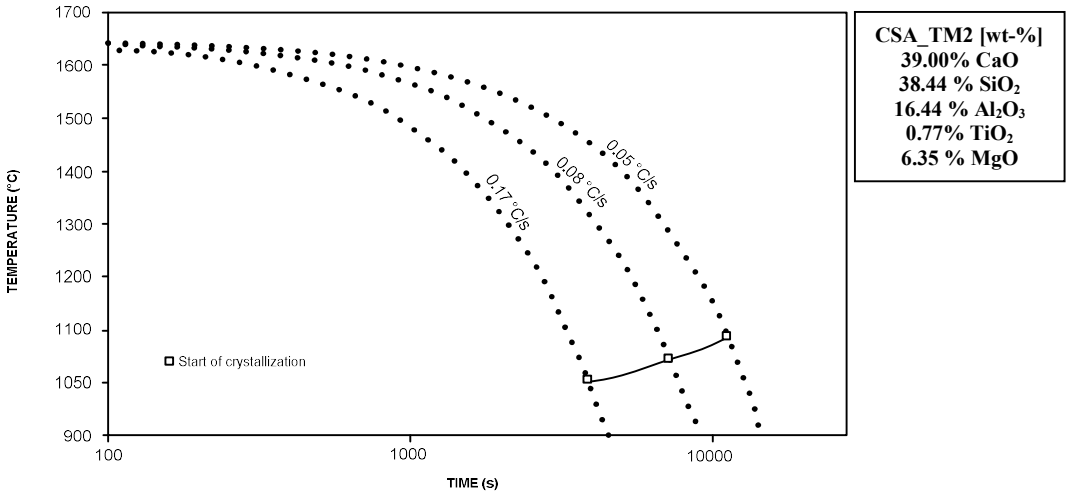

Figure 4.1.6 CCT diagrams of the CSA_TM2 mold flux in inert atmosphere.

When compared to the previous crystallization results, the effect of the addition of MgO on the crystallization behavior of TiO_2-bearing mold powders is evident. The increment of MgO

content from 4.60 wt-% to 6.35 wt-% enhances the crystallization of the mold slag systems CSA, suggesting a minimum content about 7 wt-% MgO to promote crystallization.

Figure 4.1.7 shows the viscosity profile of CSA_TM2 mold powder. Compared to the viscosity of the other mold powders, the viscosity at 1300°C of the CSA_TM2 was very high (385.3 P). As the temperature of 1300°C is lower than that determined as T_{br} (1307.68°C), the viscosity measured value lies into the region where the viscosity increases very fast due to precipitation of crystals.

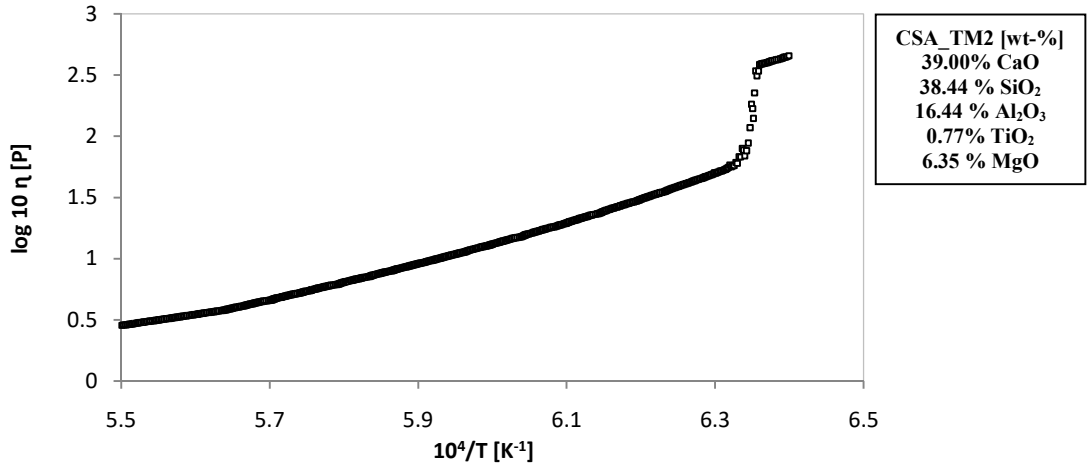

Figure 4.1.7 Viscosity profile of CSA_TM2 mold powder obtained from rotation viscometer measurements.

4.1.1.5 CSA_TM3 Mold Powder

The CCT curves of the CSA_TM3 mold flux exhibited a considerable increase on the cooling rate range (**Figure 4.1.8**). The critical cooling rate has an increment of 1.16°C.s^{-1} with increasing MgO content (from 6.35 wt-% to 9.13 wt-%). For higher MgO content (13.40 wt-%), the increment in the critical cooling rate was less preeminent, performing 0.34°C.$^{s-1}$. The viscosity measured at 1300°C for the CSA_TM3 mold flux was 97.59 P (**Figure 4.1.9**).

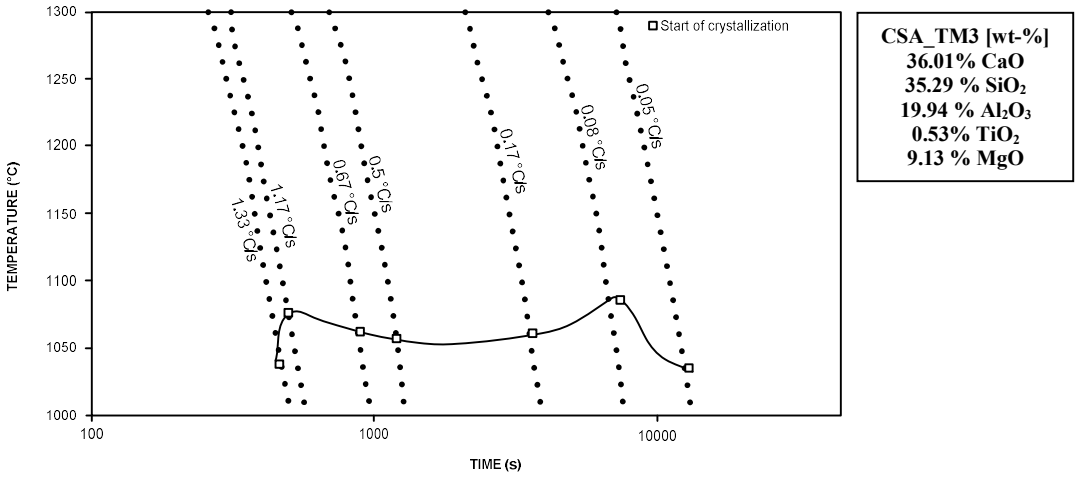

Figure 4.1.8 CCT diagrams of the CSA_TM3 mold powder in inert atmosphere.

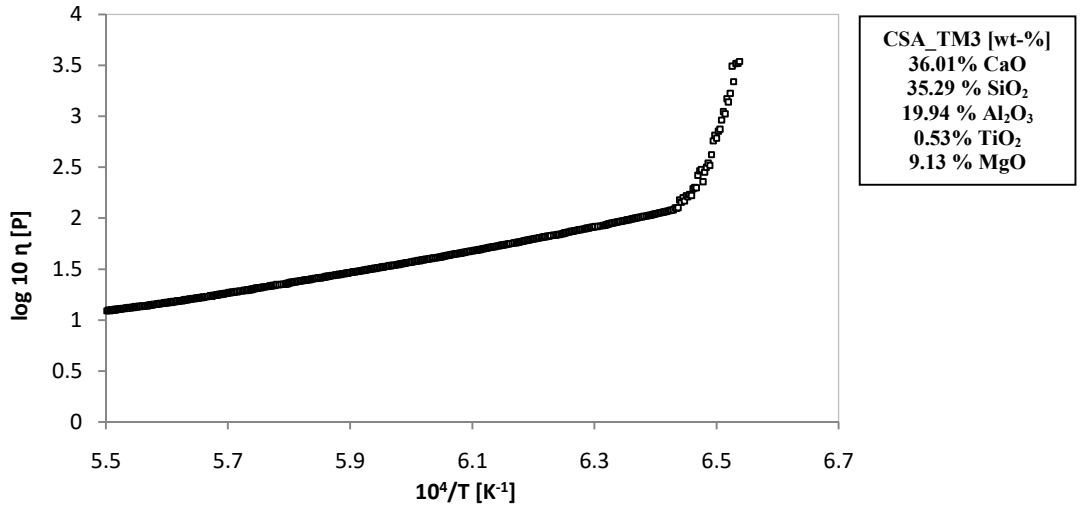

Figure 4.1.9 Viscosity profile of CSA_TM3 mold powder obtained from rotation viscometer measurements.

A decrease of crystallization temperature with increasing cooling rate was observed as a tendency for most of samples. At a given temperature, a higher cooling rate implies in a more viscous behavior of the melt, requiring a greater driving force (undercooling) for crystallization. This suggests the existence of a relationship between viscosity and cooling rate. Considering that crystal growth rate is dependent on atomic mobility, an increase of viscosity will act as a barrier for atomic diffusion and structural rearrangement of molecules, retarding the crystallization onset, *i.e.* the crystallization temperature tends to decrease with increasing cooling rate. A limit for nucleation and growth of crystals, CCR, is expected to occur, even though high cooling rates provide the necessary undercooling for crystallization.

Figure 4.1.10 shows the crystallization temperature as a function of the cooling rate. An increase of critical cooling rate with increasing MgO content can be observed. The crystallization temperature range is wider at both ends of magnesium oxide content interval. Furthermore, for the mold fluxes tested, the presence of TiO_2 mitigates the effect of MgO on the crystallization temperature.

Prapakorn and Cramb [11] show CCT curves carried out in DHTT for the slag system CaO-Al_2O_3-MgO with different MgO contents. The mold fluxes were tailored to present a CaO/Al_2O_3 ratio around to the unit. They found an increase of the critical cooling rate increasing the MgO content, from 15°C.s^{-1} (7 wt-% MgO) up to 23°C.s^{-1} (9 wt-% MgO). The discrepancy between the CCRs reported by Prapakorn and Cramb and this work, 1.67°C.s^{-1} (15 wt-% MgO) may be attributed to the strong glass forming tendency of SiO_2. The effect of lowering CCR is more evident for slags with addition of titanium dioxide, the higher the TiO_2 content, the higher the tendency to form glass.

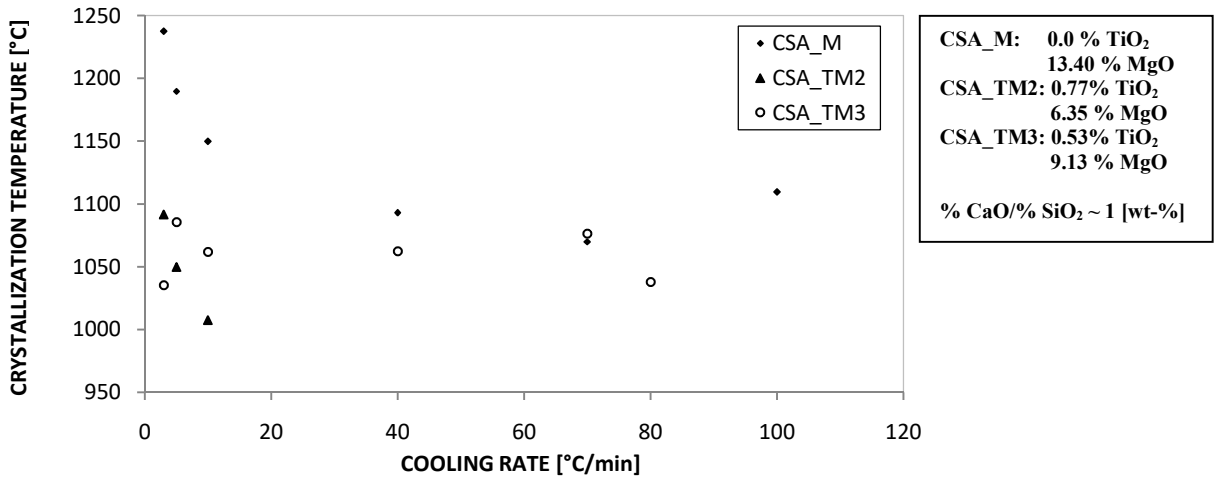

Figure 4.1.10 Effect of the MgO content and cooling rate on the crystallization temperature.

Regarding to the effect of TiO_2 content on mold powders, the absence of crystallization in the slags with 1 and 5 wt-% TiO_2,– even with the addition of 5 wt-% MgO (CSA_TM1) – denotes its strong glass former character. Such behavior is consistent with the tendency of TiO_2 to work as a network former oxide in a range 1 – 7 wt-% TiO_2 [12]. Similar results were found by Klug [8] for CaO-SiO_2-(18.1 wt-%) TiO_2 (CST) slag system; although the addition of Na_2O to the CST system enables the crystallization with evident effect on the critical cooling rate. From **Figure 4.1.10**, it can be seen a crystallization temperature drop with addition of TiO_2. On the other hand, Li *et al.* [13] – from CCT diagrams constructed using DTA technique – reported an increase of crystallization temperature of CaO-Al_2O_3-based mold flux with increasing titanium dioxide content, from 0 to 10 wt-%, and an enhancement of overall crystallization. Such divergence between the results on the crystallization behavior may be related to differences in the slag composition; presence of fluorides (CaF_2 and NaF) and other oxides (LiO_2, Na_2O, etc.) alter the crystallization characteristics of the slag. Comparison of the viscosity results from the viscometer measurements exposes the complexity which involves the variation of slag properties with their chemical composition (**Figure 4.1.11**).

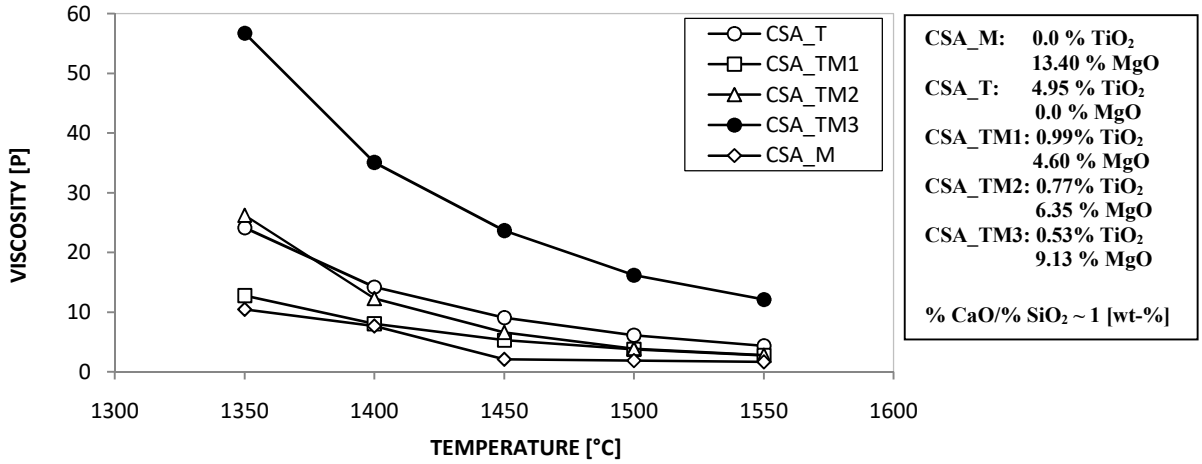

Figure 4.1.11 Viscosity- temperature profile of the mold powders at a temperature range above the T_{br}.

Ohno and Ross [14] found that TiO_2 in slags under reducing atmosphere acts as a network former, increasing the degree of polymerization of the slag and, consequently, the viscosity (TiO_2 behaves as a weak acidic oxide when in a basic slag system). Several researchers have been pointed to the fact that additions TiO_2 tend to decrease the slag viscosity [13,15-19]. Xin *et al*. [20] found two distinct behaviors of titanium dioxide: (i) reduction of viscosity with increasing TiO_2 for amounts below 6 wt-% and, (ii) increase of viscosity for amounts of TiO_2 above 6 wt-%. The viscosity reduction with TiO_2 additions is in accordance with the results of the present study for the TiO_2 content range investigated.

The effect of TiO_2 additions on lowering viscosity is more evident at lower temperatures, while above 1450°C the effect is strongly attenuated. Similar results were reported by Sohn *et al*. [16] for CaO-SiO_2-17 wt-% Al_2O_3-10 wt-% MgO slag system with additions 5 and 10 wt-% TiO_2 and distinct CaO/SiO_2 close to unity. It is obvious that, beside of different amounts of components of (CaO-SiO_2-Al_2O_3-MgO-TiO_2), the presence of other components as B_2O_3, LiO_2, Na_2O and CaF_2, as well as different V-ratios affect the properties of mold powders. The viscosity results obtained from rotate viscometer measurements showed an increase of the viscosity with increment of the TiO_2 amount at lower temperature, while to high temperatures (above 1500°C) the effect of TiO_2 in the reduction of viscosity is strongly attenuated.

From the viewpoint of the MgO in the CSA_TM(1, 2 or 3) slags, an increase of viscosity with increasing magnesium oxide content is observed. Following the compositional MgO/TiO_2 trend, the slag containing 15 wt-% MgO (CSA_M) should exhibit the highest viscosity; however, the opposite behavior was observed. Increasing MgO content from 5 wt-% (CSA_TM1) to 10 wt-% (CSA_TM3) promoted the viscosity increment; the increase of viscosity was much more expressive for the CSA_TM3 mold powder than the others. Contrasting results were found by Xin *et al*. [20]. Whitin 3.0 – 8.0 wt-% MgO range, a decrease about 0.16 P for each 1.0 wt-% average increase in the amount of MgO was reported. Nevertheless, a minor effect of MgO on viscosity was observed.

For the CSA_TM1, CSA_TM2 and CSA_TM3 slags (containing both TiO_2 and MgO) an increase of viscosity with increasing MgO content was observed. These results are in accordance with those reported by Song *et al*. [7] (see **Table 4.1.1**); whereas, a decrease of viscosity was observed with increasing TiO_2 content, with viscosity values for CSA_TM3 being markedly higher with additions of MgO from 5 wt-% (CSA_TM1) to 10 wt-% (CSA_TM3). Without the presence of TiO_2, for the slag containing 15 wt-% MgO (CSA_M), the lowest viscosity values were found. Without the presence of MgO, containing 5 wt-% TiO_2 (CSA_T), viscosity values were intermediate, equivalent to CSA_TM2 mold flux. Feng *et al*. [21] point to a decrease in the viscosity values with increasing MgO content for a CaO-SiO_2-Al_2O_3-V_2O_5 with different MgO and TiO_2 contents (CaO/SiO_2 = 1.07). The same behavior was observed by the authors with respect to TiO_2 additions.

Break Temperature

With one exception (CSA_T, **Figure 4.1.5**), all slags exhibited break temperature. This is in agreement with the results obtained by He *et al.* [22], in which no obvious T_{br} for CaO-SiO_2-TiO_2 mold fluxes systems with high titanium dioxide content was observed. Feng *et al*. [21]

reported an initial decrease, followed by a subsequent increase of T_{br} with increasing TiO_2 content from 5 wt-% to 9 wt-%. The absence of T_{br} for CSA_T mold powder is in accordance with its strong tendency to form glass. The break temperature is an important property of mold powders, since it indicates the temperature upon which the caster mold lubrication potential of the liquid slag breaks down. It represents the crystallization onset [9,22]; for instance, the viscosity of CSA_M mold flux increases strongly from approximately 1269.90°C – which is the break temperature for this slag.

Based on the concept of T_{br}, it is possible to establish a relation between break temperature from viscosity measurements and temperature correspondent to onset of crystallization, from SHTT continuous cooling experiments, for a cooling rate of 0.17°C.s^{-1}. A good agreement between the break temperature from viscosity measurement and continuous cooling for CaO-Al_2O_3 system have been reported, suggesting a correspondence between rotation viscometer and SHTT continuous cooling results [8]. Sridhar *et al*. [9] propose the following equation to calculate the T_{br} from dynamic measurements of slag viscosity based on their chemical composition:

$$T_{br} = 1120 - 8.43\%Al_2O_3 - 3.30\%SiO_2 + 8.65\%CaO - 13.86\%MgO - 18.40\%Fe_2O_3 - 3.21\%MnO - 9.22\%TiO_2 + 22.86\%K_2O - 3.20\%Na_2O - 6.46\%F \quad (4.1)$$

The mold powders investigated in the present study do not contemplate all components of the **Equation (4.1)**. Therefore, only the components which integrate the slag systems proposed were considered. **Table 4.1.2** presents the T_{br} results from **Equation (4.1)**, the T_{br} obtained from viscosity measurements, the viscosity at 1300°C and the start of the crystallization at a cooling rate of 0.17°C.s^{-1}.

Table 4.1.2 Comparison of the T_{br} calculated, T_{br} measured and the temperature of onset of crystallization from a cooling rate of 0.17°C.s^{-1}.

Slag system	Calculated T_{br} [9] [°C]	Measured T_{br} [°C]	Viscosity [P] at 1300°C	Onset of crystallization (from CCT cooling rate of 0.17 °C.s^{-1}) [°C]
CSA_M	1146.28	1269.90	16.50	1149.75
CSA_TM1	1137.46	1121.42	21.73	no crystallization
CSA_TM2	1082.38	1307.68	385.30	1007.43
CSA_TM3	999.65	1281.45	97.59	1061.87
CSA_T	1050.40	no break temperature	43.72	no crystallization

From the **Table 4.1.2** it is possible to note a considerable difference between the calculated and the measured break temperatures. The measured T_{br} are higher than those obtained from **Equation (4.1)**. The exception was the CSA_TM1 mold powder, for which the break temperature deviation lies in the range proposed by Sridhar *et al*. [9] of ± 20 K. On the other hand, when comparing the calculated T_{br} with the onset of crystallization at a cooling rate of 0.17°C.s^{-1}, such discrepancy is attenuated. The difference between measured break temperature and the start of crystallization is attributed to the different measurement conditions of the applied techniques. In the SHTT the sample is stable, *i.e.* it was not submitted to any kind of external force (shear strain). In the rotating viscometer there is a shear strain on the molten slag caused by the rotation of the molybdenum bob. Such shear

strain affects the crystallization behavior of the slag [10,23]. The higher break temperature observed with the viscometer, in comparison with the onset of crystallization temperature, may be attributed to shear strain. The shear strain present in the viscosity measurements promotes the crystallization at higher temperatures. Such phenomenon is clearly visible in the CSA_TM1 mold flux, where a T_{br} was measured, but no crystallization was detected under the undisturbed conditions of SHTT experiment, as previously mentioned. The results in the **Table 4.1.2** show an increase of the T_{br} with decreasing of MgO content up to a maximum (7 wt-% MgO), returning to decrease with subsequent reduction of the MgO content. The increment of content of some oxides as MgO in mold fluxes will decrease the T_{br} [9]. On the other hand, an increase of the break temperature of coal slag with addition of magnesia has been observed [24].

From the CCT diagrams (**item 4.1.1**) it could be seen that the crystallization temperature decreases with increasing cooling rate as a consequence of the accelerated raise of viscosity [25]. Abrupt changes of the temperature require a larger time to rearrange the structure of the slag. The heat loss rate of the slag is higher than the velocity of ordering of the melt structure; thus, beyond the diffusivity barrier imposed by the increase of viscosity to the nucleation and crystal growth, the required undercooling for crystallization will increase. Taking the T_{br} as the start of crystallization, it is possible to verify that the break temperature decreases with increasing cooling rate, until the point where its physical meaning not any more exist. At this point, the critical cooling rate was exceeded and the material will exhibit only glassy structure.

Crystalline Phases

X-Ray diffraction (XRD) analysis was applied to determine the crystal phases obtained in the CCT diagrams. The slag preparation and the XRD diagrams are shown in the **Appendix B**. The present *sub-item* will discuss only the results provided from thermal history (ii) described in the **Appendix B**. The XRD analysis for the CSA_M slag samples (**Figure 4.1.12)** indicated the presence of the follow crystalline phases: akermanite ($Ca_2MgSi_2O_7$), spinel ($MgAl_2O_4$) and quartz (SiO_2). Some peaks show concomitant precipitation of akermanite and spinel, and akermanite and silica. XRD results from Park *et al*. [26] for solidified CaO-SiO_2-20 wt-% Al_2O_3-10 wt-% MgO-5 wt-% CaF_2 (CaO/SiO_2 = 1) system pointed to the presence of melilite – defined as a solid solution between gehlenite ($Ca_2SiAl_2O_7$) and akermanite ($Ca_2MgSi_2O_7$) – spinel ($MgAl_2O_4$) and anorthite ($CaAl_2Si_2O_8$). These results are consistent with those found in the present study. **Figure 4.1.12** shows the solidified microstructure of the CSA_M mold flux from SEM analysis and the respective XRD pattern. The samples for XRD and SEM analysis were submitted to slow cooling from 1600°C to room temperature in nitrogen atmosphere. The SEM of the solidified CSA_M mold powder shows a microstructure composed of an akermanite matrix (light gray) with spinel and some well dispersed small quartz crystals.

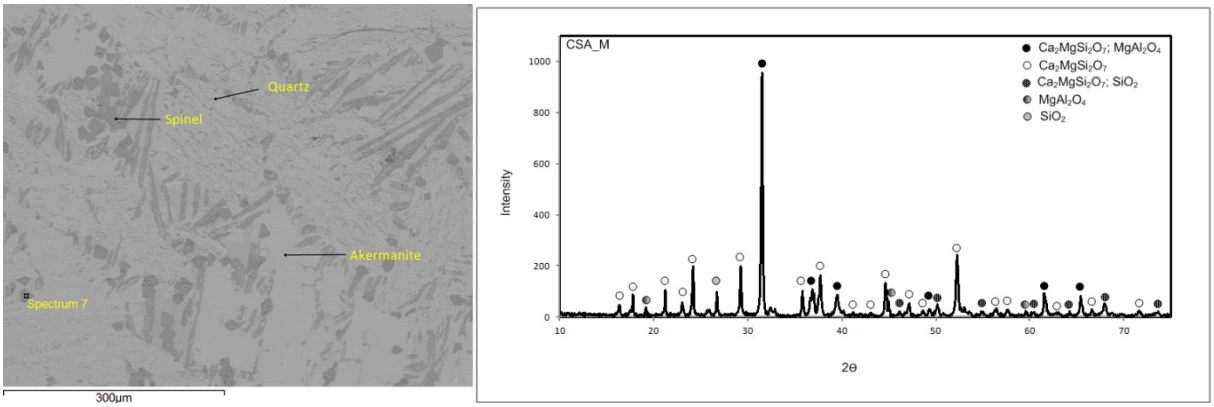

Figure 4.1.12 EDS mapping and XRD pattern of the CSA_M mold powder holding at 1600°C and continuously cooled at a low cooling rate.

The backscattering electron images of CSA_T and CSA_TM slag system are available in the **Appendix B**.

CSA_T mold powder exhibited the formation of gehlenite ($Ca_2Al_2SiO_7$) with some rutile (TiO_2) clusters (**Figure B.9**). XRD analysis results indicate the presence of melilite ($Al_2Ca_2Mg_{0.5}O_7Si_{1.5}$) [27] in all slag samples compositions of the CSA_TM(1, 2 and 3) systems; with additional SiO_2 phase in the CSA_TM1 mold powder (**Figure B.10**); and ($Al_2CaMg_{0.5}O_6Si_{1.5}$), plus silica in the CSA_TM3 (**Figure B.12**). For CSA_TM2 sample, only melilite was detected (**Figure B.11**), although SEM image apparently exhibits the SiO_2 phase. Following the increase of MgO content, there is a replacement of gehlenite (present in melilite) by spinel.

The existence of a slight bulge between $2\theta = 20°–40°$ in the baseline of CSA_T mold powder XRD analysis result (**Figure B.3**) is related to the presence of amorphous (vitreous) material [28]. This is consistent with crystallization behavior exhibited by the CSA_T and CSA_TM1 mold powders, where no crystal precipitation was observed; additionally, the viscosity-temperature profile of the CSA_T (contain highest TiO_2 content) do not exhibited inflection point (or T_{br}). Such baseline bulge is also visible to a lesser extent in the XRD result of CSA_TM1 mold powder (**Figure B.4**), which suggests an increase in crystallinity of the mold powder with the addition of MgO.

This fact is in accordance with the CCT and viscosity experimental results, where a strong reduction of crystallization tendency with increasing TiO_2 content could be observed. Similar results were found by Wang *et al*. [29] where an reduction on crystallization temperature and crystallization tendency with the addition of TiO_2 to the P-bearing steelmaking slags; both results are consistent with those found by Wang *et al*. [15], which reported a decreasing of crystallization tendency for slags with increasing TiO_2 content. XRD analysis results of samples with low TiO_2 (up to 3 wt-%) showed the presence of gehlenite ($Ca_2Al_2SiO_7$) and di-calcium silicate (α-Ca_2SiO_4) as main crystalline phases. As mentioned, these slags exhibited no obvious inflection points in viscosity curves. For the slag without break temperature (slags with or above 5 wt-% TiO_2), no crystal was found in the XRD patterns. No T_{br} was exhibited by these slags. As previously mentioned, T_{br} is related to the point at which the first solid

precipitated in the melt. Nevertheless, the XRD analysis of CSA_T sample indicates the presence of some crystal phases. This suggests that the precipitation of crystals was not enough to promote any significant alteration in the viscosity.

In order to estimate which crystal phases are thermodynamically able to precipitate for the slag system proposed, thermodynamic simulations were carried out by means of the *FactSage 6.4* thermochemical software (**Appendix C**). The crystalline phases obtained from thermodynamic simulations are summarized in the appearance order with the decreasing of temperature in the **Table 4.1.3**. Some crystalline phases results provided by *FactSage* apparently do not agree with some of the crystalline phases determined by XRD analysis. According to the *FactSage* FToxid database documentation, there is a limitation of the available data of systems containing Ti for the group of components Al_2O_3, CaO, MgO, TiO_2 among others. Furthermore, due to the lack of experimental data, the liquid phase model for ternary and higher-order systems is only estimated. On the other hand, the Ostwald's step rule establishes that the parent phase which will crystallize first is not the more thermodynamically stable phase, but a metastable phase that is closest in free energy to the parent phase. The Ostwald's rule is supported by several experimental results; however, it is not a universal rule. In addition, this fact can be related to different crystallization pathways of the materials which do not follow the thermodynamic precepts. Durinck *et al*. [30] bring out to the substantial difference between the phase predicted by the thermodynamic equilibrium model and the experimental results. The solidification process of the slag occur in a non-equilibrium state, since kinetics factors as time, in which plays an important role in determination of precipitated phases, is not contemplated by the thermodynamic. Finally, from the XRD results, it is possible to observe an appearing of Mg-melilite phase with increasing MgO content; in the present study, such phase is a conjunction of the gehlenite and arkemanite species. Similar results are reported by Feng *et al*. [21], where melilite is the basic phase founded in slags with different MgO and TiO_2 contents. Gehlenite specie is present only in the CSA_T mold flux. With additions of MgO to the mold powders as CSA_TM1, CSA_TM2 and CSA_TM3, the proportion of akermanite increase in relation to the gehlenite one until only akermanite, as in the CSA_M mold flux. Also, a strong reduction of crystallization tendency with increasing TiO_2 content could be noted. Analyzing the XRD patterns it is possible to verify this effect (see **Appendix B**, **Figures B.3** and **B.4**).

One relevant aspect is the fact that the mold powder working in real processing condition is exposed to severe thermal gradients and operational parameters, such as mold oscillation frequency, mold water cooling flow, casting speed and atmospheric humidity, which may alters significantly the crystallization behavior of the slags. Considering these conditions, experiments that are able to reproduce, as close as possible, the crystallization behavior of the mold fluxes at casting operation are more useful to industrial mold fluxes design. The continuous casting operational conditions do not occur isothermally but in a continuously cooling process [31]. Therefore, the CCT diagrams are more representative of the real thermal environment which the molten slag is submitted during the solidification. Cramb [31] pointed to necessity of developing CCT diagrams based on the actual continuous casting processing where there is an intense thermal gradient between the steel shell (hot side) and the copper

mold wall (cold side). The application of the DHTT with a difference of temperature between both thermocouple following the cooling curves of hot and cold sides might provide more representative results.

Table 4.1.3 Crystalline phases from XRD analysis and those obtained from thermodynamic simulations.

MOLD FLUX SAMPLES	CRYSTAL PHASES	
	XRD	*FactSage 6.4*
CSA_M	$Ca_2MgSi_2O_7$ (akermanite) $MgAl_2O_4$ (spinel) SiO_2 (quartz)	$MgAl_2O_4$ (spinel) $Ca_2MgSi_2O_7$ (akermanite) Mg_2SiO_4 (fosterite) $Mg_2Si_2O_6$ (clinoenstatite)
CSA_T	$Ca_2Al_2SiO_7$ (gehlenite) TiO_2 (rutile)	$Ca_2Al_2SiO_7$ (gehlenite) $CaAl_2Si_2O_8$ (anorthite) $CaTiO_3$ (perovskite) $CaSiO_3$ (pseudo-wollastonite) $Ca_3Al_2Si_3O_{12}$ (garnet)
CSA_TM1	$AlCa_2Mg_{0.5}O_7Si_{1.5}$ (melilite) SiO_2 (quartz)	$Ca_2MgSi_2O_7$ (akermanite) $CaAl_2Si_2O_8$ (anorthite) $CaTiO_3$ (perovskite) $CaSiO_3$ (pseudo-wollastonite)
CSA_TM2	$AlCa_2Mg_{0.5}O_7Si_{1.5}$ (melilite)	$Ca_2MgSi_2O_7$ (akermanite) $CaAl_2Si_2O_8$ (anorthite) $CaTiO_3$ (perovskite) $CaSiO_3$ (pseudo-wollastonite)
CSA_TM3	$AlCa_2Mg_{0.5}O_7Si_{1.5}$ (melilite) $AlCaMg_{0.5}O_6Si_{1.5}$ SiO_2 (quartz)	Titania-spinel $Ca_2MgSi_2O_7$ (akermanite) $CaAl_2Si_2O_8$ (anorthite) $CaTiO_3$ (perovskite)

As aforementioned (see **Chapter 2 - section 2.5**), the heat flow crossing the mold slag layers deals with severe temperature gradient, and the rate in which the slag is cooled can alter the crystallization behavior predict mainly by CCC and TTT diagram. For instance, a study performed by Petajajarvi *et al*. [32] correlates the crystallization behavior result from SHTT measurements of commercial mold slags, and the heat flux obtained from an industrial caster. The results exhibited an opposite behavior between heat flux and crystallization. The mold slag with higher crystallization tendency showed the highest heat flux, instead a higher inhibition of the heat flux, as expected. According to the authors, the viscosity and the break temperature are dominating factors over the basicity and crystallization tendency, when the thermal properties are considered. However, external factors – as presence of the humidity in the atmosphere and the dynamism of the industrial caster as well as the intense thermal gradient – affect directly on the kinetics of crystallization of the mold slag. Isothermal analysis or TTT diagram of the crystallization behavior of the mold powders is extremely useful in the characterization of the slags, providing the onset of crystallization at several temperatures. The effect of water vapor on crystallization at different temperatures can also be evaluated. Furthermore, information about the crystallization temperature range (maximum and minimum temperatures where the crystallization occurs) can be obtained.

4.1.2 Time-Temperature-Transformation (TTT) Diagrams

Preliminary Experiments

The crystallization behavior of five mold powders constituted by CaO, SiO_2, Al_2O_3, MgO and TiO_2 oxides was investigated using the single hot thermocouple technique (SHTT). The humid atmosphere used were an argon-water vapor gas mixture with water vapor partial

pressures of 3.384 kPa (0.0334 atm) and 12.349 kPa (0.1219 atm), corresponding to 100% humidity at 26°C and 50°C, respectively. First of all, an experimental series in humid atmosphere was carried out taking as base the slag sample referred to as CSTNA_3 (31.6 wt-% CaO, 48.1 wt-% SiO_2, 1.1 wt-% Al_2O_3, 15.5 wt-% TiO_2 and 3.7 wt-% Na_2O), from crystallization studies conducted by Klug [8]. The preliminary experiments have two main purposes: (i) adjustment of the water vapor partial pressure in order to ensure a more precise humid content in the experimental atmosphere gas mixture, and (ii) to observe the effect of water vapor on the crystallization behavior of the slag. The results for a mixture of argon + 3.35 % H_2O are presented in the **Figure 4.1.13.**

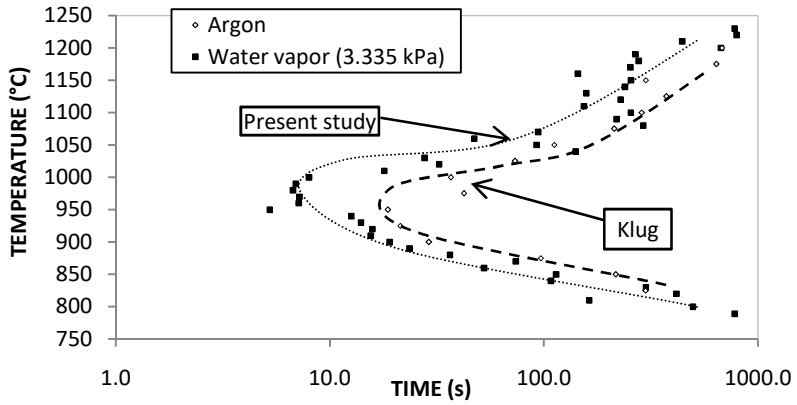

Figure 4.1.13 TTT curves of CSTNA_3 in argon [8] and humid atmospheres for a water vapor pressure of 0.334 atm (3.335 kPa).

TTT diagram shows a decrease of incubation time in presence of humid atmosphere. For instance, the nose at 950°C (the nose is defined by Jung *et al.* [33] as the critical minimum time required to form a given degree of crystallization, here referred as the nose point) was reduced about 13.4 seconds with introduction of water vapor in the atmosphere. This effect is more prominent in an intermediate temperature range (about 950°C – 1050°C); and seems to be more discrete at lower temperatures. In addition, an increase in the extent of crystallization temperature range and no significant dislocation of the nose position can be observed. The CSTNA_3 differ in components of the mold fluxes analyzed in the present study by presence of Na_2O rather than MgO. In the Na_2O-SiO_2 system, the addition of Na_2O to pure silica promote a sharp decrease in the *liquidus* temperature; for the MgO-SiO_2 system, additions beyond 2 mole% MgO leads to a region of liquid immiscibility. Such behavior suggests that Na_2O is a more effective network modifier than MgO [34]. Studies about the solubility of water in alkali borate melts have been shown a decrease of solubility with increasing alkali oxide content [35]. Additions of K_2O and Na_2O to alkali borate melts promote a decrease of H_2O solubility until a minimum; in the case of Li_2O this minimum in water solubility was not reached [35,36]. The effect of MgO oxide on the solubility of water in the mold powders will be discussed later.

4.1.2.1 CSA_M Slag System

Inert Atmosphere Experiments

Figure 4.1.14 shows the TTT diagram of the CSA_M slag system in argon atmosphere. Two nose points were indentified (at 1000°C and 1090°C). The existence of double noses in the

TTT diagram is generally related to the occurrence of different crystallization events (more than one kind of crystals) [37]. According to thermodynamic calculations carried out with *FactSage*, the first precipitated crystals are spinel ($MgAl_2O_4$) and akermanite ($Ca_2MgSi_2O_7$) which appears about 1538°C and 1393°C, respectively. Such results are in accordance with the XRD – although the calculated crystallization temperatures are above that the experimental – in which the main possible phases detected were $Ca_2MgSi_2O_7$ and $MgAl_2O_4$ (see **Appendix B**, **Figure B.3**). The thermochemical simulation results are available in the **Appendix C**.

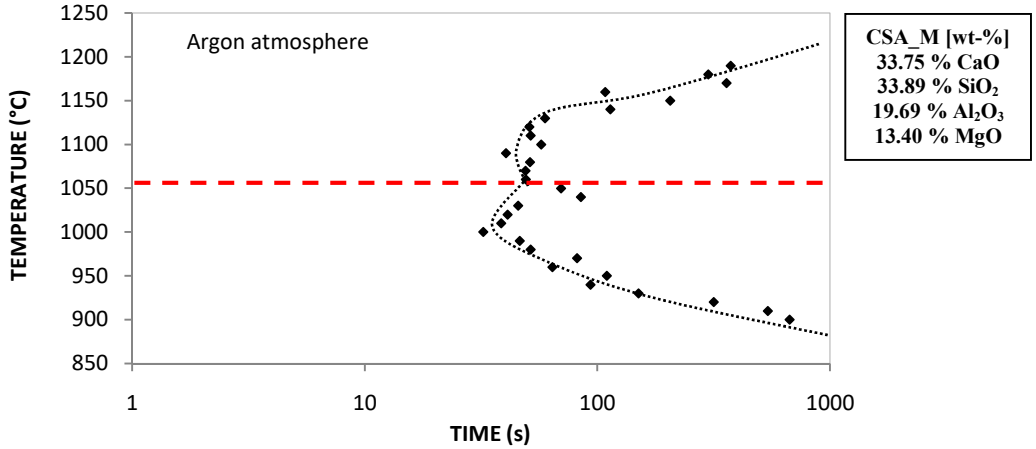

Figure 4.1.14 TTT diagram of CSA_M mold powder from SHTT measurements carried out in inert atmosphere.

In order to situate the thermal region for crystallization of CSA_M slag system (33.75 wt-% CaO, 33.89 wt-% SiO_2, 19.69 wt-% Al_2O_3 and 13.40 wt-% MgO), the TTT diagram was compared to results found in literature for slags with similar composition. The results obtained by Prapakorn *et al*. [11] for a MgO-bearing slag (CAM3: 44.88 wt-% CaO, 46.06 wt-% Al_2O_3 and 9.03 wt-% MgO), and by Kashiwaya *et al*. [37] for a blast furnace (BF) slag (42.99 wt-% CaO, 33.52 wt-% SiO_2, 13.77 wt-% Al_2O_3 and 6.28 wt-% MgO) are shown in the **Figure 4.1.15**. The presence of double noses for all slags is observed. The positions of the nose points of BF in relation to temperature are at 1250°C and 1000°C; while for the CSA_M the noses are positioned at 1090°C and 1000°C. The XRD results from TTT diagram of BF at the nose temperatures pointed to the presence of gehlenite and merwinite ($Ca_3MgSi_2O_6$). For CAM3 slag, the X-ray diffraction results exhibit a mixture of $Ca_3Al_2O_6$ and $Ca_3Al_4MgO_{10}$ at temperatures above 1200°C; for temperatures below 1200°C, the crystalline phase is a mixture of $Ca_5Al_6O_{14}$ and $MgAl_2O_4$. Considering the compositional similarity between both CSA_M and BF slags, the crystalline phases are suitable inasmuch as gehlenite and akermanite are constituents of the melilite. **Figure 4.1.16** shows the pseudo-ternary phase diagram of *liquidus* surface for the system CaO-SiO_2-Al_2O_3 with 10 and 15 wt-% MgO, for BF and CSA_M, respectively [12].

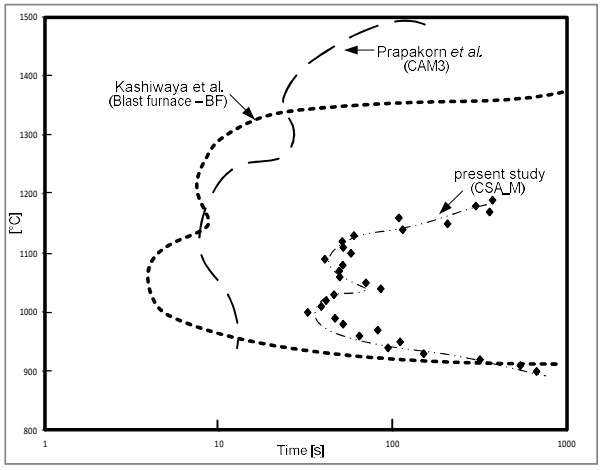

Figure 4.1.15 Time-temperature-transformation curves of CSA_M, CAM3 [11] mold powders and blast furnace (BF) [37].

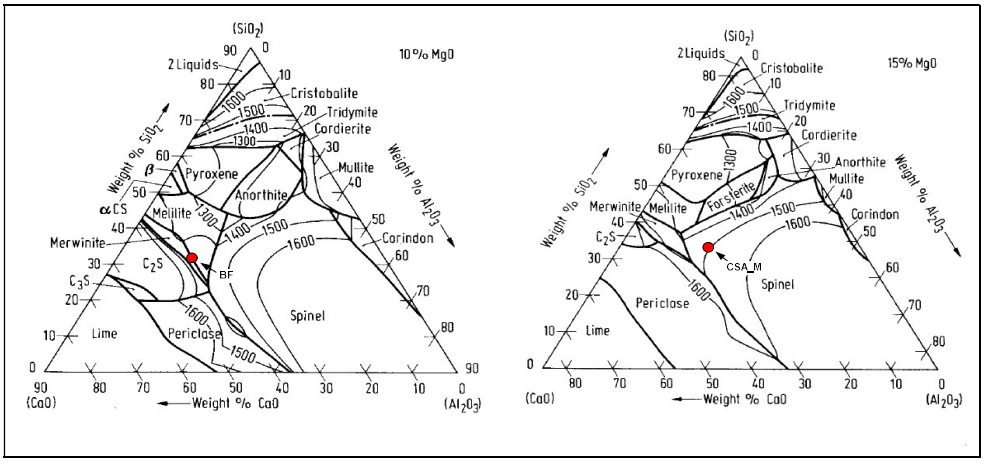

Figure 4.1.16 Pseudo-ternary diagrams of *liquidus* surface for the CaO-SiO_2-Al_2O_3 with 10 wt-% and 15 wt-% MgO [12]; the red points represent the blast furnace (BF) [37] for 10 wt-% MgO and CSA_M mold flux for 15 wt-% MgO diagrams, respectively.

Although the compositional similarity can be extended to the three mold slags – regarding to the major components – the differences in the crystallization temperature range and incubation are significant. The TTT curve from Prapakorn *et al*. [11] (CAM3) exhibited the highest crystallization temperatures and the largest crystallization temperature range. In the case of BF and CSA_M slags, the presence of SiO_2 in the chemical composition, with concomitant reduction of Al_2O_3 content, promoted the narrowing of the crystallization temperature range and a reduction in the temperature of crystallization, *i.e.* the first crystals raise at lower temperatures than those exhibited by the CAM3 ternary slag system. The effect of the binary basicity (wt-% CaO/wt-% SiO_2) must also be taking account, since an increase on the crystallization rate of the slags with increasing basicity has been reported [38-40]. Even a little difference in the basicity can alters significantly the incubation time. The basicities of the CSA_M (present study) and the BF slag are 0.973 and 1.285, respectively; however, in the Prapakorn's work is a ternary system without SiO_2 in his constitution. Therefore, an analysis of the influence of the binary basicity on the crystallization is prejudiced for comparison. As

can be seen in the **Figure 4.1.15**, the incubation time of the BF slag is shorter than that of CSA_M.

Regarding to the influence of the chemical composition, the MgO content has also strong influence on the crystallization kinetics of the mold fluxes. For the case of the three slags showed above, the incubation time increase by increasing the quantity of MgO from 6.28 to 13.40 wt-%. As will be discussed later, the incubation time of the mold powders investigated in the present study decreases with increasing MgO content. It is worth to keep in mind that the binary basicity of the mold fluxes were tailored to be the same for all slags and equal to unity ($CaO/SiO_2 = 1$); thus, the effect of the binary basicity on the crystallization rate of the slags could be ignored. Focusing back on the three cases exposed in the **Figure 4.1.15**, the effect of MgO content exhibited opposite behavior, *i.e.* the incubation time increases with increasing MgO.

Water Vapor Atmosphere Results

The TTT diagrams in water vapor atmosphere for CSA_M mold powder are shown in the **Figure 4.1.17**. For a water vapor partial pressure of 0.0344 atm (3.34 % H_2O – water vapor 1), the effect of humidity on crystallization rate and crystallization temperature range was not significant. A similar behavior was observed for a water vapor partial pressure of 0.1219 atm (12.19 % H_2O – water vapor 2). In order to provide a better visualization of the effect of water vapor on the crystallization behavior of CSA_M mold flux, the TTT curves obtained from CSA_M experiments carried out in argon atmosphere and in water vapor atmospheres at two different water partial pressures of are shown in the **Figure 4.1.18**.

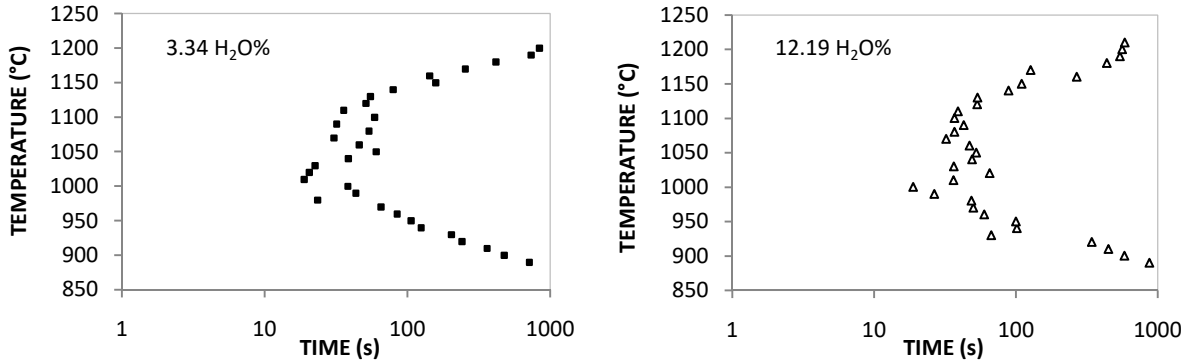

Figure 4.1.17 TTT curve of CSA_M mold powder in humid atmosphere with water vapor partial pressure of 0.0334 atm and 0.1219 atm, respectively.

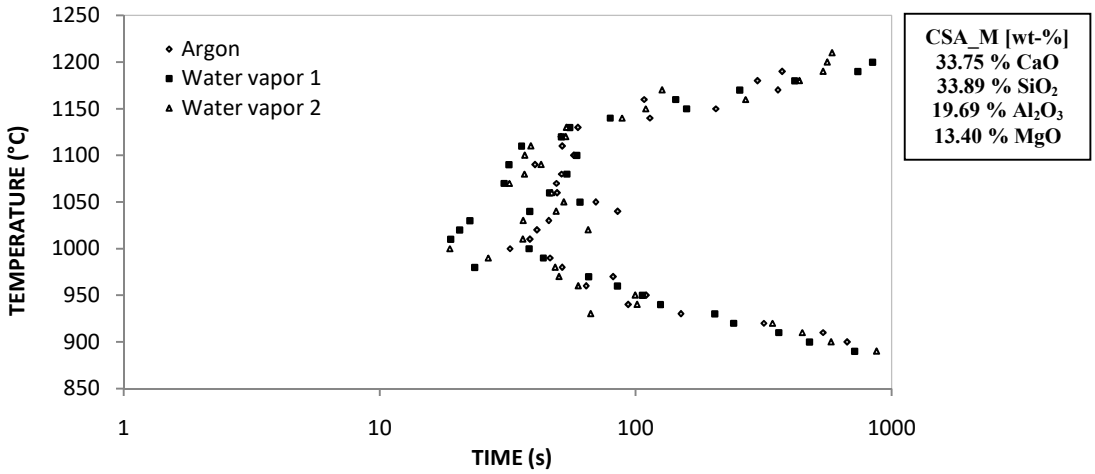

Figure 4.1.18 TTT diagrams of CSA_M mold powder in inert atmosphere, 0.0334 atm (water vapor 1) and 0.1219 atm (water vapor 2).

The TTT diagram shows a double nose for both inert and humid atmospheres. These two regions – above and below 1050°C – indicates the formation of two different crystal phases, as previously discussed [4,37]. The presence of water minimizes the incubation time, but in a subtle way, depending on the temperature range. **Figure 4.1.19** shows the incubation time deviation (Δt) – which was considered as the difference between the incubation time of the mold powder in inert and the humid atmospheres; the indexes 1 and 2 correspond to the difference of incubation time between argon and water vapor 1 and argon and water vapor 2, respectively. Positive values of Δt indicate shorter incubation time, whereas negative values indicate longer incubation times. From **Figure 4.1.19** it is possible to observe positive values of Δt for a wide temperature range. Nevertheless, this trend exhibits different behaviors at temperature range extremes. At low temperatures (around 900°C and 960°C), the values of the incubation time deviation are positive, with some dispersion. In these temperatures, the effect of the lower water content was pronounced; further increment in the water vapor content increased the incubation time. At high temperature range (between 1150°C and 1190°C) Δt was intermittent showing positive and negative values; however, the negative values were more prominent, showing a higher tendency to retard the crystallization onset. As with the lower temperature range, the lower water vapor content was more effective than the higher one. In the **Figure 4.1.19** the notation $\Delta t1$ and $\Delta t2$ indicates the measurements carried out in water vapor 1 (3.34 % H_2O) and water vapor 2 (12.19 % H_2O), respectively.

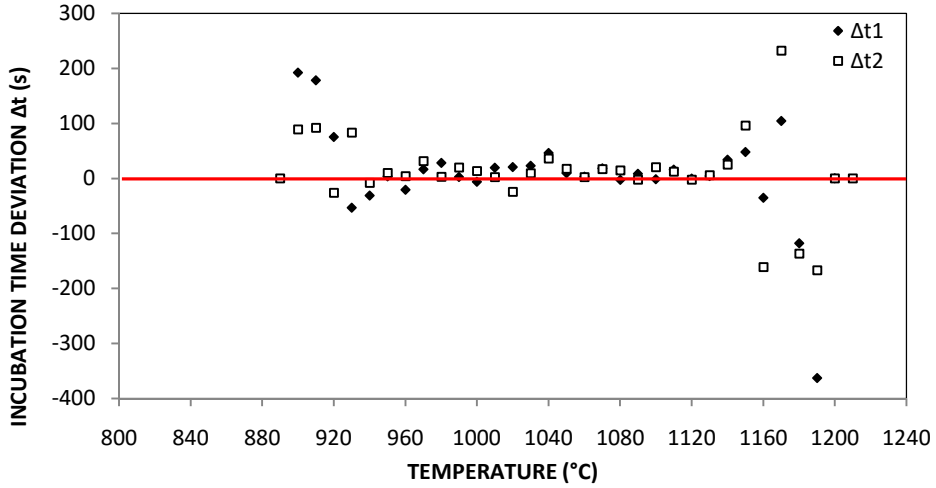

Figure 4.1.19 Incubation time deviation as effect of water vapor in the atmosphere for CSA_M mold powder.

At intermediary temperature range (between 960°C and 1140°C), the effect of the water vapor on the crystallization kinetics was subtle regarding to the enhancement of the rate crystallization, indicating a low effect of water vapor on the crystallization. Similar results were reported by Parpakorn *et al.* [11] for a CaO-Al_2O_3-MgO ternary system using DHTT. The crystallization temperature range was kept unaltered in presence of humidity. At high temperatures (about 1300°C – 1500°C) the TTT diagram shows an increase of the incubation time with increasing water partial pressure; while at low temperatures (about 950°C – 1100°C) the opposed behavior could be observed – the incubation time has become shorter in the presence of water vapor. Nevertheless, the difference of the incubation time between the different water vapor partial pressures is negligible. For intermediary temperatures, the effect of water vapor on the crystallization rate is not significant. Results from continuous cooling experiments for the same slag system showed a considerable delay in crystallization onset for lower cooling rates in humid atmosphere; this difference in crystallization temperatures decreases with increasing the cooling rate until the crystallization is promoted in presence of water vapor. As previously discussed, the crystallization temperature decreases with increasing cooling rate due to changes in the viscosity of the mold slags.

According to Prapakorn *et al*. [11], MgO additions make the solidification of the slag less sensitive to atmospheric humidity. This apparent insensibility to the water influence on crystallization behavior in MgO-bearing slags can be related to condition of magnesia in the slag structure. As referred in **Chapter 2 - section 2.4**, increasing alkali earth oxides content decrease water solubility if it replaces an alkali oxide in the structure of the slag [41]. Sosinsky *et al*. [42] draw attention to the ambiguity effect of MgO on the solubility of water in the molten slags. Iguchi and Fuwa [43] reported an increase on the solubility of water as CaO is replaced with MgO. On the other hand, the results obtained by Zuliani *et al*. [44] pointed to a minimum effect on the water vapor solubility when lime is replaced by magnesia. However, based on the CSA_M results, the relation between solubility of water and his effect on the crystallization behavior is unknown. This issue will be taken up later (**section 4.2**).

From **Figure 4.1.19**, it is possible sketch out some consideration about the influence of temperature on the crystallization behavior of the mold slag, mainly on the extremes of the

crystallization temperature range. Cramb [45] reported an enhance of crystal growth velocity in isothermal experiments below to 1170°C for CaO-Al_2O_3-MgO slag system. For temperatures above 1170°C it was observed a hinder of the growth velocity. Prapakorn *et al.* [11] found that water hinders crystallization only at temperatures above 1200°C for the same slag system studied by Cramb. In the present study, the incubation time deviation exhibited some negative values at temperatures higher than 1150°C. At low temperatures, the incubation time decreases with increasing water vapor content in the atmosphere. Such behavior suggests an influence of temperature on the effect of water on the crystallization characteristics of the slag.

Figure 4.1.20 shows images taken *in situ* of the CSA_M sample in three different atmospheres – inert and water vapor atmospheres (0.0334 atm and 0.1219 atm) at 1100°C. The images represent the progress of crystallization from the liquid state to a certain degree of crystallization in a similar time interval, except to those that correspond to the onset of crystallization, since they are different due to effect of atmosphere on the crystallization. From the images, the delay of crystallization onset of the sample in presence of water can be observed (**Figures 4.1.20 (b)** and **(f)**); however, the incubation time slightly decreases with increasing water content (**Figures 4.1.20 (d)**, **(h)** and **(l)**).

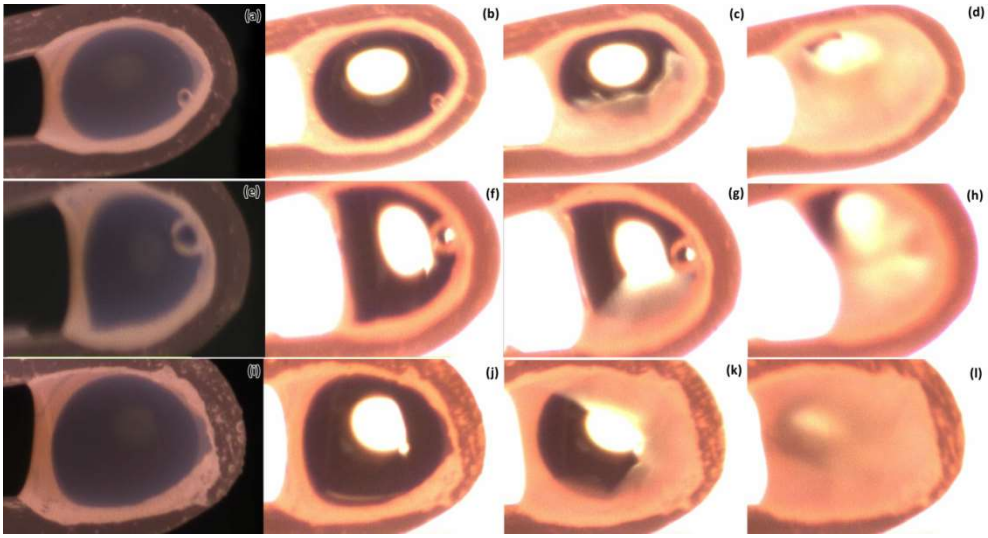

Figure 4.1.20 Effect of water on the crystallization of the CSA_M slag samples; images (a), (e) and (i) are liquid slag at 1650°C in argon, 0.0334 atm and 0.119 atm H_2O partial pressures, respectively. The other images were taken at 1100°C: images (b), (c) and (d) in argon atmosphere in 38.97s (onset of crystallization), 118.72s and 211.63s, respectively; images (f), (g) and (h) in a partial pressure of 0.0334 atm of H_2O in 50.23s (onset of crystallization), 118.77s and 211.70s, respectively; and images (j), (k) and (l) in a partial pressure of 0.1219 atm H_2O in 36.91s (onset of crystallization), 118.76s and 211.70s, respectively.

Results obtained from FTIF-IR and Raman analysis indicate that the presence of water vapor in the atmosphere increases the degree of polymerization of silicate anions of the slags, and consequently the viscosity [1]. According to the authors, water stabilizes the more polymerized silicate anions rather than the depolymerized monomers. Shelby [41] reported a large effect of hydroxyl on viscosity and T_g of glasses as a consequence of formation of additional non-bridging species in the network caused by conversion of these non-bridging oxygens into non-bridging hydroxyls. The formation of these non-bridging species allows the

relaxation of the structure and motion of the flow units to occur at lower temperatures, leading to the reduction of viscosity. According to the water mechanisms reactions showed in the **Chapter 2** (**Equations (2.28) – (2.31)**) the formation of non-bonding OH^- due to the reaction with atmospheric water vapor implies in the polymerization of the melt; such mechanism is suggested to occur in depolymerized melts (basic slags). The polymerization leads to "stiffening" of the silicate melt structure and, consequently, increasing its viscosity.

Although the effect of water on the viscosity of slags and glasses reported by Mohassab and Sonh [1] and Shelby [41] are in a sense conflicting, both effects may be present, depending on the temperature. At high temperatures, the water dissolved in the slag acts as a network former, increasing the degree of polymerization and, consequently, the viscosity. Such increment on the viscosity affects the mobility of the germ nuclei, retarding the nucleation and crystal growth. On the other hand, the water seems to act as a network modifier, promoting the depolymerization of slag due to formation of non-bridging hydroxyls. Such contradictory function exerted by water may be related to stability of water at high temperatures. The gaseous system C-O-H is composed by a large number of different species which have low thermodynamic stability at high temperatures [1]. According to the thermodynamic calculation carried out with *FactSage*, the water decomposes at 1600°C, showing the following equilibrium composition: 99.5 mol% H_2O, 0.29 mol% H_2 and 0.12 mol% O_2. However, water is stable in a temperature range between 950°C and 1200°C (range of temperature upon which crystal precipitation has occurred in the present study). The decomposition of water in this range of temperature produces the follow components: 99.975 – 99.999 mol% H_2O, 0.000 – 0.015 mol% H_2 and 0.000 – 0.007 mol% O_2. Since in the experimental temperature range over 99.9 mol% is H_2O, the possible effect of decomposition of water on the crystallization of slags is considered negligible. Although the influence of temperature on the solubility of water vapor in the slag has been reported as low or even negligible [42,46,47], its effect on the crystallization rate in presence of humidity was evident. Thus, the influence of the triple relation temperature/water solubility/viscosity on the crystallization behavior of the slags requires a more elaborated analysis and discussion.

Figure 4.1.21 shows the visual aspect from an optical microscope of a CSA_M sample taken at 940°C for experiment carried out in a water vapor partial pressure of 0.1219 atm (12.349 kPa).

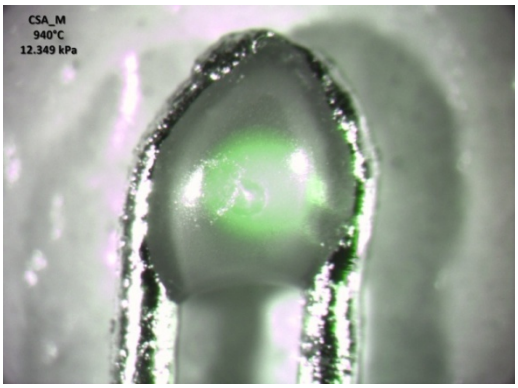

Figure 4.1.21 Optical microscope image of a CSA_M sample took after a SHTT in a water vapor partial pressure of 12.19 %H_2O at 940°C.

Crystallization morphology of CSA_M system

The nucleation and crystal growth of the CSA_M mold fluxes was predominantly heterogeneous at high temperatures for both inert and humid atmosphere. In lower temperatures the crystal nucleation was predominantly homogeneous. Fine crystals dispersed in the slag bulk were formed in temperatures between 890°C – 1010°C; with some columnar crystals growing from the thermocouple surface. At first, the columnar structure fraction was very low, increasing as temperature increases. For a temperature range of 1020°C – 1110°C only columnar crystals were observed. Theses columnar crystals were formed in different places along of thermocouple surface. In some cases the crystal growth took place at different times from distinct crystallization sites in a same sample. However, the formed crystals attained similar sizes and merged forming a 'wall', which growths towards the center of the sample. Equiaxied crystals emerged concomitantly with columnar structure at temperatures above 1120°C. The maximum crystallization (fully crystalline sample) was archived only at temperatures above 990°C. A markedly decrease of the crystalline fraction was observed at higher temperatures; the columnar structure is replaced by few dendritic crystals formed in discrete points of thermocouple surface. The presence of water in atmosphere do not promoted any variation on the crystal morphology. The crystal morphology images of a CSA_M slag sample at different temperatures are shown in the **Figure 4.1.22**. The different structures of the solidified samples denote a markedly influence of the solidification thermal conditions as reported by Orrling *et al*. [48].

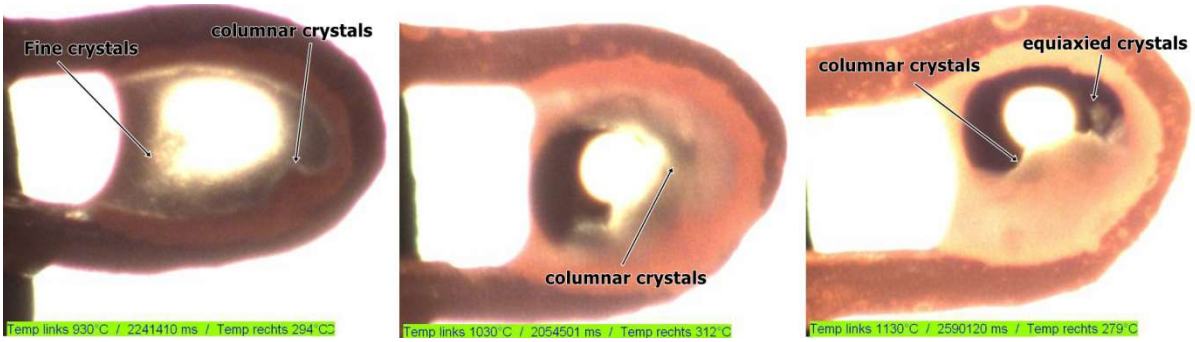

Figure 4.1.22 Crystal morphology of the CSA_M samples at 930°C, 1030°C and 1130°C, respectively.

4.1.2.2 CSA_T Slag System

Inert Atmosphere Results

TTT diagram of the CSA_T system (5 wt-% TiO2) from measurements carried out in argon atmosphere is shown in **Figure 4.1.23**. For this mold powder the crystallization tendency was very low, which is in accordance to the results obtained in the CCT experiments – where no crystal had precipitated, regardless of the cooling rate applied. The crystallization temperature range is very narrow, exhibiting evident crystal formation only at temperatures between 1000°C and 1020°C. Furthermore, the samples never reached full crystallization during the experimental time (see **Figure 4.1.27).** The presence of TiO_2, even at low contents, may affect the visualization of crystallization onset due to its effect on the transparency of the sample. Significant quantities of metal oxides as FeO, MnO and TiO_2 increases the translucency of the samples, making it difficult to observe the crystallization onset [31,49]. This problem is

aggravated at lower temperatures. Owing to this factor the onset of crystallization, which could be occurring at low temperatures, probably can be hidden by the enhancement of opacity of the sample. The beginning of crystallization have been reported as 0.5% crystalline fraction for experiments using SHTT [4,50].

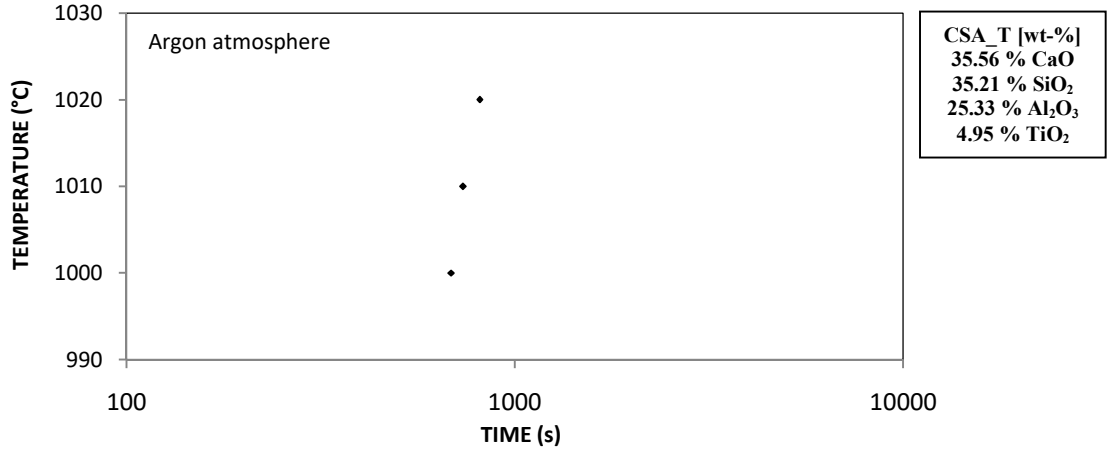

Figure 4.1.23 TTT diagram of CSA_T mold powder from SHTT measurements carried out in inert atmosphere.

TiO_2 has been widely investigated as a central component in F-free mold powders to replace CaF_2. Since it can lead to formation of crystals with high melting point (as perovskite – $CaTiO_3$), it has been pointed out as suitable candidate to replace cuspidine as a predominate crystal to controlling the horizontal heat transfer in the mold level [22,38,51,52]. However, in the present study, the addition of 5 wt-% TiO_2 was not enable to promote the crystallization of the slag, denoting a strong network forming characteristic of the titanium dioxide. Crystallization results reported by Klug [8] for the ternary system CaO-SiO_2-TiO_2 using the SHTT showed a large crystallization temperature range (940°C – 1100°C). DTA results obtained by Nakada and Nagata [51] for the CaO-SiO_2-TiO_2 slag systems exhibited two different crystallization temperature range, depending on the TiO_2 content: the slag with higher titanium dioxide content promoted the appearance of crystals at a high temperature range; while slag with lower TiO_2 content exhibited crystallization at a low temperature range. On the other hand, Rocabois *et al*. [53] reported that additions of TiO_2 as nucleating agent to mold powders containing less than 30 wt-% SiO_2, does not decrease the onset of crystallization and the crystallization rate remains unchanged.

Based on crystallization results reported by literature, it is important to point out the wide TiO_2 content range investigated – beside the presence of different oxides – which may modify the titanium role in the structure of the molten slag. TiO_2-rich melts probably forms titanium cations with sixfold oxygen coordination [Ti^{6+}], while in SiO_2-rich melts, a fourfold coordination cation [Ti^{4+}] can be formed [54,55]. Most TiO_2-bearing mold powders found in the literature regard to F-free mold powders and slags is considerably high (12.05 - 37.19 wt-% TiO_2) [8,22,51,56]; although crystallization results of Ti-bearing mold slags with low titania content are also reported for some researches (1.1 - 9.9 wt-% TiO_2) [38,52]. In all of these studies just mentioned above, for slags containing TiO_2, the presence of crystal phases such as $CaTiO_3$, $CaSiTiO_5$ and $CaSiO_3$ were detected. Electron Probe Micro Analysis (EPMA) results reported by Nakada *et al*. [51] show the formation of glassy phase in most of

the mold powders tested, either together with crystalline phases or fully glassy. Results based on Raman spectroscopy have been shown that Ti^{4+} ion can also act as a network forming cation, enhancing the oxygen bridging [57]. According with Mysen and Neuville [58], the structural role of the Ti^{4+} in alkali silicate melts and glasses is a complex function of Ti concentration and temperature. At low TiO_2 content, Ti^{4+} acts predominantly as a network modifier; whereas Ti^{4+} assumes a four-fold coordination either as TiO_2-cluster or in substitution for Si^{4+} in the structure, or a combination of both, *i.e.*, it acts as a network former at high TiO_2 content. As will be seen later, the Ti^{4+} ion works as a network former, although the TiO_2 content of the mold powder systems in present study is very low compared to that reported in literature (0.5 – 5 wt-% TiO_2). As a comparative of the crystallization behavior of the CSA_T mold powder (5 wt-% TiO_2), the TTT curves obtained by Zhang *et al*. [38] for MS-4 (5.5 wt-%TiO_2), MS-5 (4.89 wt-%TiO_2) and MS-6 (5.60 wt-%TiO_2), and by Klug [8] for CST_2 (18.1 wt-% TiO_2) and CSTNA_3 (15.5 wt-%TiO_2) are shown in the **Figure 4.1.24**.

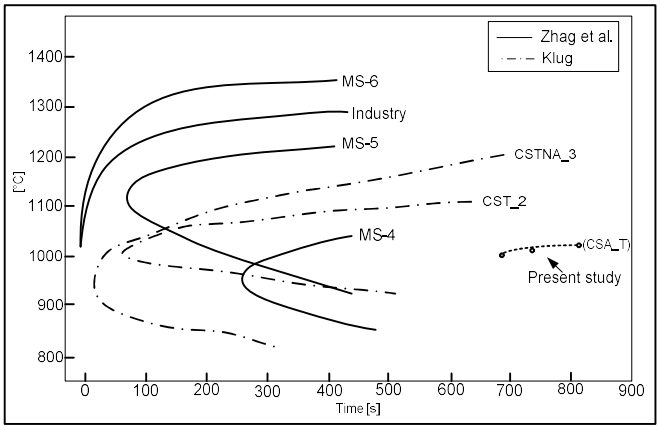

Figure 4.1.24 Comparison of the TTT curves of CSA_T mold powder with TiO_2-bearing slags with different compositions from literature [8,38].

From the **Figure 4.1.24** it is possible to observe the discrepancy of incubation time and temperature crystallization range between the slags, even for those with similar TiO_2 content (case of CSA_T and MS-4, -5 and -6). In this case, it is obvious the influence of the other components on the crystallization behavior of the mold powders.

Water Vapor Atmosphere Results

Figure 4.1.25 shows the TTT diagram of the CSA_T mold powder in humid atmosphere for the water vapor 1 (0.0334 atm) and water vapor 2 (0.1219 atm), respectively. The effect of water vapor on the crystallization behavior of the slag was well pronounced: the temperature crystallization range was markedly improved, increasing from a narrow range in argon (1000°C – 1020°C) to a wide one (940°C – 1050°C) accompanied by a reduction of the incubation time; however, such behavior was properly verified for lower water vapor partial pressure. For higher water vapor partial pressure, the increasing in the crystallization temperature range was less intense.

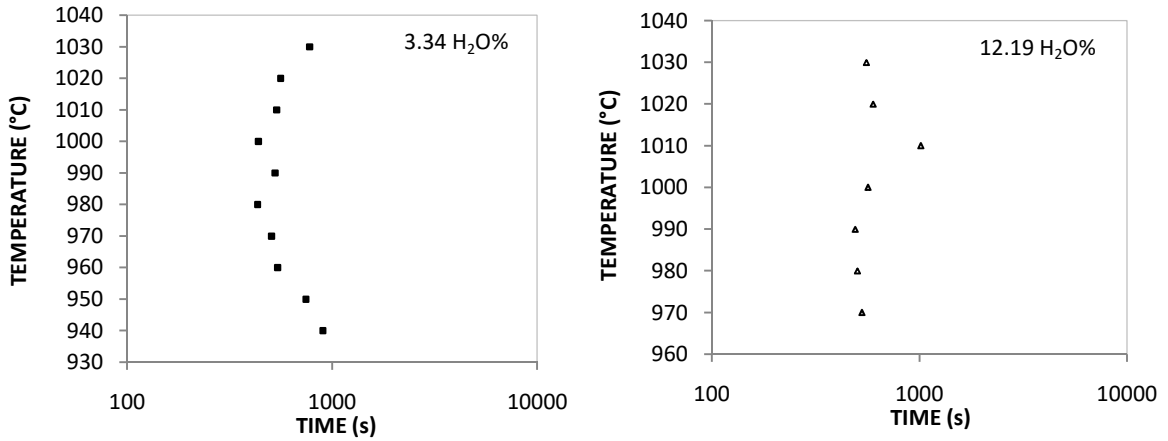

Figure 4.1.25 TTT curve of CSA_T mold powder in humid atmosphere with water vapor partial pressure of 0.0334 atm and 0.1219 atm.

An apparent formation of two noses, one above and other below 990°C can be observed. These noses became more evident in higher water vapor content (**Figure 4.1.25**); however, there was an upward displacement of the noses with increasing water vapor partial pressure. The comparison between the incubation times in argon and in water vapor atmosphere is prejudiced due to the low crystallization temperature range exhibited by the sample in inert atmosphere. The confrontment of these results in different atmospheres and partial pressures are shown in the **Figure 4.1.26**. Notwithstanding that the interaction of the slag sample with water vapor promoted a mild decrease of the incubation time, it do not changes significantly with further increase of water vapor partial pressure.

One interesting phenomenon that could be observed was an apparent relation between the experimental temperature, the water vapor partial pressure and the nucleation and crystal growth. The quantity of crystals decreases with increasing temperature and water vapor partial pressure. **Figure 4.1.27** shows images taken *in situ* from CSA_T samples at two different temperatures. All these images were taken at the end of the experimental time (20 min); consequently they represent the maximum crystallization reached by the samples within the stipulated time; the low crystallization tendency is evident. An increasing of the number of crystals could be observed as the slag sample was kept in contact with humid atmosphere. However, the number of crystals decreased with increasing water content. The quantity of crystals was lower even those obtained in dry atmosphere. Such behavior suggests that high water contents hinder the crystallization of the slag. This effect was more pronounced at higher temperatures. As the isothermal temperature was increased, the size of the crystals had a little increment, but accompanied by reduction of the quantity of crystals. The maximum crystallization rate occurs at a temperature significantly low compared to that for maximum crystal growth rate, *i.e.* at relatively high temperature, the nucleation rate is low and the crystal growth is high. As the temperature decreases, the drive force for nucleation increases; however, the mobility of atoms or ions decreases, promoting a reduction of crystal growth rate [59,60].

Regarding to the influence of water vapor and temperature on the crystallization behavior, a comparison with the CSA_M results shows great influence of chemical composition on the

effect of water on the crystallization behavior of slags. Results reported by Cramb [45] and Orriling *et al.* [61] exhibited a strong increase of the crystallization rate for a $CaO\text{-}Al_2O_3$ system; on the other hand, Prapakorn *et al*. [11] and Cramb [45] pointed to a mitigation of influence of water on the crystallization of $CaO\text{-}Al_2O_3\text{-}MgO$ slag system. As previously mentioned, the less sensitivity of the slag to the effect of water is attribute that the presence of MgO.

As could be observed, the presence of water vapor enlarged the crystallization temperature range of mold powder containing 5 wt-% TiO_2. For the sake of exemplification, at temperatures in which any crystal nucleation was observed in the experiments in argon atmosphere during experimental time – 20 minutes – some crystallization occurred when this same sample was exposed to the humid atmosphere during the same experimental time. This effect was more pronounced for water vapor 1 than that with higher partial pressure, more precisely at lower temperatures.

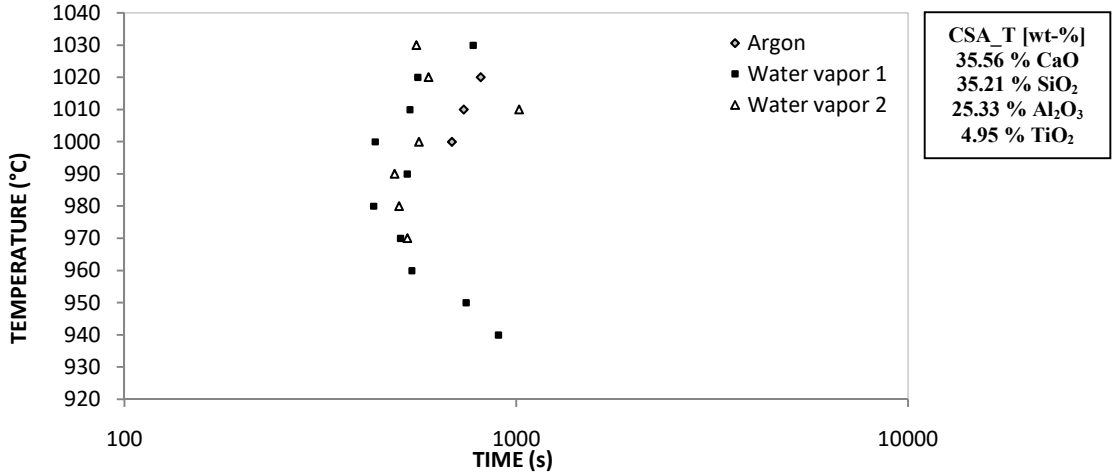

Figure 4.1.26 TTT diagrams of CSA_T mold powder in inert atmosphere, 0.0334 atm and 0.1219 atm.

Bearing in mind the definition of T_{br}, changes in the viscosity caused by water necessarily will promote alteration on the break temperature, thus an increase of the crystallization temperature range suggest that the water acts toward to the increase of break temperature. Hurley *et al*. [24] reported an increase of viscosity and T_{br} (referred by authors as critical temperature) of coal slag in presence of an air+ 10 % water vapor mixture. For the CSA_T mold powder, water acts as a crystallization agent, promoting crystal precipitation at temperatures above the highest temperature obtained in argon atmosphere; this suggests a decrease of viscosity in presence of humid atmosphere. Conversely, there is a shortening of the crystallization temperature range with the increment of water vapor in the atmosphere, suggesting an increase of viscosity with increasing water vapor partial pressure.

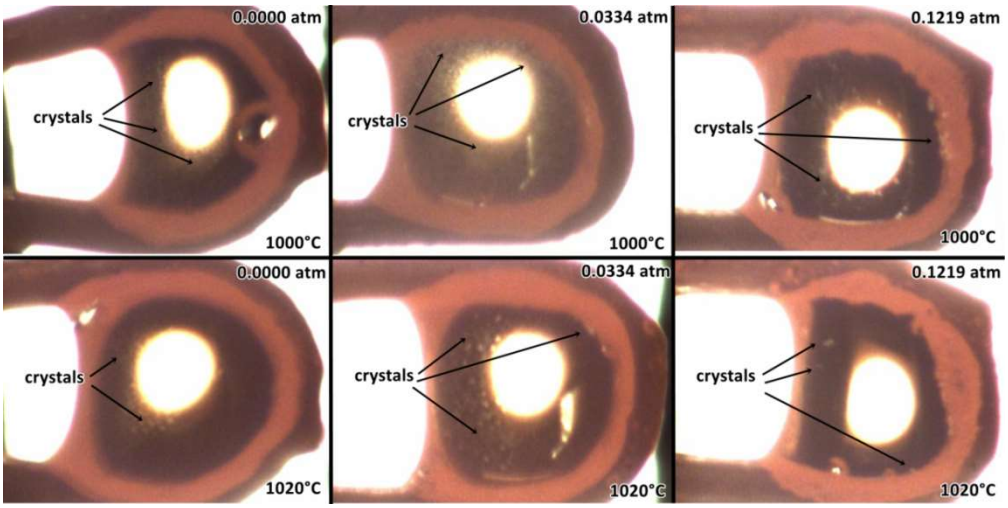

Figure 4.1.27 Effect of water atmosphere content and temperature on the crystallization behavior of the CSA_T mold powder.

According to Shelby, [41] the effect of water concentration on the glass transition temperature (T_g) and on the isothermal viscosity of glasses is more evident for glass former oxides. A reduction of T_g with increasing water content have been reported for several glasses and melts [35,62,63]. Since in the present study, the TiO_2 seem to act as network former oxide, it is expected a decrease of the glass transition temperature of the slag when in presence of water. This decreasing of the T_g can be thought to increase the tendency to precipitate crystal. Fokin *et al*. [64,65] reported an increase of maximum nucleation rate with decreasing the reduced glass transition temperature T_{gr} (defined as the ratio between the T_g and the melting point or *liquidus* temperature); *i.e.* the crystallization is favored with reduction of T_g. Nevertheless, as T_{br} as T_g are phase transition temperatures and they can increase or decrease, depending on the applied cooling rate [41,66]. Results from differential thermal analysis (DTA) has pointed out to a decrease of glass-formation and crystallization temperatures of potassium metaphosphate with increasing the content of residual water by ΔT_g = 40°C and ΔT_{cr} = 80°C, respectively [67]. Although these temperatures are not properly a property, they are a useful indicator of the approximate temperature where the supercooled liquid converts to a solid on cooling, in the case of T_g [41]; and as the starting of crystals precipitation [9].

Result provided by X-ray photoelectronic spectroscopy (XPS) indicated a decrease in the fraction of bridging oxygen (O^0) and non-bridging oxygen (O^-), while the fraction of free oxygen (O^{2-}) increases with increasing TiO_2 content (0 – 10 wt-%) – for a CaO-SiO_2 17 wt-% Al_2O_3 and 10 wt-% MgO system [16]. Such increasing of the O^{2-} concentration in the melt probably gives rise to a slag with lower polymerization degree. According to reaction for highly basic slags (**Chapter 2 – Equation (2.31)**), water reacts with the free oxygen ions promoting the depolymerization of the slag. This would imply in an increase of tendency of the slag forms crystals. Therefore, although the CSA_T system exhibited a strong trend to form glass structure, the crystallization behavior was improved in presence of humidity.

Water solubility results indicate an increase of hydroxyl capacity (C_{H_2O}) with increasing of MgO content in slags [42,43,68]; whereas TiO_2 addition decreases the water vapor solubility in the melt [69]. Comparing the C_{H_2O} results to the crystallization behavior represented by

TTT diagrams, the higher the hydroxyl capacity, the lower the effect of water on the crystallization behavior of the slag. Such behavior indicates that, as temperature, the melt structure is an important factor on the effect of water on the crystallization. Hydroxyl capacity calculations are preformed using *FactSage* (see **Section 4.2** – **Figure 4.2.3**).

Crystallization morphology of CSA_T system

Figure 4.1.28 shows an optical microscope image of CSA_T sample taken after isothermal experiments exposed to argon-12.19 H_2O% gas mixtures at 1000°C for 20 minutes. It was observed two different kind of crystallization: heterogeneous (from internal surface of thermocouple) and homogeneous (from the sample melt bulk). The heterogeneous crystallization was characterized by formation of columnar crystals growing toward the center of the sample (positive temperature gradient). For homogeneous crystallization, very fine crystals dispersed in the melt bulk were observed. Again, the morphology and size of the crystals were dependent of temperature. At higher temperatures, the crystals were predominantly equiaxial with a few sites of heterogeneous crystallization (columnar crystals). At lower temperatures, only homogeneous crystallization was observed, and the size of the crystals became smaller (see **Figure 4.1.27**). Considering that the crystal growth is diffusion controlled, the viscosity increases with decreasing temperature, acting as a 'blockage' to ion mobility. Based on the result obtained, the effect of the water on the morphology and the crystal growth is not so clear. There was a slight increase in the crystal size with addition of water to the atmosphere. With the increment of water vapor partial pressure, the increase of crystal was much more inconspicuous. For higher temperature, the increase of the crystal size was a little more evident, ratifying the influence of temperature on the crystal growth rate; however, a strong reduction of the crystal density with increment of water vapor partial pressure was unexpected.

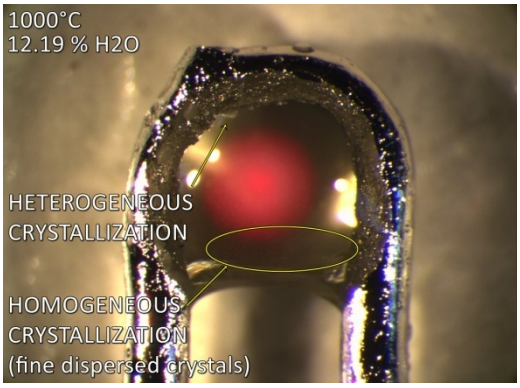

Figure 4.1.28 Optical microscope image of CSA_T sample after SHTT isothermal experiment at 1000°C in argon – 0.1219 % H_2O gas mixture.

4.1.2.3 CSA_TM1 Slag System

Inert Atmosphere Experiments

The CSA_TM1 system shows a similar crystallization trend of that exhibited by CSA_T mold powder. Addition of 5 wt-% MgO with concomitant reduction of TiO_2 content (from 5 wt-% to 1 wt-%) did not provided any improvement on the crystallization behavior of the slag system. Apparently, this composition was easier to form glass than the other TiO_2-bearing

mold powder. For instance, the crystallization temperature range is reduced to only two crystallization points: at 1040°C and 1050°C with an average incubation time of 560.86 s and 427.45 s, respectively. Comparing to the TTT diagram obtained from CSA_T measurements performed at the same experimental conditions, there was a considerable reduction in the crystallization temperature range. Although crystallization has been occurred for a reduced temperature range, the crystallization temperatures were higher and the incubation times were shorter than those exhibited by CSA_T mold flux.

Water Vapor Atmosphere Results

In contrast to the behavior exhibited by the CSA_T mold powder, the crystallization range of the CSA_TM1 system remained unchanged in presence of water vapor. Crystal precipitations also occurred only at 1040°C and 1050°C, but with a strong increment in the incubation time (539.69 s and 524.89 s, respectively). Similar effect on the incubation time was observed by Cramb [45] and Prapakorn *et al*. [11], where the presence of water dissolved in the slag hindered the crystallization onset at temperatures higher than 1170°C. Assuming the diffusivity as governing mechanism of crystal growth, the delay on the crystallization onset at the referred temperatures can be attributed to an increase of the ion mobility barrier due to structural changes of the slag caused by the water. According to Mohassab and Sohn, [1] there is an increase of the polymerization degree of silicate anions of a multicomponent slag (CaO-SiO_2-Al_2O_3-MgO-MnO-FeO-$Ca_2P_2O_7$-FeS), leading to an increase of its viscosity.

Furthermore, the influence of MgO addition on the reduction of the effect of water vapor on the crystallization behavior reported by Prapakorn and Cramb [11] is apparently reduced by the TiO_2 addition. This can be attributed to structural changes promoted by compositional variations. As aforementioned, Raman results of glasses and melts containing Ti showed that Ti^{4+} can be present in at least three different structural positions (as Si^{4+} replacement, TiO_2 clusters, and as a network modifier), which is a function of temperature and TiO_2 content [58].

Further increase in the water atmosphere content (12.19% H_2O) promoted an expressive expansion of the crystallization temperature field (**Figure 4.1.29**); being the enlargement of the crystallization temperature range more pronounced at lower temperatures. Similar behavior was observed for the CSA_T mold slag, however, for the lower water vapor pressure. This effect is in accordance to that reported by Orrling [3], were the presence of water vapor in the atmosphere not only increased the nucleation and crystal growth rate, as expanded region of thermal stability of the crystalline phase.

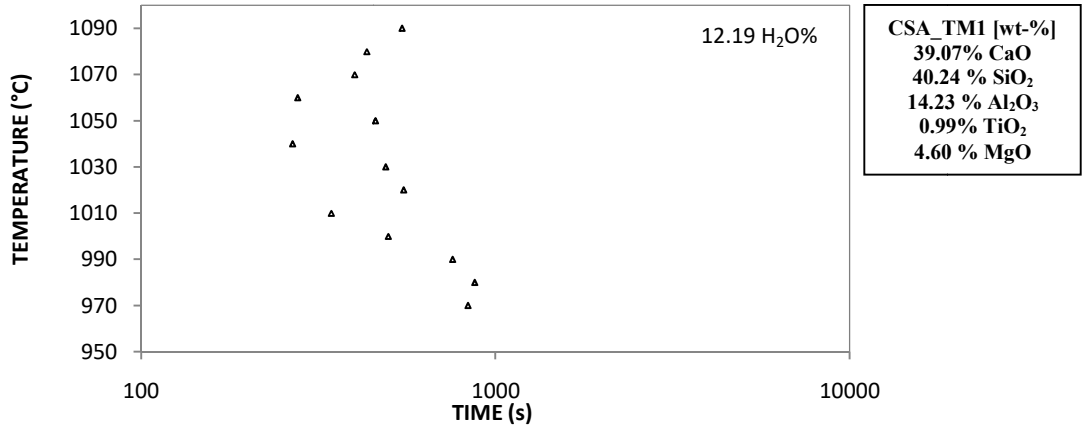

Figure 4.1.29 TTT diagram of CSA_TM1 mold powder in an atmosphere with a water vapor partial pressure of 0.1219 atm.

From **Figure 4.1.29** it is possible to observe some scattering of the experimental data at the temperature range from 1000°C to 1060°C. In the SHTT experimental images, some peculiarities (in the direction of decreasing temperature) were identified: (i) at the 1090°C – 1060°C temperature range, a mass motion similar to Marangoni convection was noticed; (ii) at 1050°C no mass convection was found; (iii) at the 1040°C – 1030°C temperature range, a less intense mass convection was detected; (iv) and finally, from 1020°C to 970°C no longer mass motion was detected. **Figure 4.1.30** shows a sequence of images take *in situ* of a CSA_TM1 sample at 1090°C with atmosphere containing 12.19% of water. Migration of few crystals from the center toward sample periphery during the growing step can be observed Many of the crystals proved unstable, dissolving after reaching the peripheral region of the samples (e.g. crystal indicated as number 1 in the **Figure 4.1.30**).

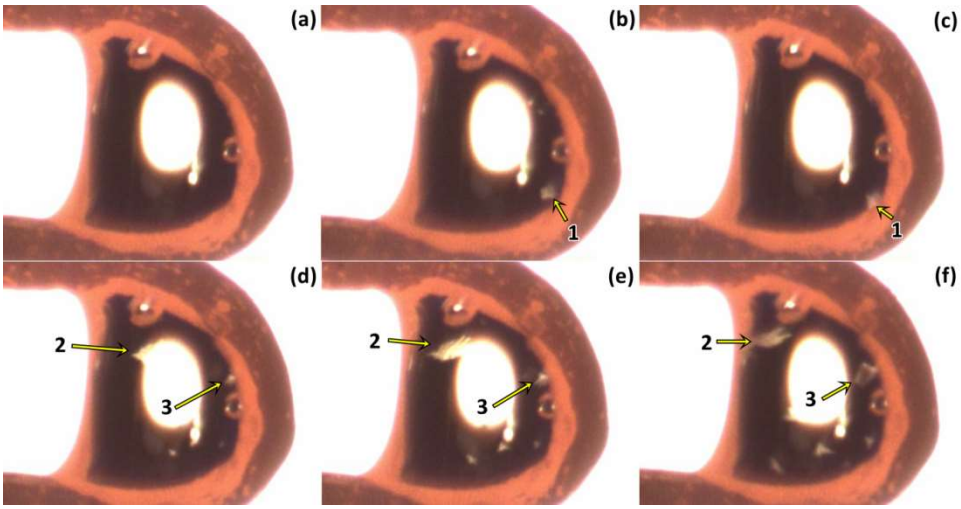

Figure 4.1.30 CSA_TM1 sample at 1090°C and 12.19 % H_2O: (a) 133.73 s (no crystallization); (b) 532.54 s; (c) 625.87 s; (d) 993.32 s; (e) 1057.47 s; (f) 1175.21 s.

Crystal motion was observed during the isothermal experiments. Initially, some crystals forming around the sample core migrate to its peripheral region. Over time, crystals formed on the thermocouple side move toward the center of the sample. In both cases, the crystals which reached the peripheral sample zone were not stable. The movement of the crystals advanced slowly and became slower as the temperature decreases due to the increase of

viscosity. Assuming that in isothermal experiments, the temperature of the sample is homogenous, *i.e.* absence of temperature gradient throughout the sample, the crystal motion cannot be attributed to the Marangoni effect.

Large bubbles were observed in the experiments carried out in presence of humidity (**Figure 4.1.31**). In the most of the cases, the bubbles disappear after spending some time at high temperature; however, some bubbles were trapped during the quenching process. Bubbles may cause some interference on the overall temperature distribution through the sample (formation of thermal gradient zones); besides it can acts as nucleation sites (heterogeneous crystallization) [70]. However, in the present study, the occurrence of crystallization on the bubble surface was not detected. Swanson [71] observed that the presence of vapor bubbles – present in certain bulk composition of synthetic granitic systems – did not act as nucleation sites for feldspars or quartz. However, it is worth to emphasize that, in the case of geological experiments, high pressures are involved in the crystallization processes, which are far away of the scope of the present study.

Due to the low crystallization tendency (strong glass network former character) of the CSA_TM1 mold powder, the analysis of the effect of water on the incubation time is somehow impaired. However, based on the few crystallization points available from measurements in argon and water vapor 1 (3.34 % H_2O), a considerable hindering of the crystallization took place when in the measurement carried out in humid atmosphere. Such effect was also observed in the CSA_M system at high temperatures and in higher water vapor partial pressure. Unfortunately, the absence of a wider crystallization temperature range for the referred atmospheres it is not favorable to a more refined analysis about the effect of water on the crystallization hindering. On the other hand, the crystallization rate was markedly improved with the increase the water vapor partial pressure to 0.1219 atm (water vapor 2). Such behavior can be attributed to a decrease of the viscosity promoted by the depolymerization of the slag structure in presence of higher water content in the atmosphere.

According to Mohassab and Sohn [1], the higher the water vapor content in the gas atmosphere, the higher the degree of polymerization of the silicate in the slag. Although the experiments carried out by Mohassab and Sohn only contemplated the glassy portion of the sample (low presence of crystals) at high temperature (1550°C), the results can be extended to the crystallization behavior of the mold powders. Bringing these results for the crystallization field, the polymerization of the silicate anions would imply in an increase of the viscosity. As aforementioned, such increase of the isothermal viscosity naturally imposes a ‘barrier’ to the atom mobility, affecting directly the nucleation and the crystal growth rate. The crystallization results obtained for the mold powders discussed until now (CSA_M, CSA_T and CSA_TM1) indicate that the effect of the water on the crystallization rate can acts neither as a network former or a network modifier, *i.e.* it will polymerize or depolymerize the silicate structure, depending of the chemical composition of the slag. Moreover, there is an apparent influence of the temperature regarding to the effect of water in the crystallization rate.

Crystallization morphology of CSA_TM1 system

The morphology of the crystals of the CSA_TM1 mold powder was similarly to that exhibited by CSA_T system, independently of the existence of crystal movement during the growth phase in some slag samples. For the temperature range 1060°C – 1090°C, in which the crystal migration was more intense, the crystallization was predominantly homogeneous, being composed by equiaxed morphology (see **Figure 4.1.31**). At temperatures between 1030°C and 1040°C, a reduction of the crystal migration was observed. The reduction on the mobility of the growing crystal follows the temperature decreasing. In this temperature range the precipitated crystals exhibited a morphology predominantly equiaxied dendrites. In some experiments at 1040°C (approximately 50%) heterogeneous crystallization took place forming a columnar crystal which grew from the thermocouple surface toward the core of the sample. At temperatures below 1030°C, small equiaxied crystals were formed. A gap in this morphological trend was observed at 1050°C. For this temperature the crystal morphology was purely columnar; probably a consequence of heterogeneous crystallization on the thermocouple wall.

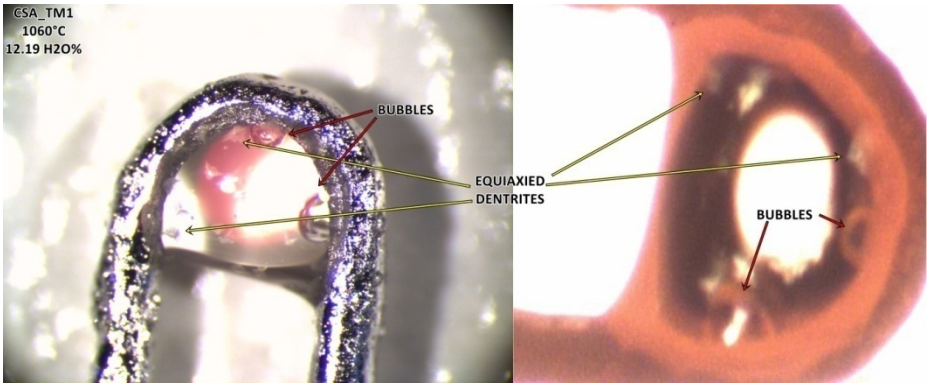

Figure 4.1.31 Optical microscope and take *in situ* images from SHTT measurements of CSA_TM1 sample at 1060°C and 12.19 % H_2O atmosphere.

4.1.2.4 CSA_TM2 Slag System

Inert Atmosphere Experiments

The isothermal measurement results of CSA_TM2 mold powder in argon atmosphere are shown in the **Figure 4.1.32**. The temperature crystallization range was significantly increased with the increment of MgO content (to 7 wt-%) accompanied by the reduction of TiO_2 content (from 1 wt-% to 0.75 wt-%); however, the crystallization tendency of the slag remained low, reinforcing the strong network former tendency of the TiO_2. For instance, at the temperature range where the crystallization rate was more intense (1070°- 1090°C), the maximum crystalline percentage was between 50 % and 85 %; the incubation time was shorter than that showed by CSA_T and CSA_TM1 samples, but longer than that obtained by CSA_M mold flux.

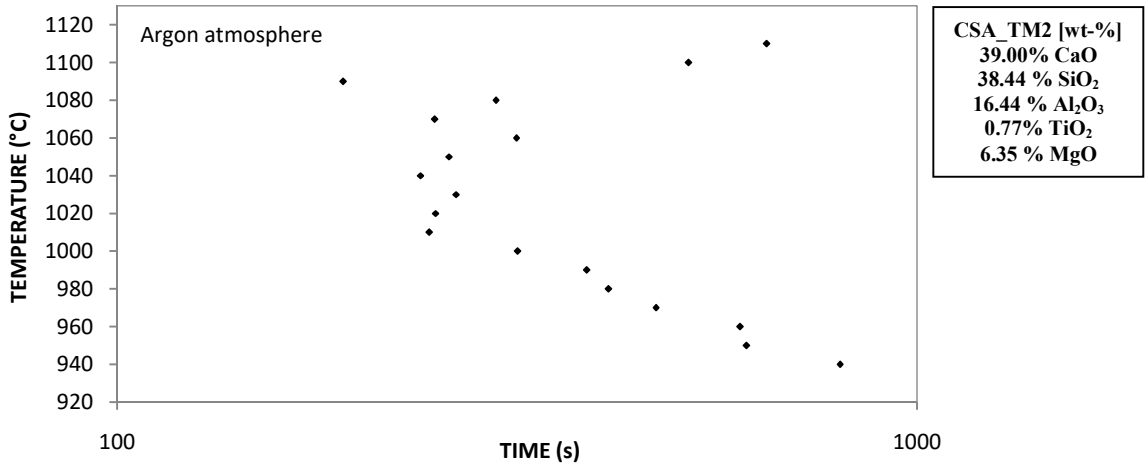

Figure 4.1.32 TTT diagram of CSA_TM2 mold powder from DHTT measurements carried out in inert atmosphere.

Compared to the others TiO_2-beraing mold powders, the increase of the extent of crystallization was more intense at the higher temperatures; this can be attributed to the effect of the higher MgO content, which was able to promote an increase in the crystallization temperature of the slag system. Some data scattering at temperatures between 1010°C and 1070°C was observed. Such scattering was a problem to accurately identify the inflexion point or nose position of the curve (shortest incubation time point). Nevertheless, it is possible to observe the formation, however tenuous, of two noses (one below and other above 1050°C); the inflexion points were estimated in 239.5 s and 249.4 s at 1040°C and 1070°C, respectively.

Water Vapor Atmosphere Results

The effect of the water vapor on the crystallization tendency of the CSA_TM2 mold powder for an Ar-3.34 H_2O% and an Ar-12.19 H_2O% gas mixtures are shown in the **Figure 4.1.33**.

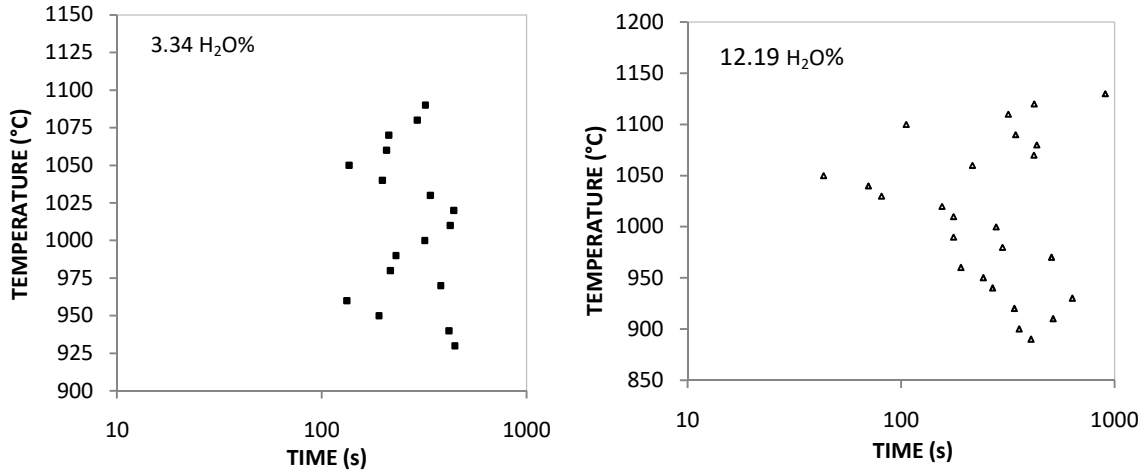

Figure 4.1.33 TTT curve of CSA_TM2 mold powder in humid atmosphere with a water vapor partial pressure of 0.0334 atm and 0.1219 atm, respectively.

As can be seen in **Figure 4.1.33**, there is a reduction of the scattering data and a clear formation of a double nose occurred in presence of the Ar-3.34 H_2O% gas mixture. For this

water vapor partial pressure, a displacement of the TTT curve about 10°C down was observed. The occurrence of the double nose regions – above and below 1020°C – the nose positions were, approximately, 132.7 s and 135.8 s at 960°C and 1050°C, respectively.

Sporadic crystallization occurred in the temperature range of 1110°C – 1140°C; however, the crystallization started few seconds after archive the isothermal temperature. In this case, the crystallization occurred in the same site of some thermocouples; this suggests that the thermocouple surface works as a nucleation site (no longer crystallization was observed after replacement of the thermocouples). Due to these reasons, the experimental data from crystallization which took place in such conditions was ignored. Also it is worth to remember that each point in the TTT diagram is an average of the several experiments results for each isothermal temperature, where the discrepant results (data with significant deviation) were suppressed.

As aforementioned, the existence of the two distinct curves can be related to two separate nucleation events, *i.e.* the occurrence of more than two kind of crystals [4]. However, the results obtained from X-ray diffraction for the CSA_TM2 samples continuously cooled at argon atmosphere had indentified only one crystalline phase ($AlCa_2Mg_{0.5}O_7Si_{1.5}$ – see **Table 4.1.3** and **Appendix B**, **Figure B.6**). Some studies have been shown that the presence of dissolved water in the molten slag can alters the precipitated crystal phase. For instance, the molecular level of Al_2O_3 and SiO_2 mixtures in synthesized mullite ($3Al_2O_3.2SiO_2$), from sol-gel method, decreases with increasing water content using different precursors. Results of DTA and XRD indicates the crystallization of Al-poor mullite at 1000°C in absence of water (ethanol-based alkoxide solution); for low water content, Al-rich and spinel crystallize together; and only spinel crystallized using water-based alkoxide solution. The authors attributed a water content dependence of the chemical homogeneity in the precursor to the formation of lager oligomers (compound of low molecular weight comprised of a few monomer units) with increasing water concentrations [72].

As previously discussed, change on the crystalline phase in presence of water was observed by Orrling [3], in which the precipitated phase were $Ca_5Al_6O_{14}$ and the $Ca_3Al_2O_6$ for a sample cooled at $1°C.s^{-1}$ in argon atmosphere, while the precipitated phase was $Ca_{12}Al_{14}O_{33}$ for the same cooling rate in humid atmosphere (see **Chapter 2, pg. 50**). This change in the crystal phase was also observed in samples from isothermal experiments: the same crystalline phases ($Ca_5Al_6O_{14}$ and $Ca_3Al_2O_6$) were found for samples held at 1200°C in argon atmosphere; whereas, for a sample held at 1400°C in saturated water vapor atmosphere, the precipitated phases were determined as been $Ca_3Al_2O_6$ and $CaAlO_4$. It is important to note the difference of temperature between the above mentioned isothermal experiments (about 200°C), which can be an influent factor on the crystal phase, beyond of the atmosphere. However, thermodynamic simulations results of CSA_TM2 mold slag in humid atmosphere did not exhibited change in the crystal phase with introduction of water in the atmosphere (see **Section 4.2 Thermodynamic Simulation Results** and the **Appendix C**).

Influence of water on the activation energy for crystallization has been also reported by some researches. Wagstaff and Richards [73] found a marked decrease in the activation energy for

crystallization of cristobalite with increasing of H_2O concentration, from 134 kcal.mole^{-1} to 77 kcal.mole^{-1}. This is in accordance with the reduction of the energy barrier for nucleation. Assuming that crystal growth rate is limited by mass transfer in the liquid, a reduction of the viscosity of the slag due to the incorporation of OH^- ions in the melt can be a reason of the increase of crystal growth rate in humid atmosphere. Orrling [3] suggests that the interface kinetics is affected by a decrease in the interface energy between crystal and liquid melt, reducing the barrier for nucleation, as reported by Wagstaff *et al*. [73] and Li *et al*. [74]. In the case of the previous mold powder (CSA_TM1), in special, the crystallization was markedly improved in presence of water vapor, but only for higher water vapor content. The introduction of 3.34 % H_2O was not enough to promote any alteration in the crystallization behavior of the slag. Such insensitivity to water was unexpected and, due to experimental limitation, any explanation in present work about this will be merely speculative.

The determination of both inflexion point and formation of the double-nose were hindered for the CSA_TM2 mold flux due to an intense scattering of the results with the increment of the water vapor partial pressure (from 3.34 % H_2O to 12.19 H_2O%). **Figure 4.1.34** shows a comparative of the crystallization data obtained from measurements carried out in argon atmosphere and the different water contents of the CSA_TM2 system, where the data scattering occurred in 12.19 % H_2O atmosphere can be clearly seen. The scattering of the data in HTT measurements have been attributed to many factors, namely: (i) presence of impurities in the slag will affect the crystallization behavior, mainly in the beginning of the crystallization; (ii) enhancement of crystallization due to the water content in the slag; (iii) optical properties of the slag, which is an important property to visualization of the crystals and finally; (iv) the size of the crystal at beginning of the crystallization, which is important with respect to its visualization. The last will depend of the resolution of the optical system [37].

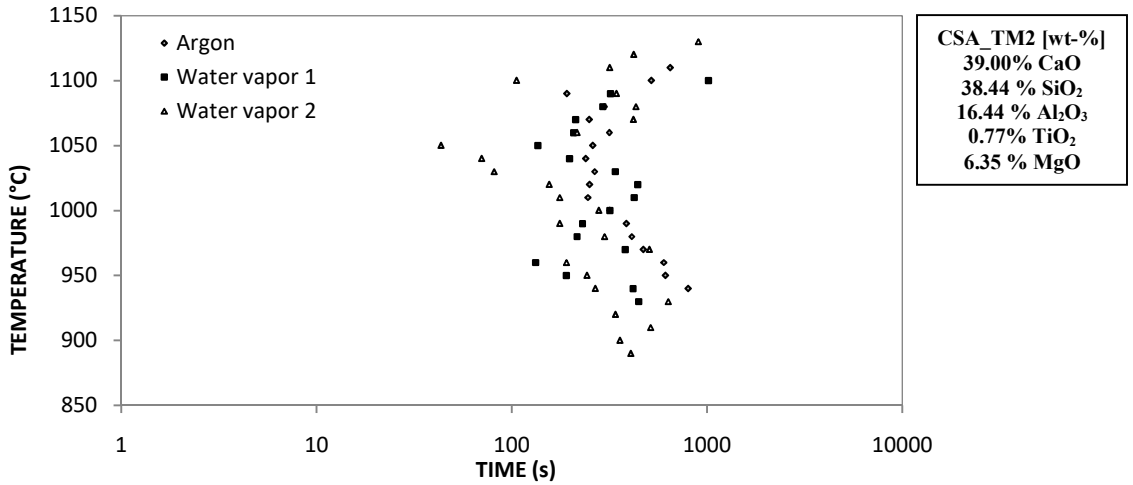

Figure 4.1.34 TTT diagrams of CSA_TM2 mold powder in inert atmosphere, 0.0334 atm (water vapor 1) and 0.1219 atm (water vapor 2).

Despite the high scattering of data is a barrier to a clear interpretation of the influence of water on the crystallization tendency of the CSA_TM2 slag system, its effect on the incubation time could be better evaluated considering the incubation time deviation (Δt).

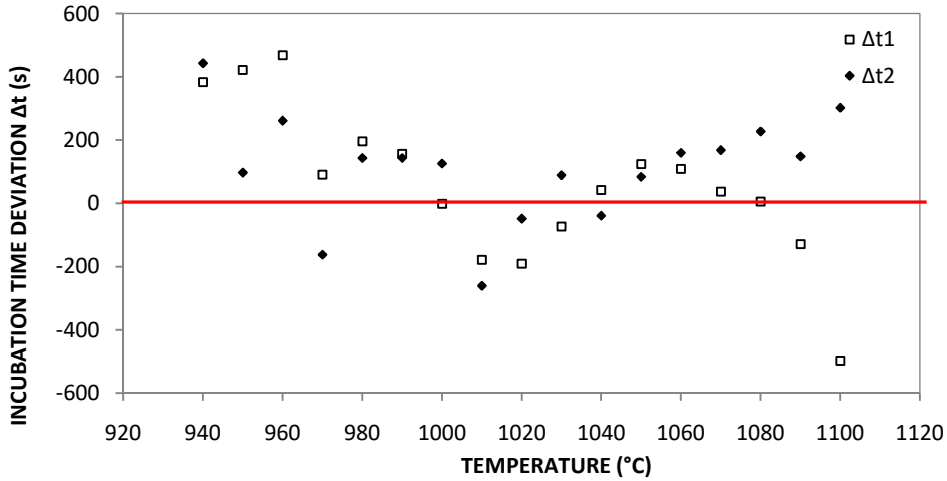

Figure 4.1.35 Incubation time deviation as effect of water vapor in the atmosphere for the CSA_TM2 mold powder.

In the **Figure 4.1.35** it is possible to observe a similar trend regarding to the effect of different water vapor pressures on the incubation time – *Δt1* and *Δt2* – until a temperature about 1060°C. At temperatures above 1060°C, the incubation time shows opposite trends for each water vapor content presents in the Ar-H_2O gas atmosphere. At temperatures between 940°C – 1000°C, the water vapor promoted a positive effect on the crystallization rate, being more intense for measurements carried out in higher water vapor partial pressure. In this "low" temperature range, there is an apparent hindering of crystallization with increase of water content in the atmosphere. For a short intermediate temperature range (approximately 1000°C - 1030°C) a negative effect was predominant, *i.e.* the start of "visible" crystallization was retarded with addition of water in relation to that obtained in inert atmosphere. At temperatures above 1040°C, the crystallization rate of the slag back to being favored, mainly by the higher water vapor pressure; however, at temperatures higher than 1060°C the incubation time exhibited opposite effect on crystallization rate, according to the water content in the atmosphere: negative to lower water content (water vapor 1) and positive to higher water content (water vapor 2). Similar behavior was observed in the CSA_M mold flux for both water vapor contents, but the hindering of crystallization was less prominent.

Crystallization morphology of CSA_TM2 system

Crystal nucleation of the CSA_TM2 exhibited a similar behavior with respect to morphology to the CSA_M mold flux. The main difference lies in the temperature range, which the CSA_TM2 is shorter than that of CSA_M mold powder. In the temperature range of 940°C – 990°C, the crystals were fine and dispersed. Columnar crystal growth was observed in a temperature range of 1000°C – 1080°C, derived from the thermocouple surface; however, the columnar crystal fraction was very low and increased with increasing temperature. The maximum crystallization (fully crystalline sample) was archived only at the temperature of 1090°C. The samples exhibited a decrease of the crystalline fraction at higher temperatures. Identically to the CSA_M samples, the columnar structure did not developed beyond a few dendritic crystals formed in discrete points of thermocouple surface. Again, presence of water in atmosphere did not promoted any variation on the crystal morphology. **Figure 4.1.36** shows the visual aspect of the crystal morphology at different temperatures.

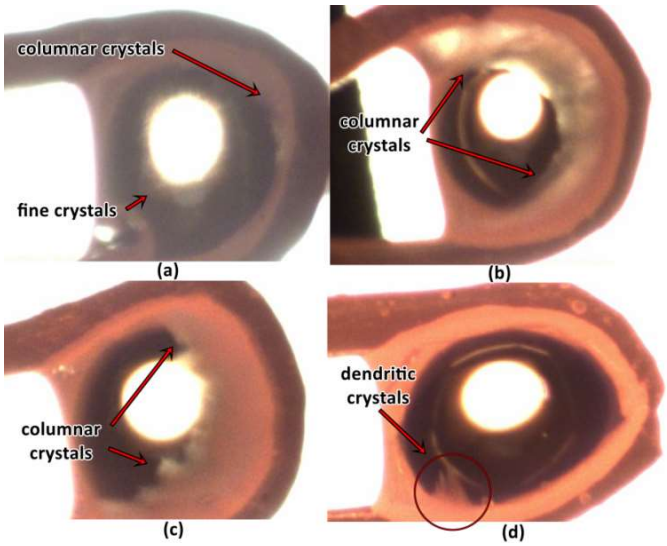

Figure 4.1.36 Morphological aspect of the CSA_TM2 crystal samples at different temperatures: (a) 950°C; (b); 1000°C (c) 1050°C and (d) 1100°C.

4.1.2.5 CSA_TM3 Slag System

Inert Atmosphere Experiments

Figure 4.1.37 shows the TTT diagram of the CSA_TM3 mold powder from experiments carried out in argon atmosphere. Compared to the previous TiO_2-bearing mold powders, the crystallization temperature range was enlarged with increasing MgO content from 7 wt-% to 10 wt-%. This slag composition exhibited a clear double nose positions (temperature correspondent to the shorter incubation time) at 1130°C and 990°C. The double nose has been shown to be characteristic of MgO-bearing mold powders of the present study and those found in literature [11,37]. The upper nose curve has narrow crystallization temperature range and with longer incubation time, about 483.18 s; while the nose lied below 1090°C encompasses a larger temperature range and the incubation time at nose position was about 58.68 s. The CSA_TM3 system exhibited high crystalline fraction, even at low temperature, making up about 100 % crystalline structure for a temperature range of 1020°C – 1150°C. For temperatures below 1000°C, the crystalline fraction decrease gradually, as expected, once the increase of slag sample viscosity is a barrier to ion mobility assuming a crystallization growth controlled by mass diffusion.

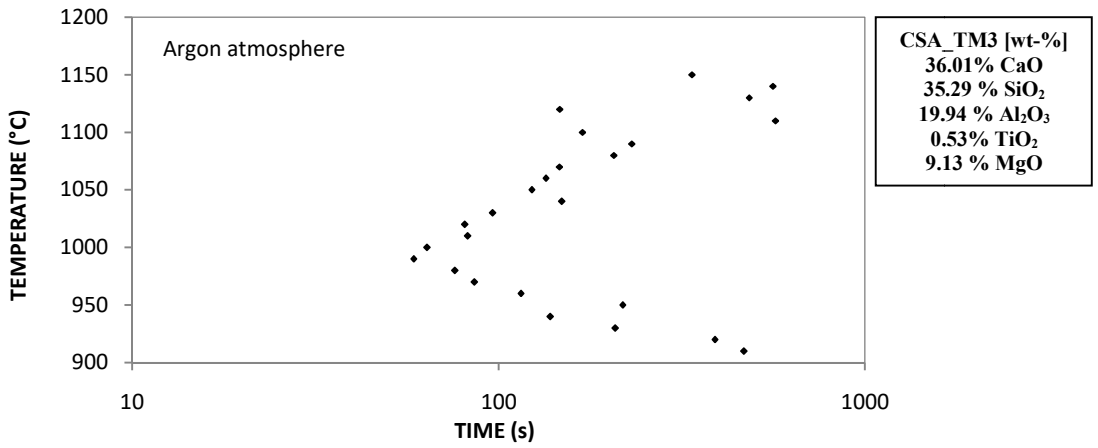

Figure 4.1.37 TTT diagram of CSA_TM3 mold powder from SHTT measurements carried out in inert atmosphere.

Water Vapor Atmosphere Results

The effect of water vapor on the crystallization behavior of the CSA_TM3 system at isothermal conditions is shown in **Figure 4.1.38**. Similarly to CSA_TM2 mold powder, the insertion of water into the atmosphere promoted a narrowing of the crystallization temperature range at the higher temperatures – from 1150°C to 1130°C – with a concomitant enlargement at lower temperature – from 910°C to 900°C. There was also a decrease of the temperature of the upper nose position – from 1130°C to 1080°C – and a lower nose position rise – from 990°C to 1000°C. For this slag, the general effect of water on the crystallization was a subtle displacement of the TTT curve to down and to left. The crystallization field at high temperatures (C curve above 1050°C) was enlarged by presence of water. The incubation time for upper and lower nose position was 30.0 s and 76.98 s, respectively.

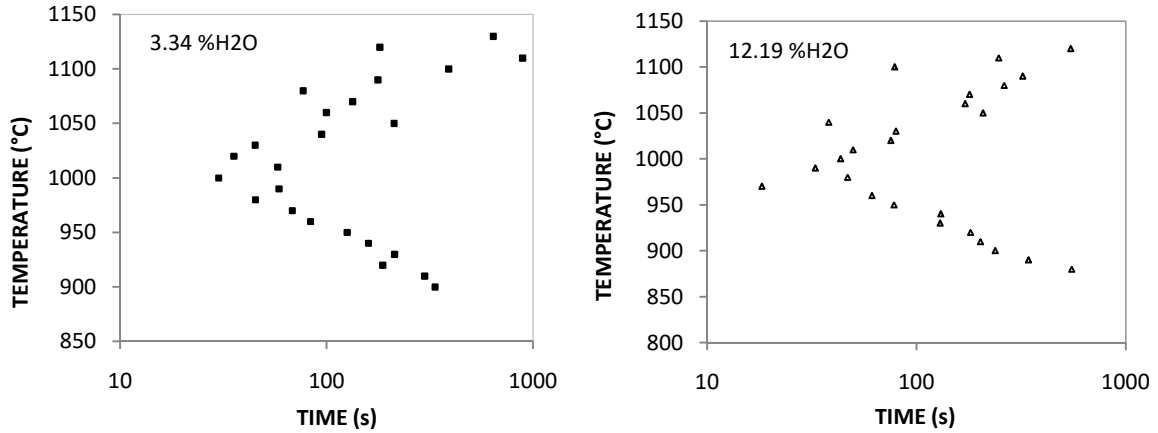

Figure 4.1.38 TTT curve of CSA_TM3 mold powder in humid atmosphere with water vapor partial pressure of 0.0334 atm and 0.1219 atm, respectively.

At first view, the increase of the water vapor content promotes the displacement of the TTT curve little more down and the incubation time became subtly shorter than that obtained at lower partial vapor pressure. The nose positions remain unaltered with increment of water content from 3.34 % H_2O to 12.19 % H_2O. An important characteristic was a decreasing of crystallization temperature of about 30 °C for higher temperatures. Such decreasing of crystallization temperature can be related to increasing of viscosity reported by Mohassab and Sohn [1], as a consequence of stabilization of more polymerized silicate anions. This argument was also applied for those mold powders which exhibited a certain degree of hindering of crystallization at higher temperatures, which also occurred for the present mold powder as can be seen in the **Figure 4.1.39** and **Figure 4.1.40**. Comparing the isothermal crystallization results for the different atmospheres (**Figure 4.1.39**) it is possible to verify that the lower nose position remains practically unchanged, while the upper nose position is substantially altered.

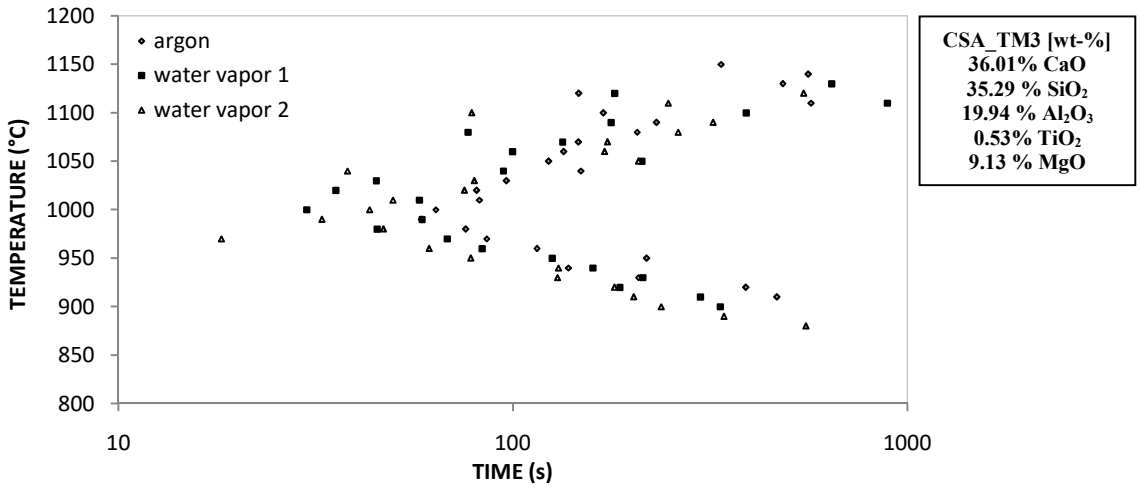

Figure 4.1.39 TTT diagrams of CSA_TM3 mold powder in inert atmosphere, 0.0334 atm (water vapor 1) and 0.1219 atm (water vapor 2).

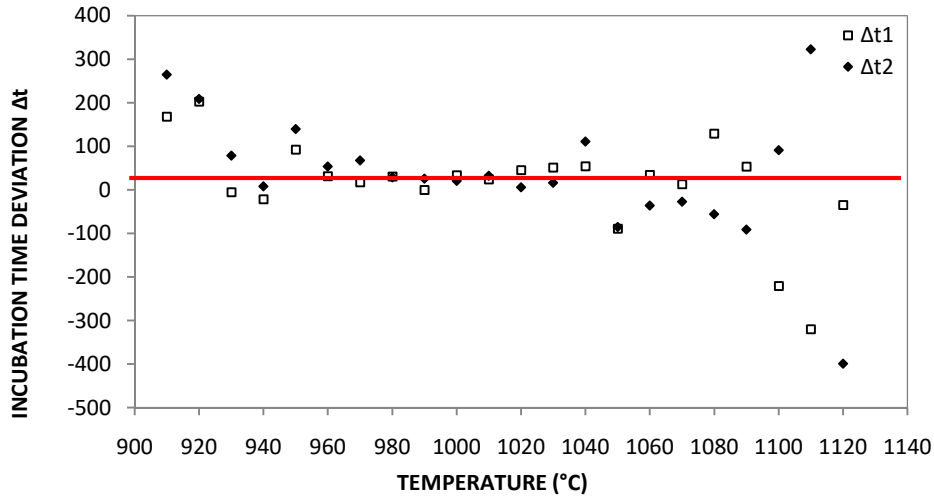

Figure 4.1.40 Incubation time deviation as effect of water vapor in the atmosphere for CSA_TM3 mold powder.

Figure 4.1.40 shows the deviation of the incubation time as effect of water content on the crystallization. Following the same observed characteristic of water influence on the crystallization behavior of the previous mold powders, the incubation time at low temperatures exhibited positive values, in a general way. For a temperature range of 910 °C – 970 °C, the incubation time was improved with introduction of water in the system, becoming shorter with increasing water content in the atmosphere. On the other hand, the incubation time deviation is predominantly negative at high temperatures, denoting a tendency to retard the crystallization.

Crystallization morphology of CSA_TM3 system

The morphology of the crystals is similar to the other MgO-bearing mold powders analyzed in the present study. At low temperatures, the crystals are fine and the nucleation is predominantly homogeneous. With the increase of temperature, the crystals became larger and a concomitant heterogeneous nucleation could be observed. In the temperature range from 1030°C to 1150°C, the crystal morphology was essentially columnar crystals with some

dendritic growth, attaining 100% crystal fraction. At this point, heterogeneous crystallization is predominant.

4.1.3 General Discussion

In order to establish a better visualization of the effect of different atmospheres on the crystallization behavior based on slag chemical compositions, the TTT diagrams of the five mold powders investigated were grouped by applied atmosphere. **Figure 4.1.41** shows the TTT results from measurements carried out in argon atmosphere.

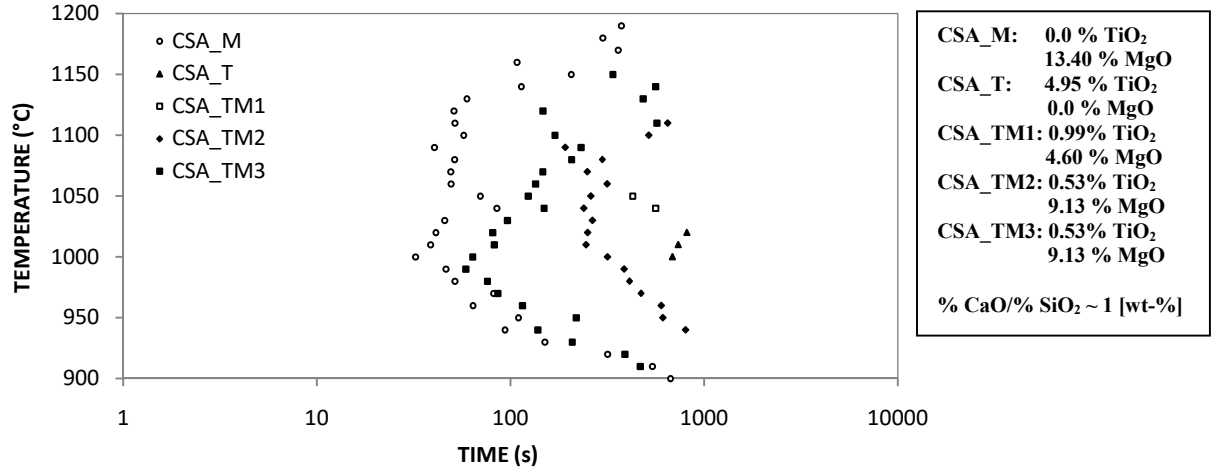

Figure 4.1.41 Comparison of the TTT diagrams of the mold powders investigated in argon atmosphere.

From TTT diagram in inert atmosphere was possible to observe that the CSA_M and CSA_T positioned at the extremes of the diagram, representing the maximum and minimum incubation time and temperature crystallization range, respectively (although the shorter crystallization temperature range is exhibited by the CSA_TM1 mold flux). The effect of the MgO on the crystallization tendency of the mold powders was evident. Additions of MgO from 0 wt-% (CSA_T) to 5 wt-% (CSA_TM1), 7 wt-% (CSA_TM2), 10 wt-% (CSA_TM3) and 15 wt-% (CSA_M) exhibited an accentuated increase of the crystallization temperature range and a shortening of the incubation time. Another visible characteristic was the formation of double nose for additions above 7 wt-% MgO, which suggests the occurrence of two separate nucleation events. **Figure 4.1.42** shows the visual aspect of the CSA_M slag sample take *in situ* from the nose positions, more precisely at 1000°C and 1090°C. Cramb [45] reported change in the position and the shape of TTT curves as MgO content increases – for a CaO-SiO_2-MgO based slags with binary basicity about 1. Increasing the MgO content from 0.0 wt-% to 3.6 wt-% moves the curve slightly upward in temperature and toward lower incubation times. Further MgO additions, from 3.6 to 7.1wt-%, promoted the formation of a double nose curve with distinct incubation times. The nose formed at higher temperatures has higher incubation times than those of the nose formed at lower temperatures. In the present study, similar behavior was obtained for the MgO-bearing mold powders. Nevertheless, addition of 5.0 wt-% MgO (CSA_TM1) does not promoted any significant change with respect to crystallization temperature range, being similar to that exhibited by that with absence of magnesium oxide (CSA_T) – there was a little shortening of the crystallization

range accompanied by a raise of the crystallization temperature – which denotes a low crystallization tendency of these slags (glass structure formers).

The extension of crystallization is dependent of both temperature and chemical composition, *i.e.* the fraction of crystalline phase obtained during the pre-determinate experimental time (20 min) varies with the temperature, type and contents of the components. The percentage of crystal phase was higher in the temperature range around the noses of the TTT curves. However, in many cases, the slag sample did not achieve the full crystallization during the experimental time. For instance, the crystalline fraction of the CSA_T mold powder was restrict to few small crystals in all the crystallization temperature range, not being greater than 20% - 25%, approximately. On the other hand, the extent of crystallization was enhanced with MgO additions. The percentage of crystalline phase is increased considerably with additions of MgO above 5 wt-%, which promoted full crystallization for a lager crystallization temperature range. Assuming the nucleation and growth of the crystals as controlled by mass diffusion, the crystallization behavior of the slags can be attributes to structural changes as a response to temperature changes, which is clearly reflect on the viscosity of the slag. In addition, the increment of MgO content increases the crystal growth velocity of the slag systems, since the slag structure is also a function of its chemical composition. Similar effect was also observed by Prapakorn and Cramb [11] and Jung and Sohn [33] for the CaO-Al_2O_3-MgO system.

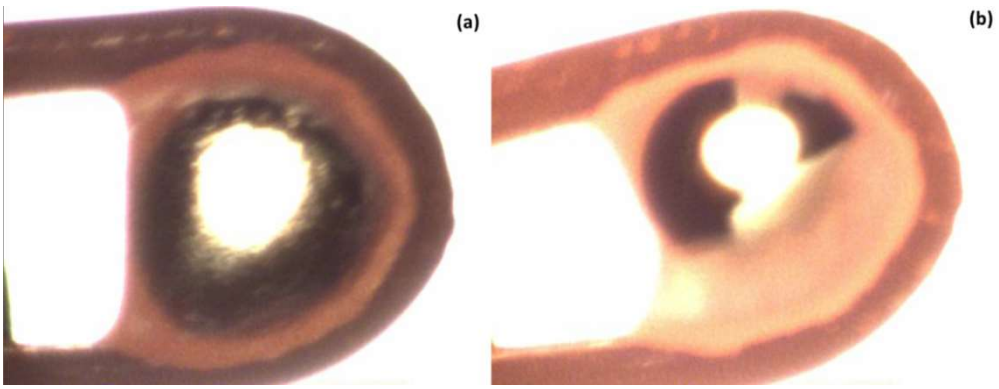

Figure 4.1.42 Visual aspect of CSA_M slag samples: (a) at 1000°C and 222.5s and (b) at 1090°C and 147.9s.

The isothermal temperature affects the crystal morphology significantly [8,31,38]. **Figure 4.1.42(a)** shows two different crystal morphologies at 1000°C: (i) columnar grains formed on the thermocouple surface growing towards the center of the sample and (ii) dispersed equiaxed crystals formed into the slag bulk. In the **Figure 4.1.42(b),** only columnar crystals growth is observed at the temperature of 1090°C. These temperatures correspond to the nose temperatures of the C curves formed above and below 1040°C of the CSA_M mold powder. Similar behavior was found by Klug [8] for slags containing Na_2O. The morphology of crystals changed from dendritic appearance at high temperatures to small and dense crystals. For temperatures below 900°C, very fine crystals were formed and the density of crystals increased until it appears “cloud-like” morphology. In the present study, such crystal morphological phenomena as a function the temperature was observed in all investigated

mold powders. According to Avrami [75], the crystallization rate varies with the temperature. At high undercooling temperatures, the crystallization rate is low. As the temperature is taking lower, the time to the formation of crystals becomes shorter until reaches a minimum, becoming higher upon further lowering undercooling temperatures. Avrami attributes such behavior as the "rigidity of the phases involved with respect to the movements of the constituent particles". The nucleation rate tends to increase with decreasing temperature, while the mobility of atoms or ions decreases with decrease of temperature. At a certain low temperature, the nucleation rate is high and the crystal growth rate is low; the opposite behavior at a certain high temperature. Therefore, there is a specific intermediate temperature where both nucleation and crystal growth rates are equivalents [59]. Zhang *et al*. [38] attributed the morphology change as a function of the temperature to decreasing of ion mobility as the undercooling temperature is continuously reduced. Based on this fact, the authors concluded that the formation of very fine crystals occurs due to the low ion mobility and high nucleation rate. On the other hand, high ion mobility and crystal growth are responsible to the formation of equiaxed individual dendrite crystal. In the present study, the most of cases showed heterogeneous crystal growth at higher temperatures associated to columnar dendrite crystal morphology. As the temperature is reduced, the homogeneous crystal growth became evidently stronger and equixed crystals rose into the melt bulk. For further temperature reductions, the crystal growth mechanism became predominant homogeneous and the crystals were increasingly fine. Some crystals with morphology needle-like dendrites preceded the formation of columnar dendrite. In these cases, the crystal growth was exclusively homogeneous. **Figure 4.1.43** shows the evolution of the crystal growing of CSA_M mold powder at 1190°C.

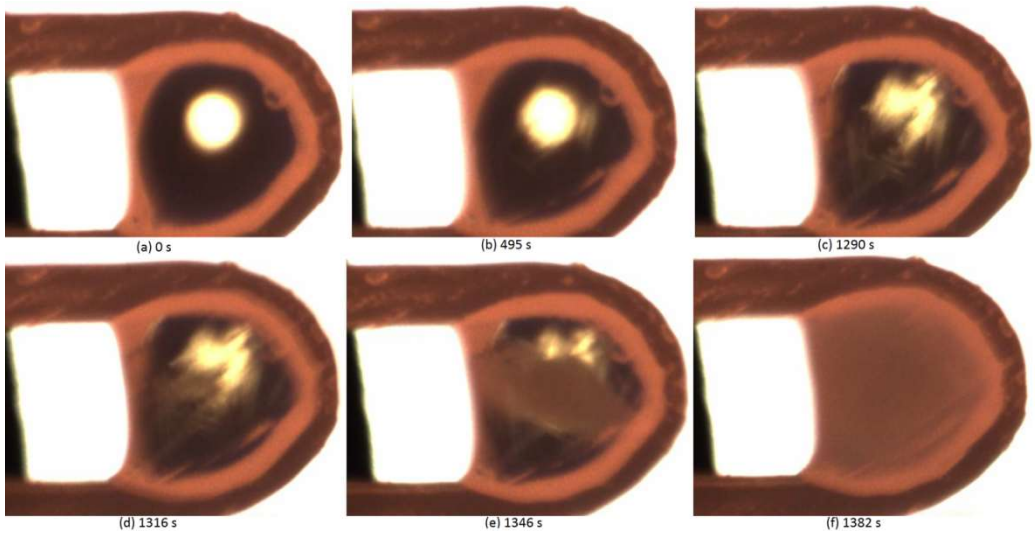

Figure 4.1.43 Crystal morphology evolution of CSA_M mold powder in argon atmosphere and 1190°C.

4.1.3.1 Effect of Water Vapor Atmosphere

An interesting aspect which could be observed in the SHTT measurement results was the influence of temperature on the effect of water vapor on the crystallization behavior of the mold powders. For instance, for a same mold powder, the crystallization kinetics at higher temperature range differs from those at intermediate and lower temperature range. In a general way, a shortening of the incubation time was observed at temperatures below 1000°C,

approximately. In this temperature range, the incubation time deviation exhibited positive values, *i.e.* the crystallization was improved at such a temperature range. At intermediate temperatures, between 950°C and 1080°C – according to the mold powder composition – the effect of water on the crystallization was markedly reduced (the changes in the incubation time was considered negligible). However, at temperatures higher than 1080°C – approximately – water tends to hinder the crystallization onset (reflected in the negative values of the incubation time deviation). Such effect was clearly observed for CSA_M, CSA_TM2 and CSA_TM3 mold powders (see **Figures 4.1.19**, **4.1.35** and **4.1.40**, respectively). Similar results were obtained by Prapakorn and Cramb [11]. For instance, the crystallization temperature range exhibited by the CaO-Al_2O_3-MgO (9.03 MgO wt-%) system was about 950°C – 1500°C. When in presence of water vapor atmosphere, the incubation time of the mold powders increases promoting an inhibition of the crystallization onset. The referred authors conclude that, for this slag system, water hinders the crystallization at temperatures above 1200°C, as aforementioned. On the other hand, at low temperatures, the incubation time became shorter with increasing water vapor atmospheric content, but still higher than those at argon atmosphere. In the present study, the evaluation of influence of the water on the incubation time of the CSA_T and CSA_TM1 systems is disfavored due to their low crystallization tendency exhibited in argon atmosphere measurements. The crystallization temperature range was very narrow, even at lower water vapor partial pressure in the case of the CSA_TM1 mold powder.

In general, water has shown a strong effect toward the enhancement of the crystallization rate in a large range of different slag systems and glasses. As reported by Orrling [3] for a binary CaO-Al_2O_3 system, and by Orrling and Cramb [61] for the CaO-SiO_2-Al_2O_3-Na_2O-CaF_2 system, the presence of water in the atmosphere increases significantly the nucleation and crystals growth rates. Similar results were obtained in the experiments performed with Na_2O-bearing mold flux in humid atmosphere in the present study (see **Figure 4.1.13**). In the same way that the chemical composition influences the slag crystallization behavior, its influence on effect of water on the crystallization is equally evident. Such influence can alters the way as water acts either on enhancement or retardation of the crystallization. For the sake of specificity, results obtained from humid atmosphere measurements using HTT (single or double) for different oxide systems are shown in the **Figure 4.1.44**. Comparing all systems shown in the **Figure 4.4.44**, it is possible to observe the effect of addition of MgO (CAM3) [11] and SiO_2 (CSA_M) on the crystallization behavior of CaO-Al_2O_3 binary system (CA) [3], and its relation with the effect of water on the crystallization rate. For the CA system, the extension of crystallization range increased significantly in presence of water vapor; however, for temperatures lower than 1350°C, the onset of crystal precipitation are not available. With "addition" of MgO to the CA slag system (CAM3) an increment of crystallization temperature range can be observed. Such behavior can be related to the network breaker characteristic of the MgO. The covalent oxygen bondings of silicon tetrahedron are broken by Mg^{2+} cations, creating non-bridging oxygens. The increase of the number of the non-bridging in the melt structure decreases the degree of polymerization of the slag, leading to a reduction of the viscosity.

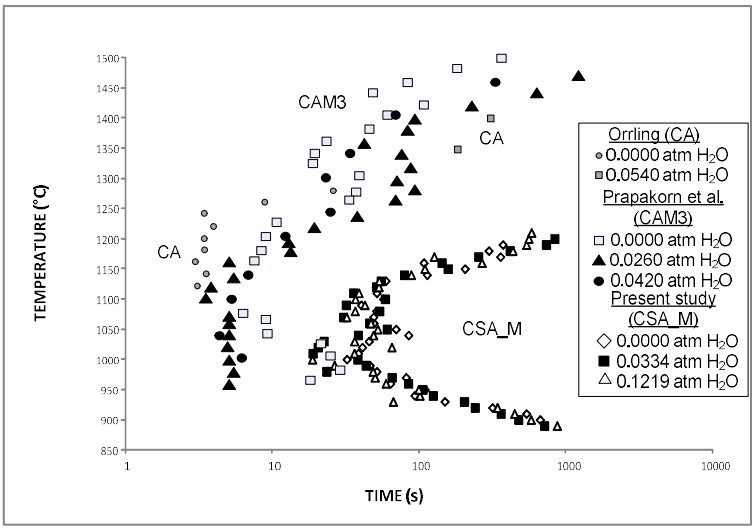

Figure 4.1.44 Comparison of the effect of chemical composition and water vapor on the crystallization behavior of: 48.83 wt-% CaO – 49.32 wt-% Al_2O_3 (CA) [3], 44,88 wt-% CaO – 46.06 wt-% Al_2O_3 – 9.03 wt-% MgO (CAM3) [11] and 33.75 wt-% CaO – 33.89 wt-% SiO_2 – 19.69 wt-% Al_2O_3 – 13.4 wt-% MgO (CSA_M) systems.

Conversely to the effect of the MgO, the "introduction" of SiO_2 to the system (CSA_M) promoted the narrowing of the temperature crystallization range, the increasing of incubation time and the lowering of crystallization temperature, as expected. This reflects directly on the structure of the slag. Silicon dioxide is well-known as a network former; it forms structural chains in the polymeric network of the melt, decreasing the number of non-bridging oxygens and, consequently, increasing its degree of polymerization. For all slag systems showed in **Figure 4.1.44** the binary basicity was approximately 1 (considering the CA binary basicity as CaO/Al_2O_3 ratio).

Unfortunately, experimental solubility data for the slags referred in the **Figure 4.1.44** are not available; however, water solubility data from slags with similar chemical composition are found in the literature, providing a good prediction of the influence of determined oxides on the water capacity of the slags (which definition is found in **Chapter 2**, **section 2.4**). Daya [47] compares the water solubility data of several oxide systems as is shown in the **Figure. 4.1.45**; for instance, taking the slag labeled with the number (1) [76] (50 wt-% CaO - 50 wt-% Al_2O_3) as a reference – and for a specific water vapor pressure (0.2 $atm^{1/2}$) – additions of MgO (slags (6) [69] and (7) [43]) or SiO_2 ((2) [69], (3) [46], (4) [77] and (5) [69]) decrease the water solubility. The water solubility have been reported to be proportional to the square root of the partial pressure of water vapor and increase with increasing the basicity of the slag [46,76,77].

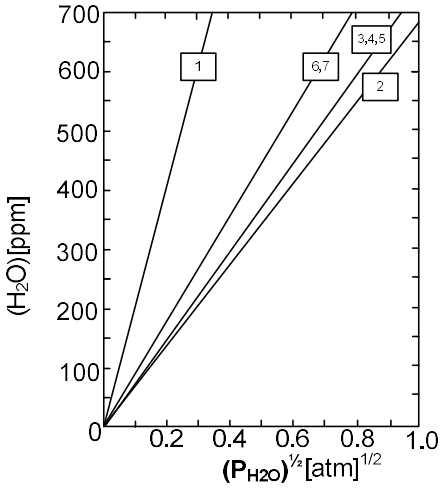

Figure 4.1.45 Solubility data for molten slag systems: (1) 50 wt-% CaO –50 wt-% Al_2O_3 at 1600°C [76]; (2) 37 wt-% CaO – 63 wt-% SiO_2 at 1500°C [69]; (3, 4, 5) 40 wt-% CaO – 40 wt-% SiO_2 – 20 wt-% Al_2O_3 from 1350°C to 1550°C [46,69,77]; (6, 7) 35 wt-% CaO – 45 wt-% SiO_2 – 20 wt-% MgO from 1475°C to 1575°C [43,44]. Figure adapted from Daya [47].

Bringing the water solubility data to the field of the effect of water on the crystallization of the slags, as those showed in the **Figure 4.1.44**, it is possible to suggest that the presence of SiO_2 apparently decreases the solubility of water in the melt; in addition, it alters the incubation time deviation (Δt) of the CSA_M mold powder compared to the CAM system. Based on the data shown in the **Figure 4.1.45**, the follow water solubility sequence can be suggested: CA > CAM3 > CSA_M. A superficial analysis can lead to a direct relationship between water solubility and crystallization enhancement. For the sake of specification, the higher water solubility, the higher the effect of water on the crystallization. However, such relationship was not observed in the crystallization behavior of the mold powders investigated in the present study. The TTT curves obtained from measurements carried out in water vapor atmospheres with H_2O partial pressures of 0.0334 atm and 0.1219 atm are shown in the **Figure 4.1.46** and **Figure 4.1.47**, respectively. The addition of water vapor to argon atmosphere produced some interesting aspects regarding to the displacement of TTT curves among the different compositions. One is the accentuated hindering of crystallization exhibited by the CSA_TM1 sample, upon which the incubation time became larger than that obtained with the CSA_T mold powder in argon atmosphere. In addition, the presence of the humid atmosphere promoted an expressive increase of the crystallization temperature range of the slags which has exhibited strong glass-forming feature, as CSA_T and CSA_TM1 slag systems. Such effect shows be mitigated with increasing crystallization tendency of the mold flux.

Silicate melts are formed by a distribution of structural anionic units with different NBO/T, which proportion depends on SiO_2 content and the type of metal cation present. The abundance of some structural specie – with higher or lower NBO/T – determines the overall degree of polymerization of the slag [58]. However, the presence of water alters the abundance of this species; the proportion of the more polymerized anionic structures can either increase or decrease with increasing water content [1,78].

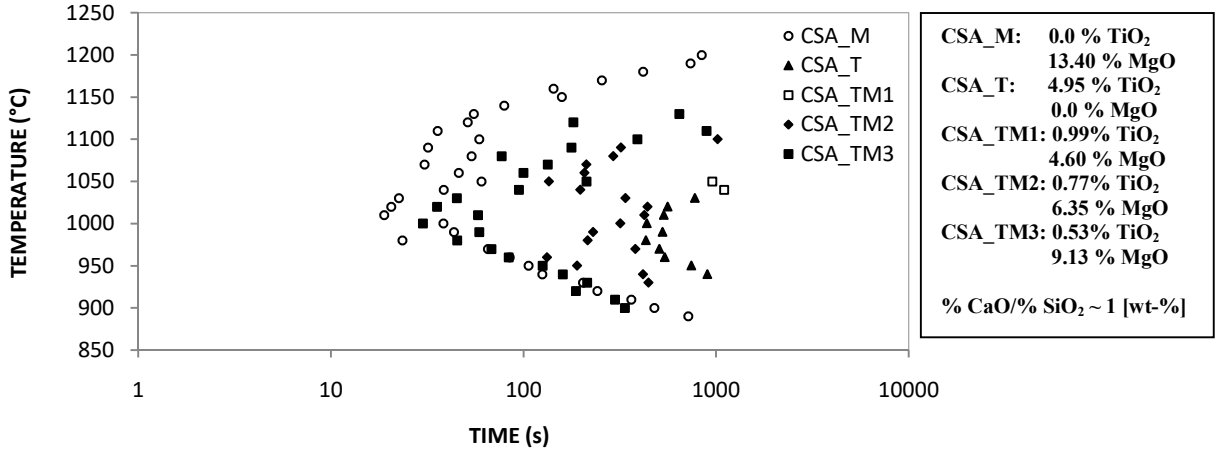

Figure 4.1.46 Comparison of the TTT diagrams of the mold powders investigated in the water vapor partial pressure of 0.0334 atm.

As discussed so far, the CSA_T and CSA_TM1 mold powders exhibited a markedly tendency to form glass. Samples of referred slags do not exhibit any trace of crystallization during continuous cooling process, even at lower cooling rates (see **sections 4.1.1.2** and **4.1.1.3**). In the isothermal experiments, the crystallization was restricted to few isothermal temperatures, with a crystallization temperature range not higher than 30°C. In presence of humid atmosphere, the extent of crystallization of the CSA_T mold powder increased considerably, even in the lower water vapor partial pressure. Regarding to the CSA_TM1 mold flux, such effect of water on the crystallization was perceptible only with higher water content in atmosphere. Water solubility simulation performed using the thermodynamic tool *FactSage 6.4* (see **section 4.2, Figure 4.2.3**) showed the lowest H_2O solubility for the CSA_T and CSA_TM1 mold fluxes, respectively.

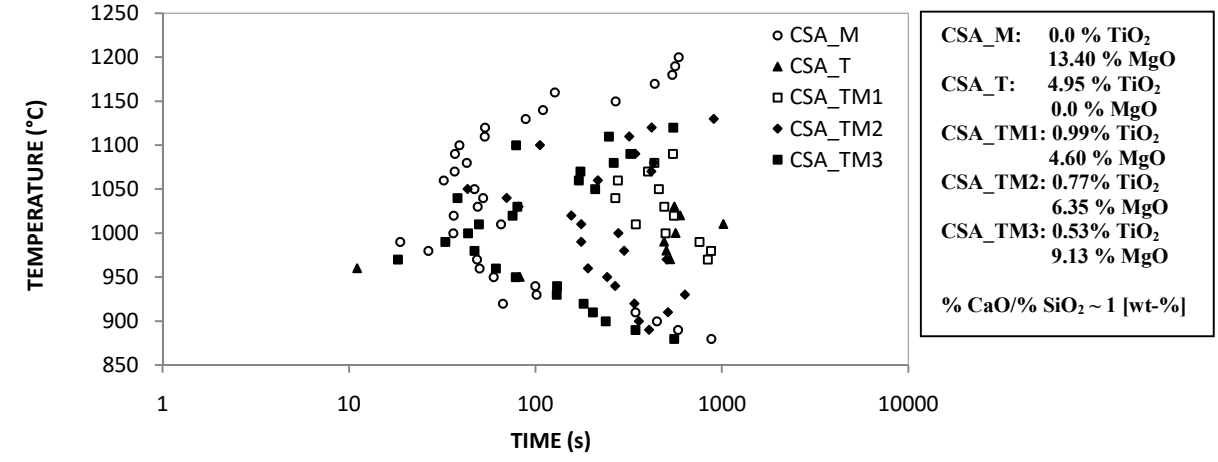

Figure 4.1.47 Comparison of the TTT diagrams of the mold powders investigated in the water vapor partial pressure of 0.1219 atm.

These results indicate that water solubility and its effect on the crystallization are independent events. This fact can be dealt with on some aspects. One concerns to the relation chemical composition–water solubility. Comparing the crystallization behavior of the mold powders in different atmospheres, it is possible to note controversy results concerning to water solubility

and effect of water on crystallization kinetics of the slags. Based on the experimental and predicted data reported in literature, MgO-bearing mold fluxes are more susceptible to dissolve water, and such "predisposition" to water dissolution increases with increasing magnesia content [43,68]. On the other hand, the solubility of water decreases with increasing TiO_2 content [69]. In addition, the relating data of water solubility from **Figure 4.1.45** and the TTT diagrams shown in the **Figure 4.1.44** indicates that the effect of water on crystallization is higher for slag with higher water capacity. When such information is confronted with the crystallization behavior of the mold powders in present study, it would be expected a more prominent effect of water on the crystallization kinetics of mold powders with higher MgO content. However, the TiO_2 based slag systems were more reactive to water content than MgO-bearing mold powder. In this context, the relationship between water solubility and the effect of water on the crystallization behavior is unclear.

Other aspect is concerned to the relation water vapor partial pressure–water solubility. According to a large number of experimental results found in the literature, the solubility of water in slags and molten glasses increase with increasing the partial pressure of water [76,77,79]. However, such an increase in the water content in the mold powder was not necessarily translated as improvement of the crystallization rate of the slag. For the CSA_M mold powder, the increase of the partial pressure had few influence on the crystallization rate, *i.e.* as the crystallization temperature range as the incubation time do not exhibited significant changes in presence of water vapor atmosphere. Other interesting characteristic found in the experimental results was a subtle reduction of the crystallization extent at high temperatures with increasing water vapor partial pressure. Furthermore, there was an enlargement of the crystallization temperature range toward the lower temperatures. Such effect was observed for CSA_TM2 and CSA_TM3 mold powders. In the case of the mold powders less susceptible to dissolve water, namely CSA_T and CSA_TM1, the response to the presence of humid atmosphere as well as to the increase of pressure of water showed some similarity, however, both slags present some peculiarities. The CSA_T mold powder exhibited considerable enlargement of the crystallization temperature range with addition of moisture to the argon atmosphere. Further increasing of humidity in the atmosphere promoted a reduction of the crystallization temperature range about 30°C at lower temperatures. In the case of the CSA_TM1 mold powder, the introduction of water vapor into the atmosphere does not alter the crystallization temperature range, which remained very narrow. On the other hand, the crystallization temperature range was enlarged about 70°C at the lower temperatures region with increasing the water content in the atmosphere.

The most remarkable behavior observed is the apparent influence of temperature on the effect of water vapor on the crystallization. In general, water promotes, in a certain degree, the hindering of the crystallization onset at higher temperatures. For lower temperatures, such onset of crystallization has an inverse behavior, *i.e.*, the incubation time became shorter in presence of humidity. This effect could be well observed in the MgO-bearing mold powders (see **Figures 4.1.18**, **4.1.34** and **4.1.39)**. Similar results were reported by Prapakorn and Cramb [11] and Cramb [45] for a $CaO\text{-}Al_2O_3\text{-}MgO$ based slag (see **Figure 4.1.44**). The authors pointed out that the water hinders the crystallization of the high temperature phases

($3CaO.Al_2O_3$+$3CaO.2Al_2O_3.MgO$), while the crystallization behavior of the phases formed at low temperature ($3CaO.2Al_2O_3$+$MgO.Al_2O_3$) is not affected by the presence of dissolved water in the slag. It was concluded that the addition of MgO to CaO-Al_2O_3 system minimize or eliminate the effect of water on the crystallization behavior of the slag. However, this relationship between temperature and the water effect on the crystallization path is hitherto unclear. In their study, about the role of water in the structure of slags, Mohassab and Sohn [1] concluded that H_2O stabilizes the more polymerized silicate anions rather than the depolymerized monomers. Such stabilization of more polymerized silicate anions results in an increasing of the degree of polymerization and, consequently, the viscosity of the slag. They were based on XRD analysis in addition to NBO/T (non-bridging oxygen atoms/number of atoms in tetragonal coordination), as well FTIR-RAS (Fourier transform infrared-reflection absorption spectroscopy) and Raman spectroscopy, for slag samples with CaO/SiO_2 equal to the unit. The samples were quickly quenched from 1550°C in ice water. This succinct description of the referred study was necessary, at this point, it intends to clarify the experimental conditions in which the results were obtained. In a previous work based on Raman spectroscopy results, Mysen *et al*. [80] report that water tends to form non-bridging oxygens in silicate melts with three-dimensional network structure. For melts with non-bridging oxygens, water acts towards the increase of the degree of polymerization of the slag network. Such a behavior was attributed to the reaction of water with non-bridging oxygen and network modifiers forming Si-OH bonds and M(OH) or $M(OH)_2$ complexes, where M is a modifying cation. Cao *et al.* [81] reported a beneficial effect of water to formation of amorphous substances in detriment of crystalline ones for coal slags at high temperatures. On the other hand, a depolymerization effect of water on the structure of these same coal slags was also observed. For coal slags with high SiO_2-Al_2O_3, the polymerization degree was enhanced with increasing water vapor proportion in the atmosphere [82].

The increasing in viscosity promoted by stabilization of the more polymerized silicate anions can be related to the hindering of crystallization onset at high temperatures. Since the mass diffusivity of the slag is frequently considered as the inverse of the Einstein-Stokes viscosity, an increase of viscosity will act as a barrier to ion mobility according to **Equation 2.41**, reproduced below.

$$D_L = \frac{kT}{6\pi r\eta} \qquad (\mathbf{2.41})$$

where η is liquid viscosity [61].

However, the conclusions reported by Mohassab and Sohn [1] and Mysen *et* al. [80] can be related to the hindering of crystallization only at high temperatures. For intermediate and low temperatures, the role of water on the crystallization behavior remains unclear. The crystallization results obtained from SHTT exhibited, in a general way, three distinct characteristics, as previously mentioned: (i) hindering of the crystallization onset at high temperatures, (ii) relatively insensitive to water vapor at intermediate temperatures, and (iii) enhancement of crystallization rate at low temperatures. Assuming mass diffusion as the

control process of crystal growth, it is worth to consider the viscosity-temperature dependence of the slag: viscosity variations with temperature impose different mass-transfer rates.

Given that the viscosity of the slag is related to its structural condition – the higher the degree of polymerization, the higher the viscosity of the melt – it is expected that changes in the structure of the slag will occur with the variation of temperature. For instance, the NBO/T index of $Na_2Si_2O_5$-$Na_2Ti_2O_5$ melts and glasses slightly increase when they are heated above the T_g; with a maximum value reached at a specific temperature range [58]. This increase in the NBO/T value was attributed to changes in the degree of polymerization of the melt with the temperature by altering the proportion or abundance of the anionic structural units or species, as will be discussed below.

Based on the SHTT crystallization results, reinforced by those reported by Prapakorn and Cramb [11], it is evident the influence of the temperature on the way as the water acts on the structure of the slag. Such influence of temperature will affect directly the role of water on the nucleation and growth of the crystal. In the present study, water acts as a network former, increasing the degree of polymerization of the slag at higher temperatures. On the other hand, water decreases the degree of polymerization of the slag, and accordingly the viscosity at lower temperatures. For the higher temperatures, such propose is supported by the study carried out by Mysen *et al*. [80] and Mohassab and Sohn [1], in which an increase of viscosity with increasing water vapor content was reported.

As aforementioned, NBO/T provides a measure of the degree of depolymerization of the slag. Although this structural parameter do not differentiate between the effects of different cations on the silicate structures [66], as well as the binary basicity, it have been used continuously as a polymerization index of the slag structure. The NBO/T has been correlated to slag properties as viscosity, water capacity, thermal diffusivity and so on. The **Table 4.1.4** shows the nominal NBO/T for the mold fluxes of the present study calculated using the **Equations** (**2.2)**, (**2.3**) and (**2.4**) (**Chapter 2**).

Table 4.1.4 Calculated nominal non-bridging oxygen atoms per number of tetrahedrally-coodinated atoms (NBO/T) of the mold fluxes.

MOLD FLUX	NBO/T (NOMINAL)
CSA_T	0.680
CSA_TM1	1.394
CSA_TM2	1.423
CSA_TM3	1.366
CSA_M	1.560

According to the nominal NBO/T results, the investigated mold powders are predominantly composed by different anionic structural units as sheet (NBO/T = 1) and chain or single ring (NBO/T = 2); except to CSA_T system, where the structure comprehend three-dimensionally (3D) interconnected (NBO/T = 0) and sheet units. This is in accordance with the expression suggested by Mysen *et al*. [83] (**Equation 4.2**) which describe the equilibrium between anionic units for binary melts with NBO/T between 1.0 and 2.0:

$$3Si_2O_6^{4-}\ (chain) = 2Si_2O_5^{2-}\ (sheet) + \ 2SiO_4^{4-}\ (monomer) \qquad (\mathbf{4.2})$$

For a NBO/T between 0.1 and 1.0, the equilibrium of coexisting anionic species is expressed in the **equation 4.3** as follow:

$$2Si_2O_5^{2-}\ (sheet) = 2Si_2O_6^{4-}\ (chain) + \ 2SiO_2\ (3D) \qquad (\mathbf{4.3})$$

The mold fluxes that are situated into this NBO/T range differ in the proportion of each structural units in the melt *i.e.* which kind of structural unit is predominant.

Assuming that the equations (**4.2**) and (**4.3**) describes adequately the anionic equilibrium of the mold powders, the higher reactivity of CSA_T mold powder (NBO/T between 0 – 1) in presence of water can involve the possible presence of three-dimensional units in the structure. Based on the crystallization measurements result carried out with the SHTT, it was possible identify a higher reactivity of water with the more polymerized melts.

Changes in the structural units in more polymerized species of the NaO_2-SiO_2 and CaO-MgO-SiO_2 systems when in presence of water have been reported by Myssen [78]. Such changes were attributed to the formation of bonds between some OH groups and the network modifier metal instead of breaking oxygen bridges by hydroxyl ions (e.g., Na..OH, Ca..OH and MgO..OH). On the other hand, a decrease in the polymerization degree of the NaO_2-Al_2O_3-Si_2O-H_2O system due to an increasing of the proportion of the less polymerized species as detriment of the more polymerized species was also reported. According to the dissolution mechanism (see **Chapter 2, section 2.4**), H_2O can acts a polymerizing or depolymerizing agent of the silicate melt, according to the slag basicity. For instance, in acidic slags, water tends to react with doubly bonded oxygen, promoting the depolymerization of the slag. When in basic slag, water can acts either as polymerization or depolymerization agent. In the case of highly basic slags, water reacts with free oxygen ions causing depolymerization of the slag. In the present work, all slag systems investigated were tailored intentionally to have the same basicity (about unity). According to Mohassab and Sonh [1], such a basicity is considered moderately basic. Thus, it would be expected that the effect of water on the crystallization of the slag exhibit similar behavior in all slags. However, the influence of water was distinct for some slag, namely CSA_T and CSA_TM1 systems. Based in the results obtained in the present study, the utilization of the basicity of the slag as a parameter related to the effect of water on crystallization of slag seems not be appropriate. On the other hand, the degree of polymerization seems to provides a better parameter to explain the interaction water-slag crystallization.

The effect of water on the viscosity of glasses, silicate melts and slags varies according to the chemical composition. For instance, the effect of hydroxyl on the viscosity of glasses is evident for glass former oxides, as commercial vitreous silica and vitreous boric oxide; for silica-lime glasses, such effect is smaller. It is suggested that addition of more non-bridging

species has little additional effect on the viscosity of fragile[1] melts due to its high structural disruption [41]. Measured viscosity values of coal slags showed no substantial difference between measurements carried out in atmospheric air and in an air + 10% H_2O mixture [24]. In turn, an increase of the viscosity in presence of water was reported by Mysen *et al* [80] and Mohassab *et al.*[1] in melt silicates and ironmaking slags, respectively.

Important physicochemical properties of the slags – as viscosity – are directly connected to structure of these systems [84]. Taking into account the temperature dependence of viscosity, changes in the viscosity are related to structural changes as a consequence of variations of the proportions of anionic unities. Accordingly, the degree of polymerization of a slag may also change with the temperature, as well as it implicates directly on the kind and proportion of the anionic species will constitute the slag structure. For a determined mold powder, the extent of polymerization is altered according to the temperature; thus, the both dissolution reactions for basic slags (described by **Equations 2.29** and **2.30** – **Chapter 2**) may occur at different temperature ranges. Accordingly to anionic model proposed by Mysen *et al*. [83] (see **Chapter 2** – **equations 2.6**, **2.7** and **2.8**), there are three distinct compositional regions (or NBO/T) in which a combination of three anionic structural units may occur. Assuming that the degree of polymerization of the mold powders is altered with the temperature (increasing or decreasing), the types and proportions of structural anionic units present in each NBO/T range will also change with the temperature. This suggests that a determined slag will exhibit different structural anionic units which will interact with the water in distinct manner, according to the temperature.

At higher temperatures, the viscosity of the slag decreases as a consequence of increasing number of non-bridging oxygen. Thus, it will be expected an increase of the proportion of the anionic species with higher NBO/T as monomers (SiO_4^{4-}), dimmers ($Si_2O_7^{6-}$) and chains ($Si_2O_6^{4-}$), at the expense of the lower ones as sheet ($Si_2O_5^{2-}$) and three-dimensional units (SiO_2). When in presence of humid atmosphere, the degree of polymerization tends to increase, promoting the retardation of the onset of crystallization in high temperatures. According to Mohassab *et al*. [1], water promotes the stabilization of the more polymerized anionic unit instead the depolymerized monomer. Assuming the stabilization of the more polymerized structure by water in the present study, such phenomenon was observed only in the higher temperature range. This is consistent with the results reported by Mohassab *et al*., take account that their slag samples were quenched from a considerably high temperature (1550°C). In practice, such stabilization of the more polymerized structures results in an increase of viscosity. Considering the mass diffusion as a crystal growth control process, an increase of viscosity implicates in a hindering of the crystallization onset. Nevertheless, such behavior was not completely observed.

At intermediate temperatures, the effect of water on crystallization is apparently mitigated, *i.e.* the crystallization behavior of the slag did not exhibit significant alterations in presence of water compared to its behavior in inert atmosphere. This suggests that in these temperatures,

[1] Fragile melts are characterized by less defined short range order, high configurational degeneracy, and ionic bonds. Their structures disintegrate rapidly with increases in temperature above T_g [32].

the distribution of polymerized and the depolymerized silicate anions tend to be more "equilibrated", even in presence of humidity.

On the other hand, the viscosity of the slag is high at lower temperatures as a consequence of increment of the degree of polymerization (lower NBO/T). At this temperature range, the rate of crystallization was enhanced in presence of water in the atmosphere. Such effect of water vapor on the crystallization can be attributed to the depolymerization of the slag structure and accordingly decreasing the viscosity. Therefore, the effect of the water on the crystallization behavior of the present systems varies with its extent of polymerization degree which, in turn, changes with the temperature. Water acts toward to polymerization the more depolymerized anionic units; and as a depolymerizing agent of the more polymerized structural units. Mysen *et al*. [80] reported that H_2O increases the NBO/T in highly polymerized silicate melts; while in melts with high depolymerization degree, H_2O results in decreased NBO/T.

Naturally, the chemical composition of the slag has strong influence on the stabilization of the coexisting three-dimensionally interconnected units. The type of metal cation present affects the distribution of structural units in the slag [12]. For instance, the presence of Mg^{2+} stabilizes the SiO_2 and SiO_4^{4-}structural units, which are the extreme cases of polymerizing silicate anions; however, the overall NBO/T ratio remains unchanged [12]. Based on the **Equation 4.2**, such behavior suggests that the SiO_4^{4-}anionic units are more stabilized by presence of MgO than $Si_2O_6^{4-}$ and $Si_2O_5^{2-}$. This fits well with the crystallization trend of the present mold fluxes where the crystallization rate and temperature range of crystallization were enhanced with increasing MgO content.

The effect of the temperature on the water solubility has been reported as low or even irrelevant at temperatures over 1370°C [42,46,47]. Assuming that the solubility of water is unaffected to temperature variations, it has not been treated as a relevant factor on the crystallization behavior of the mold powders investigated in the present study. However, it is worth to keep in mind that the structure of the slag changes with the temperature, and this has direct influence on the solubility capacity of the slag systems. A relationship between the hydroxyl capacity and NBO/T of the mold fluxes are shown in the **Section 4.2**.

In a general way, that the water acts as a depolymerization agent in highly polymerized slags (NBO/T between 0.1-1.0) and in highly depolymerized slags (NBO/T > 2), independently of temperature. For instance, water increased significantly the crystallization temperature range of the CSA_T mold powder (NBO/T < 1), while the crystallization rate of slags with NBO/T > 2 as the CSATN_3 [8] (see **Item 4.1.2**, **Figure 4.1.13**) and others [61], was improved by H_2O in the gas atmosphere. For the slags with higher NBO/T, the structure is so disrupted due to high concentration of NBO so that water is not able to polymerize the structure. Shelby and McVay [62] reported that the presence of Na_2O in sodium trisilicate glasses provides a high depolymerization to the structure – due to a formation of a high concentration of NBO – that additional depolymerization due to small additions of water (as much as 1 mol% H_2O) do not provide significant decrease in the degree of polymerization. In the case of the slag with intermediate polymerization degree (2 > NBO/T > 1) water tends to polymerize the more depolymerized anionic units at high temperatures, increasing the viscosity; conversely, water

act toward to the depolymerization of the more polymerized structural units at lower temperatures. It was the case of the CSA_M, CSA_TM1, CSA_TM2 and CSA_TM3 mold powders, where the effect of the water on crystallization is a function of the temperature.

Based on the SHTT measurements results carried out in argon and water vapor atmospheres, with some “support" from Raman spectroscopy analysis results reported in literature [1,78,80], it is possible to suggest that the occurrence of structural changes with temperature affects the proportion of the structural unities which, in turn, affects the effect of water on the crystallization behavior. In other words, structural changes promoted by temperature denote the amphoteric characteristic of water, which have reflex on the crystallization behavior of the mold fluxes. In addition, the solubilized water may alter the abundance of determined coexistent anionic specie in detriment of another one. Assuming mass diffusivity as the limiting process to crystal nucleation and crystal growth, either the crystallization rate improvement at lower temperatures, or the crystallization hindering at higher temperatures are a consequence of the viscosity variations caused by the reported structural changes. In the present work, it is suggested that such “distinct” crystallization behavior promoted by the presence of water as function of temperature occurs more intensely for mold powders with a nominal NBO/T between 1 and 2.

References

[1] Mohassab, Y., Sohn, H. Y. Analysis of Slag Chemistry by FTIR-RAS and Raman Spectroscopy: Effect of Water Vapor Content in H_2-H_2O-CO-CO_2 Mixtures Relevant to a Novel Geen Ironmaking Technology. *Steel Research International* **2014**, *85*.

[2] Wang, W., Yan, X., Zhou, L., Xie, S., Huang, D. Influences of Basicity and Li_2O on the Properties of Fluorine-Free Mold Flux for the Casting of Medium Carbon Steels. *Metallurgical and Materials Transactions B* **2016**, *47B*, 963-976.

[3] Orrling, C. Crystallization Phenomena in Slags. Carnegie Mellon University, 2000.

[4] Kashiwaya, Y., Cicutti, C. E., Cramb, A. W. An Investigation of the Crystallization of a Continuous Casting Mold Slag Using the Single Hot Thermocouple Technique. *ISIJ Internacional* **1998**, *38*, 357-365.

[5] Orrling, C., Fang, Y., Phinichka, N., Sridhar, S., Cramb, A. W. Observing and Measuring Solidification Phenomena at High Temperatures. *JOM* **1999**, *51*.

[6] Orrling, C., Cramb, A. W., Tilliander, A., Kashiwaya, Y. Obeservations of the Melting and Solidification Behavior of Mold Slags. *Iron & Steel Society* **2000**, *27*, 53-63.

[7] Song, M., Shu, Q., Sichen, D. Vicosities of the Quarternary Al_2O_3-CaO-MgO-SiO_2 Slags. *Steel Research International* **2011**, *82*, 261-268.

[8] Klug, J. L. Crystallization control for fluorine-free slags using the Single Hot Thermocouple Technique. UFRGS-Brazil / TU Bergakademie Freiberg-Germany, 2012.

[9] Sridhar, S., Mills, K. C., Afrange, O. D. C., Lörz, H. P., Carli, R. Break temperatures of mould fluxes and their relevance to continuous casting. *Ironmaking and Steelmaking* **2000**, *27*, 238-242.

[10] Seidel, T., Friedrich, C. Influence of shear rate and temperature of the crystallization of spontaneous crystallizing glass-ceramic. *Journal of Materials Science* **1992**, *27*, 263-269.

[11] Prapakorn, K., Cramb, A. W. Initial Solidification Behavior in Continuous Casting: The Effect of MgO on the Solidification Behavior of CaO-Al_2O_3 Based Slags. *MS&T* **2004**, 3-10.

[12] Mills, K. C.: *Slag Atlas*; 2nd Edition ed.; Verlag Stahleisen GmbH Düsseldorf, 1995.

[13] Li, J., Shu, Q., Hou, X., Chou, K. Effect of TiO_2 Addition on Crystallization Characteristics of CaO-Al_2O_3-based Mould Fluxes for High Al Steel Casting. *ISIJ Internacional* **2015**, *55*, 830-836.

[14] Ohno, A., Ross, H. U. Optimum slag composition of the blast furnace smelting of titaniumferous ores. *Canadian Metallurgical Quarterly* **1963**, *2*, 259-279.

[15] Wang, Z., Shu, Q., Chou, K. Viscosity of Fluoride-Free Mold Fluxes Containing B_2O_3 and TiO_2. *Steel Research International* **2013**, *84*, 766-776.

[16] Sohn, I., Wang, W., Matsuura, H., Tsukiashi, F., Min, D. J. Influence of TiO_2 on the Viscous Behavior of Calcium Silicate Melts Containing 17 mass% Al_2O_3 and 10 mass% MgO. *ISIJ Internacional* **2012**, *52*, 158-160.

[17] Shankar, A., Görnerup, M., Lahiri, A. K., Seetharaman, S. Experimental Investigation of the Viscosities in CaO-SiO_2-MgO-Al_2O_3 and CaO-SiO_2-MgO-Al_2O_3-TiO_2 Slags. *Metallurgical and Materials Transactions B* **2007**, *38*, 911-915.

[18] Li, J. L., Shu, Q., Hou, X., Chou, K. C. Effect of TiO_2 addition on viscosity and structure of CaO-Al_2O_3 based mould fluxes for high Al steel casting. *Canadian Metallurgical Quarterly* **2015**, *54*, 85-91.

[19] Zhang, G. H., Chou, K. C., Zhang, J. l. Influence of TiO_2 on viscosity of aluminosilicate melts. *Ironmaking and Steelmaking* **2014**, *41*, 47-50.

[20] Xin, Q., Wen, G., Tang, P. Viscosity and Viscosity Estimate Model of Fluoride-Free and Titanium-Bearing Mold Fluxes. *Journal of Iron and Steel Research International* **2010**, *17*.

[21] Feng, C., Chu, M-S., Tang, J., Qin, J., Li, F., Liu, Z-G. Effects of MgO and TiO_2 on the viscous behaviors and phase compositions of titanium-bearing slag. *International Journal of Minerals and Materials* **2016**, *23*, 868-880.

[22] He, S., Huang, Q., Zhang, G., Lu, Y., Wang, Q. Solidification Properties of CaO-SiO_2-TiO_2 Based Mold Fluxes. *Journal of Iron and Steel Research International* **2011**, *18*, 15-19.

[23] Müller, R., Zanotto, E. D., Fokin, V. M. Surface crystallization of silicate glasses: nucleation sites and kinetics. *Journal of Non-Crystalline Solids* **2000**, *274*, 208-231.

[24] Hurley, J. P., Watne, T. M., Nowok, J. W. The Effect of Atmosphere and Additives on Coal Slag Viscosity. 691-694.
[25] Zhou, L., Wang, W., Zhou, K. Viscosity and Crystallization Behavior of F-free Mold Flux for Casting Medium Carbon Steels. *ISIJ Internacional* **2015**, *55*, 1916-1924.
[26] Park, J. H. Solidification structure of CaO-SiO_2-MgO-Al_2O_3 (-CaF_2) systems and computational phase equilibria: Crystallization of $MgAl_2O_4$ spinel. *Computer Coupling of Phase Diagrams and Thermochemistry* **2007**, *31*, 248-437.
[27] Tang, X., Zhang, M., Guo, M., Zhang, Z., Wang, X. Non-isothermal Crystallization Kinetics of Mineral Wool Fibers. *Journal of University of Science and Technology Beijing* **2011**, *12*.
[28] Lacefield, W., Clare, A.: Handobook of biomaterials evaluation. Second Edition ed., 1999; pp 144.
[29] Wang, Z., Sun, Y., Sridrar, S., Zhang, M., Zhang, Z. Investigation on Viscosity and Nonisothermal Crystallization Behavior of P-Bearing Steelmaking Slags with Varying TiO_2 content. *Metallurgical and Materials Transactions B* **2017**, *48*, 527-537.
[30] Durinck, D., Jones, P. T., Blanpain, B., Wollants, P. Slag Solidification Modeling Using the Scheil-Gulliver Assumptions. *Journal of American Ceramic Society* **2007**, *90*, 1177-1185.
[31] Cramb, A. W. The Solidification Behavior of Slags: Phenomena Related to Mold Slags. *ISIJ International* **2014**, *54*, 2665-2671.
[32] Petajajarvi, M., Klug, J. L., Hooli, P., Heller, H. P., Scheller, P. R.: Industrial mould slags for continuous casting of stainless steel - analysis of the crystallisation behaviour using the Single Hot Thermocouple Technique. In *Ninth International Conference on Molten Slags, Fluxes and Salts (MOLTEN)*: Beijing, China, 2012.
[33] Jung, S. S., Sohn, I. Crystallization Behavior of the CaO-Al_2O_3-MgO System Studied with a Confocal Laser Scanning Microscope. *Metallurgical and Materials Transactions B* **2012**, *43B*, 1530-1539.
[34] Waseda, Y., Toguri, J. M.: *The Structure and Properties of Oxide Melts*; World Scientific Publishing Co. Pte. Ltd., 1998.
[35] Shelby, J. E. Diffusion and solubility of water in alkali borates melts. *Physics and Chemistry of Glasses* **2003**, *44*, 106-112.
[36] Franz, H. Solubility of Water Vapor in Alkali Borates Melts. *Journal of American Ceramic Society* **1966**, *49*, 473-477.
[37] Kashiwaya, Y., Nakauchi, T., Pham, K. S., Akiyama, S., Ishii, K. Crystallization Behavior Concerned with TTT and CCT Diagrams of Blast Furnace Slag Using Hot Thermocouple Technique. *ISIJ Internacional* **2007**, *47*, 44-52.
[38] Zhang, Z. T., Li, J., Liu, P. Crystallization Behavior in Fluorine-Free Mold Fluxes Containing TiO_2 / ZrO_2. *Journal of Iron and Steel Research International* **2011**, *18*, 31-37.
[39] Zhou, L., Wang, W., Ma, F., Li, J., Wei, J., Matsuura, H., Tsukihashi, F. A Kinetics Study of the Effect of Basicity on the Mold Fluxes Crystallization. *Metallurgical and Materials Transactions B* **2012**, *43B*, 354-362.
[40] Lu, B., Wang, W., Li, J., Zhao, J., Huang, D. Effect of Basicity and B_2O_3 on the Crystallization and Heat Transfer Behaviors of Low Fluorine Mold Fluxes for Casting Medium Carbon Steels. *Metallurgical and Materials Transactions B* **2013**, *44B*, 365-377.
[41] Shelby, J. E.: *Introduction to Glass Science and Technology*; Second ed.; The Royal Society of Chemistry: Cambridge, 2005.
[42] Sosinsky, D. J., Maeda, M., McLean, A. Determination and Prediction of Water Vapor Solubilities in CaO-MgO-SiO_2 Slags. *Metallurgical Transactions B* **1985**, *16B*, 61-66.
[43] Iguchi, Y., Fuwa, T. The Solubility of Water in Liquid CaO-SiO_2-MgO, with and whitout "FeO" at 1550°C. *Transactions ISIJ* **1970**, *10*, 29-35.
[44] Zuliani, D. J., Iwase, M., McLean, A. The Thermodynamics of Water Vapour Dissolution in CaO-MgO-SiO_2 Slags. *Trans. ISIJ* **1982**, *1*, 61-67.
[45] Cramb, A. W. *Quantifying the thermal behavior of slags*: Pittsburgh, PA2003.
[46] Walsh, J. H., Chipman, J., King, T. B., Grant, N. J. Hydrogen in Steelmaking Slags. *Journal of Metals - Transactions AIME* **1956**, 1568-1576.

[47] Daya, Z. A. The Thermodynamics of Water Vapour Dissolution in Tundish Fluxes. University of Toronto, 1997.
[48] Orrling, C., Tilliander, A., Kashiwaya, Y., Cramb, A. W. Observations of the melting and solidification behavior of mold slags. *I&SM* **2000**, *20*, 53.
[49] Kölbl, N., Marschall, I., Harmuth, H. Single Hot Thermocouple Technique for the Characterization of the Crystalliztion Behavior of Transparent or Translucent Liquids. *Journal of Materials Science* **2011**, *46*, 6248-6254.
[50] Orrling, C., Sridhar, S., Cramb, A. W. *In situ* Observations and Thermal Analysis of Crystallization Phenomena in Mold Slags. *High Temperature Materials and Processes* **2001**, *20*, 195-199.
[51] Nakada, H., Nagata, K. Crystallization of $CaO-SiO_2-TiO_2$ as a Candidate for Fluorine Free Mold Flux. *ISIJ International* **2006**, *46*, 441-449.
[52] Qi, X., Wen, G., Tang, P. Investigation on heat transfer performance of fluoride-free and titanium-bearing mold fluxes. *Journal of Non-Crystalline Solids* **2008**, *354*, 5444-5425.
[53] Rocabois, P., Pontoire, J. N., Lehmann, J., Gaye, H. Crystallization of Al_2O_3-CaO-SiO_2 based oxide inclusions. *Journal of Non-Crystalline Solids* **2001**, *282*, 98-109.
[54] Turkdogan, E.T.: *Physicochemical properties of molten slags and glasses*; The Metal Society: London, 1983. pp. 201-208.
[55] DeVries, R. C., Roy, R., Osborn, E. F. Phasa Equilibria in the System $CaO-TiO_2-SiO_2$. *Journal of the American Ceramic Society* **1955**, *38*, 158-171.
[56] McRae, L. B., Pothas, E., Jochens, P. R., Howat, D. D. Physico-Chemical Properties of Titaniferous Slags. *Journal of the South African Institute of Mining and Metallurgy* **1969**, 577-594.
[57] Wang, Z., Shu, Q., Chou, K. Structure of $CaO-B_2O_3-SiO_2-TiO_2$ Glasses: a Raman Spectral Study. *ISIJ Internacional* **2011**, *51*, 1021-1027.
[58] Mysen, B. O., Nouville, D. Effect of temperture and TiO_2 content on the structure of $Na_2Si_2O_5-Na_2Ti_2O_5$ metls and glasses. *Geochimica et Cosmochimica Acta* **1995**, *59*, 325-342.
[59] Mizuno, H., Esaka, H., Shinozuka, K., Tamura, M. Analysis of theCrystallization of Mold Flux for Continuous Casting of Steel. *ISIJ Internacional* **2008**, *48*, 277-285.
[60] Okui, N. Relationship between crystallization temperature and melting temperature in crystalline materials. *Journal of Materials Science* **1990**, *25*, 1623-1631.
[61] Orrling, C., Cramb, A. W. The Effect of Water Vapor on Mold Slag Cristallization. *Metallurgical and Materials Transactions B* **2000**, *31B*, 403-406.
[62] Shelby, J. E., McVay, G. L. Influence of water on the viscosity and thermal expansion of sodium trisilicate glasses. *Journal of Non-Crystalline Solids* **1976**, *20*, 439-449.
[63] Davis, M. J. The effect of water on the viscosity of silicate melts: A configurational entropy approach. *Geochimica et Cosmochimica Acta* **1998**, *63*, 167-173.
[64] Fokin, V. M., Zanotto, E. D., Schmelzer, J. W. P. Homogeneous nucleation versus glass transition temperature of silicate glasses. *Journal of Non-Crystalline Solids* **2003**, *321*, 52-65.
[65] Fokin, V. M., Nascimento, M. L. F., Zanotto, E. D. Correlation between maximum crystal growth rate and glass transition temperature of silicate glasses. *Journal of Non-Crystalline Solids* **2005**, *351*, 789-794.
[66] Mills, K., C.: *The Estimation of Slag Properties*, 2011.
[67] Min'ko, N. I., Varavin, V. V. Effect of water in the structure and properties of glass (review). *Glass and Ceramics* **2007**, *64*, 71-74.
[68] Zorzato, M. G. Análise Termodinâmica da Incorporação da Hidrigênio pelo Aço Líquido através da Escória da Refino Secundário (portuguese). Universidade Federal do Rio Grande do Sul - UFRGS, 2013.
[69] Iguchi, Y., Ban-Ya, S., Fuwa, T. The Solubility of Water in Liquid $CaO-SiO_2$, with Al_2O_3, TiO_2 and FeO at 1550°C. *Transactions ISIJ* **1969**, *9*.
[70] Davis, M. J., Ihinger, P. D. Heterogeneous crystal nucleation on bubbles in silicate melt. *American Mineralogist* **1998**, *83*, 1008-1015.
[71] Swanson, S. E. Relation of nucleation and crystal-growth rate to the development of granitic textures. *American Mineralogist* **1977**, *62*, ^966-978.

[72] de Oliveira, T. C., Ribeiro, C. A. Brunelli, D. D., Rodrigues, L. A., Thim, G. P. The kinetic of mullite crystallization: Effect of water content. *Journal of Non-Crystalline Solids* **2010**, *356*, 2980-2985.
[73] Wagstaff, F. E., Richards, K. J. Kinetics of Crystallization of Stoichiometric SiO_2 Glass in H_2O Atmospheres. *Journal of American Ceramic Society* **1966**, *49*, 118-121.
[74] Li, X., Yin, X., Zhang, L., He, S. The devitrification kinetics of silica powder heat-treated in different conditions. *Journal of Non-Crystalline Solids* **2008**, *354*, 3254-3259.
[75] Avrami, M. Kinetics of Phase Change. I*. *Journal of Chemical Physics* **1939**, *7*, 1103-1112.
[76] Schwerdtfeger, K., Schubert, H. G. Solubility of Water in $CaO-Al_2O_3$ Melts at 1600°C. *Metallurgical Transactions B* **1978**, *9B*, 143-144.
[77] Sachdev, P. L., Majdic, A., Schenck, H. Solubility of Water in Lime-Alumina-Silica Melts. *Metallurgical Transactions* **1972**, *3*, 1537-1543.
[78] Mysen, B. O. Water-melt interaction in hydrous magmatic systems at high temperature an pressure. *Progress in Earth and Planetary Science* **2014**, *1:4*.
[79] Yokokawa, T. Gas solubilities in molten salts and silicates. *Pure & Applied Chemistry* **1986**, *58*, 1547-1552.
[80] Mysen, B. O., Virgo, D., Harrison, W. J., Scarfe, M. Solubility mechanisms of H_2O in silicate melts at high pressures and temperatures: a Raman spectroscopic study. *American Mineralogist* **1980**, *65*, 900-914.
[81] Cao, X., Kong, L., Bai, J., Ge, Z., He, C., Li, H., Bai, Z., Li, W. Effect of water vapor on coal slag ash viscosity under gasification condition. *Fuel* **2019**, *237*, 18-27.
[82] Cao, X., Kong, L., Bai, J., Zhao, H., Ge, Z., Li, H., Bai, Z., Li, W. Effect of water vapor on viscosity behavior of coal slags with high silicon-aluminum level under gasification condition. *Fuel* **2020**, *260*.
[83] Mysen, B. O., Virgo, D., Scarfe, C. M. Relations between the anionic structure and viscosity of silicate melts - a Raman spectroscopic study. *American Mineralogist* **1980**, *65*, 690-710.
[84] Mills, K. C. The Influence of Structure on the Physico-chemical Properties of Slags. *ISIJ Internacional* **1993**, *33*, 148-155.

4.3 Thermodynamic Simulations Results

4.3.1 Water Solubility Predictions

In the present section, the results of calculations of water solubility in the $CaO\text{-}SiO_2\text{-}Al_2O_3\text{-}MgO\text{-}TiO_2$ slag systems – carried out using *FactSage 6.4* for two distinct water vapor partial pressures – are presented below. The thermodynamic calculation results are confronted to the crystallization behavior experimental results from SHTT measurements.

The thermodynamic calculations were validated by means of experimental water solubility data provided by Iguchi, Ban-ya and Fuwa [1], and Iguchi and Fuwa [2]. Curves of *iso*-hydroxyl capacity or *iso*-water capacity (*iso*-C_{OH}) from solubility data of $CaO\text{-}SiO_2\text{-}MgO$, $CaO\text{-}SiO_2\text{-}Al_2O_3$ and $Ca\text{-}SiO_2\text{-}TiO_2$ ternary systems were adopted as guidelines (**Figure 4.2.1**). Thus, the chemical composition of the investigated mold powders (see **Table 3.2**) were adjusted to ternary slag systems and inserted in its correspondent ternary hydroxyl capacity (C_{OH}) diagram. This adjustment was carried out suppressing the components that were not contemplated by the three ternary diagrams, $CaO\text{-}SiO_2\text{-}MgO$ (CSM), $CaO\text{-}SiO_2\text{-}Al_2O_3$ (CSA) and $CaO\text{-}SiO_2\text{-}TiO_2$ (CST). The chemical composition of the adjusted mold powders is shown in the **Table 4.2.1**. The binary basicity (CaO/SiO_2) was kept constant equal to unity.

Table 4.3.1 Adjusted chemical composition of the mold powders used in the thermodynamic calculations and concentration values H, H_2O and hydroxyl capacity (C_{OH}).

Ternary system	Mold flux sample	Components			H [ppm]	H_2O [ppm]	C_{H2O} [ppm $atm^{-1/2}$]
		CaO	SiO_2	MgO			
$CaO\text{-}SiO_2\text{-}MgO$	**CSM1**	40.74	40.74	18.52	96.172	865.548	1413.434
	CSM2	47.06	47.06	5.88	50.322	452.898	739.5793
	CSM3	45.78	45.78	8.43	55.647	500.823	817.8405
	CSM4	43.75	43.75	12.50	67.013	603.117	984.8859
		CaO	SiO_2	Al_2O_3			
$CaO\text{-}SiO_2\text{-}Al_2O_3$	**CSA1**	36.84	36.84	26.32	35.959	323.631	528.4872
	CSA2	38.82	38.82	22.35	36.753	330.777	540.1566
	CSA3	42.55	42.55	14.89	38.728	348.552	569.1830
	CSA4	41.19	41.19	17.62	37.948	341.532	557.7194
	CSA5	39.11	39.11	21.79	36.883	331.947	542.0672
		CaO	SiO_2	TiO_2			
$CaO\text{-}SiO_2\text{-}TiO_2$	**CST1**	46.67	46.67	6.67	34.478	310.302	506.7210
	CST2	49.38	49.38	1.23	40.257	362.313	591.6547
	CST3	49.51	49.51	0.98	40.557	365.013	596.0637
	CST4	49.65	49.65	0.71	40.884	367.956	600.8696
		CaO	Al_2O_3				
$CaO\text{-}Al_2O_3$*	**CA1**	44.44	55.56	-	38.756	348.808	1559.916
	CA2	50.00	50.00	-	48.028	433.869	1940.320
	CA3	54.55	45.45	-	60.474	544.269	2432.045
T = 1550°C and P_{H2O} = 0.370078 atm (0.375 bar)							

*Water vapor partial pressure = 0.0507 bar and T = 1600°C.

The thermodynamic calculations were set to the temperature of 1550°C and a water vapor partial pressure of 0.375 bar; same conditions whereon the hydroxyl capacities of the ternary diagrams were constructed [1,2]. The data of absorbed hydrogen content by the slag systems were converted to water content by the **Equation 4.4**

$$\frac{1}{2}\,O^{2-}{}_{(slag)} + \frac{1}{2}\,H_2O_{(gas)} = OH^-{}_{(slag)} \qquad \textbf{(4.4)}$$

The hydroxyl capacity (also named as water capacity – C_{H2O}) was calculated using the **Equation (2.34)** – reproduced as follows

$$C_{OH} = \frac{ppm\ H_2O}{(p_{H_2O})^{1/2}} \quad (2.34)$$

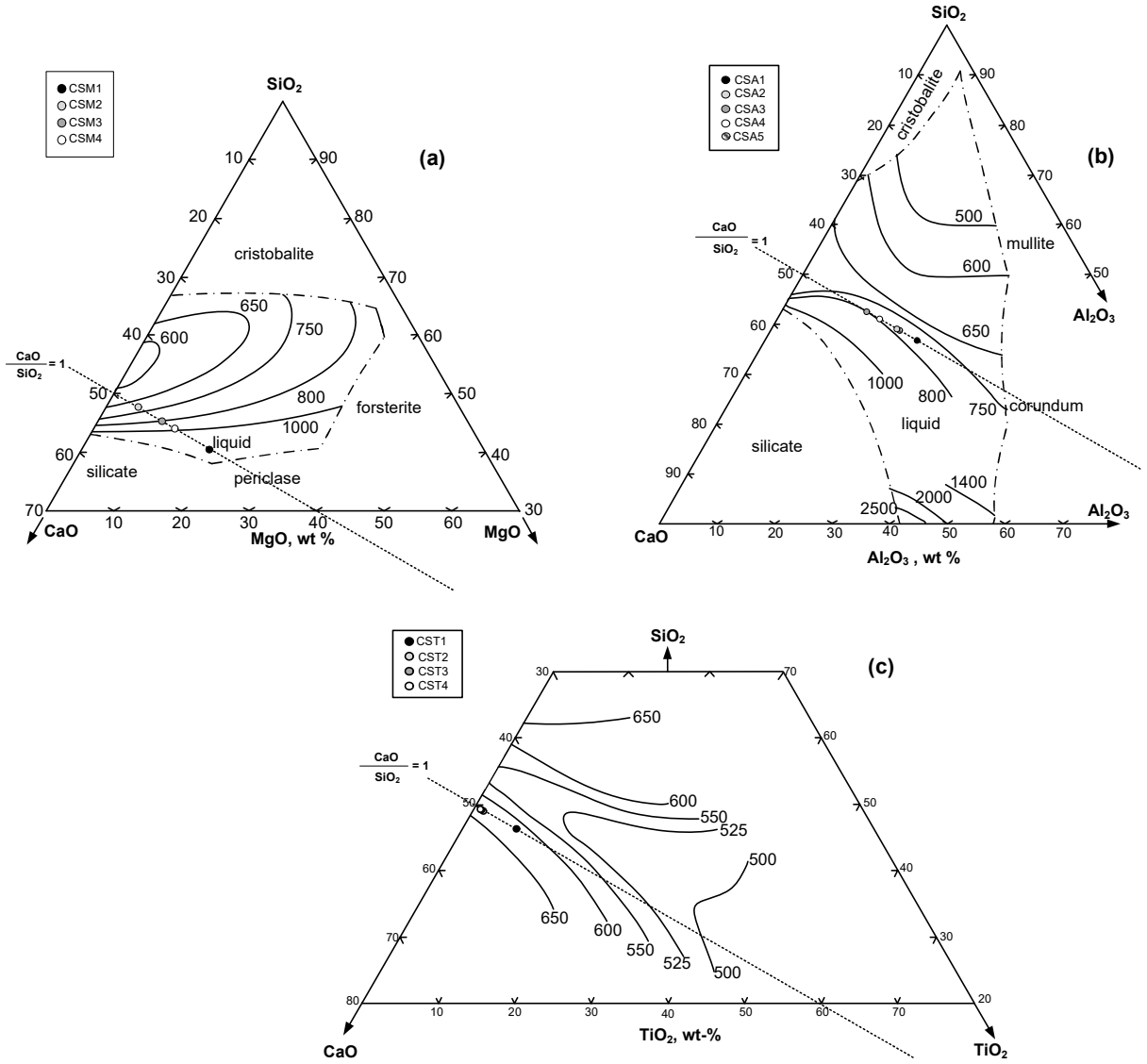

Figure 4.2.1 Iso-hydroxyl capacities ternary diagrams for (a) CaO-SiO_2-MgO; (b) CaO-SiO_2-Al_2O_3, and (c) CaO-SiO_2-TiO_2 ternary slag systems at 1550°C and 0.375 bar. Figure adopted by (a) Iguchi and Fuwa [2]; and (b) and (c) Iguchi, Ban-ya and Fuwa [1]. The dotted line represents the CaO/SiO_2 ratio.

The hydroxyl capacities results for the ternary systems containing MgO (**Figure 4.3.1(a)**) showed good agreement with the *iso*-C_{OH} curves from experimental solubility data. The CSM system exhibited the highest hydroxyl capacities, as expected [3-5] with the larger water solubility range. For the CSA (**Figure 4.3.1(b)**) and CST (**Figure 4.3.1(c)**) ternary systems, the calculated C_{OH} results showed some discrepancies with the experimental data: according to the *iso*-C_{OH} ternary diagrams, the hydroxyl capacities of the CSA compositions are in a range of 750 – 800 ppm $bar^{-1/2}$; whereas for the calculated data the solubility data lies in a range between 520 – 570 ppm $bar^{-1/2}$. Similarly, C_{H_2O} experimental data for the CST

composition exhibited a range of 600 – 650 ppm $bar^{-1/2}$ while the calculated capacities are between 500 and 600 ppm $bar^{-1/2}$. A certain divergence in experimental results can also be seen in the literature; for instance, the water solubility results from CaO-SiO_2-MgO system reported by Sosinsky *et al*. [3] are lower than those from Iguchi *et al*. [2].

Figure 4.2.2 (see also **Table 4.2.1**) shows the hydroxyl capacity data from *FactSage* calculations. The hydroxyl capacities of the CSA and CST ternary systems are lower and close to each other in a very narrow solubility range, in contrast to those obtained with the CSM system. This suggests that Al_2O_3 and TiO_2 behave similarly regarding to water solubility potential within the chemical composition range investigated, *i.e.*, TiO_2 at low content is found as Ti^{4+}, which has a role equivalent to Al^{3+} in the structure, acting as network forming element. According to Mills [6], TiO_2 in steelmaking slags works as network former in a range 1 - 7 wt-%. With respect to the influence of chemical composition, it is possible to observe a substantial increase of water solubility with increasing MgO content; conversely, there is a slight decrease of water solubility with increasing content of Al_2O_3 and TiO_2.

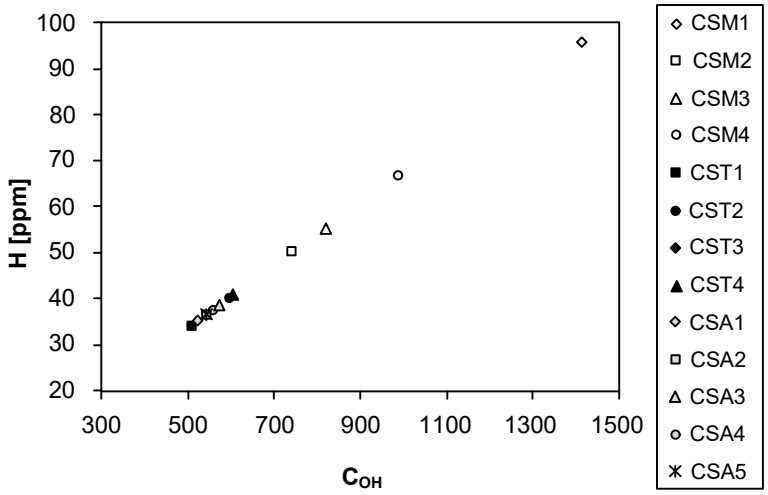

Figure 4.2.2 C_{OH} calculated from *FactSage* water solubility results for the CSM, CSA and CST ternary systems.

Considering the experimental error range inherent to the experimental procedures, the C_{H_2O} calculated data for ternary systems are assumed to be in good agreement with the experimental results, giving support to the thermodynamic prediction of higher order systems. It is noteworthy that, despite the discrepancy in some systems, the water solubility in the ternary slags shows the same tendency between experimental and calculated data.

The water solubility thermodynamic calculations, based on the chemical composition of the *original* mold fluxes (see **Chapter 3**, **Table 3.2**), are shown in the **Figure 4.2.3**. Two different aspects can be highlighted: (i) the effect of water vapor partial pressure and (ii) the influence of chemical composition on the water solubility of the slags. The solubility of water increases linearly with square root of partial pressure of water, which is in accordance with an extensive literature concerned to water solubility from atmosphere in slags, glasses and oxide melts [3,7-11]. The water vapor partial pressures used for the calculations were approximately the same applied in the isothermal crystallization experiments in the present study.

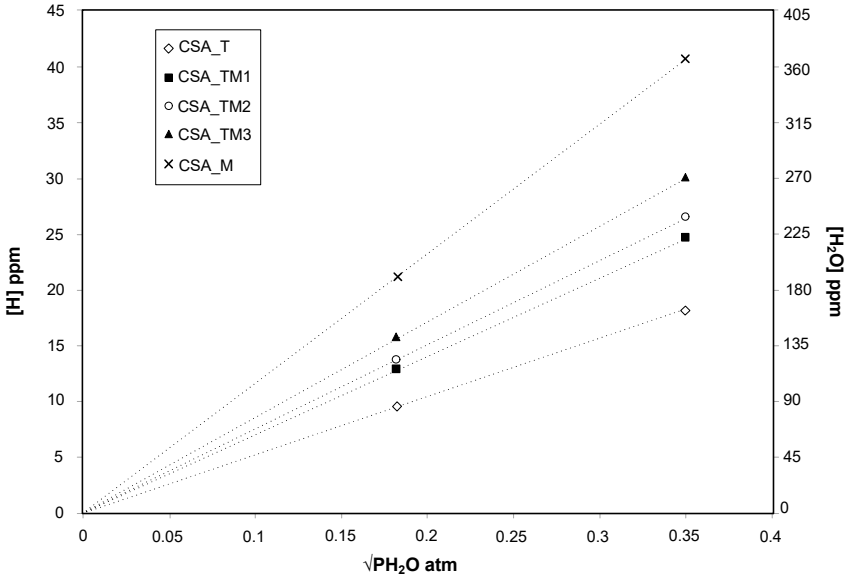

Figure 4.2.3 Water solubility of the mold powders as a function of water vapor partial pressure at 1550°C from thermodynamics calculation using the *FactSage*.

Concerning the chemical composition, the results for higher order systems are consistent with the tendency exhibited by the ternary systems discussed earlier; *i.e.*, the water solubility increase with increasing MgO concentration in the slag. Reverse effect was demonstrated by Al_2O_3 and TiO_2 additions (**see Figure 4.2.1(a) and (b)**). The calculation results are consistent with the tendency exhibited by the ternary systems discussed earlier. These data are also in agreement with those from experimental [1-3,11-14] and from mathematical model estimations [4,5,15] reported in literature. For example, Jung [4] – by means a thermodynamic model – reported a general tendency of increasing water capacity with additions of MgO into the $CaO\text{-}SiO_2\text{-}Al_2O_3$ system.

Ban-Ya *et al*. [15] point out to the fact that, despite the water vapor solubility in the molten slag have the same characteristic behaviors, a quantitative analysis of the water dissolution as a function of composition and temperature, in a wide slag compositional range, has not yet been established. Thereby, the aim of these thermodynamic calculations was not to quantify the water content absorbed by slag from the atmosphere, but to evaluate the solubility trend of the slags and establish a relation with the crystallization behavior of each slag system.

As mentioned in the **section 4.1**, the CSA_T and CSA_TM1 mold powders were more susceptible to changes in their crystallization behavior when in presence of water vapor atmosphere. The crystallization extend (or crystallization temperature range) of CSA_T was markedly enlarged with addition of 3.34 % H_2O to the atmosphere. In the case of CSA_TM1 mold flux, such effect on extend of crystallization temperature range was observed only for the higher water vapor content (12.19 % H_2O) in the argon mixture.

The solubility of gases in glasses, slags and oxide melts has been reported as a function of structure of the slag [16]. For example, at a given pressure and temperature, the solubility of CO_2 in silicate melts is preferentially associated with NBO's of the melt. Correlations with NBO/T pointed to an increase CO_2 solubility with increasing non-bonding oxygen [17-19]. In the present work, a correlation between the nominal NBO/T and C_{OH} for CA, CSM, CSA,

CST and CSA_TM systems was investigated based on the results which are shown in the **Figure 4.2.4** together other with experimental data from literature [3,13,14,20-22].

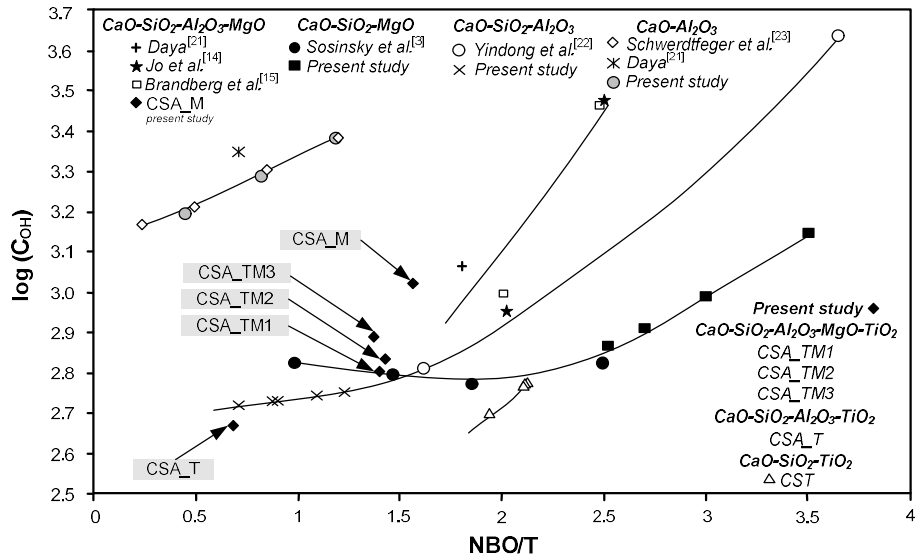

Figure 4.2.4 Water capacity of the mold slag as a function of the number of non-bridging oxygen atoms per number of tetrahedrally-coordinate atoms at 1550°C for CA, CSM, CSA, CST and CSA_TM systems together with experimental data from Sosinsky *et al.* [3], Jo *et al.* [13], Brandberg *et al*. [14], Daya [20], Yindong *et al*. [21] and Schwerdtfeger *et al.* [22].

From the **Figure 4.2.4** it is possible to observe the existence of a trend toward an increase of the hydroxyl capacity with increasing NBO/T, *i.e.* the higher the degree of depolymerization, the higher the water solubility in the slag. Similar tendency was observed by Deubener *et al*. [23] where OH concentrations are significantly higher in more depolymerized sodium trisilicate (NBO/T ≈ 0.66) than in the fully polymerized rhyolitic glass (NBO/T ≈ 0). Study conducted by Le Losq *et al.* [24] – based on variations of water solubility with ionic radius of the alkali oxide at a given temperature and pressure – concluded that the existence of a relationship between chemical composition, solubility mechanisms and melt structure affects the water solubility in tetrasilicate melts. Mysen [25] reported an increase of molar water concentration with increasing NBO/T of Na_2O-SiO_2 glass system for high pressure (1.5 GPa).

Other important aspect observed is the existence of distinct C_{OH} curves as a function of NBO/T ratio for each oxide system, *i.e.* the use of the NBO/T as a structural parameter to predict the hydroxyl capacity of the mold fluxes can be applied only to similar oxide systems, independent of the order of system: binary, ternary or higher order systems. Different hydroxyl capacity values were obtained for distinct oxide systems with a same fixed NBO/T value. Such behavior can be attributed to the presence and proportion of different anionic structural unities, which can be altered by the type of coordinating cations and temperature in a multicomponente melt, denoting a high influence of the chemical composition on the water solubility potential. Although Bouhifd *et al.* [26] suggest that the calculated NBO/T values should be treated only as a guideline – once non-bridging oxygens can be present in the nominally full polymerized compositions – it can be used to reveal the existence of a water solubility-slag structure relationship.

The slag basicity index has also been used as a representative structural parameter of the slags [27,28]. As aforementioned in the **Chapter 2 - item 2.1.1.2**, the concept of binary basicity is somewhat questionable due to the high structural disruption of the melt, which constantly alters the concentration of the non-bridging oxygens. Even structural parameters as NBO/T and *Q*-notation experience problems to describe the structure since they do not take account the effect of different cations on the slag structure [6,28,29]. In this case, the optical basicity is suggested as being an appropriate method to characterize slags according to their chemical composition. The formula of optical basicity and the data used to calculation are described in the **Chapter 2**. Relation of optical basicity (Λ) and water vapor capacity was calculated using the following equation suggested by Sosinsky *et al*. (**Equation 2.38**) [30].

$$\log C_{H_2O} = 12.04 - 32.63\Lambda + 32.71\Lambda^2 - 6.62\Lambda^3 \quad (\mathbf{2.38})$$

Table 4.2.2 shows the estimated C_{H_2O} values calculated by means *FactSage*.

Table 4.2.2 Optical basicity and water capacity results derived from **Eq. 4.6** and *FactSage* calculations.

Mold Flux	Λ*	log (C_{H2O})	C_{H2O} (Eq. 4.6)	C_{H2O} (*FactSage*)	log (C_{OH}) (FactSage)
CSA_T	0.646	2.826	670.821	469.676	2.672
CSA_TM1	0.655	2.839	691.826	639.765	2.806
CSA_TM2	0.660	2.848	705.231	687.291	2.837
CSA_TM3	0.661	2.851	709.187	780.309	2.892
CSA_M	0.664	2.856	718.797	1056.882	3.024

*Calculed using the Pauling eletronegativity data [6] (see **Table 2.1**).

Hydroxyl capacity results from *FactSage* simulations show some alternating result when compared to those from **Eq. 2.38**. The simulated C_{H_2O} of mold powders with highest MgO level was higher than that obtained from **Eq. 2.38**. Opposite result was obtained for the highest TiO_2 mold powder, where the calculated C_{H_2O} was higher than that provided by *FactSage* simulation. **Figure 4.2.5** shows a comparison between the data obtained from *FactSage* simulations and from **Eq. 2.38** calculations for all proposed systems in the present study (see **Table 3.1** and **Table 4.2.1**). On the other hand, the difference between C_{H_2O} data derived from *FactSage* and **Eq. 2.38** calculations of CSA(_TM1, _TM2 and _TM3) systems were lower than those exhibited by the CSA_T and CSA_M mold powders. In addition, the C_{H_2O} *FactSage* results of these slags systems were lower than those provided by **Eq. 2.38**.

Figure 4.2.5 shows a comparison between the *FactSage* C_{OH} values and the hydroxyl capacity data as a function of the optical basicity found in the literature. The quaternary systems – namely CSA_M and CSA_T mold powders – show the highest deviations from the optical basicity curve (**Eq. 2.38**). Nevertheless, the estimated C_{OH} values lie within the experimental data dispersion; furthermore, CSA_M system shows good agreement with Daya's [20] experimental point for an equivalent system (36 wt-% CaO, 35.8 wt-% SiO_2, 18.5 wt-% Al_2O_3 and 9.7 wt-% MgO). It can also be seen that experimental points concerning the TiO_2-bearing system (CST and CSA_T) show lowest water capacity values. The thermodynamic calculation results show a large variation of the hydroxyl capacity in a very narrow optical basicity range – except for CaO-Al_2O_3 binary system.

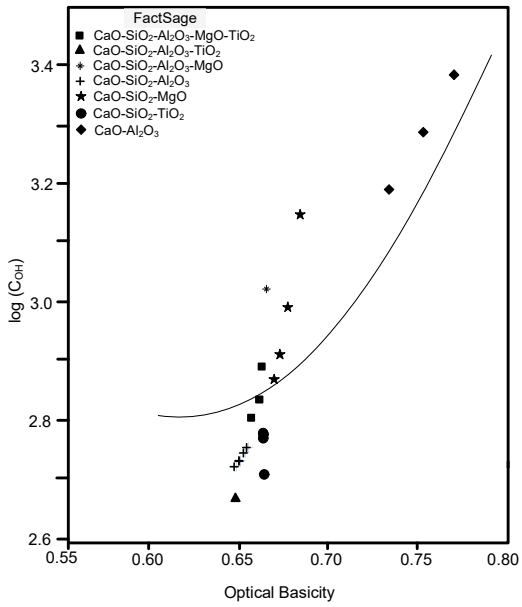

Figure 4.2.5 Comparison between *FactSage* hydroxyl capacity results (C_{H2O}) and equation 4.6 (solid line) data as a function of Optical basicity (Λ).

FactSage C_{OH} values were also compared to literature data as a function of the optical basicity (derived from Pauling electronegativity) based on the **Equation 2.39**, suggested by Daya [20].

$$\log C_{H_2O} = 41.92 - 164.92\Lambda + 226.42\Lambda^2 - 100.31\Lambda^3 \qquad (\mathbf{2.39})$$

The results are shown in **Figure 4.2.6**. A large dispersion of experimental results around the minimum of hydroxyl capacity can be seen. In addition, for the $CaO\text{-}Al_2O_3$ system, data calculated by *FactSage* show better adjustment with the Daya's curve. The ternary systems – CSM, CSA and CST – show a C_{OH} distribution that corroborates the information giving in **Figure 4.2.2**, with MgO-bearing mold powder at higher and wider position than fluxes containing alumina and titania, above and below the C_{OH} curve as a function of Λ, respectively. The quartenary systems – CSA_M and CSA_T mold fluxes – show the highest deviations from the optical basicity curve (**Eq. 2.39**). Nevertheless, the estimated C_{OH} values lie within the experimental data dispersion; furthermore, CSA_M shows a relatively good agreement with Daya's [20] experimental point (36 wt.% CaO, 35.8 wt.% SiO_2, 18.5 wt.%, Al_2O_3 and 9.7 wt.% MgO) of an chemically equivalent system. It can also be seen that experimental points concerning the TiO_2-bearing system (CST and CSA_T) show lowest hydroxyl capacity values. Summarizing, the effect of the chemical composition on the hydroxyl capacity of the ternary systems is reproduced for the higher order systems.

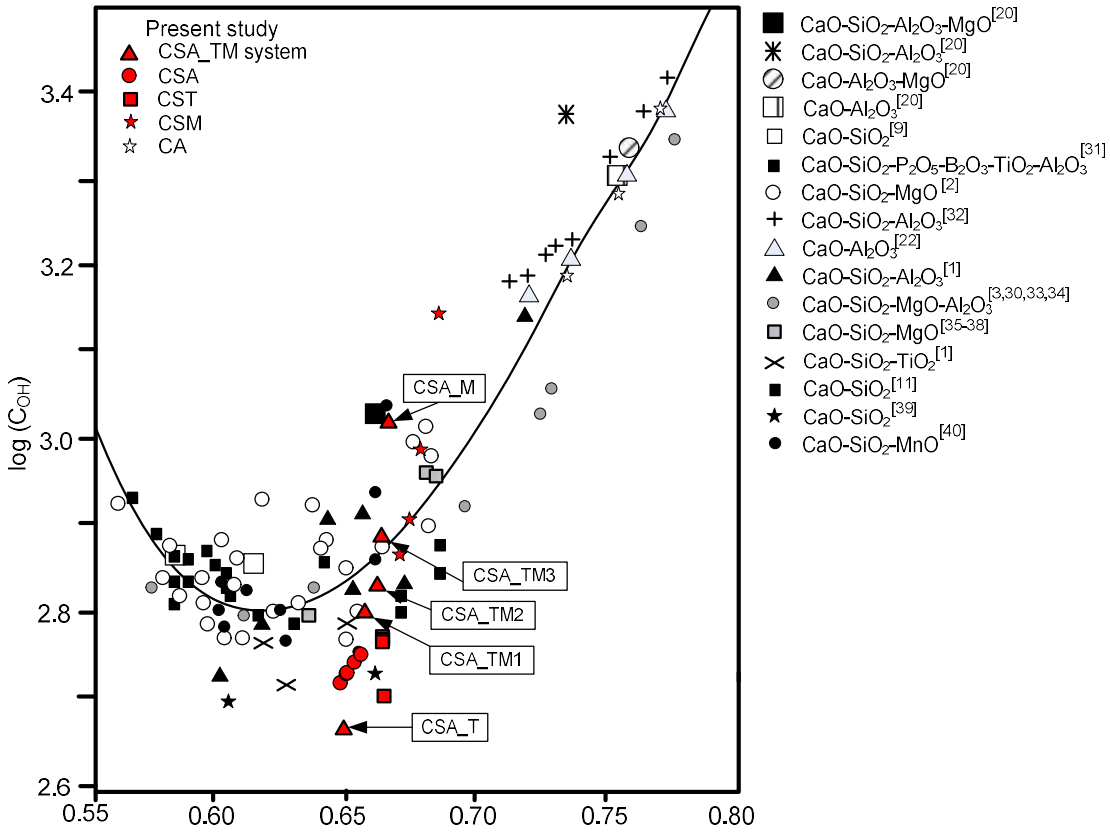

Figure 4.2.6 *FactSage* water capacity (C_{H2O}) as a function of Optical basicity (Λ); comparison of mold fluxes proposed in the present study and from different slag systems available in the literature [1-3,9,11,20,22,30-40]. Figure adapted from Daya [20].

In the **Fig. 4.2.6**, a minimum of C_{OH} as a function of the optical basicity can be clearly seen; in case of other usual indices to express basicity, a minimum at about unity basicity or near to the metasilicate composition has also been reported [3,15,31,41]. As the mold powders tailored from the CSA_TM system were proposed to have a CaO/SiO_2 ratio equal to unity, C_{OH} data distribution around the region of minimum solubility in the curve was expected; however, the mold fluxes exhibited a large water capacity distribution data for a narrow Λ range – yet, still within the experimental data scatter.

Based on the reliability of calculated data, such a hydroxyl capacity variability exposes the high sensitivity to the chemical composition of the *FactSage*, *i.e.* small changes in a component content of the oxide system reflects in a large variation in hydroxyl capacity results. This fact raises the question that, although the optical basicity provides a unique curve for a large chemical composition range – differently to NBO/T index – it is not an adequate parameter to serve as a basis for the hydroxyl prediction of the fluxes under study. It can be seen for the ternary system containing TiO_2 that slags with approximately the same optical basicity may present variations in hydroxyl capacity. Assuming that the structure of the slag has an important role on the water solubility control, such variability in H_2O capacity may indicate that the relation water capacity-slag structure needs complementary information. According to Mills [29], the NBO/T ratio is probably superior to Λ as a measure of the depolymerization, however, it shows some limitations when used to predict water solubility, as previously mentioned.

The curve characteristic of the solubility plotted in terms of basicity is attributed to the amphoteric behavior of the water dissolved in the melt, *i.e.* it can act either as a polymerizing agent in acidic slags or as a depolymerizing agent in basic slags. The calculated optical basicity values lie in a range which indicates a basic character to the mold fluxes, according to the different dissolution mechanisms represented by the reactions **2.28 – 2.31** [4,19,21]. Nevertheless, the amphoteric behavior of water is not reveled taking C_{OH} as a function of NBO/T, *i.e.* , the possible existence of a minimum in solubility could not be confirmed for the oxide systems investigate; since such a minimum in solubility has been found as a function of the slag basicty, and the fact that the basicity of all proposed oxide systems – ternary, quaternary and quinary – is equivalent ($CaO/SiO_2 = 1$), the observation of a minimum when H_2O is expressed as a functions of NBO/T is obscured. However, based on the observations made from results showed in the **Fig. 4.2.4**, the existence of a minimum in solubility correlated to structural assignment is not expected.

Comparing the water solubility results with their respective crystallization results (TTT diagrams – see **section 4.1**), it is possible to observe that the effect of water vapor on crystallization of the slags is more pronounced in those with lower water solubility (CSA_T and CSA_TM1mold powders) than those slags with high water solubility capacity. Such slags have higher polymerization degree than the others, indicating that water have a stronger crystallization effect on the more polymerized mold powders. This is in accordance with the water solubility reaction mechanisms presented in the **Chapter 2** (**reactions 2.28 – 2.31**). The CSA_TM1 and CSA_TM2 mold powders, which are more polymerized than the CSA_TM3, exhibited higher hydroxyl capacity (the values of NBO/T are showed in **Table 4.1.4**). Bouhifd *et al.* [26] reported more intense effect of water on the T_g of aluminosilicate glasses in the more polymerized melts albite (NBO/T = 0) than those with lower degree of polymerization phonolite (NBO/T = 0.19) and trachyte (NBO/T = 0.21), as previously mentioned in **Chapter 2 - section 2.4**. On the other hand, the effect of water on T_g of the leucogranite DK89 (NBO/T = 0) was equivalent to that the phonolite and trachyte melts. Assuming the basic nature of the investigated mold powders, the solubility must to follow one of the reaction mechanisms represented by **reaction 2.29** and **reaction 2.30**. As concluded from the TTT experimental results (**section 4.1**), both solubility mechanisms can occur for a same mold flux as a function of the temperature. This implicates in a structural rearrangement by means of a change in the proportion of the coexisting anionic unities; thus, a change in the basicity could be also expected.

Structural parameters of the slag as NBO/T and optical basicity can be calculated from its chemical composition, giving a good indicative of the degree of polymerization of the slags. Nevertheless, the effect of the temperature on the structure of the slag – which is reflected on the slag properties as viscosity – is not contemplated by such parameters; even experimental results about the effect of water on the structure of the molten silicate and slags are restricted to high temperature (above T_{liq}).

Thus, it is possible to establish a relation between the structure and the water capacity, and its effect on the crystallization behavior of the slags. The structure of the slag dictates the ability of slag to dissolve water – higher polymerized melts are less able to solubilize water than

those with lower degree of polymerization. In addition, the structure of the slag is affected by the temperature, not to the point to significantly alter the overall degree of polymerization, but enough to influence the effect of water on the crystallization behavior of the mold flux.

4.2.2 Some observations about the structural parameters

The structural parameters adopted in the present work to describe the degree of polymerization of the proposed mold powders – NBO/T and Λ – are calculated based on the chemical composition of the slags (**Equations 2.2 – 2.4** and **2.10**, respectively). These equations do not take account the effect of temperature on the structure of the slag. Such a temperature influence on the structure of the slag, in some way, may perhaps be irrelevant in the steelmaking processes, since they usually occur at high temperatures (above the melting temperature of the slag). Nevertheless, for continuous casting, the temperature changes are essential in the solidification process and on the structural variations, which have strong influence on several physicochemical parameters of the slag. Thus, these structural parameters must to be "faced" as a polymerization index which provides a structural tendency of the slag based on its chemical composition. As previously metioned, Bouhifd *et al*. [26] suggest that the NBO/T should be treated as a guideline, because nominally fully polymerized compositions can contain some non-bridging oxygens. Even these parameters are calculated from the bulk chemistry, qualitative discrepancies can occur. For example, assuming Ti^{4+} tetrahedrally-coordinated and Mg^{2+} as a network breaker, it would be expected an increase of polymerization with increasing TiO_2 content – with concomitant decreasing MgO content. This tendency could be observed from optical basicity results, where a polymerization hierarchy obtained was CSA_T > CSA_TM1 > CSA_TM2 > CSA_TM3 > CSA_M. On the other hand, the NBO/T calculated values show the CSA_TM3 more polymerized than CSA_TM1 and CSA_TM2 mold fluxes. In this case, the difference between the NBO/T and Λ values in the present study shows an advantage of optical basicity over the NBO/T ratio. According to Mills [29], the optical basicity can provide an alternative measure of the degree of polymerization. When corrected to compensates the cations used for charge balancing of the alumino-silicate, the optical basicity has advantages over the NBO/T – which is reported as superior to optical basicity – since these cations do not contributes to the depolymerization of the melt. Although these peculiarities about NBO/T ratio, it is a strong and widely used parameter to represent the degree of polymerization of the silicates melts and slags. In the present work, the calculated NBO/T is referred as nominal and was adopted as the main polymerization degree parameter, providing a good polymerization tendency index of the mold fluxes investigated.

References

[1] Iguchi, Y., Ban-Ya, S., Fuwa, T. The Solubility of Water in Liquid CaO-SiO_2, with Al_2O_3, TiO_2 and FeO at 1550°C. *Transactions ISIJ* **1969**, *9*.

[2] Iguchi, Y., Fuwa, T. The Solubility of Water in Liquid CaO-SiO_2-MgO, with and whitout "FeO" at 1550°C. *Transactions ISIJ* **1970**, *10*, 29-35.

[3] Sosinsky, D. J., Maeda, M., McLean, A. Determination and Prediction of Water Vapor Solubilities in CaO-MgO-SiO_2 Slags. *Metallurgical Transactions B* **1985**, *16B*, 61-66.

[4] Jung, I-H. Thermodynamic Modeling of Gas Solubility in Molten Slags (II) - Water. *ISIJ Internacional* **2006**, *46*, 1587-1593.

[5] Zorzato, M. G., Morales, B. B., Bielefeldt, W. V., Vilela, A. C. F.: Thermodynamic analysis of hydrogen pick-up in steel through moist slags. In *67th ABM International Congress*: Rio de Janeiro - Brazil, 2012.

[6] Mills, K. C.: *Slag Atlas*; 2nd Edition ed.; Verlag Stahleisen GmbH Düsseldorf, 1995.

[7] Russell, L. E. Solubility of Water in Molten Glass. *Journal of Society Glass Technology* **1955**, *41*, 304T-317T.

[8] Tomlinson, J. W. A note of the solubility of water in a molten sodium silicate. *Journal of Society Glass Technology* **1956**, *40*, 25T-31T.

[9] Walsh, J. H., Chipman, J., King, T. B., Grant, N. J. Hydrogen in Steelmaking Slags. *Journal of Metals - Transactions AIME* **1956**, 1568-1576.

[10] Franz, H. Solubility of Water Vapor in Alkali Borates Melts. *Journal of American Ceramic Society* **1966**, *49*, 473-477.

[11] Sachdev, P. L., Majdic, A., Schenck, H. Solubility of Water in Lime-Alumina-Silica Melts. *Metallurgical Transactions* **1972**, *3*, 1537-1543.

[12] Iwamoto, N. Gas Solubility of Slag. *Transactions JWRI* **1976**, *5*, 135-142.

[13] Jo, S-K., Kim, S-H. The Solubility of Water Vapour in CaO-SiO_2-Al_2O_3-MgO Slag System. *Steel Research International* **2000**, *71*, 15-21.

[14] Brandberg, J., Sichen, D. Water Vapor Solubility in Ladle-Refining Slags. *Metallurgical and Materials Transactions B* **2006**, *37B*, 389-393.

[15] Ban-Ya, S., Hino, M., Nagasaka, T. Estimation of Water Solubility in Molten Silicates by Quadratic Formalism Based on the Regular Solution Model. *ISIJ Internacional* **1993**, *33*, 12-19.

[16] Mysen, B. O. Water-melt interaction in hydrous magmatic systems at high temperature an pressure. *Progress in Earth and Planetary Science* **2014**, *1:4*.

[17] Brooker, R. A., Kohn, S. C., Holloway, J. R., McMillian, P. F. Structural controls on the solubility of CO_2 in silicate melts Part I: bulk solubility data. *Chemical Geology* **2001**, *174*, 225-239.

[18] Guillot, B., Sator, N.: Carbon dioxide in silicate melts: A molecular dynamics simulation study. In *Laboratorie de Physique Théorique de la Matière Condensée*: Université Pierre et Marie Curie (Paris 6).

[19] Turkdogan, E.T.: *Physicochemical properties of molten slags and glasses*; The Metal Society: London, 1983. pp. 201-208.

[20] Daya, Z. A. The Thermodynamics of Water Vapour Dissolution in Tundish Fluxes. University of Toronto, 1997.

[21] Yindong, Y., Daya, Z. A., Sommerville, I. D., McLean, A. Water Vapor Solubility in Tundish Slags. *Journal of Iron and Steel Research International* **1998**, *5*, 7-14.

[22] Schwerdtfeger, K., Schubert, H. G. Solubility of Water in CaO-Al_2O_3 Melts at 1600°C. *Metallurgical Transactions B* **1978**, *9B*, 143-144.

[23] Deubener, J., Müller, R., Behrens, H., Heide, G. Water and the glass transition temperature of silicate melts. *Journal of Non-Crystalline Solids* **2003**, *330*, 268-273.

[24] Le Losq, C., Mysen, B. O., Cody, G. D. Water and magmas: insights about the water solution mechanisms in alkali silicate melts from infrared, Raman and ^{29}Si solid-satate NMR strectroscopies. *Progress in Earth and Planetary Science* **2015**, *2*.

[25] Mysen, B. O. The solution of H_2O in peralkaline alumosilicate melts at high pressure with implications for properties of hydrous melts. *Geochimica et Cosmochimica Acta* **2007**, *71*, 1820-1834.
[26] Bouhifd, M. A., Whittington, A., Roux, J., Richet, P. Effect of water on the heat capacity of polymerized aluminosilicate glasses and melts. *Geochimica et Cosmochimica Acta* **2006**, *70*, 711-722.
[27] Mills, K. C., Yuan, L., Jones, R. T. Estimating the physical properties of slags. *The Journal of the Southern African Institute of Mining and Metallurgy* **2011**, *111*, 649-658.
[28] Mills, K. C. Structure and Properties of Slags Used in the Continuous Casting of Steel: Part 1 Conventional Mould Powders. *ISIJ Internacional* **2016**, *56*, 1-13.
[29] Mills, K. C. The Influence of Structure on the Physico-chemical Properties of Slags. *ISIJ Internacional* **1993**, *33*, 148-155.
[30] Sosinsky, D. J, Sommerville, I. D., McLean, A.: Sulphide, Phosphate, Carbonate and Water Capacities of Metallurgical Slags. In *Process Technology Conference ISS-AIME*, 1986; Vol. 6; pp 697-703.
[31] Fukushima, T., Iguchi, Y., Ban-Ya, S., Fuwa, T. The Solubility of Water in the Liquid Silicate. *Trans ISIJ* **1966**, *6*, 19-26.
[32] Do, T. T., Lange, K. W.: Determination of the Solubility and Apparent Diffusion Coefficient of Water Vapour in Synthetic Slags. In *3rd. International Conference on Molten Slags and Fluxes*; Institut of Metals: London, 1989; pp 117-124.
[33] Sosinsky, D. J. Application of Optical Basicity Concepts to Metallurgical Slags. University of Toronto, 1990.
[34] Sommerville, I. D., Sosinsky, D. J.: Solubility, Capacity, and Stability of Species in Metallurgical Slags and Glasses. In *Pyrometallurgical for Complex Materials and Wastes*; M. Nilmani, T. L. J. R., Ed.: Melbourne, Autralia, 1994; pp 73-91.
[35] Zuliani, D. J. Thermodynamic and Kinetic Aspects of Water Vapour Dissolution in Molten Slags. University of Toronto, 1982.
[36] Zuliani, D. J., Hasegawa, M., Heard, R. A., Sosinsky, D. J., McLean, A.: Hydrogen Dissolution Reactions and their Influence on the Production of Low Sulfur Steel. In *International Symposium of Physical Chemistry of Iron and Steelmaking*, 1982; pp l-40 - l-46.
[37] Zuliani, D. J., Iwase, M., McLean, A. The Thermodynamics of Water Vapour Dissolution in CaO-MgO-SiO_2 Slags. *Trans. ISIJ* **1982**, *1*, 61-67.
[38] Zuliani, D. J., Sosinsky, D. J., McLean, A. In *Thermodynamic and kinetic aspects of water vapour dissolution in molten CaO-MgO-SiO2 slags*1984.
[39] Davies, M. W., Spassov, A. Solubility of Water Vapour in Slags. *JISI, London* **1967**, *205*, 1031-1033.
[40] Iguchi, Y., Fuwa, T.: *Hydrogen in Liquid Silicates*; Editions Science et Industrie ed., 1972; Vol. 2. pp. 1-3.
[41] Imai, M., Ooi, H., Emi, T. On Hydrogen Equilibria in the System Water Vapour-Molten Slag-Molten Iron. *Tetsu-to-Hagané* **1964**, *50*, 878-887.

Chapter 5 – Conclusions

Taking the main functions of mold powders (lubrication and horizontal heat transfer control) into account and their importance regarding the quality of final product, the study of crystallization behavior assumes an important role for the optimization of the continuous casting process. In the present Chapter, the findings and conclusion based on in-*situ* crystallization behavior results using the SHTT, with support of thermodynamics calculations, are as following.

Crystallization Behavior

Inert Atmosphere

TiO_2 as a glass former: CCT and TTT diagrams constructed from SHTT experiments in inert atmosphere showed TiO_2 as a effective glass former in the content range used in the mold powders investigated (0.5 wt-% - 5.0 wt-%), *i.e.* titania component do not was, in low quantity, on its own a crystallization agent. On the other hand, the crystallization rate was markedly improved as MgO was incorporated to the mold powder composition (up to 5 wt-% MgO), providing the expanse of the temperature crystallization range and decreasing the incubation time.

MgO increases the CCR: The critical cooling rate (CCR) exhibited a huge increase (from $0.17°C.s^{-1}$ to $1.33°C.min^{-1}$) with increasing MgO content from 7 to 10 wt-%; for further addition (up to 15 wt-% MgO), the increase in the CCR was attenuated (from $0.17°C.s^{-1}$ to $1.37°C.s^{-1}$).

Distinct effect of MgO (and TiO_2) on the viscosity: the CSA_M slags system (15 wt-% MgO) exhibited the lowest viscosity values; on the other hand, for the slags containing TiO_2 and MgO concomitantly (CSA_TM1, CSA_TM2 and CSA_TM3) the viscosity increases with increasing MgO content – where the highest viscosity values was observed for the CSA_TM3 mold slag (10 wt-% MgO). For CSA_T mold powder (5 wt-% TiO_2) the viscosity values showed intermediary values (similar to CSA_TM2 system).

Relation between T_{br} and start of crystallization: Comparison between measured break temperature and the temperature of onset crystallization (from CCT experiments at a cooling rate of $10°C.min^{-1}$) shows higher values for the measured T_{br} than those obtained with the continuous cooling measurements. This may be attributed to the presence of an external force (shear strain), characteristic of the rotating cylinder, which can promotes the crystallization. This can be inferred from the existence of a T_{br} in the sample CSA_TM1, in which case no crystals traces were detected during the continuous cooling measurements.

Effect of Humidity

The effect of water vapor on the crystallization behavior of the mold powder is a function of the temperature:

TTT diagrams from SHTT measurements carried out in water vapor atmosphere exhibited – inside of the respective crystallization temperature range of each mold powder – the hindering of crystallization at higher temperatures. At intermediary temperatures, the effect of water on crystallization was negligible. On the other hand, an increase in the crystallization rate (shortening of the incubation time) at lower temperatures could be observed. Such a behavior was more evident in the mold powders with higher nominal NBO/T (calculated based on the chemical composition).

The structure of the slag changes with temperature and dictates the role of water on the crystallization behavior (polymerization/depolymerization): The behavior aforementioned reveals the amphoteric character of water on the crystallization tendency of the mold powders. The effect of water on the crystallization of the slags is affected by temperature.

A reason for this phenomenon can be attributed to the structural changes caused by temperature variations. Based on the crystallization results, with some support from Raman spectroscopy found in the literature, it is suggested that water interacts according to the polymerization degree of the slag, which, in turn, is temperature dependent.

The temperature implicates directly on the type and the proportion of the coexisting anionic structural units in the melt: (i) at higher temperatures, the proportion of more depolymerized anionic structure is higher, and the water acts as a polymerizer agent (as **Equation 2.19**), increasing the viscosity of the melt. Such increment on the viscosity affects the mobility of the germ nuclei, retarding the nucleation and crystal growth; (ii) at lower temperatures, the proportion of more polymerized anionic structures is higher, and water acts as a depolymerizer agent (as **Equation 2.20**), decreasing the viscosity. This enhances the ion diffusivity, and accordingly the crystallization rate.

Influence of the chemical composition of the slag on the distinct crystallization behavior in presence of water as a function of the temperature: The mold powders proposed in the present study were assumed as slightly basic. The results suggest that the change in the structure of slag with temperature, which alternates the effect of water on the crystallization tendency of slag, occurs for a nominal (bulk) range about $1.0 < NBO/T < 2.0$ – in the present study, the CSA_M, CSA_TM1, CSA_TM2 and CSA_TM3 mold powders are exhibit this condition. For $NBO/T < 1.0$, the mold flux is highly polymerized; in this case, water tends to depolymerize the slag, leading to an increase of NBO/T – condition exhibited by CSA_T mold flux (as **Equation 2.18**). For highly depolymerized slags ($NBO/T > 2$), the structure is so disrupted that any additional effect promoted by water tends to depolymerize the slag, enhancing the crystallization rate, as exhibited by CSTNA mold powder.

The crystal morphology remains unaltered in presence of humid atmosphere: The presence of water in atmosphere do not promoted significant changes on the crystal morphology.

Thermodynamic Calculations

Water solubility equivalence between TiO_2 and Al_2O_3: The water capacities of the CSA and CST ternary systems are lower and close to each other, in a very narrow solubility range. In contrast, the water capacities of the CSM systems were much higher and well distributed in a large solubility range. This suggests similar behavior between Al_2O_3 and TiO_2 regarding to water solubility potential, within the chemical composition range investigated, *i.e.*, TiO_2 at low content is assumed be present as Ti^{4+}, which has a role equivalent to Al^{3+} in the structure, acting as network forming element.

Water solubility is a function of the chemical composition of the mold powders: The water capacity of the CSM ternary system increases substantially with increasing MgO content; while the water solubility of the CST and CSA ternary systems decreases with additions of TiO_2 and Al_2O_3, respectively. The same behavior was also observed in the water solubility of the CSA_TM compositions, where the H_2O solubility increases with increasing MgO content, with TiO_2 and Al_2O_3 exhibiting inverse effect.

Water solubility increases with increasing degree of depolymerization of the slag: A relationship between water solubility and the structure of the mold powders could be established. Correlation between C_{OH} and NBO/T exposes a trend to increase water capacity with increasing NBO/T. This suggests that the higher the degree of depolymerization, the higher the water solubility of the slag.

Relation C_{OH}-NBO/T are distinct according to the oxide system: distinct C_{OH} curves as a function of NBO/T ratio for each oxide system were observed, indicating that the use of the NBO/T as a structural parameter to predict the hydroxyl capacity of the mold powders can be applied only within similar oxide systems – independent of the order of system: binary, ternary or for higher order systems, individually – denoting a high influence of the chemical composition on the water solubility potential of the slags.

No minimum in water solubility was observed: Since the mold slags proposed in the present study have a CaO/SiO_2=1, which could to implicates in the presence of a minimum in solubility; the possible existence of such minimum could not be confirmed; however, the existence of a minimum in solubility correlated to the polymerization degree of the slag (NBO/T) has no fundamental reason and was not expected.

Water capacity increases linearly with increasing $\sqrt{p_{H_2O}}$: Thermodynamic calculations confirm the linear relation between water solubility and the square root of water vapor partial pressure well established in the literature.

Water Solubility and Crystallization Behavior

Relation between crystallization behavior results and solubility calculations:

Mold powders with lower water capacity are more sensitive to the effect of water on the crystallization behavior: The slags with lower water solubility (CSA_T and CSA_TM1) - strongly glass forming tendency - exhibited markedly increase of crystallization rate and enlargement of crystallization temperature range. In the case of CSA_TM1, in special, the crystallization was markedly improved in presence of water vapor, but only at higher water vapor pressure. The introduction of 3.34 % H_2O do not was enough to promote any alteration in the crystallization behavior of the slag.

For slags systems with higher water solubility as CSA_M mold powder, the effect of water on the crystallization was less intense, mainly with respect to changes in the crystallization temperature range.

Chapter 6 - Proposal to Future Work

The effect of water vapor on the slag properties and its influence on the main slag functions is still a wide study field. Crystallization behavior is an important factor in mold powder design due its direct influence on the main duties, lubrication and horizontal heat transfer control in the caster mold, since it affect several thermo- and physicalchemical properties. Aiming to enhance the knowledge and improve the understanding about the atmosphere interaction with the slag, the following studies are proposed:

- Study of the influence of the structural changes (degree of polymerization) of the slag with the temperature and its consequence on effect of water on the crystallization behavior (polymerization/depolymerization).

- Investigate the influence of the cooling rate on effect of water on the crystallization behavior of the slags.

- Investigation of the effect of water on the viscosity of mold powders and the relation water capacity (or water solubility)/crystallization tendency of the slags.

- Analyze the influence of water content on the thermophysical properties of the slags.

- Analyze the effect of water on the thermal diffusivity of slags using radiation techniques as the infrared radiation emitter.

Appendix A – Complementary Calibration: validation of the SHTT accuracy with the $CaO\text{-}Al_2O_3$ (CA) binary system

The CA system was chosen as a complement of calibration measurements for SHTT setup. Since the experimental calibration was performed using pure components as CaF_2, the utilization of a binary oxide system is suitable to verify the accuracy and reliability of the results obtained from the SHTT measurements. The CCT curves and the crystallization temperatures are compared to results found in the literature using the same technique. The CA oxide system contains some SiO_2 and MgO impurities in very low contents (0.01 and 0.19 wt-%, respectively) so that their presence could be considered negligible. **Figure A.1** shows the CCT diagram of the CA system. The observed melting temperature for the CA system was 1433.75°C, approximately, while the *Factsage* provides a *liquidus* temperature of 1538°C.

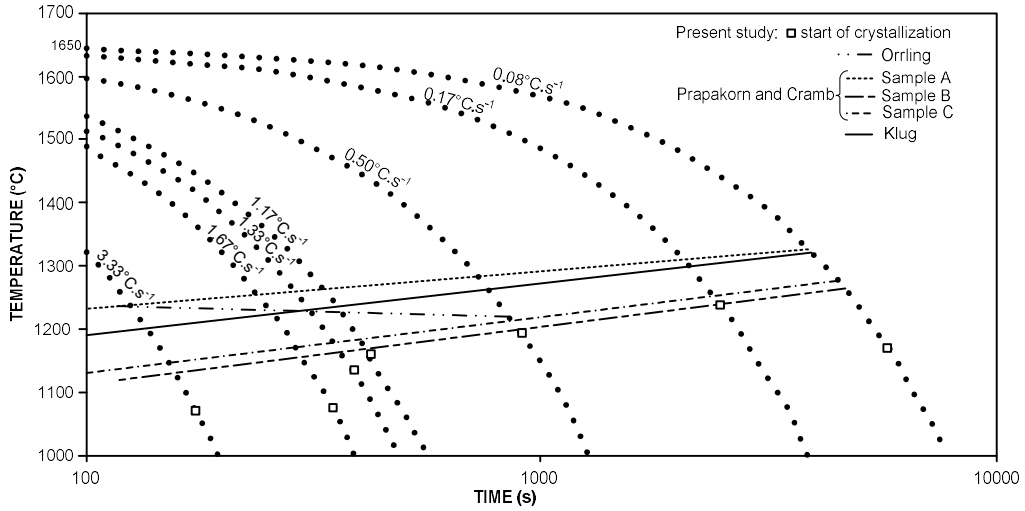

Figure A.1 CCT curves of the CA binary system (48.89 wt-% CaO – 49.93 wt-% Al_2O_3) and those reported by Klug [1] (43.7 wt-% CaO – 56.3 wt-% Al_2O_3); Prapakorn and Cramb [2] where: Sample A (48 wt-% CaO – 52 wt-% Al_2O_3), Sample B (50 wt % CaO – 50 wt-% Al_2O_3) and Sample C (53 wt-% CaO – 47 wt-% Al_2O_3); and Orrling[3] (48.83 wt-% CaO – 49.32 wt-% Al_2O_3).

The start of the crystallization at 0.17, 0.50 and 1.17°C.s^{-1} cooling rates shows good agreement with the crystallization line tendency exhibited by the Sample B from the experiments carried out by Prapakorn and Cramb [2], due to their compositional proximity – CA (48.99 wt-% CaO – 49.83 wt-% Al_2O_3) and Sample B (50 wt-% CaO – 50 wt-% Al_2O_3). CA system exhibited an increase on the crystallization temperature with increasing cooling rate from 0.083 to 1.67°C.s^{-1}. For higher cooling rates, the onset crystallization temperature became lower than those indicated by the crystallization tendency line of the Sample B. Orrling [3] has observed an increase of crystallization temperature up to a cooling rate of 8°C.s^{-1}, followed by decreasing of crystallization temperature for higher cooling rates. From these preliminary results, a dependency correlation between cooling rate and crystallization temperature can be observed, *i.e.* the crystallization temperature is a function of the applied cooling rate. The critical cooling rate for the glass formation of the CA system was 3.33°C.s^{-1} while the Sample B attained a critical cooling rate of the 5°C.s^{-1}; Orrling [3] reported a critical

cooling rate of 45°C.s^{-1} for a 48.83 wt-% CaO – 49.32 wt-% Al_2O_3 (with 1.85 wt-% SiO_2) slag system.

An interesting aspect which is important to make mention is the superheating temperature and time which the sample is held before the cooling start. According to Avrami [4], temperature and duration of superheating can alter the effective number of germ-nuclei. Klug [1] reported an increase of incubation time as superheating time is extended. In the present study, the sample stated to cooling as from 1650°C and maintained in this temperature for 5 minutes; Klug [1], Prapakorn and Cramb [2], and Orrling [3] the parameters are 1700°C for 1 min, 1600°C for 5 min and 1550°C, respectively[1].

Based on the results, the distinct crystallization behavior (crystallization temperature and CCR) observed for the CaO-Al_2O_3 system can be attributed to the differences on component contents, the superheating temperature and time in which the samples are maintained.

References

[1] KLUG, J. L. Crystallization control for fluorine-free slags using the Single Hot Thermocouple Technique. UFRGS-Brazil / TU Bergakademie Freiberg-Germany, 2012.
[2] PRAPAKORN, K.; CRAMB, A. W. Initial Solidification Behavior in Continuous Casting: The Effect of MgO on the Solidification Behavior of CaO-Al_2O_3 Based Slags. *MS&T* **2004**, 3-10.
[3] ORRLING, C. Crystallization Phenomena in Slags. Carnegie Mellon University, 2000.
[4] AVRAMI, M. Kinetics of Phase Change. I*. *Journal of Chemical Physics* **1939**, *7*, 1103-1112.

[1] The time of superheating was not informed by Orrling in his study.

Appendix B - EDS and XRD Results

Scanning electron microscopy (SEM) and energy dispersive spectroscopy (EDS) analyses were conducted with slag sample originated from two different thermal histories (i) isothermal and (ii) continuous cooling treatments. In the (i) the EDS analyses were performed with slag samples taken directly from the SHTT crystallization measurement in isothermal experimental conditions for measurements carried out in inert and humid atmospheres. The chosen isothermal temperatures of the mold powders were 1050°C for CSA_M, CSA_TM1, CSA_TM2 and CSA_TM3 samples, and 1000°C for the CSA_T sample. The preparation of the mold flux samples are described in the **Chapter 3**, **Section 3.1 - Materials and Samples Preparation**. In the (ii) the mold powders were heated at a heating rate of 0.25 °C.s^{-1} and melted at 1600°C for 15 minutes in an electrical furnace in an argon atmosphere. After, the samples were left to rest inside the closed furnace per approximately 24 hours to room temperature. The X-ray diffraction (XRD) analyses were performed using the same mold fluxes from thermal treatment (ii).

SEM images and corresponding EDS results (from SHTT experiments)

Table B.1 EDS of crystals taken from SHTT samples in argon and two different water vapor pressures.

	Atmosphere		
Element	argon	3.34 %H_2O	3.34 %H_2O
	wt%	wt%	wt%
C	15.84	10.93	24.39
O	37.69	40.77	31.17
Mg	8.72	9.76	7.95
Al	11.02	11.8	9.91
Si	15.39	16.21	14.19
Ca	11.23	10.53	12.3
Ti	0.11	0	0.09

CSA_M

	Atmosphere		
Element	argon	3.34 %H_2O	3.34 %H_2O
	wt%	wt%	wt%
C	4.59	22.97	10.17
O	38.2	38.37	32.85
Mg	0.05	0.12	0.26
Al	15.84	11.15	14.9
Si	20.61	13.17	19.08
Ca	18.65	12.82	20.34
Ti	2.05	1.4	2.43

CSA_T

	Atmosphere		
Element	argon	3.34 %H_2O	3.34 %H_2O
	wt%	wt%	wt%
C	17.41	12.39	6.47
O	33	38.79	34.05
Mg	3.04	0.06	1.31
Al	7.62	13.75	8.57
Si	18.52	16.99	24.17
Ca	19.98	16.13	24.38
Ti	0.44	1.88	0.77

CSA_TM1

	Atmosphere		
Element	argon	3.34 %H_2O	3.34 %H_2O
	wt%	wt%	wt%
C	33.19	9.64	6.09
O	26.57	34.05	32.67
Mg	3.07	4.62	4.68
Al	6.44	9.96	10.43
Si	12.7	19.93	21.29
Ca	17.63	21.34	24.33
Ti	0.38	0.46	0.51

CSA_TM2

	Atmosphere		
Element	argon	3.34 %H_2O	3.34 %H_2O
	wt%	wt%	wt%
C	15.66	9	7.57
O	32.37	36.41	33.52
Mg	6.31	7.77	6.88
Al	10.96	12.16	12.04
Si	16.72	18.64	19.01
Ca	17.69	15.84	20.71
Ti	0.28	0.19	0.28

CSA_TM3

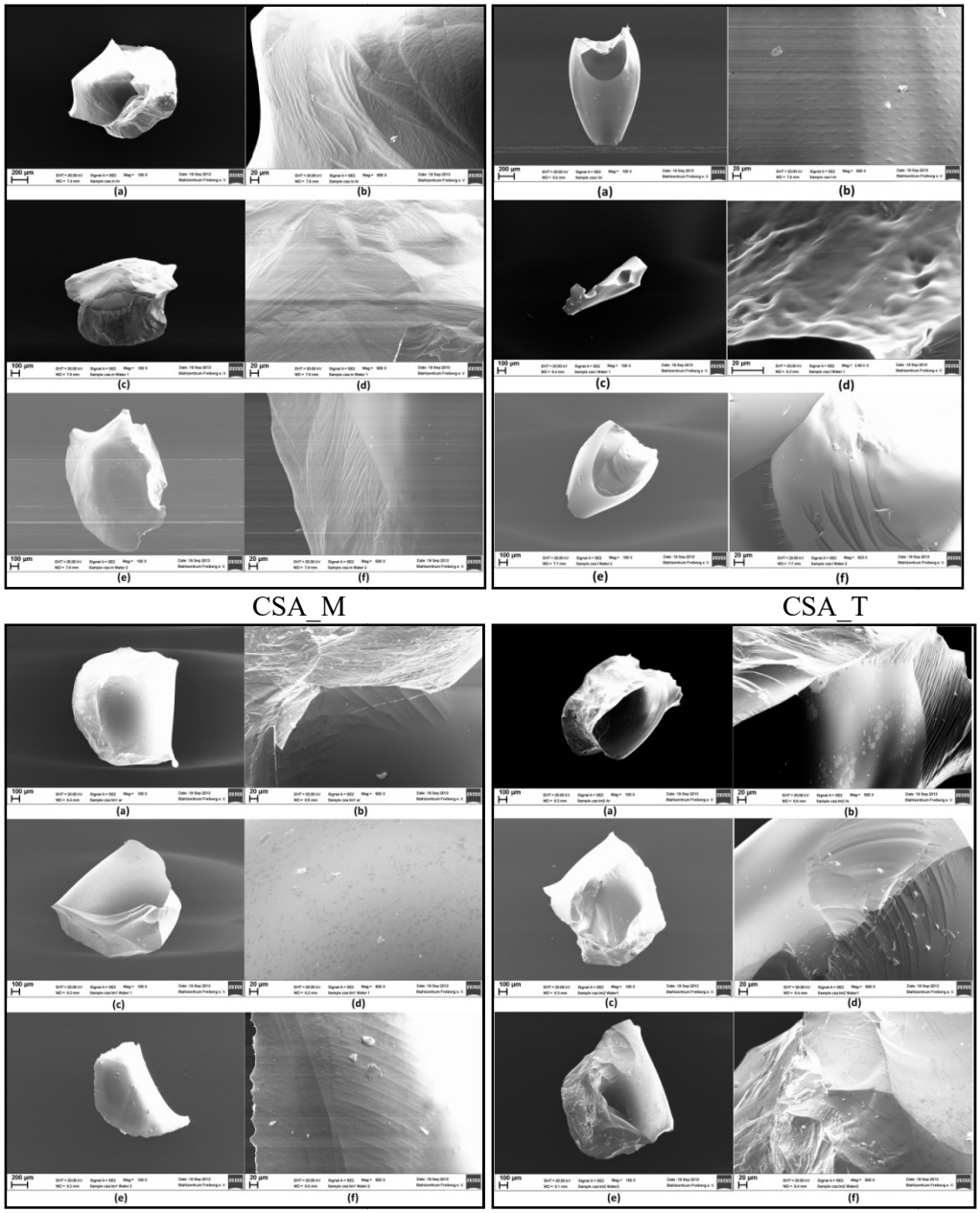

CSA_M CSA_T

CSA_TM1 CSA_TM2

Figure B.1 EDS images taken from SHTT measurements of the CSA_M, CSA_T, CSA_TM1 and CSA_TM2 mold powders samples from different atmospheres carried out at 1050°C (except CSA_T analyzed at 1000°C); images (a) and (b) from measurements in argon atmosphere; images (c) and (d) from measurements in water vapor partial pressure of 0.0334 atm and; images (e) and (f) from measurements in water vapor partial pressure of 0.1219 atm.

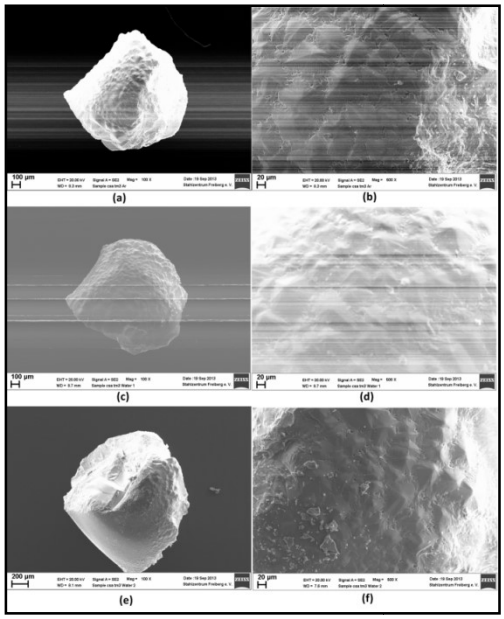

CSA_TM3

Figure B.2 EDS images taken from SHTT measurements of the CSA_TM3 mold powder samples from different atmospheres carried out at 1050°C; images (a) and (b) from measurements in argon atmosphere; images (c) and (d) from measurements in water vapor partial pressure of 0.0334 atm and; images (e) and (f) from measurements in water vapor partial pressure of 0.1219 atm.

X-ray diffraction patterns (from natural cooling treatment)

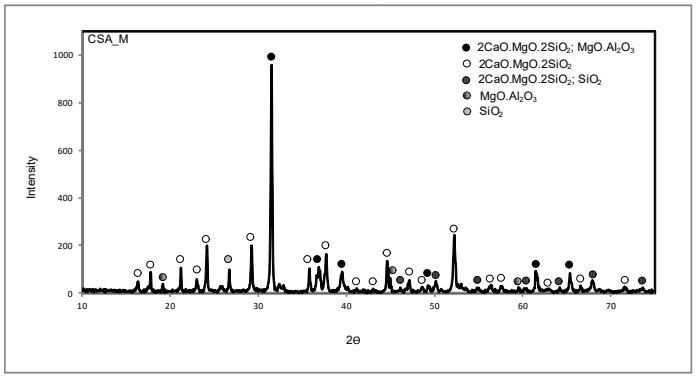

CSA_M [wt-%]
33.75 % CaO
33.89 % SiO_2
19.69 % Al_2O_3
13.40 % MgO

Figure B.3 X-ray diffraction pattern of CSA_M mold powder slowly cooled until room temperature.

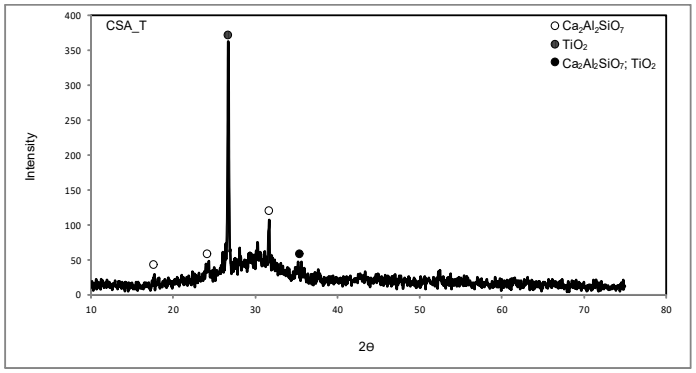

CSA_T [wt-%]
35.56 % CaO
35.21 % SiO_2
25.33 % Al_2O_3
4.95 % TiO_2

Figure B.4 X-ray diffraction pattern of CSA_T mold powder slowly cooled until room temperature.

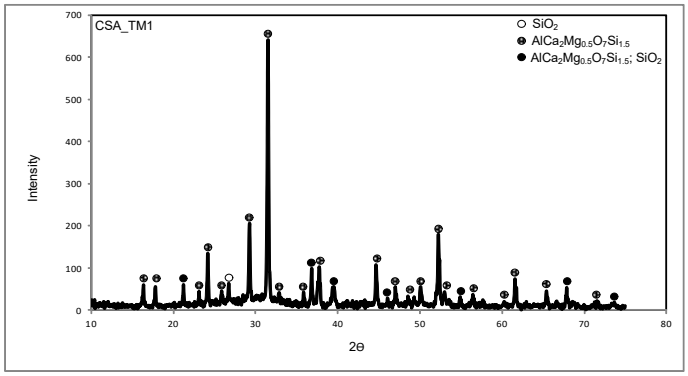

CSA_TM1 [wt-%]
39.07% CaO
40.24 % SiO_2
14.23 % Al_2O_3
0.99% TiO_2
4.60 % MgO

Figure B.5 X-ray diffraction pattern of CSA_TM1 mold powder slowly cooled until room temperature.

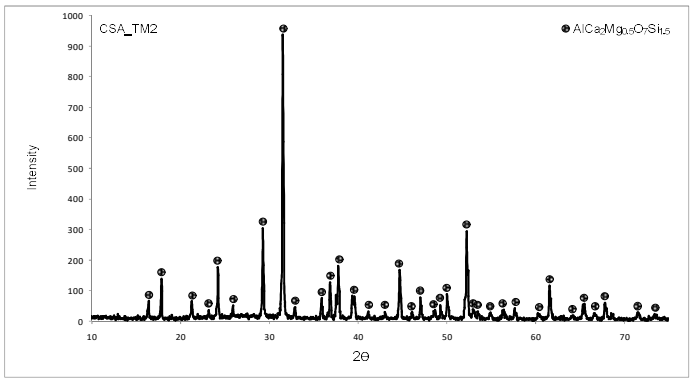

CSA_TM2 [wt-%]
39.00% CaO
38.44 % SiO_2
16.44 % Al_2O_3
0.77% TiO_2
6.35 % MgO

Figure B.6 X-ray diffraction pattern of CSA_TM2 mold powder slowly cooled until room temperature.

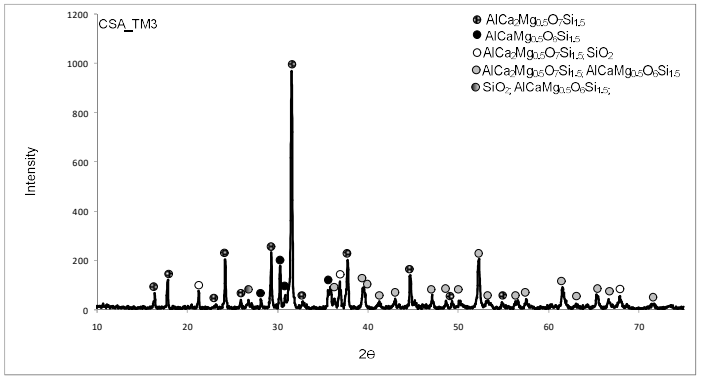

CSA_TM3 [wt-%]
36.01% CaO
35.29 % SiO_2
19.94 % Al_2O_3
0.53% TiO_2
9.13 % MgO

Figure B.7 X-ray diffraction pattern of CSA_TM3 mold powder slowly cooled until room temperature.

SEM images and corresponding EDS analysis (from natural cooling)

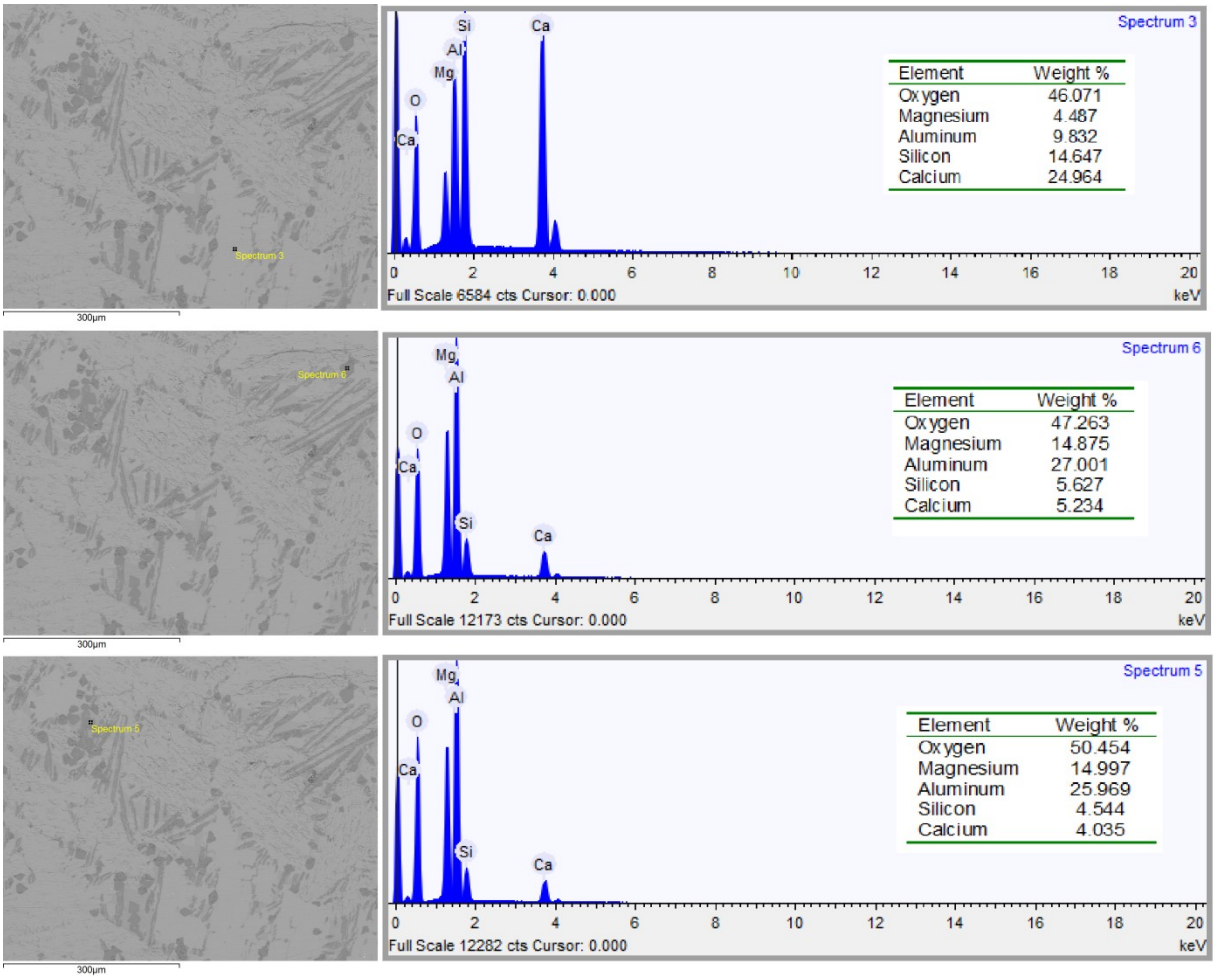

Figure B.8 SEM images and the corresponding EDS of the CSA_M slag samples after melting and natural cooling.

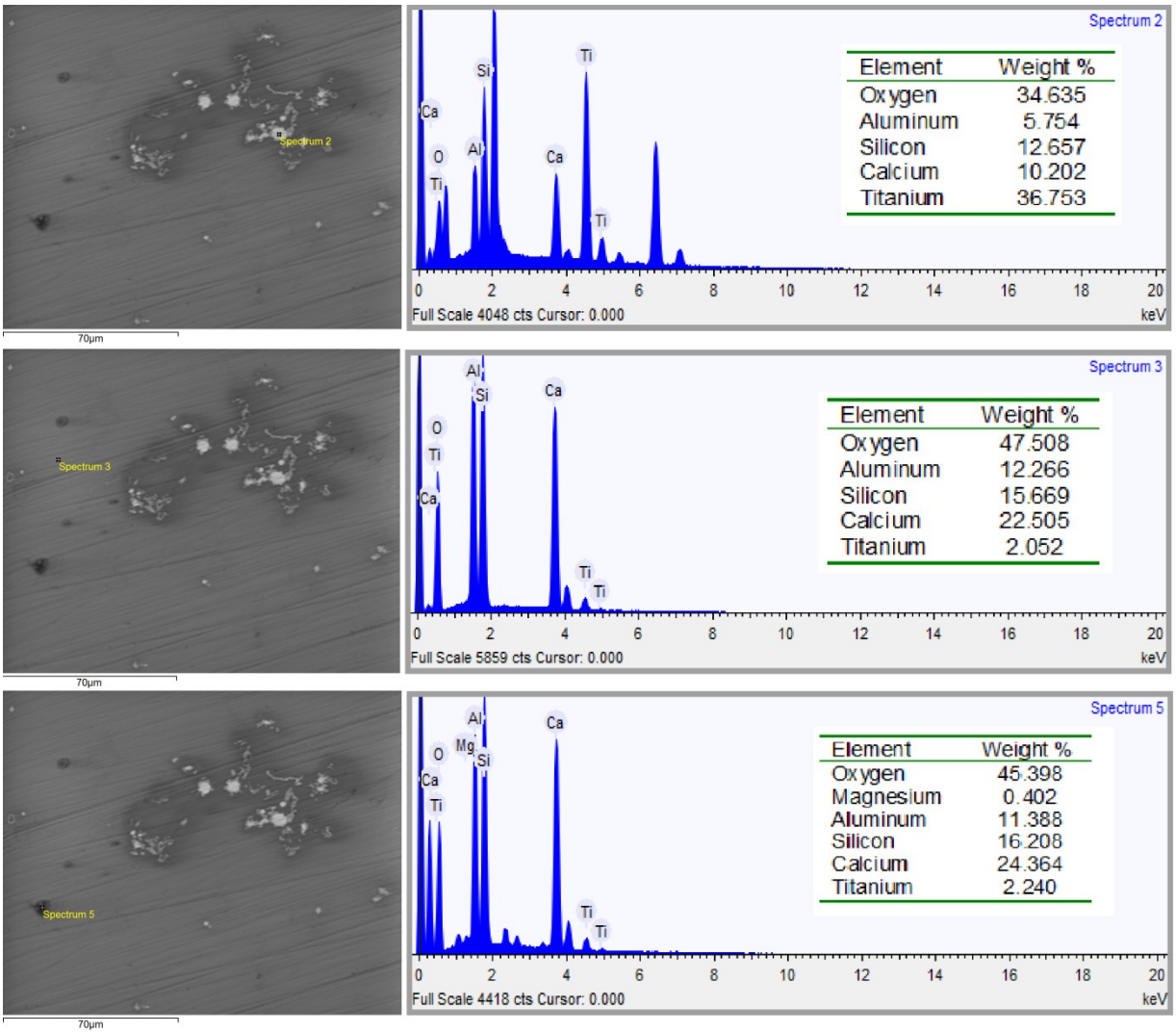

Figure B.9 SEM images and the corresponding EDS of the CSA_T slag samples after melting and natural cooling.

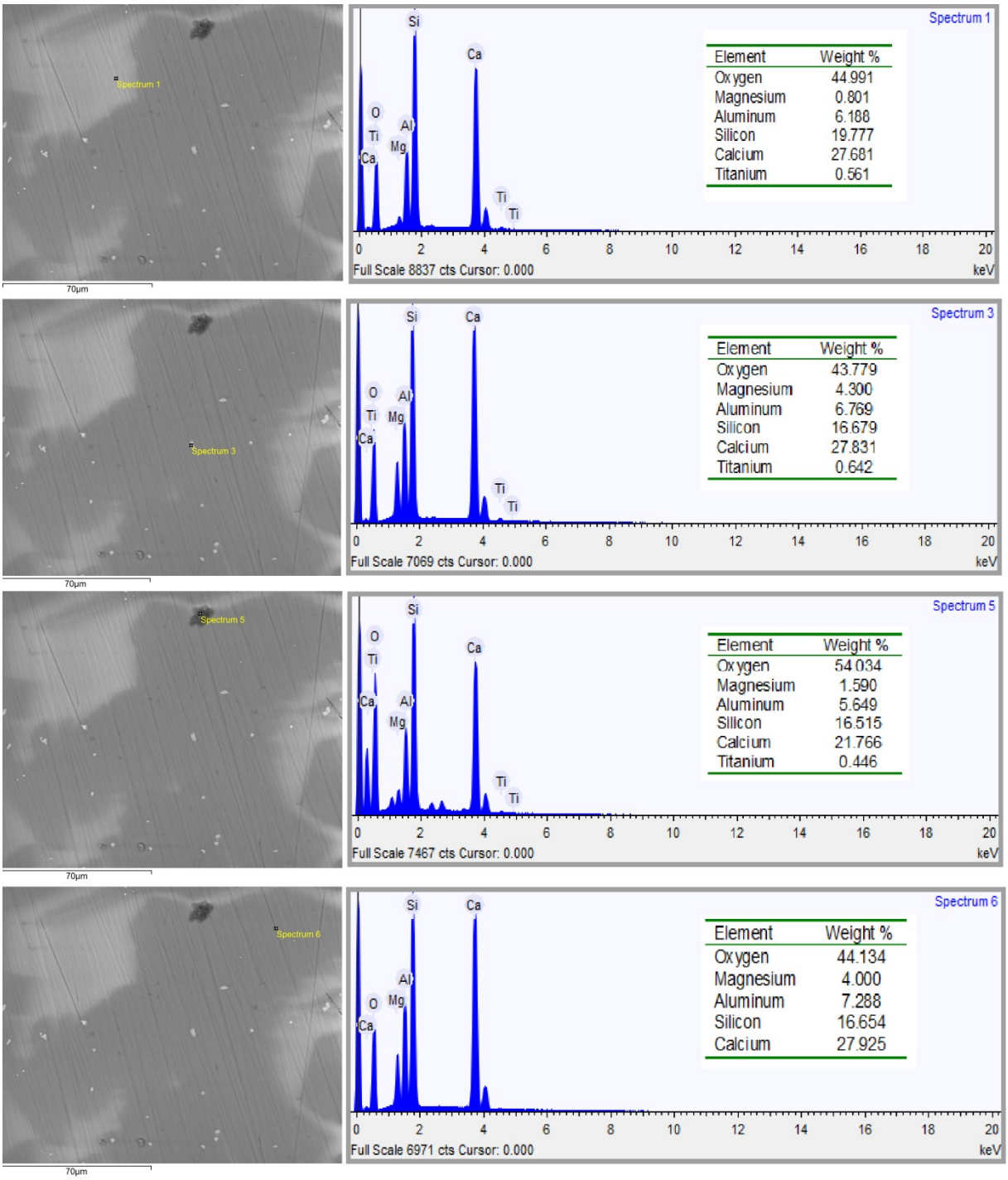

Figure B.10 SEM images and the corresponding EDS of the CSA_TM1 slag samples after melting and natural cooling.

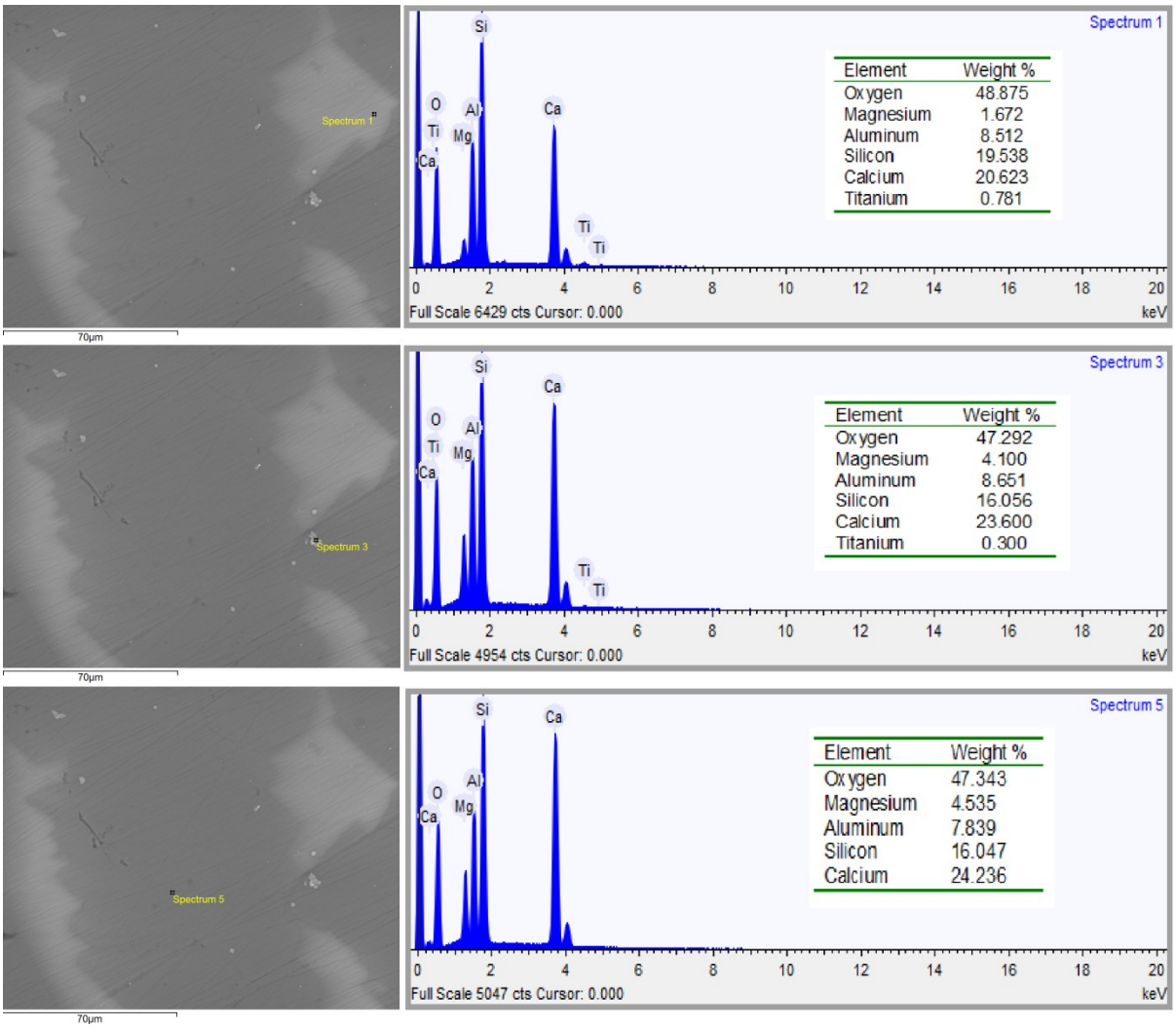

Figure B.11 SEM images and the corresponding EDS of the CSA_TM2 slag samples after melting and natural cooling.

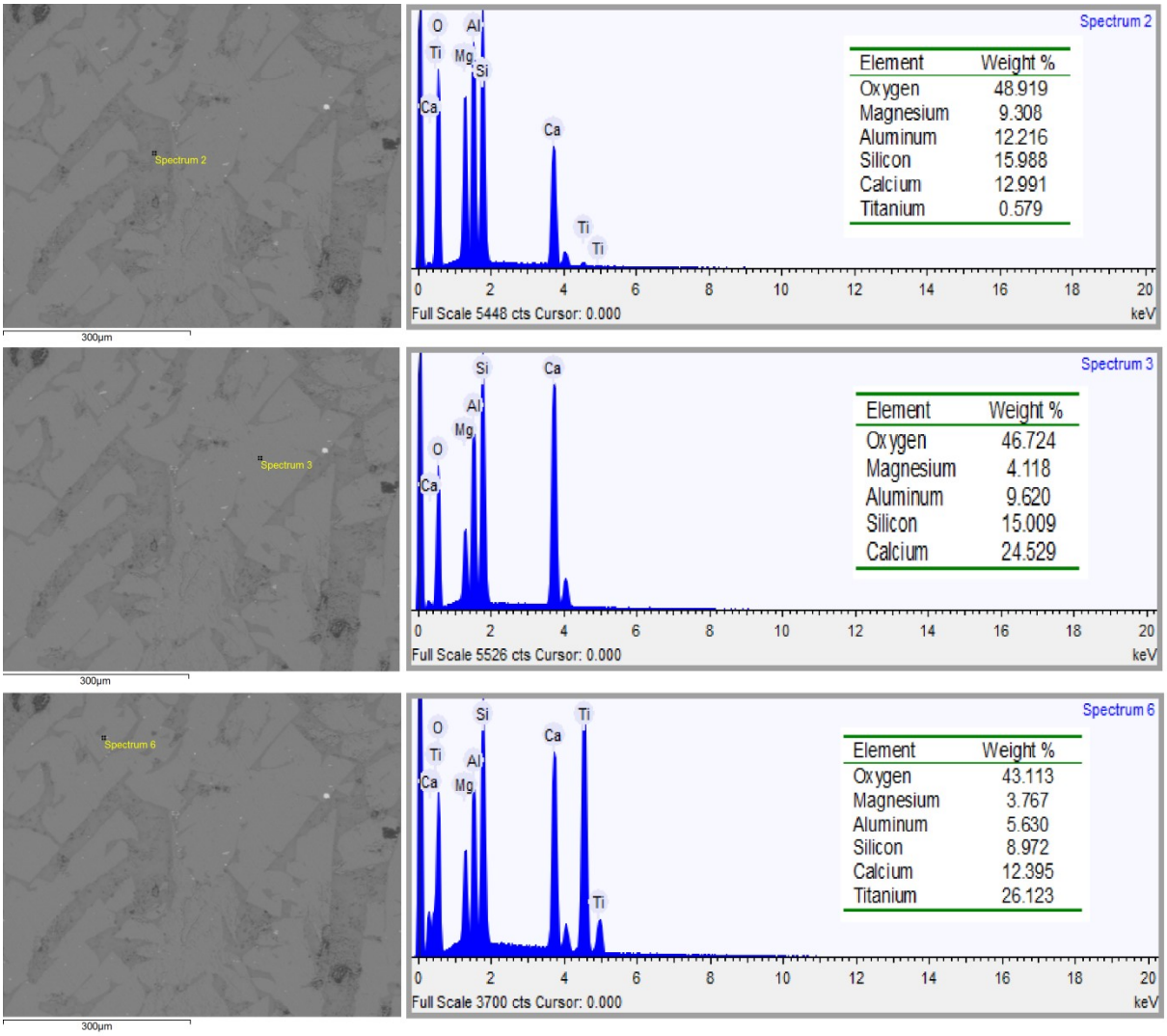

Figure B.12 SEM images and the corresponding EDS of the CSA_TM3 slag samples after melting and natural cooling.

Appendix C - Equilibrium Phases Calculations

FactSage 6.4 software was applied aiming to predict the crystalline phases that thermodynamically are able to precipitate during solidification of the mold powders for the different atmosphere conditions applied in the SHTT crystallization measurements. The following database were used in the thermodynamic calculations, according to *FactSage* database documentation: solution phase (FACT-SLAG); and the FToxid compound database, which contains all stoichiometric solid and liquid oxide compounds evaluated/optimized to be thermodynamically consistent with the FToxid solution database. The calculation results for inter and humid atmospheres are shown follow.

CSA_M (33.75 wt-% CaO - 33.89 wt-% SiO_2 - 19.69 wt-% Al_2O_3 - 13.40 wt-% MgO)

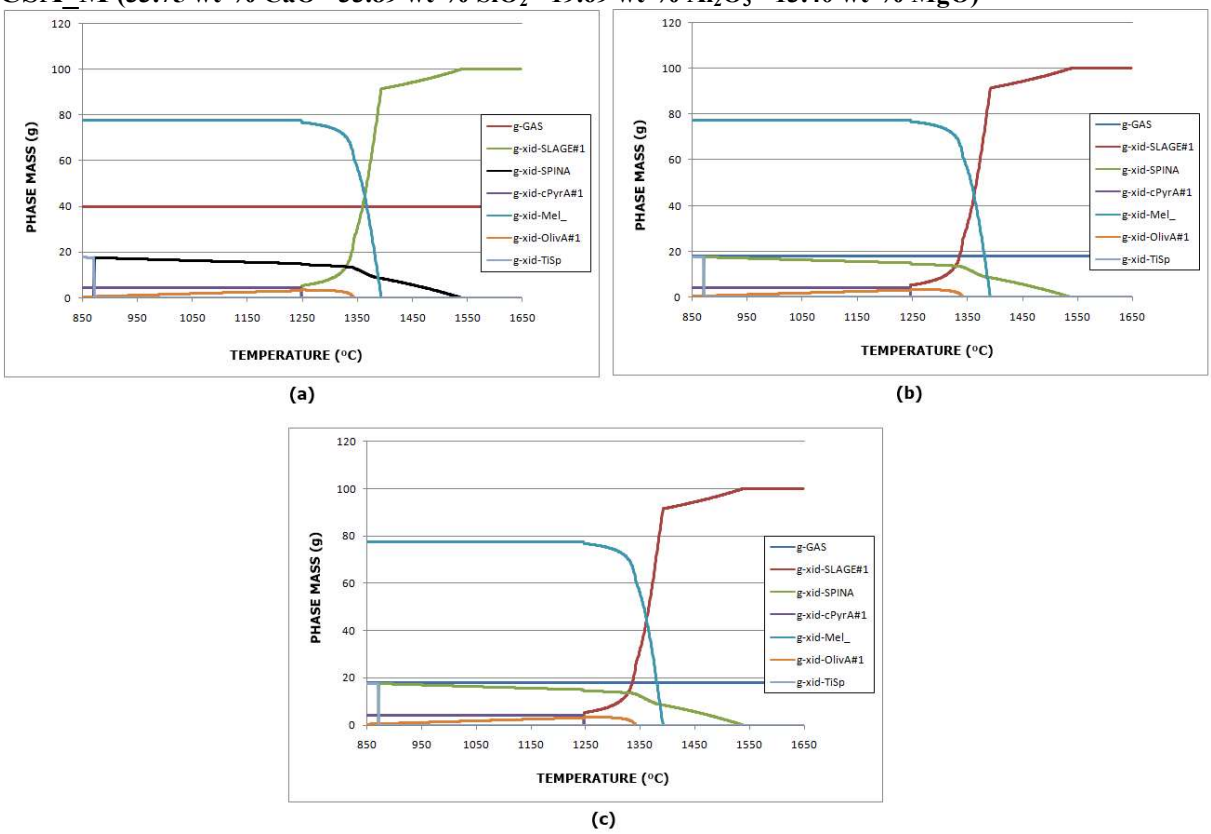

Figure C.1 Crystalline phases formation of the CSA_M mold powder (a) in argon atmosphere; and humid atmospheres (b) with 0.0334 atm H_2O; and (c) with 0.1219 atm H_2O.

CSA_T (35.56 wt-% CaO - 35.21 wt-% SiO_2 - 25.33 wt-% Al_2O_3 - 4.95 wt-% TiO_2)

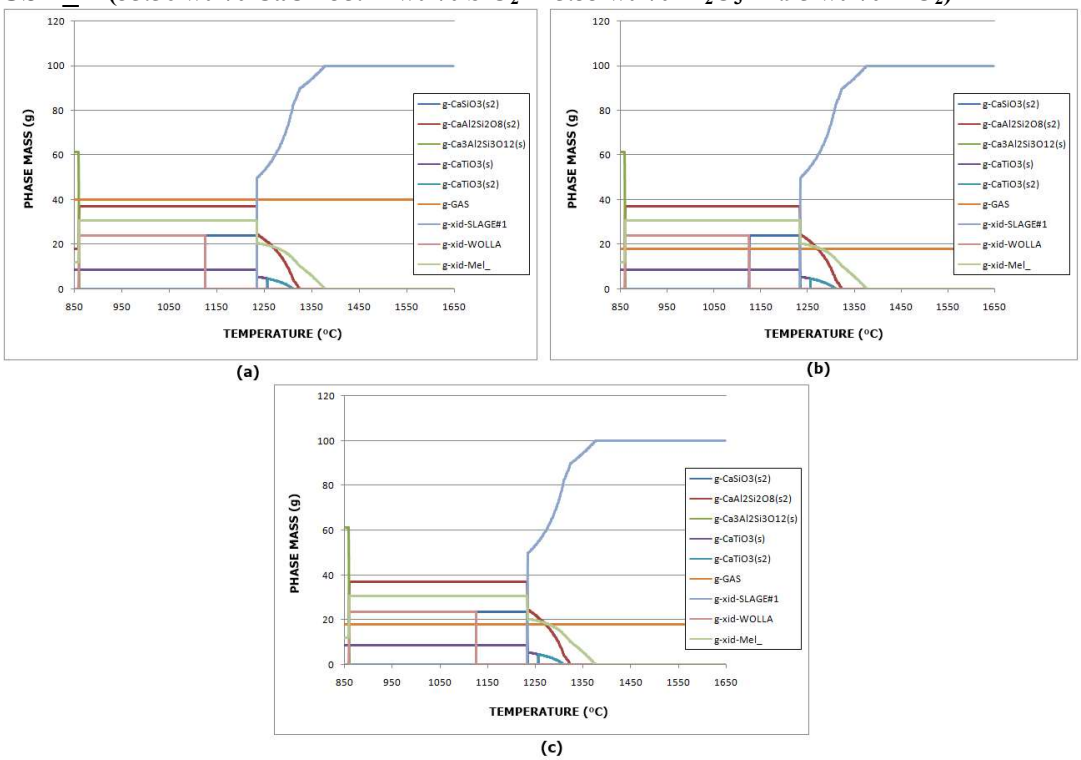

Figure C.2 Crystalline phases formation of the CSA_T mold powder (a) in argon atmosphere; and humid atmospheres (b) with 0.0334 atm H_2O; and (c) with 0.1219 atm H_2O.

CSA_TM1 (39.07 wt-% CaO - 40.24 wt-% SiO_2 - 14.23 wt-% Al_2O_3 – 0.99 wt-% TiO_2 4.60 wt-% MgO)

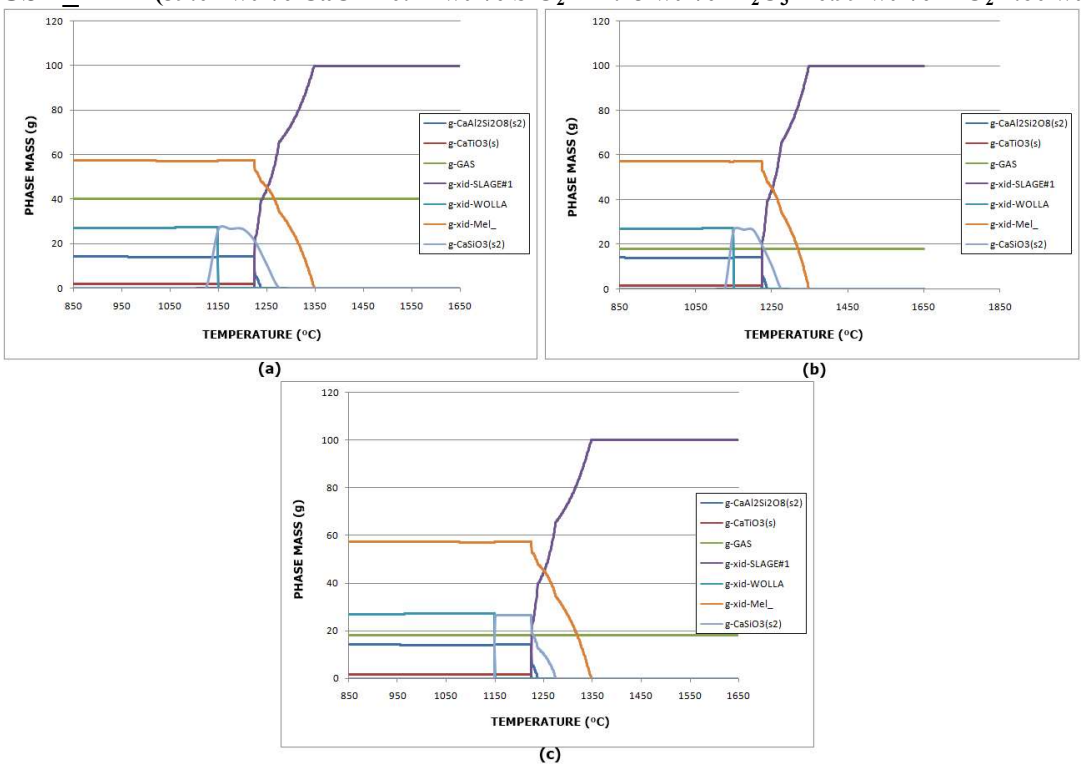

Figure C.3 Crystalline phases formation of the CSA_TM1 mold powder (a) in argon atmosphere; and humid atmospheres (b) with 0.0334 atm H_2O; and (c) with 0.1219 atm H_2O.

CSA_TM2 (39.00 wt-% CaO - 38.44 wt-% SiO_2 - 16.44 wt-% Al_2O_3 – 0.77 wt-% TiO_2 6.35 wt-% MgO)

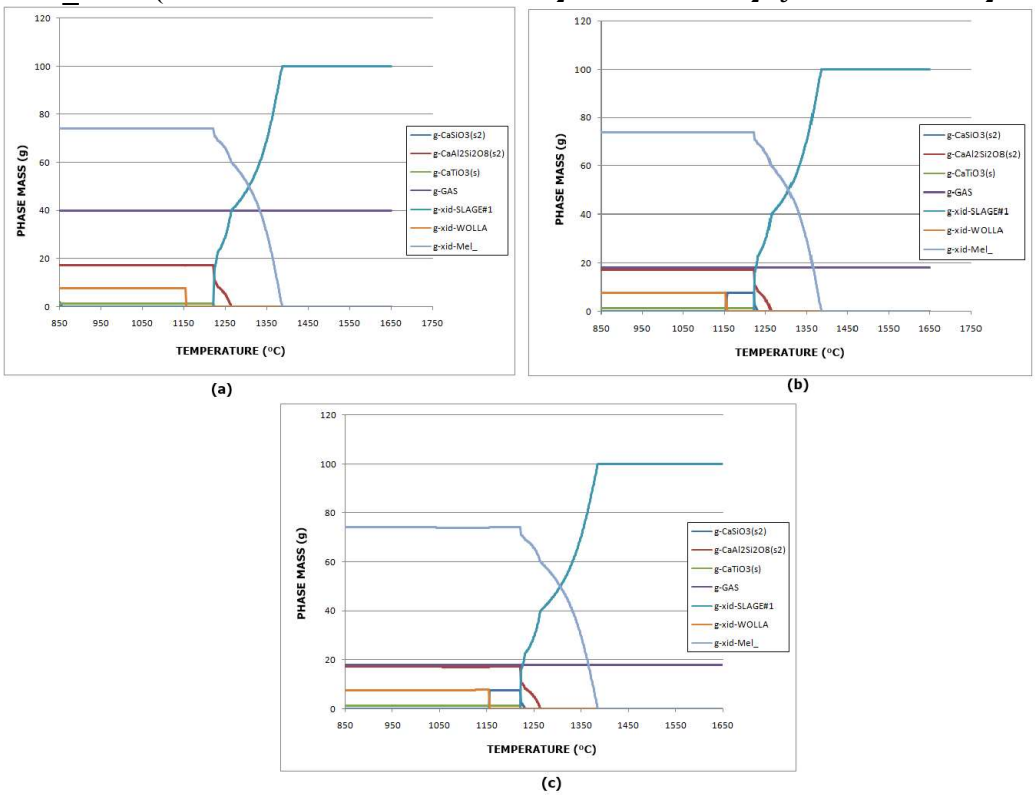

Figure C.4 Crystalline phases formation of the CSA_TM2 mold powder (a) in argon atmosphere; and humid atmospheres (b) with 0.0334 atm H_2O; and (c) with 0.1219 atm H_2O.

CSA_TM3 (36.01 wt-% CaO - 35.29 wt-% SiO_2 - 19.94 wt-% Al_2O_3 – 0.53 wt-% TiO_2 9.13 wt-% MgO)

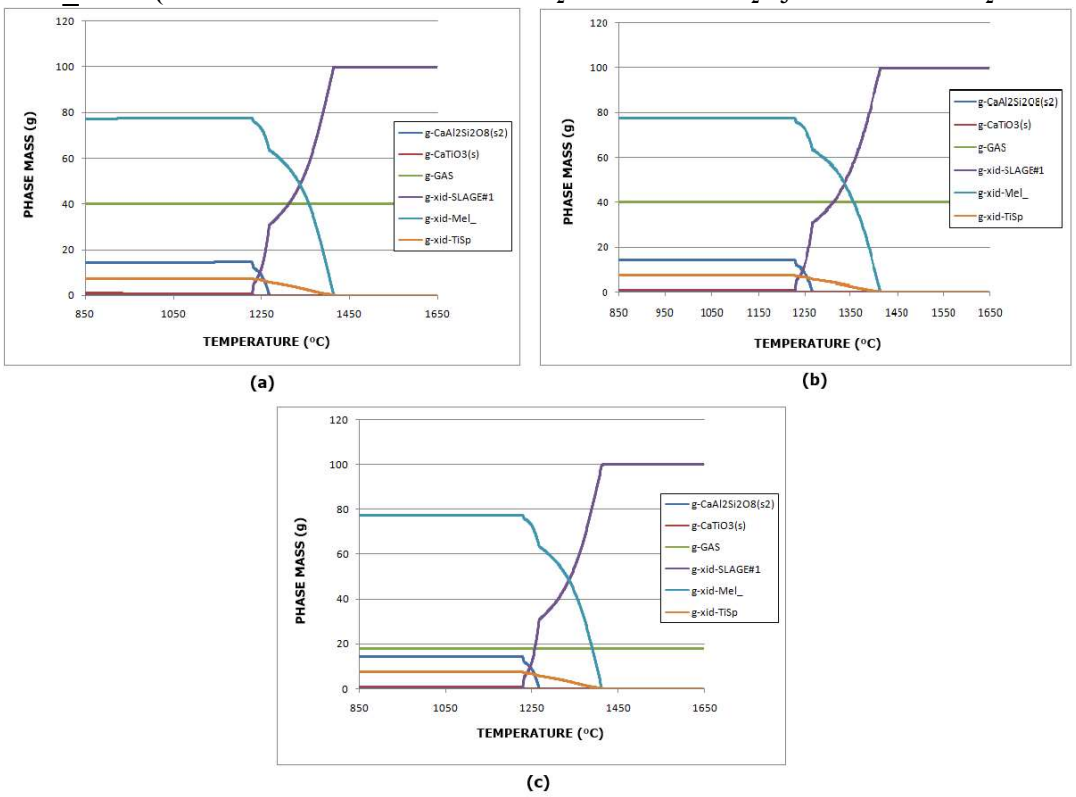

Figure C.5 Crystalline phases formation of the CSA_TM3 mold powder (a) in argon atmosphere; and humid atmospheres (b) with 0.0334 atm H_2O; and (c) with 0.1219 atm H_2O.

Some observations:

There is a decreasing of the crystallization temperature of the 1st crystal with increase water content in the atmosphere.

The thermodynamic simulation result do not exhibited phase change in presence of water in the atmosphere. However, there is an increase of the crystal phase amount with increasing the water vapor partial pressure in the gas mixture Ar-H_2O. Although kinetic factors are not considered by the thermodynamic precepts, the increase content of the first crystalline precipitate can be interpreted as an indicative of the increase of the crystallization rate with the presence of water in the atmosphere.

The crystalline phase $CaSiO_3$(s2) in the CSA_TM1 mold powder simulation in argon and 0.0334 atm H_2O (**Figure C3(a)** and **(b)**, respectively) was simulated using temperature range between each data (step) of 25°C instead a step of 1°C as used in the simulation in 0.1219 atm H_2O atmosphere (**Figure C3(c)**).